Causes and consequences of widespread ocean anoxia in the past

Niels A.G.M. van Helmond

Utrecht Studies in Earth Sciences No. 70

LPP Contribution Series No. 40

ISBN 978-90-6266-372-9
ISNN 2211-4335

USES No. 70
LPP Contributions Series No. 40

Author contact: n.vanhelmond@uu.nl or nielsvanhelmond@gmail.com

Cover: Amadeus segment (OAE1c), Fiume Bosso section, close to Urbino, Umbria-Marche, Italy (November 2010).

Copyright © 2014 N.A.G.M. van Helmond. All rights reserved. No part of this publication may be reproduced in any form, by print or photo print, microfilm or any other means, without written permission by the author.

Printed in the Netherlands by WPS, Zutphen.

Causes and consequences of widespread ocean anoxia in the past

Oorzaken en gevolgen van zuurstofschaarste in de oceanen in het verleden

(met een samenvatting in het Nederlands)

Proefschrift

ter verkrijging van de graad van doctor aan de Universiteit Utrecht op gezag van de rector magnificus, prof. dr. G.J. van der Zwaan, ingevolge het besluit van het college voor promoties in het openbaar te verdedigen op

dinsdag 13 januari 2015 des middags te 2.30 uur

door

Niels Antonius Gerardus Martinus van Helmond

geboren op 26 augustus 1987 te Deurne

Promotoren:

Prof. dr. H. Brinkhuis
Prof. dr. A. Sluijs

Copromotoren:

Dr. F. Sangiorgi
Dr. B. van de Schootbrugge

Dit proefschrift werd mede mogelijk gemaakt door financiële steun van Stichting LPP en Statoil.

Members of the dissertation committee:

Prof. dr. Jack J. Middelburg
Utrecht University, the Netherlands

Prof. dr. Jörg Pross
Ruprecht-Karls-Universität Heidelberg, Germany

Prof. dr. Gert-Jan Reichart
Royal NIOZ & Utrecht University, the Netherlands

Prof. dr. ir. Stefan Schouten
Royal NIOZ & Utrecht University, the Netherlands

Prof. dr. Silke Voigt
Goethe-Universität Frankfurt, Germany

Voor mijn ouders,

Contents

11 Chapter 1: General Introduction and Synopsis

27 Chapter 2: Marine productivity leads organic matter preservation in sapropel S1: palynological evidence from a core along the path of the Nile River outflow

Niels A.G.M. van Helmond, Rick Hennekam, Timme H. Donders, Frans P.M. Bunnik, Gert J. de Lange, Henk Brinkhuis and Francesca Sangiorgi
(in revision for Quaternary Science Reviews)

45 Chapter 3: A perturbed hydrological cycle during Oceanic Anoxic Event 2

Niels A.G.M. van Helmond, Appy Sluijs, Gert-Jan Reichart, Jaap S. Sinninghe Damsté, Caroline P. Slomp, and Henk Brinkhuis
Geology 42, 123-126, (2014)

61 Chapter 4: Freshwater discharge controlled deposition of Cenomanian-Turonian black shales on the NW European epicontinental shelf (Wunstorf, North Germany)

Niels A.G.M. van Helmond, Appy Sluijs, Jaap S. Sinninghe Damsté, Gert-Jan Reichart, Silke Voigt, Jochen Erbacher, Jörg Pross and Henk Brinkhuis
Climate of the Past Discussions 10, 3755-3786 (2014)

83 Chapter 5: Equatorward migration of dinoflagellates during the Plenus Cold Event, Oceanic Anoxic Event 2

Niels A.G.M. van Helmond, Appy Sluijs, Nina-Maria Papadomanolaki, A. Guy Plint, Darren R. Gröcke, Martin A. Pearce, James S. Eldrett, João Trabucho-Alexandre, Bas van de Schootbrugge and Henk Brinkhuis
(under review for Geology)

97 Chapter 6: Spatial extent and degree of oxygen depletion in the deep proto-North Atlantic Basin during Oceanic Anoxic Event 2

Niels A.G.M. van Helmond, Itzel Ruvalcaba Baroni, Appy Sluijs, Jaap S. Sinninghe Damsté and Caroline P. Slomp
Geochemistry, Geophysics, Geosystems 15 (2014)

121 Chapter 7: Reassessing the nitrogen isotope composition of sediments from the proto-North Atlantic during Oceanic Anoxic Event 2

Itzel Ruvalcaba Baroni, Niels A.G.M. van Helmond, Iana Tsandev, Jack J. Middelburg and Caroline P. Slomp
(under review for Paleoceanography)

147 References

173 Summary in Dutch (Samenvatting in het Nederlands)

181 Acknowledgements (Dankwoord)

185 Curriculum Vitae

1

General Introduction and Synopsis

"The beginning is the most important part of the work."

Plato, in: *The Republic (~380 B.C.)*

1. Ocean oxygenation

Oxygen plays a fundamental role for all aerobic life, in both the terrestrial and marine realm. Atmospheric oxygen concentrations are homogeneously distributed and relatively constant over long periods of time, i.e. millions of years (Berner et al, 1989). Oceanic oxygen concentrations, on the other hand, vary with space and time, and large changes may occur relatively rapidly, for example, over the last deglaciation (Jaccard and Galbraith, 2012), within decades (Jilbert and Slomp, 2013), or even seasonally (Tyson and Pearson, 1991). Decreasing oxygen concentrations in marine environments affect the growth and the metabolism of macroorganisms and ultimately may cause their death (Gray and Ying, 2002). Sea water oxygen concentrations thereby influence the distribution, diversity and biomass of marine life (e.g., Childress and Seibel, 1998). Furthermore, oxygen is a key element for most major biogeochemical cycles, because it determines whether microbial processes, occurring in the water column and in the surface sediments, are aerobic or anaerobic. For example, in anoxic environments, microbes can no longer use oxygen as a terminal electron acceptor to oxidize organic matter (e.g., Gruber, 2004; Dalsgaard et al., 2005) and anaerobic processes such as dissimilatory iron oxide reduction and sulfate reduction may become important (Jørgensen, 1982; Lovely and Phillips, 1988). Under fully anoxic conditions, bacteria are also unable to store polyphosphate in their cells (Gächter et al., 1988; Ingall et al., 1993), thus contributing to enhanced release of phosphorus (P) to the water column. Ultimately, this may lead to a positive feedback loop between ocean deoxygenation, enhanced P release and increased primary productivity and organic matter supply (van Cappellen and Ingall, 1996). Thus, changes in marine oxygen concentrations are closely linked to major perturbations in the cycles of carbon, nutrients and changes in global climate (Keeling and Garcia, 2002; Matear and Hirst, 2003).

A wide range of physical and biogeochemical processes controls ocean oxygenation. Most of the present day surface ocean is in near equilibrium with the atmosphere and is well oxygenated as a result of air-sea gas-exchange and oxygen production linked to biological activity, i.e. photosynthesis by phytoplankton. The solubility of oxygen in seawater is, however, also largely determined by temperature and salinity, which vary on both spatial and temporal scales (Sarmiento et al., 1998; Matear et al., 2000; Plattner et al., 2001; Bopp et al., 2002; Keeling and Garcia, 2002). In sub-surface waters, respiration of organic matter consumes oxygen and reoxygenation solely takes place through mixing with oxygen-rich waters (Wilkin et al., 1997). The interaction between ocean circulation and biogeochemistry therefore leads to a complex distribution of dissolved oxygen in the ocean interior. In some regions the amount of dissolved oxygen in the water column is consumed more rapidly than it can be resupplied through mixing, resulting in persistent oxygen-deficit zones, commonly referred to as oxygen minimum zones (OMZs).

In the modern ocean, OMZs often occur along the western continental margins, where wind-driven currents cause coastal upwelling of nutrient-rich waters (Fig. 1), which stimulate phytoplankton growth. In these regions the high marine primary productivity leads to a significant decrease in oxygen concentrations in sub-surface waters as a result

of enhanced respiration of organic matter. A fraction of the produced organic matter is exported to the seafloor, where it may be sequestered for long periods of time (millions of years), through burial in marine sediments. For example, estimates of carbon export to sediments in the northeast Pacific Ocean suggest that the presence of an OMZ greatly increases the amount of organic carbon preserved in marine sediments (Devol and Hartnett, 2001).

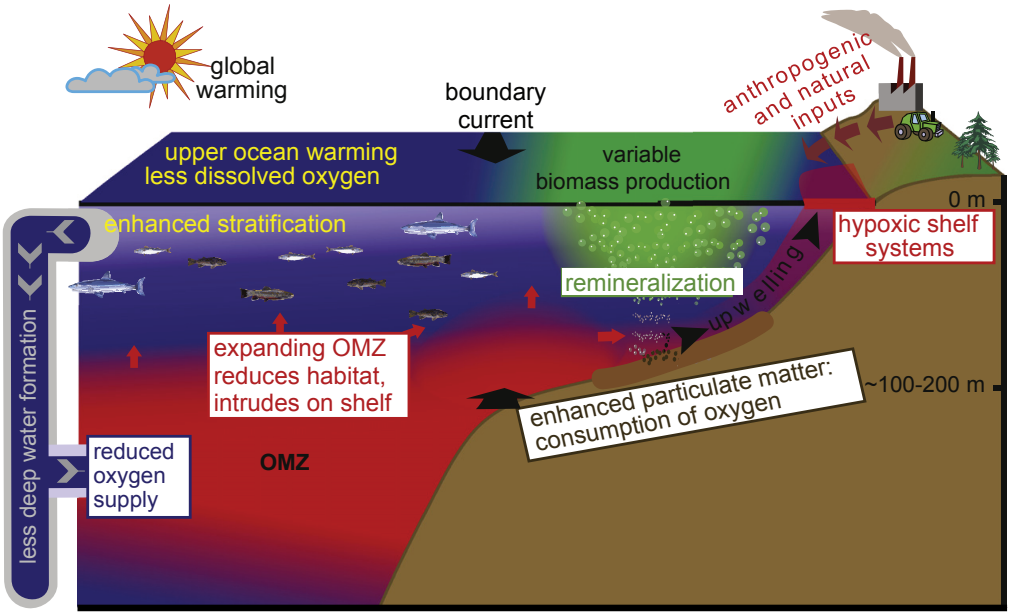

Figure 1. *Schematic illustration of interactions of open ocean oxygen minimum zones (OMZ, red) with hypoxic shelf systems and dead zones (Diaz and Rosenberg, 2008) on continental shelves of eastern ocean boundaries (modified from Stramma et al., 2010).*

Currently, OMZs extending into the open ocean are common in the East Pacific (e.g., Paulmier et al., 2006), Atlantic Ocean (e.g., Stramma et al. 2008), Gulf of Mexico (Rabalais et al., 2002) and in the Arabian Sea (e.g., Naqvi et al, 2006). In addition, enclosed or semi-enclosed basins may also develop low-oxygen conditions, such as the Baltic Sea (Conley et al., 2002), the Black Sea (Jørgensen, 1982), the Cariaco Basin (Scranton et al., 2001) and fjords or inlets (Anderson and Devol, 1973), e.g., the Framvaren Fjord (Jacobs et al., 1985) and Saanich Inlet (Presley et al., 1972).

Today's sub-surface ocean is predominantly well-oxygenated due to a conveyor-belt circulation that transports cold, dense, oxygen-rich waters from high latitudes to the abyssal zone. Human activity is, however, altering the dynamics and biogeochemistry of the (coastal) ocean (e.g., Doney, 2010). While measurements of sea surface temperature indicate a substantial increase, observations and model studies have consistently shown

a decrease in dissolved oxygen in many regions of the world ocean over the past decades (e.g., Matear et al., 2000; Whitney et al., 2007; Stramma et al., 2008).

The expansion of OMZs in the modern ocean has been directly linked to anthropogenic CO_2 emissions that induce global warming (e.g., Bopp et al., 2002; Garcia and Keeling, 2002; Fröhlicher). As a consequence, both gas solubility and ocean ventilation decrease (Stramma et al., 2012). In coastal zones, primary productivity may increase due to enhanced anthropogenic nutrient inputs (Diaz and Rosenberg, 2008) thus creating an increased oxygen demand in bottom waters. Global warming is expected to continue further expanding OMZs, which, ultimately, may even lead to severe, long-term depletion of oxygen in the deep ocean (Oschliess et al., 2008; Shaffer et al., 2009).

An increasing number of studies on dissolved oxygen in sea water is now providing a better understanding of the drivers of modern anoxia and key information on which regions are sensitive to the development of anoxia in the near future. However, our knowledge of marine biogeochemical responses to changes in ocean oxygenation, as well as feedbacks on the biosphere and climate is still relatively limited. Oxygenation of the ocean has varied significantly in strength and extent in the geological past. Anoxic periods are typically accompanied by major perturbations of carbon, nitrogen (N), P and other elemental cycles, which leave behind a biological and geochemical footprint in marine sediments (e.g., Mort et al., 2007; Jenkyns et al., 2010; Gill et al., 2011; Algeo et al., 2014), creating an archive of Earth's environmental conditions.

2. Ocean anoxia in the geological past

During particular intervals in Earth's history, dark, finely grained, often laminated marine lithofacies have been deposited. These are generally rich in organic matter (organic carbon content >1%; Creaney and Passey, 1993) and sulfides (e.g., Arthur et al., 1979) and are usually devoid of fossil traces of benthic life. These types of sediments are commonly referred to as 'black shales'. These sediments were formed in dysoxic or anoxic bottom waters (e.g., Schlanger and Jenkyns, 1976; Summerhayes, 1987; Arthur and Sageman, 1994), which developed through various factors, such as restrictions in ocean circulation, elevated primary productivity and temperature-driven changes in solubility. Specific causes for and consequences of the different anoxic periods through the geological past may differ with space and time, although their occurrence has generally been linked to greenhouse conditions (e.g., Arthur and Sageman 2005; Strauss, 2006; Jenkyns et al., 2010). The geological record documents anoxia on time scales of decades (e.g., Jilbert and Slomp, 2013) to hundreds of thousands of years (Jenkyns, 2010), from single isolated basins to quasi-global scale and ranging from shallow coastal zones to the deepest parts of the open ocean (e.g., Schlanger and Jenkyns, 1976; Jenkyns, 2010).

A good example of basin-scale marine anoxia in the recent geological past is provided by the reoccurring organic-rich sediment horizons, commonly referred to as sapropels (e.g., Rohling, 1994) that have been deposited in the Eastern Mediterranean Sea from the Miocene into the Holocene. Maxima in northern hemisphere insolation during precession

minima caused an intensification of the monsoon system on the North African continent (Fig. 2; e.g., Rossignol-Strick et al., 1985; Hilgen, 1991; Gasse et al., 2000). Subsequently, enhanced river discharge, e.g., Nile discharge, largely impacted the Mediterranean anti-estuarine circulation, resulting in stratification of the water column. Ultimately, slowdown or even total shutdown of deep water formation resulted in enhanced preservation of organic matter at the sea floor and thus the formation of the sapropels (e.g., Rohling, 1994 and references therein). Several other studies suggest that enhanced productivity in the Eastern Mediterranean was the dominant factor in sapropel formation (e.g., Calvert and Pedersen, 1992; Gallego-Torres et al., 2011). A recent study has, however, shown that enhanced productivity alone cannot explain sapropel formation (Reed et al., 2011).

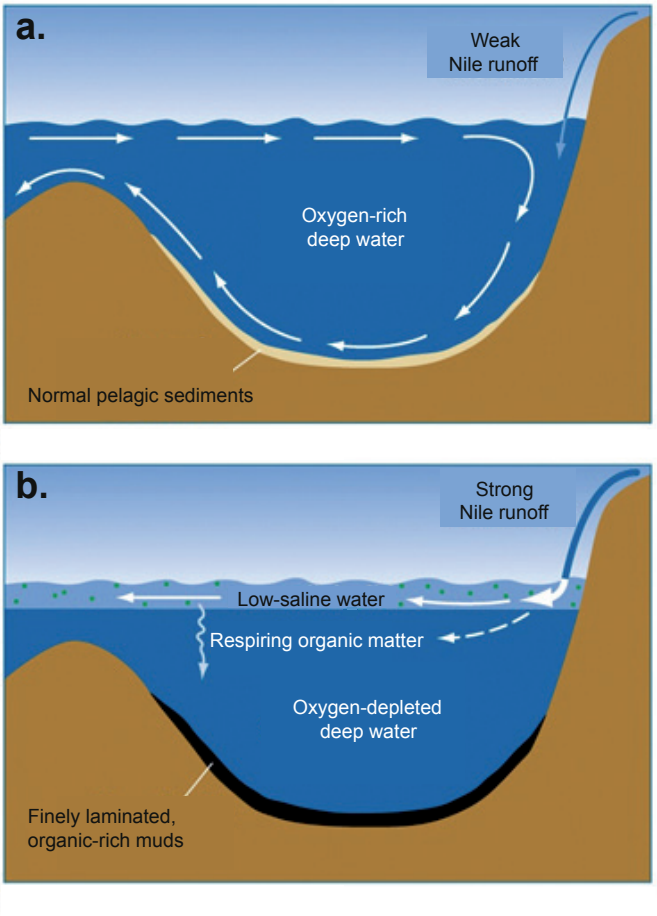

Figure 2. *Schematic illustration of Eastern Mediterranean oceanography and sapropel formation (modified from Ruddiman, 2000). (a) The situation during weak summer monsoons. (b) The situation during strong summer monsoons, i.e., precession minima.*

Regional to global scale ocean anoxia have been identified for some phases within the Precambrian (>541 Ma; Condie et al., 2001) and the Paleozoic (~541-251 Ma; e.g., Berry and Wilde, 1978; Leggett et al., 1981). The Mesozoic era in particular is characterized by multiple periods of widespread ocean anoxia, which have been termed "Oceanic Anoxic Events" (OAEs; Schlanger and Jenkyns, 1976; Fig. 3), with typical durations ranging from a few hundreds of thousands of years, up to a million years. OAEs that are of global significance are the early Toarcian OAE (termed 'Posidonienschiefer event', T-OAE, ~182 Ma; Mazzini et al., 2010), the Lower Aptian OAE (Selli event, OAE1a, ~120 Ma; Malinverno et al., 2010) and Cenomanian-Turonian OAE (termed 'Bonarelli event', OAE2, ~94 Ma).

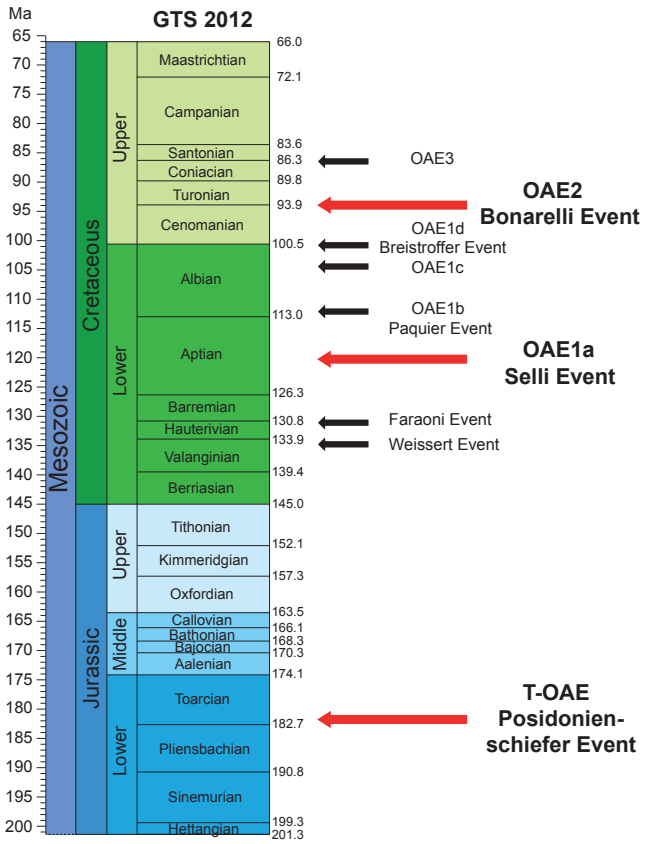

Figure 3. *The geological time scale (Gradstein et al., 2012) with arrows indicating the position of the different OAEs. Red arrows denote the most significant OAEs. Figure inspired by Jenkyns (2010).*

Most OAEs have been linked to extensive volcanism (Leckie et al., 2002) that, in some cases, may have been accompanied by the release of methane hydrates (Hesselbo et al., 2000; Beerling et al., 2002). In such a scenario, atmospheric CO_2 concentrations rose, resulting in global warming superimposed on an already warm background climate. In turn, this led to intensified chemical weathering on the continents, enhancing nutrient discharge to the ocean, leading to elevated organic matter production and large-scale ocean anoxia (Jenkyns, 2010). Additionally, volcanism was suggested to have been important for fertilization of the surface oceans, by supplying reduced metals that may have acted as micro-nutrients (e.g., Sinton and Duncan, 1997; Pálfy and Smith, 2000) and increasing sulfate availability, triggering more efficient remineralization of organic matter, fuelling primary production (Adams et al., 2010).

During most OAEs, the water column became "euxinic", a state in which the water column is anoxic and sulphidic (e.g., Jenkyns, 1988; Monteiro et al., 2012; Westermann et al., 2013). For some OAEs and in certain regions, euxinia even extended into the photic zone (e.g, Sinninghe Damsté and Köster, 1998; Pancost et al., 2004; Tzortzaki et al., 2013). Free hydrogen sulfide in the water column is toxic at low concentrations. Both anoxia and euxinia therefore have been associated with multiple mass extinctions in the marine and terrestrial realm (Meyer and Kump, 2008).

3. Oceanic Anoxic Event 2

One of the best documented and the most extensively studied of all OAEs is OAE2, which occurred close to the Cenomanian-Turonian boundary (93.9 Ma; Meyers et al., 2012a). At that time, the Atlantic mid-oceanic rift had created an oceanic basin of about 4000 by 5500 km on the Northern Hemisphere (i.e., a surface area of ~2.2×10^7 km^2), which ultimately evolved into the present-day North Atlantic Ocean. Hereafter, the basin will be referred to as the proto-North Atlantic for Cenomanian-Turonian times (Fig. 4).

The proto-North Atlantic was a semi-enclosed, restricted basin (e.g., Hetzel et al., 2009; Algeo and Rowe, 2012), with steep continental slopes (Sewall et al., 2007; Topper et al., 2011) and relatively narrow connections to the Tethys and Pacific Oceans in the East and West, respectively. High relative sea-levels during the mid-Cretaceous (Haq et al., 1987; Miller et al., 2005) led to the formation of an epicontinental seaway across the middle of the North American continent, the Western Interior Seaway. While Europe became an archipelago resulting from late Cenomanian transgression (e.g., Hancock and Kauffman, 1979), which created extensive continental shelves (Fig. 4).

The restriction of the proto-North Atlantic Basin may have favored the formation of oxygen-depleted water masses and the consequent deposition of organic-rich marine sediments even before OAE2, particularly in the southern part of the proto-North Atlantic basin (e.g., Kuypers et al., 2004b; van Bentum et al., 2009). The deposition of these organic-rich sediments, however, became globally more significant only during OAE2. The substantial increase of organic matter deposition led to enhanced burial of ^{13}C-depleted carbon, which resulted in a ^{13}C-enriched global exogenic carbon reservoir.

This is registered as a positive excursion in the stable carbon isotopic composition ($\delta^{13}C$) of sedimentary components, including organic matter and carbonates across OAE2 (e.g., Arthur et al., 1988; Tsikos et al., 2004). This positive excursion in $\delta^{13}C$, a major characteristic of OAE2 (Fig. 5), is a global phenomenon and thus can be used to correlate different OAE2 sections (e.g., Voigt et al., 2008). Recent studies show that the total duration of OAE2, from the start of the carbon isotope excursion to the termination of the plateau phase (e.g. Kuypers et al., 2002), must range from ca. 435 to 600 kyr (Sageman et al., 2006; Voigt et al., 2008; Du Vivier et al., 2014).

While extensive igneous activity, predominantly attributed to Caribbean Plateau volcanism (Snow et al., 2005; Kuroda et al., 2007; Turgeon and Creaser, 2008), was likely a major tectonic forcing behind OAE2, the resulting mechanisms leading to the onset of OAE2 and subsequent negative and positive feedbacks are, however, still not fully understood.

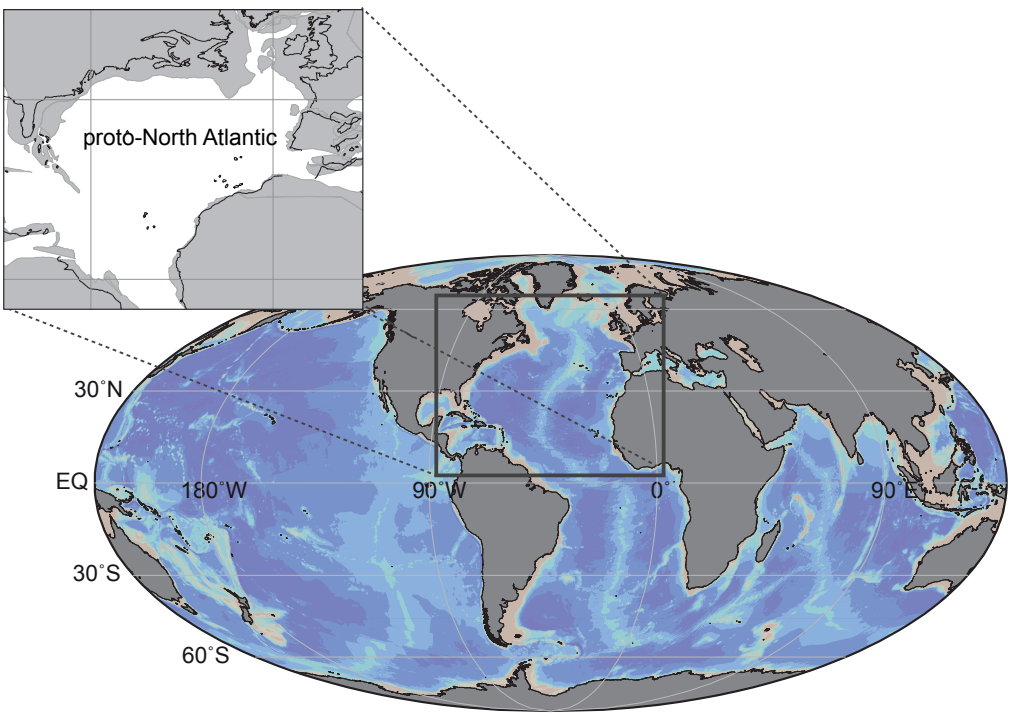

Figure 4. *Present-day map of the Earth in a Mollweide projection. Inset map shows the continental configuration around the Cenomanian-Turonian transition (~94 Ma). In dark gray are the non-submerged land masses, while the light gray areas are flooded continental shelves. The present-day map was generated with Ocean Data View; Schlitzer, R., Ocean Data View, http://odv.awi.de.2014. The paleomap was generated at http://www.odsn.de/odsn/services/paleomap/paleomap.html.*

Although OAE2 does not represent one of the "big five" mass extinctions (e.g., Raup and Sepkoski, 1982), it does rank among the eight major biological marine extinctions since the start of the Mesozoic (Raup and Sepkoski, 1986). OAE2 is associated with, generally stepwise, large biotic turnovers (extinction plus speciation) in many groups of marine biota, e.g. calcareous nannoplankton, radiolaria, molluscs and benthic and planktonic foraminfera (e.g., Elder, 1989; Kaiho, 1994; Leckie et al., 2002; Erba, 2004; Parente et al., 2008). These biotic turnovers have generally been attributed to submarine volcanism, extended OMZs and changes in nutrient levels (e.g., Leckie et al., 2002; Parente et al., 2008).

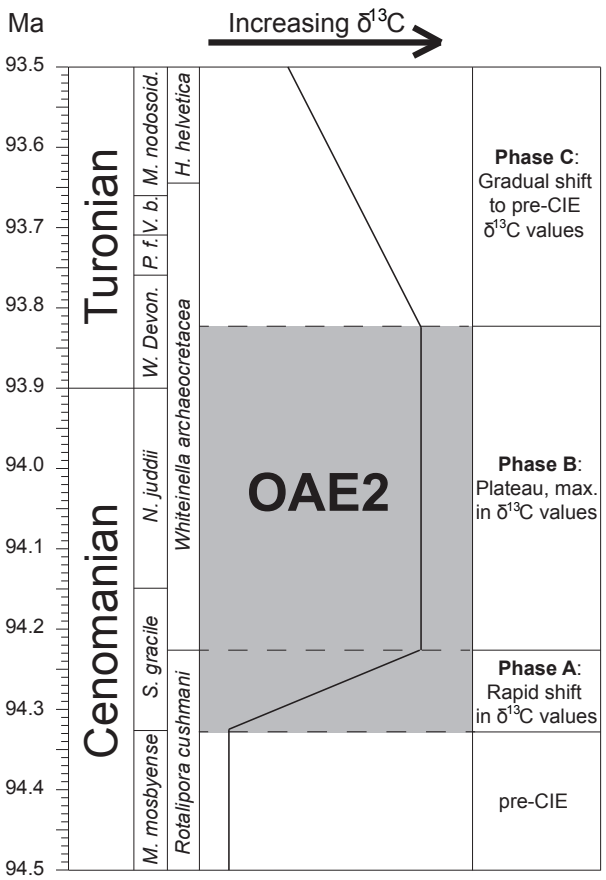

Figure 5. *Schematic representation of the for OAE2 characteristic positive carbon isotope excursion (CIE). Biozonation for the OAE2 interval at Pueblo, Colorado, USA, the Global Boundary Stratotype Section (GSSP) for the Cenomanian-Turonian boundary, after Sageman et al. (2006). Timescale after Meyers et al. (2012a). Figure inspired by Kuypers et al. (2002).*

4. Scope of this thesis

This thesis aims to further identify and quantify the causes of widespread ocean anoxia and its consequences for biogeochemical cycles, the diversity and distribution of biota, and global climate, primarily focusing on OAE2. To this end, existing data has been compiled, and augmented with newly generated paleobiological and geochemical proxy data at a suite of carefully selected sediment sequences covering the OAE2-interval. Moreover, for groundtruthing deep-time reconstructions and to allow for comparison between relatively recent and ancient mechanisms, the most recent Eastern Mediterranean sapropel, sapropel S1 has been analyzed. In particular, marine palynology, involving integrated records of marine (dinoflagellates, acritarchs, chlorophytic algae) and terrestrial (pollen, spores of higher plants) elements, has great potential to provide critical information on a wide range of paleoenvironmental conditions (e.g., Wall et al., 1977, Goodman, 1987, Stover et al., 1996; Sluijs et al., 2005). Additionally, geochemical proxies are employed to obtain information on redox conditions, nutrient availability and sea surface temperature (e.g., Brumsack, 1980; Schouten et al., 2002; Algeo and Ingall, 2007).

Among the main tools applied in this thesis are organic-walled cysts produced by dinoflagellates. Dinoflagellates are, together with diatoms and coccolithophorids, among the most prominent eukaryotic primary producers in the present-day ocean, and therefore play an important role in the global carbon cycle (Brasier, 1985). Less than 20% of the dinoflagellate species in the modern ocean produce highly resistant organic-walled dinoflagellate cysts (dinocysts), for the dormant stage of their life cycle (Fensome et al., 1996). The highly resistant organic dinocysts are often preserved in aquatic sediments that are not fully oxidized (e.g., Wall and Dale, 1966; Head, 1996), and are ecologically tied to marginal marine settings (e.g., Dale, 1996; Montresor et al., 1998). The diversity in (paleo)ecological preferences of the dinoflagellates that produce these resistant cysts is large in the modern (Zonneveld et al., 2013) and paleodomain (e.g., Pross and Brinkhuis, 2005). Therefore, dinocyst assemblages in ancient marine sediments provide key insights into surface water parameters such as runoff, stratification, sea level and water mass histories (e.g., Wall et al., 1977; Goodman, 1987; Harris and Tocher, 2003; Sluijs et al., 2005; Pross and Brinkhuis, 2005; Prince et al., 2008; Pearce et al., 2009; Zonneveld et al., 2013). Moreover, combining these with the coeval signals from land, i.e., pollen and spores of higher plants, integrated land-sea paleoenvironmental reconstructions may be established (e.g., Turon et al., 2003; Donders et al., 2009; Sluijs et al., 2009). Despite their potential in paleoenvironmental analysis, dinocysts have only rarely been employed in paleoenvironmental studies on OAE2 (Harris and Tocher, 2003; Pearce et al., 2009).

In addition, a wide range of geochemical proxies can be employed to reconstruct the paleoenvironmental conditions prior to, during, and immediately following OAE2. Studies on sedimentary P cycling show enhanced regeneration of P under low-oxygen conditions (Ingall et al., 1993; Ingall and Jahnke, 1994). Since P is a limiting nutrient in large parts of the ocean (e.g., Krom et al., 1991; Tyrrell, 1999), the regenerated P can fuel production of organic matter when upwelled into the photic zone (van Cappellen and Ingall, 1996).

Based on this the ratio of organic carbon versus the P of marine sediments (C_{org}/P_{tot}) is not only an accurate proxy for (ancient) redox conditions (Algeo and Ingall, 2007), but also provides insight in the degree of P recycling (Mort et al., 2007; Kraal et al., 2010), and thus nutrient availability. Furthermore, the concentrations of a wide range of trace metals (e.g., molybdenum (Mo) and vanadium (V))can be used to reconstruct (paleo)redox conditions in bottom waters, because they are actively scavenged from oxygen depleted marine environments, and therefore enriched in the sediment (Brumsack, 1980; Emerson and Huested, 1991; Scott and Lyons, 2012).

For temperature reconstructions, the distributions of membrane lipids derived from marine Thaumarcheota and soil bacteria, named glycerol dialkyl glycerol tetraethers (GDGTs) have been shown to reflect annual mean sea surface temperature (SST) and continental mean air temperature (MAT) and, respectively (Schouten et al., 2002; Weijers et al., 2007). Ratios of the various isomers, notably the MBT/CBT and the TEX_{86} proxies, are calibrated to temperature based on modern sediments (Schouten et al., 2002; Weijers et al., 2007; Kim et al., 2010; Peterse et al., 2012), which can be used to reconstruct past SSTs (e.g., Sluijs et al., 2006; Castañeda et al., 2010).

The implementation of the results from this thesis in ocean biogeochemical models, within the framework of a parallel PhD-project (Ruvalcaba Baroni, in press), further improves our understanding of how widespread ocean anoxia developed during OAE2. Ultimately, such integrated knowledge is required to improve projections for future ocean deoxygenation.

5. Synopsis

The relative contributions of the supply of terrestrial and marine organic matter and the preservation of this organic matter to the deposition of ancient organic-rich marine sediments, remains elusive. Even for the relatively recent and well-studied Eastern Mediterranean sapropels this debate continues. In **Chapter 2** this issue is addressed by studying sediments deposited prior to, during, and after sapropel (S1, ~10-6 calibrated kyr before present) using an integrated marine and terrestrial palynological approach, combined with bulk geochemical analyses. The studied piston core PS009PC was retrieved from offshore Israel, an area under strong influence of the Nile outflow. This resulted in high average sediment accumulation rates allowing an unusually high temporal resolution of several decades to centuries. Marine productivity, indicated by the accumulation rates (ARs) of total dinocysts and biogenic $CaCO_3$, starts to increase ~1 kyr before sapropel formation. The nutrients forcing the productivity increase likely were derived from increased Nile River discharge, as inferred from a coinciding decrease in $\delta^{18}O_{ruber}$ (Hennekam et al., 2014). A shift in the ARs of various dinocyst taxa at the onset of the sapropel is indicative of rapid (within a century) development of (seasonal) water column stratification. Pollen and spore ARs also increase prior to the onset of the sapropel, but a few centuries after the increase in marine productivity. Hence, the first shift to a highly productive marine system may have been sustained by injection of nutrients via shoaling

of the nutricline (e.g., Crudeli et al., 2006). Pollen assemblages show a gradual change across the onset of the sapropel from a savanna-like, through coastal marsh expansion, towards an open woodland assemblage, consistent with greater Nile influence and delta development. Three centuries following the onset of the sapropel, dinocyst and biogenic $CaCO_3$ ARs start to decrease, while sapropel deposition continues and concentrations of the redox sensitive elements Mo, V and C_{org}/P_{tot} ratios remain elevated, supporting persistent anoxia. We therefore conclude that high marine productivity and stratification-induced preservation in tandem triggered sapropel formation, and elevated marine productivity particularly contributed to sapropel formation during its early stages.

The occurrence of OAE2 has frequently been linked to exceptional warmth and high CO_2 concentrations (e.g., Schouten et al., 2003; Forster et al., 2007b; Barclay et al., 2010; Sinninghe Damsté et al., 2010). Consequences of this warmth for the intensity of the hydrological cycle remain poorly understood, hampering our understanding of its impact on biogeochemical cycles. **Chapter 3** reports on a newly generated, integrated geochemical and palynological dataset to reconstruct regional climate evolution, with a focus on SST and the hydrological cycle. The studied samples derive from diagenetically immature New Jersey shallow shelf sediments from the Bass River borehole, Ocean Drilling Program (ODP) Leg 174AX, which contains a stratigraphically expanded OAE2 succession. Towards OAE2, TEX_{86}^{H}-based SSTs rapidly increased from 34 to 36.5°C, and both palynological and inorganic geochemical records suggest enhanced runoff. Right after the onset of OAE2 climate temporarily became drier and SSTs dropped by ~3°C, representing the so-called Plenus Cold Event. This cooling was recognized previously and attributed to declining CO_2 concentrations resulting from globally enhanced organic carbon burial (Sinninghe Damsté et al., 2010). For the remainder of OAE2 SSTs were high, and humid conditions prevailed. After OAE2, SSTs gradually returned to pre-OAE2 values and climate became drier again. Based on the results we conclude that an acceleration of the hydrological cycle during OAE2 played a key role in supplying nutrients to coastal waters and enhancing stratification, thus contributing to the development of ocean anoxia.

Disentangling the effects of global warming, changes in the hydrological cycle and enhanced marine primary productivity on decreasing oxygen concentrations during OAE2 on a regional scale remains problematic. **Chapter 4** details the effects of these forcing factors on cyclically deposited black shales on epicontinental shelf sediments spanning OAE2, recovered in the Wunstorf core, Lower Saxony Basin (North Gemany). To this end several types of palynological and organic geochemical records are combined. Despite widely varying depositional conditions, complicating the interpretation of the obtained records, GDGT distributions indicate that SST evolution during OAE2 resembled that of previously studied sites throughout the proto-North Atlantic. Climatic cooling, again linked to the Plenus Cold Event, interrupted black shale deposition during the early stages of OAE2. For the remainder of the record, SSTs do not vary significantly across alternations between marls and black shales, suggesting that SST did not have a direct effect on the formation of the black shale horizons. Relative (i.e., with respect to marine palynomorphs), and absolute abundances of pollen and spores are appreciably

elevated during phases of black shale deposition, indicative of enhanced precipitation and run-off. The latter likely introduced additional nutrients to the epicontinental shelf, in turn resulting in elevated marine primary productivity, as shown by relatively high concentrations of cysts derived from inferred heterotrophic and euryhaline dinoflagellates. We therefore conclude that enhanced precipitation and run-off, in tandem with elevated marine primary productivity, were critical in black shale formation on the northwest European epicontinental shelf.

Species on land and in the ocean, including dinoflagellate taxa, may migrate geographically in response to (paleo)environmental perturbations (e.g., van Simaeys et al., 2005; Sluijs et al., 2007a). Pronounced global cooling during the early stages of OAE2, associated with the Plenus Cold Event, may have triggered such dinoflagellate migration events. This is predominantly suggested by the occurrence of the dinocyst morphological complex *Cyclonephelium compactum–membraniphorum* (*Ccm*) within the TEX_{86}^{H}-based SST-cooling in the Bass River record. In **Chapter 5** the global chronostratigraphic occurrence of *Ccm* is compiled, in order to confirm whether and when this species migrated and to assess its potential as a biostratigraphic marker. Our results indicate that *Ccm* was ubiquitously present at relatively high latitudes on both the Northern and Southern Hemisphere, prior to, during, and after OAE2. This while in the mid-latitudes cysts of *Ccm* were only sporadically present prior to OAE2. The consistent appearance of *Ccm* in the mid-latitudes of the Northern Hemisphere occurred during the first maximum in the positive carbon isotope excursion (CIE) associated with OAE2. This suggests that the migration of *Ccm* was geologically instantaneous, and based on the records of Bass River and Wunstorf, was linked to cooling during the Plenus Cold Event. This implies that the episode represented by the (re)-occurrence of *Ccm* in combination with the CIE, provides a good stratigraphic marker. Sustained presence of *Ccm*, at all sites except Bass River, suggests that not only temperature, but also other environmental and paleoceanographical conditions were important for the distribution of *Ccm* once it had occupied niches at lower latitudes.

The characteristics and spatial distribution of the OAE2 deposits that formed in the deep part of the proto-North Atlantic Basin remain relatively poorly described. In **Chapter 6** newly generated and compiled redox proxy data (e.g., concentrations of Mo and Mn, Fe/Al, C_{org}/P_{tot}) for five Deep Sea Drilling Project (DSDP) and ODP sites, DSDP 367, DSDP 386, DSDP 603, ODP 641 and ODP 1276 are presented. The studied sites are distributed over the deep proto-North Atlantic and were selected to reconstruct the spatial extent and degree of oxygen depletion throughout the deep proto-North Atlantic Basin during OAE2. Our results highlight that bottom waters in the entire deep proto-North Atlantic were anoxic during most of OAE2. Quantitative relations between Mo and TOC content, previously shown to document the degree of water mass restriction (Algeo and Lyons, 2006), confirm that the water circulation in the proto-North Atlantic Basin was severely restricted during OAE2, i.e., comparable with the present-day Black Sea. Finally, the Plenus Cold Event, appears to have led to temporary re-oxygenation of bottom waters in

the deep proto-North Atlantic Basin, suggesting that temperature was a crucial factor in determining deep ocean oxygen concentrations during OAE2.

The formation of widespread ocean anoxia during OAE2 has been intimately linked to enhanced marine primary productivity, partially attributed to changes in the nitrogen cycle. For several sites in the proto-North Atlantic, the OAE2-interval is characterized by exceptionally low $\delta^{15}N$ values, linked to increasing N_2-fixation (Kuypers et al., 2004b; Junium and Arthur, 2007). Published $\delta^{15}N$ values for OAE2 vary over an extremely wide range, even for similar locations (e.g., Jenkyns et al., 2007). In **Chapter 7**, existing $\delta^{15}N$ data for bulk sediments are compiled and new stable isotopic N data of bulk sediments are generated for multiple OAE2 sections in the open and coastal proto-North Atlantic. Based on these data, we show that the reported wide variation in $\delta^{15}N$ values is most likely related to the treatment of sediment samples with acid prior to analysis of the stable isotopic composition of N. Compilation of all available $\delta^{15}N$ data for the proto-North Atlantic, measured on non-acidified samples, demonstrates that the most pronounced negative shift in $\delta^{15}N$ from pre-OAE2 to OAE2 occurs in the open ocean, with $\delta^{15}N$ dropping below -3‰ for one sample. By employing a box model of N cycling for the proto-North Atlantic during OAE2, we show that N_2-fixation is the major contributor to the $\delta^{15}N$ signal, particularly in the open ocean. We also demonstrate that lateral transport and upwelling of NH_4^+ and its incomplete uptake during phytoplankton growth additionally lowers the $\delta^{15}N$ signal.

6. Concluding remarks

Widespread ocean anoxia during sapropel S1 and OAE2 times resulted from a complex interplay of various factors (Chapters 2, 3 and 4). Climate-driven changes in temperature and hydrology have been of particular importance for the occurrence of ocean anoxia during OAE2 and sapropel S1 (Chapters 2, 3 and 4). This is illustrated by the strong influence of freshwater discharge from the Nile on the formation of Eastern Mediterranean sapropel S1, which not only led to freshwater stratification induced preservation of organic matter, but also contributed to enhanced production of organic matter by delivering nutrients for marine primary productivity (Chapter 2). This mechanism was shown to be responsible for organic matter deposition during OAE2 on the flooded continental shelves as well (Chapters 3 and 4). As a consequence of the extreme warmth, likely resulting from higher levels of atmospheric CO_2 due to extensive volcanism, the hydrological cycle intensified (Chapter 3). Enhanced precipitation and runoff, as also recorded for sapropel S1 (Chapter 2), ultimately led to freshwater stratification and enhanced marine primary productivity, culminating in widespread ocean anoxia and organic carbon sequestration (Chapters 3 and 4). The regeneration of P from sedimentary organic matter in anoxic sediments acted as a positive feedback. Interestingly, pronounced cooling and drier conditions, linked to the Plenus Cold Event during the early stages of OAE2, correspond to a minimum in sedimentary organic carbon content, which can even be tracked throughout the deep proto-North Atlantic Basin, suggesting large-scale oxygenation

of the water column during this period (Chapters 3, 4 and 6). This again implies that temperature and hydrology were crucial factors in determining bottom water oxygen concentrations. The mentioned cooling episode not only diminished organic carbon sequestration, but was also shown to drive equatorward migration of dinoflagellate taxa, showing that relatively small changes in temperature during the mid-Cretaceous super-greenhouse world had significant implications for biogeographical patterns (Chapter 5). Although redox conditions varied through time and space during OAE2, the results of this study do show that most of the proto-North Atlantic was oxygen depleted during OAE2, and that the deep part was completely anoxic for most of the event (Chapter 6).

The main results and conclusions of this thesis indicate that past climatic perturbations forced a chain of events, including fresh water induced stratification and enhanced nutrient cycling, which ultimately culminated in (widespread) ocean anoxia. IPCC Working Group I, predicts, along with global warming, enhanced precipitation for mid- and high-latitude regions (IPCC, 2013). Additionally, precipitation and river discharge are shown to have become much more extreme in many regions (IPCC, 2014). The most recent IPCC output extensively reports on decreasing oxygen solubility, decreasing oceanic oxygen concentrations and expanding OMZs, already now (IPCC, 2014). These observations and projections, in combination with the main conclusions from this thesis, suggest that OMZs in the future ocean will continue to expand, and, at this moment well-oxygenated parts of the ocean, particularly coastal zones, will become prone to (seasonal) anoxia. Most notably, the work in this thesis contributes to the various positive and negative feedbacks that respectively enforce and counteract ocean deoxygenation on various time scales. Such insights will be crucial to improve projections for future trends.

2

Marine productivity leads organic matter preservation in sapropel S1: palynological evidence from a core along the path of the Nile River outflow

"To know, is to know that you know nothing. That is the meaning of true knowledge."

Socrates

Abstract

The Eastern Mediterranean sedimentary record is characterized by the widespread and distinctly periodical occurrence of organic carbon-rich layers, called sapropels. Increased productivity due to enhanced nutrient input in the photic zone and improved preservation of organic matter due to the development of dysoxic/anoxic conditions in deeper waters have been indicated as the two major factors contributing to sapropel formation. The relative contribution of productivity and preservation and their leads and lags with respect to each other remain elusive, however. Here, we address these questions by studying sediments deposited prior to, during, and after the most recent sapropel (S1, ~10-6 calibrated kyr before present) with an integrated marine and terrestrial palynological and geochemical approach. The studied core has been retrieved from an area under strong influence of the Nile outflow and has high average sediment accumulation rates allowing an unusually high temporal resolution of several decades to centuries.

Marine productivity, as deduced from the total dinocyst and biogenic $CaCO_3$ accumulation rates (ARs), starts to increase ~1 kyr prior to sapropel formation. A shift in the dinocyst taxa contributing to the productivity signal at the sapropel onset indicates the rapid development of (seasonal) water-column stratification. Pollen and spore ARs also increase prior to sapropel onset, but a few centuries after the increase in marine productivity. Hence, the first shift to a high marine productivity system may have been provided by injection of nutrients via shoaling of the nutricline. In addition, nutrients may have been partly provided from land via river input and flooding of the shelves. Pollen assemblages indicate a gradual change across the onset, from a savanna-like, through coastal marsh expansion, toward an open woodland assemblage. This is consistent with greater Nile influence and delta development. Sapropel onset is characterized by a marked shift in pollen ARs. Major shifts in pollen assemblages and signs of selective or partial decomposition of terrestrial palynomorphs are absent, however. We therefore suggest that high pollen ARs result from greater river runoff and extension of the freshwater plume of the Nile. Three centuries after the sapropel onset, marine productivity starts to decrease, while sapropel deposition continued.

High marine productivity and stratification-induced preservation in tandem triggered sapropel formation. High marine productivity appreciably contributed to sapropel formation at its early stages. Elevated concentrations of V, Mo and the organic carbon over phosphorus ratios (C_{org}/P_{tot}) suggest that preservation of organic matter was the dominant mechanism for the remainder of sapropel formation.

1. Introduction

At present, the Mediterranean Basin is generally oligotrophic and well-ventilated (Krom et al., 1991; Pinardi and Masetti 2000; D'Ortenzio and Ribera D'Alcala, 2009), and its surface sediments are typically poor in organic carbon (e.g., Calvert, 1983). However, the Eastern Mediterranean late Neogene sedimentary record is characterized by the widespread and distinctly periodical occurrence of organic carbon-rich layers, called sapropels (e.g., Kullenberg, 1952; Rohling, 1994; Robertson et al., 1998).

The currently accepted model for the formation of most sapropels proposes that maxima in insolation during precession minima caused an intensification of the monsoon system on the North African continent (e.g., Rossignol-Strick et al., 1985; Hilgen, 1991; Gasse et al., 2000; Weldeab et al., 2014). Subsequently, enhanced river discharge significantly impacted the Mediterranean water circulation, resulting in stratification of the water column. Ultimately, slowdown or total shutdown of deep-water formation resulted in enhanced preservation of organic matter at the sea floor (e.g., Rohling, 1994, and references therein). The primary cause triggering the formation of sapropels has been debated ever since their discovery (Kullenberg, 1952; Aksu et al., 1999), and productivity and preservation have been indicated as the two major contributing factors operating either separately (Williams et al., 1978; Calvert, 1990) or combined (De Lange and Ten Haven, 1983; Rohling and Gieskes, 1989; Kemp et al., 1999).

Present-day biological primary productivity is thought to be insufficient to account alone for the elevated organic carbon content observed in sapropels (Dugdale and Wilkerson, 1988; Bethoux, 1989). Elevated past primary productivity is likely to have been contributing to sapropel formation and several studies support this hypothesis (e.g., De Lange and Ten Haven, 1983; Calvert and Pedersen, 1992; Rohling, 1994; Gallego-Torres et al., 2011). Marine productivity can be boosted by freshwater input (1) directly, via nutrient input by enhanced river discharge from the Nile (e.g., Krom et al., 2002); (2) indirectly, via upward advection of the nutricline following stratification. The latter mechanism, which creates a productive Deep Chlorophyll Maximum (DCM) in the photic zone underneath a nutrient-poor surface layer, has been used to explain high productivity rates preceding and at the onset of sapropel S5 (previous interglacial, ~125 calibrated kyr before present; BP, before 1950 AD; e.g., Giunta et al., 2006; Grelaud et al., 2012) and during the most recent sapropel S1 (Gieskes and Rohling, 1989; Castradori, 1993; Crudeli et al., 2006).

For sapropel S1, deposited during the Holocene between ~10 and 6 cal. kyr BP, debate continues on the importance of marine productivity relative to organic matter preservation. Moreover, the leads and lags between productivity and preservation remain elusive. At present nannoplankton contributes ~40% to the primary productivity of the Mediterranean Sea, and diatoms and dinoflagellates account for another ~40% (Uitz et al., 2010). Despite their large contribution to the organic carbon flux (Kemp et al., 1999) sapropel S1 is usually devoid of diatoms. Calcareous nannoplankton and coccolithophores can be abundant in sapropel S1 but may suffer from selective preservation and carbonate diagenesis (e.g., Negri et al., 1999; Negri and Giunta, 2001; Crudeli et al., 2004; Thomson

et al., 2004; Crudeli et al., 2006). Remains of dinoflagellates (organic-walled dinoflagellate cysts, dinocysts) are generally abundant and well preserved in the sediments, together with pollen and spores from land plants (Cheddadi and Rossignol-Strick, 1995; Rossignol-Strick, 1999; Zonneveld et al., 2001; Sangiorgi et al., 2003; Kholeif and Mudie, 2009). So far, no palynological (dinocysts, pollen and spores) study has provided a temporal resolution sufficient to resolve pre-sapropel and sapropel productivity trends and cause-effect relationships, however.

Here we present an integrated marine and terrestrial palynological study on a piston core taken along the path of freshwater routing from the Nile (Fig. 1). The core contains a ~42 cm-thick sapropel S1, which allows analyses at unprecedented high resolution (multi-decadal to centennial scale). Our data, together with a suite of newly generated and available geochemical proxies (Hennekam et al., 2014), provide insights into regional climate, the source of nutrients, the contribution of marine productivity to sapropel S1 deposition, and the importance of preservation.

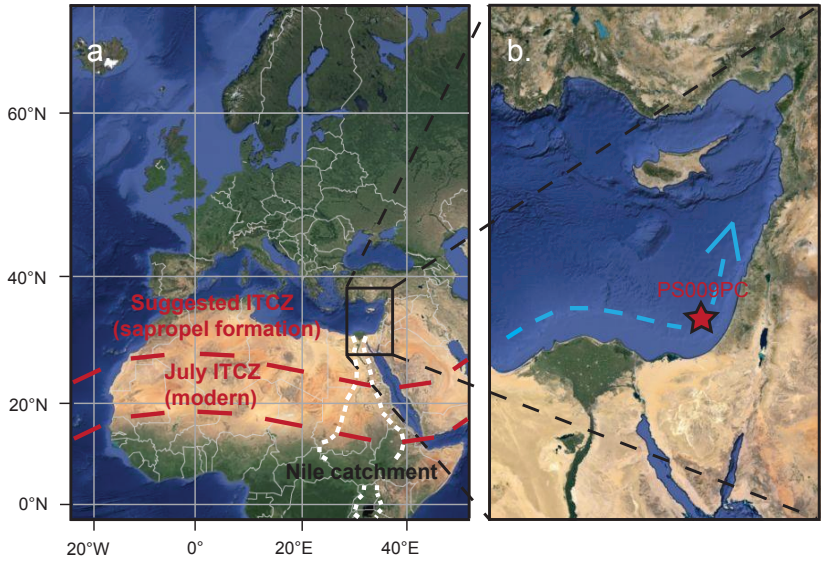

Figure 1. *(a) Satellite image of the Mediterranean region. Dashed lines indicate the Nile catchment and the assumed position of the Intertropical Convergence Zone (ITCZ) during onset of sapropel deposition and at present (Gasse, 2000). (b) Location of the studied core, PS009PC (32°07.7'N, 34°24.4'E; 552 m water depth). The blue arrow indicates the prevailing surface current in the Levantine Basin.*

2. Materials and Methods

2.1. Core location, sediments and age model

The sediment samples used in this study were taken from piston core PS009PC, recovered from the continental slope ~50 km off the coast of Tel Aviv, Israel (Fig. 1a, b; 32°07.7'N,

34°24.4'E; 552 m water depth), in the southeastern part of the Levantine Basin. Core PS009PC was recovered during the PASSAP cruise in May 2000 with RV *Pelagia*; its total length is 690 cm. The recovered sediments consist of >90% of clays and silts (Hennekam and De Lange, 2012). Surface waters in the Levantine Basin move in an anticlockwise direction (e.g., Pinardi and Masetti, 2000), implying that Nile-derived sediments, the main sediment source for the eastern Mediterranean, are transported eastward from the Nile outflow to our coring site (Weldeab et al., 2002; Fig. 1b). The sedimentary record of PS009PC may thus be expected to directly reflect changes in the outflow of the Nile and its hinterland, which makes it exceptionally well suited for the objectives of our study.

Our study focuses on the interval between 265 and 174 cm, which spans 12 to 5 cal. kyr BP, according to the age model of Hennekam et al. (2014). The sedimentation rate for this interval is high, ~12.5 cm/kyr (i.e., 1 cm = ~80 years), and relatively constant between 285.2 and 191.2 cm (13460 ± 204 and 6118 ± 169 cal. kyr BP, respectively; Hennekam et al. 2014). Sediment accumulation rates are in agreement with those found in the Nile Cone area (Stanley and Maldonado, 1977; Kholeif and Mudie, 2009), and other nearby sites (e.g., Hamann et al., 2008; Castañeda et al., 2010). Between 240 and 198 cm the two phases of sapropel S1 deposition (S1a and S1b) and its interruption are recorded. The identification of the sapropel layer, its age model and the S1a and S1b phases follow Hennekam et al. (2014). The onset of unit S1a for PS009PC is at 10.0 cal. kyr BP and its termination is at 8.2 cal. kyr BP. The onset of S1b is at 7.9 cal. kyr BP followed by its termination at 6.6 cal. kyr BP. The sapropel interruption lasts ~300 years, as in other Mediterranean S1 records (Bar-Matthews et al., 1999; Pross et al., 2009, Marino et al., 2009), and correlates well with the 8.2 kyr BP cooling event in the Northern Hemisphere (Alley et al., 1997; Rohling and Pälike, 2005).

2.2. Palynological processing

Fifty-nine sediment samples were selected with particular high sampling resolution (every 0.5 cm; 40 years) around sapropel onset. Sediment samples were freeze-dried, and crushed and homogenised using an agate pestle and mortar. Subsequently, between 0.6 and 2.5 g of sediment per sample was treated with ~10% HCl and ~38% HF to dissolve carbonates and silicates, respectively. A known amount of *Lycopodium clavatum* marker spores was added to enable quantification of the palynomorphs and their accumulation rates (ARs) to the sediment. After decantation of the solution ultrasonic separation was employed. Samples were then sieved over a 10-µm sieve, after which the remaining residues were concentrated and mounted on slides for microscope analysis. On average ~170 dinocysts per sample were counted and identified to genus or species level at 400x magnification. Dinocyst taxonomy follows Rochon et al. (1999) and Fensome and Williams (2004). Total pollen and spores were also counted in all dinocyst samples.

After dinocyst analysis 19 samples were selected for detailed pollen and spore analysis. To optimize identification of pollen and spores palynological residues were acetolysed, following Erdtman (1960). After acetolysis, samples 202.45 cm and 203.45 cm were combined (composite sample 202.95 cm; 7 cal. kyr BP), because of the small sample size,

to ensure statistically relevant counts. On average ~440 pollen and spores per sample were counted and identified. All samples and slides are stored in the collection of the Laboratory of Palaeobotany and Palynology, Utrecht University, the Netherlands.

Dinocyst and pollen and spores ARs (palynomorphs/cm^2/yr) were calculated multiplying the amount of dinocysts and pollen and spores per gram sediment dry weight (palynomorphs/g sed. dw.), by the mass accumulation rates (g/cm^2/yr) derived from Hennekam et al. (2014).

2.3. *Geochemical analysis*

Calcium (Ca), Phosphorus (P) and Molybdenum (Mo) concentrations were measured by X-ray fluorescence (XRF) at the Institute of Chemistry and Biology of the Marine Environment (ICBM) in Oldenburg, using a Philips PW 2400 X-ray spectrometer on glass beads. $CaCO_3$ content was calculated assuming that all Ca was related to $CaCO_3$, subsequently ARs were calculated multiplying the $CaCO_3$ content by the mass accumulation rates (g/cm^2/kyr) derived from Hennekam et al. (2014). Organic carbon over P ratios (C_{org}/P_{tot}) were calculated using the C_{org} dataset derived from Hennekam et al. (2014).

All measurements and analysis were performed on the same samples to optimize comparability of the signals and to avoid correlation issues (e.g., age model differences). This includes the geochemical data derived from Hennekam et al., (2014), i.e., C_{org}, vanadium (V) and stable oxygen isotopic composition of the surface dwelling planktonic foraminifer *Globigerinoides ruber* (white; $\delta^{18}O_{ruber}$)

2.4. *Approach and proxy interpretation*

Marine palynology mainly studies organic-walled dinoflagellate cysts, fossilizable resting stages produced by some dinoflagellates mostly during the sexual reproduction stage in the life cycle (Wall and Dale, 1966). Notably, most dinoflagellates are either photosynthetic, i.e. they need light and nutrients, or heterotrophic and feed on organic material and other phytoplankton (e.g., Jacobson and Anderson, 1986). Dinocysts are sensitive recorders of environmental conditions of the surface waters (e.g., Zonneveld et al., 2013). Therefore their fossil assemblages, concentrations and accumulation rates in marine sediments can be successfully employed to reconstruct palaeoenvironmental surface water conditions, providing information on nutrient availability, productivity, temperature, salinity, stratification, and oxygenation (e.g., Dale, 1996; Pross and Brinkhuis, 2005; Zonneveld et al., 2008; Zonneveld et al., 2012).

The marine sediments also yield pollen and spores, produced by terrestrial vegetation, which are transported into the marine environment mainly via river discharge and wind (e.g., Farley, 1987). Transport mode influences the type and richness of the assemblage (Hooghiemstra, 1988; Traverse, 1990), which allows determination of the relative changes in river input. Pollen transport through air and water is selective, and typically, larger, heavier types are transported less far (Holmes, 1990), affecting total diversity in the assemblage. Exception to the rule is bisaccate conifer pollen that are predominantly wind-

transported and floats on water so that their relative abundance instead increases with distance to the shore (Mudie, 1982)

Combined marine and terrestrial palynology thus provide an integrated signal of synchronous changes occurring in the marine and continental environments. Our palynological data were integrated with available geochemical data (Hennekam et al., 2014). Furthermore new geochemical data was generated, i.e., $CaCO_3$ accumulation rates (ARs), C_{org}/P_{tot} and molybdenum (Mo), providing additional information on productivity and redox conditions. All together this set of samples is optimally suited to reconstruct the palaeoenvironmental conditions during sapropel formation in high-resolution.

3. Results

3.1. Dinocysts

Core PS009PC contains abundant and well-preserved dinocysts. Assemblages are overall dominated by cysts produced by autotrophic/phototrophic dinoflagellates (Fig. 2b), mostly gonyaulacoids. Heterotrophic dinocysts, i.e., protoperidinioids (Fig. 2b) form less than 10% of the total assemblage prior to and after sapropel deposition and during its interruption. Within the sapropel protoperidinioids are relatively more abundant and represent up to 35% of the assemblage.

The total dinocyst AR (Fig. 2c, black) rapidly increases to ~75 cysts cm^{-2} yr^{-1}, between 10.8 and 10.3 cal. kyr BP. A sudden decrease to 40 cysts cm^{-2} yr^{-1} is observed from 10.3 cal. kyr BP to just before S1 onset. *Spiniferites* spp. is chiefly responsible for this pattern in the total dinocyst AR, with minor contributions of *Pentapharsodinium dalei*, *Lingulodinium machaerophorum* and protoperidinioids (*Brigantedinium* spp., *Echinidinium* spp. and *Stelladinium stellatum,* Fig. 2c, blue)

At the onset of S1 the total dinocyst AR increases again and reaches the maximum value for the entire record of 80 cysts cm^{-2} yr^{-1} at 10.0 cal. kyr BP and remains high until 9.7 cal. kyr BP. The maximum in the total dinocyst AR at the onset of S1a is mainly the result of a major increase in the AR of *L. machaerophorum*, but the ARs of *Spiniferites* spp., *P. dalei* and protoperidinioids are also high. Afterwards, the total AR rapidly drops to approximately 40 cysts cm^{-2} yr^{-1} and gradually decreases throughout the sapropel to around ~20 cysts cm^{-2} yr^{-1} at sapropel termination.

After sapropel termination the total dinocyst AR remains generally below sapropel values. Only the AR of *Operculodinium israelianum* shows a peak at 5.5 cal. kyr BP.

We also calculated the AR of oxygen-resistant dinocysts, i.e. *Nematosphaeropsis labyrinthus*, *P. dalei*, *Impagidinium* spp., *Operculodinium* spp. (according to Zonneveld et al., 1997, 2001; Versteegh and Zonneveld, 2002; Fig. 2c, red). It remains relatively constant over the studied interval, generally fluctuating between 5 and 10 cysts cm^{-2} yr^{-1}. The maxima are reached around the onset of S1a.

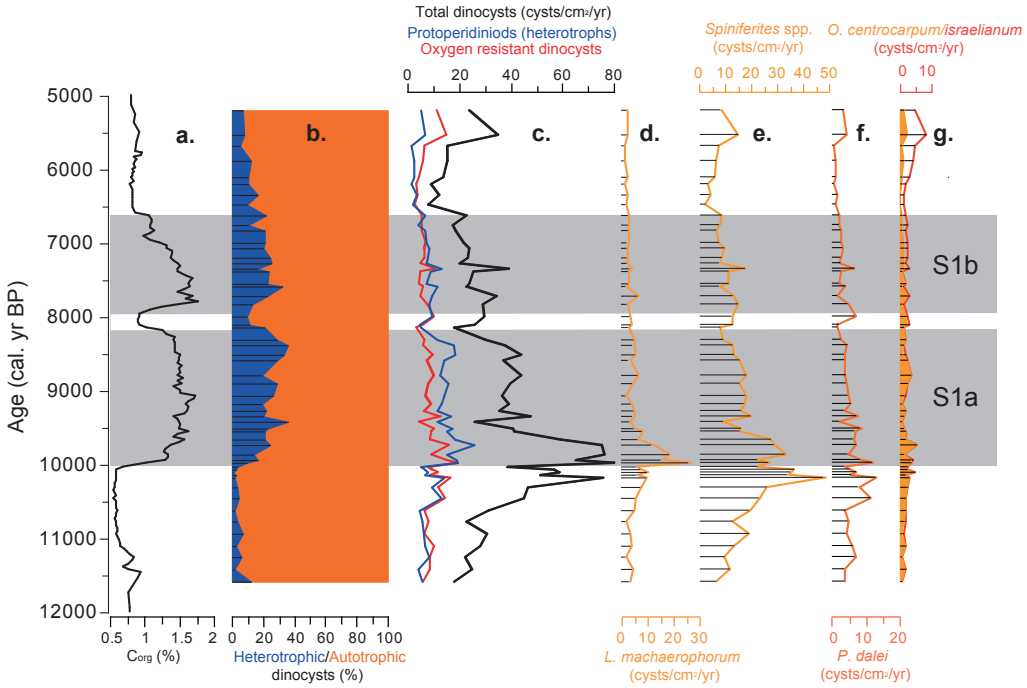

Figure 2. *Overview of selected geochemical and dinocyst data of core PS009PC. (a) Organic carbon content (C_{org}) (Hennekam et al., 2014). (b) Relative abundances of heterotrophic (blue) and autotrophic dinocysts (orange). (c) The total dinocyst accumulation rate (AR) (black), the AR of protoperidinioid cysts (blue) and the AR of oxygen resistant dinocysts (red; e.g., Zonneveld et al., 2001). ARs of Lingulodinium machaerophorum (d), Spiniferites spp. (e), Pentapharsodinium dalei (f), Operculodinium centrocarpum (orange) and Operculodinium israelianum (red) (g). Gray zones indicate the two sapropel phases S1a and S1b, respectively. The plotted age is derived from the age model for PS009PC by Hennekam et al. (2014).*

3.2. Pollen and Spores

Prior to sapropel S1 deposition, the total pollen and spores AR (Fig. 3b) increases from ~5 to ~20 grains cm^{-2} yr^{-1}, between ~10.5 and 10.0 cal. kyr BP (Fig. 3b inset). On average, about 25% of the pollen assemblages are tree pollen, dominated by *Quercus* (Figs. 3c, d), while herbs dominate the pollen assemblages, with percentages up to ~70% (Fig. 3f). Asteraceae subf. Liguliflorae and Chenopodiaceae (Fig. 3f, g) are the dominant herb pollen types. Prior to the onset of the sapropel, at 10.1 kyr BP, Chenopodiaceae increases from ~25% to almost 40% of the total pollen assemblage. The less abundant (<10%) *Ephedra fragilis,* typical of arid conditions, decreases simultaneously (Fig. 3h).

At the onset of S1a the total pollen and spores AR increases exponentially, reaching up to ~180 grains cm^{-2} yr^{-1} at 9.8 cal. kyr BP. From this maximum onwards the AR gradually decreases to 50 grains cm^{-2} yr^{-1} at the termination of S1a. Total herb pollen types gradually decrease over S1a to a rather stable value around 50% for the remainder of the record.

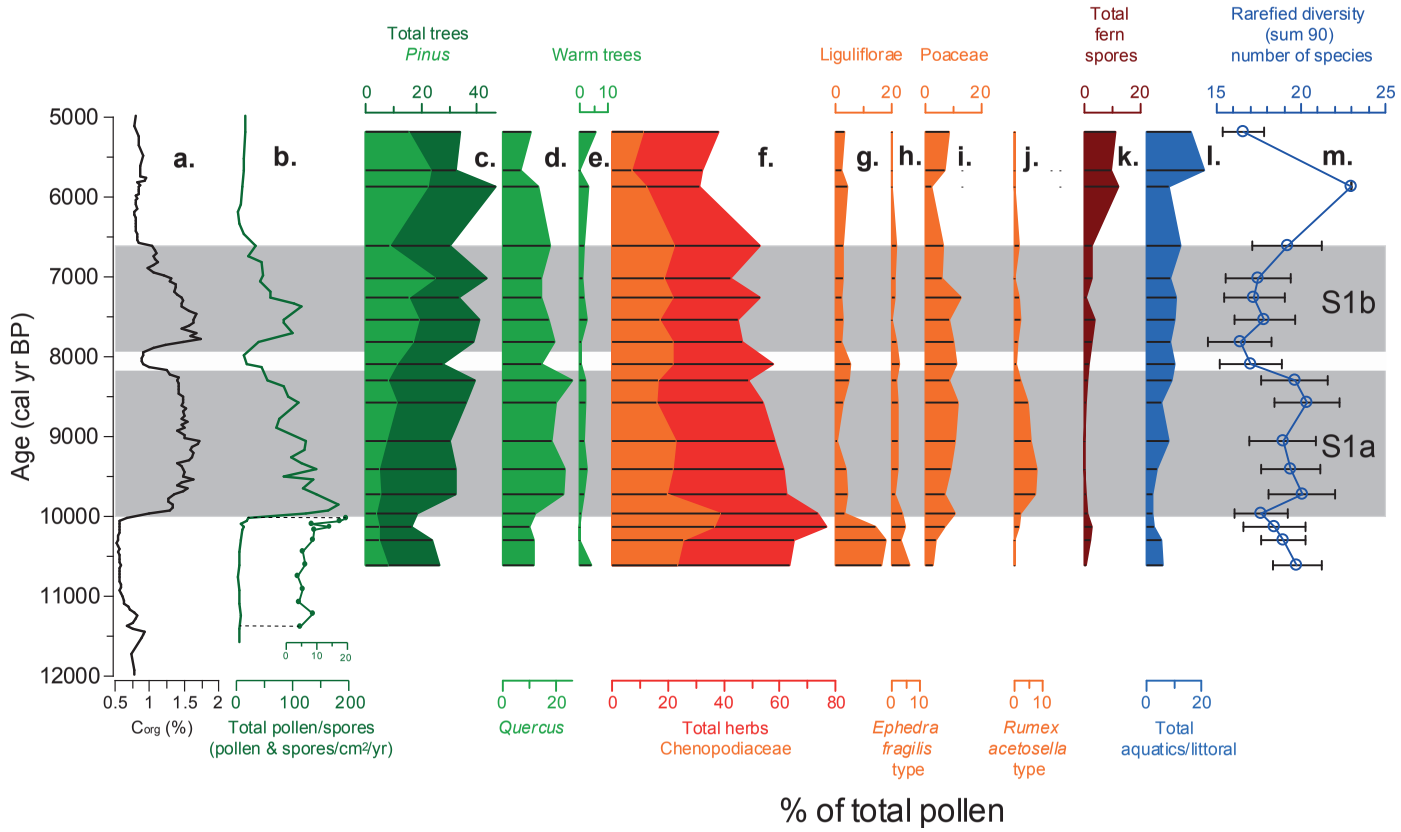

Figure 3. *Overview of selected geochemical and pollen and spores data of core PS009PC (a) Organic carbon content (C_{org}) (Hennekam et al., 2014). (b) The total pollen and spores accumulation rate, with an inset zooming in on the pre-sapropel phase. Relative abundances of total trees (dark green and Pinus (light green) (c), Quercus (d), warm trees (e), total herbs (red) and Chenopodiaceae (f), Liguliflorae (g) Ephedra fragilis type (h), Poaceae (i), Rumex acetosella type (j), total fern spores (k) and total aquatics/littoral (l). Rarefaction diversity (m). Gray zones indicate the two sapropel phases S1a and S1b, respectively. The plotted age is derived from the age model for PS009PC by Hennekam et al. (2014).*

Tree pollen, still dominated by *Quercus*, increase up to ~40% of the total pollen sum. At the onset of S1a Asteraceae subf. Liguliflorae drop from 20% to below 5%, subsequently Chenopodiaceae rapidly decrease from ~40% to around 20%. Poaceae and *Rumex acetosella* (Fig. 3i, j) become relatively more abundant during S1a. *R. acetosella* presence is mainly restricted to S1a, while Poaceae remain a relatively constant contributor to the total pollen assemblage (~10%) for the remainder of the record. Within the sapropel interruption the total pollen AR decreases to 13 grains cm^{-2} yr^{-1}, subsequently the AR rises again to above 100 grains cm^{-2} yr^{-1} in S1b. Followed by a gradual decrease, towards values below 20 grains cm^{-2} yr^{-1} after the sapropel. From the sapropel interruption onwards, *Pinus* pollen become relatively more abundant and dominate tree pollen assemblages during S1b (Fig. 3c). Aquatics/littoral pollen (Fig. 3l), predominantly composed of Cyperaceae pollen, gradually increase from <5% at the onset of the sapropel to above 10% at the termination of the sapropel. Fern spores (Fig. 3k) and pollen of thermophilous trees are only a minor constituent of the pollen assemblages (Fig. 3e), although the latter are relatively more abundant during phases of sapropel deposition.

After sapropel deposition the abundance of herb pollen types decreases further, while the abundance of tree pollen, dominated by *Pinus* pollen, remains relatively constant, i.e. between 30% and 40%. The relative abundance of fern spores and aquatics/littoral pollen increases after sapropel deposition, from less than 5% to >10% and from 10 to ~20%, respectively.

The rarefaction diversity (Fig. 3m), the palynological diversity corrected for the total number of pollen counted (Birks and Line, 1992; Sangiorgi and Donders, 2004), shows a gradual decreases towards the sapropel. Within S1a the taxa richness increases appreciably, to ~20. After S1a the richness decreases to ~17, after which it increases again after the sapropel.

3.3. Geochemistry

The $CaCO_3$ AR (Fig. 4b) has a background value of about 1.5 g cm^{-2} yr^{-1}, and starts to increase well before the marked increase in C_{org} From ~11.3 cal. kyr BP onwards, the $CaCO_3$ AR increases gradually, reaching maximum values between 9.8 and 9.2 cal. kyr BP, of 2.3 g cm^{-2} yr^{-1}. After an abrupt fall at 9.2 cal. kyr BP, the $CaCO_3$ AR gradually decreases towards sapropel termination.

The C_{org}/P_{tot} ratio (Fig. 4c) perfectly mimics the C_{org} profile (Fig. 4a). Pre-sapropel values are between 20 and 30 and sharply increase at sapropel onset, reaching relatively stable values of ~45 for S1a. During the sapropel interruption C_{org}/P_{tot} values fall close to background. At the onset of S1b the C_{org}/P_{tot} ratio sharply increases again, reaching stable values of ~50. From 7 cal. kyr BP onwards, just before sapropel termination, values gradually decrease towards background values of ~35.

Mo concentrations are generally close to zero prior to sapropel onset (Fig. 4d). At the onset of sapropel formation concentrations rapidly increase to an average of 14 parts per million (ppm), and a maximum close to 20 ppm in the middle of S1a. During the sapropel interruption, Mo concentrations decrease to ~2 ppm. In the early stages of S1b

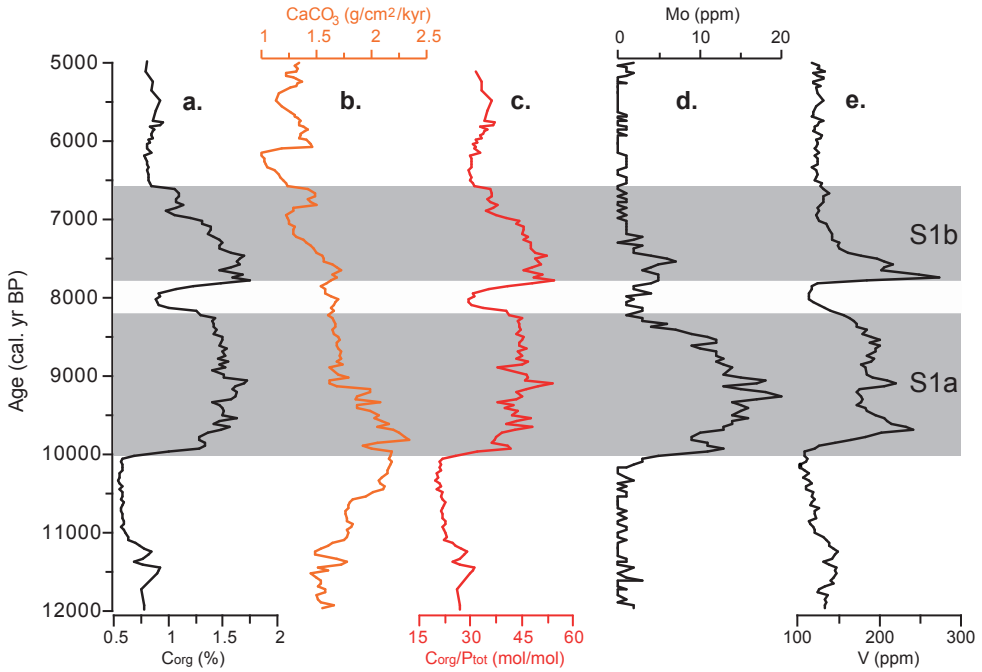

Figure 4. *Overview of geochemical data of core PS009PC (a) Organic carbon content (C_{org}; Hennekam et al., 2014). (b) $CaCO_3$ accumulation rate. (c) Organic carbon over phosphorus ratio (C_{org}/P_{tot}). (d) Molybdenum (Mo). (e) Vanadium (V; Hennekam et al., 2014). Gray zones indicate the two sapropel phases S1a and S1b, respectively. The plotted age is derived from the age model for PS009PC by Hennekam et al. (2014).*

Mo concentrations increase again to maximum values of 7 ppm, but rapidly return to background values (i.e., close to zero).

4. Discussion

4.1. Paleoproductivity and preservation signals

Most protoperidinioid cysts are formed by heterotrophic dinoflagellates, whilst gonyaulacoids are usually produced by phototrophic dinoflagellates (Harland, 1988). Heterotrophic dinoflagellates typically feed on organic detritus, other phytoplankton, and even higher trophic levels, e.g., fish (Jacobson and Anderson, 1986). Hence their relative abundance has been widely employed as a proxy for paleoproductivity (Sluijs et al., 2005). However, heterotrophic protoperidinioid cysts are more sensitive to oxidation than other cysts, and are therefore better preserved under hypoxic or anoxic conditions (Zonneveld et al., 1997, 2001; Versteegh and Zonneveld, 2002). Their occurrences, and consequently their relative abundances, in an assemblage may therefore be biased by differential preservation, such as that typically of sapropel versus non-sapropel sediment sequences. Cysts of phototrophic/autotrophic dinoflagellates (mostly gonyaulacoids) are

usually either moderately or highly resistant to oxygenation (Zonneveld et al., 1997, 2001; Versteegh and Zonneveld, 2002). Therefore their ARs provide a more reliable proxy for investigating marine productivity trends (Zonneveld et al., 2009) in sapropel and non-sapropel sediments, and will help us to distinguish between productivity and preservation.

In anoxic or near anoxic conditions V is scavenged from the water column and concentrated in the sediments (e.g., Emerson and Huested, 1991), while under euxinic conditions molybdate anions are converted to particle-reactive thiomolybdates, hence the burial of Mo (Helz et al., 1996. Additionally, C_{org}/P_{tot} can be used as an indicator for sea floor deoxygenation (Algeo and Ingall, 2007).

4.2. Pre-sapropel: ~12-10 cal. kyr BP

A distinct shift in total dinocyst ARs (Figs. 2c and 5c) starting from 10.8 cal. kyr BP suggests that marine productivity increased ~1 kyr before the sapropel onset, a feature also noted in the Aegean Sea (Casford et al., 2002). The productivity signal is primarily based on the moderately oxygen-sensitive *Spiniferites* spp., with a minor contribution of *P. dalei* (oxygen-resistant), *L. machaerophorum* (moderately sensitive) and the heterotrophic protoperidinioids (oxygen sensitive, Zonneveld et al., 1997, 2001; Versteegh and Zonneveld, 2002). Our reconstructed high productivity is further supported by a steady, synchronous increase in $CaCO_3$ AR (Fig. 5e), which in this region is suggested to be of a biogenic origin (Weldeab et al, 2003). We attribute these increases in marine productivity to enhanced nutrient input in the photic zone at least partly due to enhanced Nile River discharge. A coinciding, gradual, ~2‰ decrease in $\delta^{18}O_{ruber}$ occurs, which is largely related to reduced sea surface salinity (SSS) (Hennekam et al., 2014; Fig. 5b). Importantly, the primary productivity increase prior to sapropel formation is not matched by increases in sedimentary C_{org} (Fig. 5a), suggesting that most organic matter was remineralised upon sedimentation. An increase in the AR of phototrophic dinocysts (which require nutrients and light) together with increased $CaCO_3$ AR from biogenic origin may indicate that nutrients were injected not only directly via nutrient-rich freshwater input but also indirectly through a shoaled nutricline with the development of a DCM (Gieskes and Rohling, 1989; Castradori, 1993; Crudeli et al., 2006). We speculate that blooms of the lower photic zone coccolithophore *Florisphaera profunda*, which thrives at the DCM, could have contributed to the increased $CaCO_3$ AR. The marine productivity increase occurs during a period of increased insolation (Fig. 5g) and warming of Eastern Mediterranean surface waters (Castañeda et al., 2010; Fig. 5f), concurrent with ongoing rapid global sea level rise (e.g., Grant et al., 2012; Fig. 5h). Particularly the latter process may have further stimulated marine productivity by introducing additional land-derived nutrients from flooded shelves. Compared to the present-day productivity estimates as derived from dinocyst AR in proximity of the studied core location (Elshanawany et al., 2010), productivity was at least one order of magnitude higher than today, prior to sapropel deposition.

The brief, but noteworthy decrease in the total dinocyst AR between 10.3 and 10 cal. kyr BP coincides with a 0.7‰ increase in $\delta^{18}O_{ruber}$ (Hennekam et al., 2014; Fig. 5b),

pointing to a temporary increase in SSS perhaps resulting from a period of decreased Nile discharge.

The pre-S1 pollen assemblages are typical for a savanna-like ecosystem dominated by herbs, e.g. Asteraceae subf. Liguliflorae, Poaceae, and significant amounts of *Ephedra* characteristic for warm and arid regions (van Campo, 1984; Boessenkool et al., 2001). The increase in the total pollen and spores AR at 10.5 cal. kyr BP lags the increase in marine productivity by a few centuries, suggesting that increased sediment input (carrying pollen) was initially accommodated in the Nile delta (Fig. 1b). This would have led to expansion of coastal habitat and salt marsh environments. A relative increase in Chenopodiaceae pollen, typical for salt marsh environments (Willard et al., 2001), supports such expansion of tidally influenced brackish habitat in the Nile delta. The brief decrease observed in the total dinocyst AR, between 10.3 and 10 cal. kyr BP, is not observed in the total pollen and spores AR. This may have been caused by a relatively brief period of delta progradation and vegetation expansion due to increased Nile sediment discharge in a phase that is generally dominated by marine transgression (Stanley and Warne, 1993; Kholeif and Mudie, 2009).

Low concentrations of Mo and V reflect that overlaying waters at the studied site were well-oxygenated prior to sapropel, which is further supported by low C_{org}/P_{tot} ratios (Algeo and Ingall, 2007).

4.3. Sapropel: ~10-6.6 cal. kyr BP

A maximum in the total dinocyst and biogenic $CaCO_3$ ARs, indicative of maximum marine productivity, is reached at the onset of sapropel formation, i.e., at 10 cal. kyr BP. This productivity maximum lasts for about three centuries and coincides with maximum summer insolation at 30°N (Laskar et al., 2004; Fig.5h) and a depleted $\delta^{18}O_{ruber}$ of approximately -1.3‰, representing the highest Nile activity and lowest reconstructed SSS values for the entire Holocene (Hennekam et al., 2014). This scenario is further supported by synchronous maximum values in the Ba/Ca_{ruber} (Weldeab et al., 2014) obtained from a core in a nearby location. The maximum in the dinocyst AR mainly results from peaks of *L. machaerophorum, P. dalei* and heterotrophic protoperidinioids. High occurrences of *L. machaerophorum* have been found in eutrophic areas under the influence of river plumes (Sangiorgi and Donders, 2004; Sangiorgi et al., 2005; Zonneveld et al., 2009), in areas where (seasonal) stratification occurs. *P. dalei* is a cosmopolitan euryhaline species (Zonneveld et al., 2013). A recent study on eutrophication trends in the Mediterranean Sea reveals that cyst production of *P. dalei* increases when upper water column phosphate concentrations increase (Zonneveld et al., 2012). The large peak in the AR of both species, recorded at the onset of sapropel deposition, therefore suggests a rapid shift, within a century, towards nutrient-rich, (seasonally) highly stratified surface waters (Zonneveld et al., 2013). In this view, the sudden rapid increase in C_{org} could be explained in terms of enhanced preservation of organic matter, as bottom water ventilation most probably worsened due to freshwater stratification. However, given the different trends in the ARs of dinocysts, all with different sensitivity to oxygenation, we conclude that stratification-

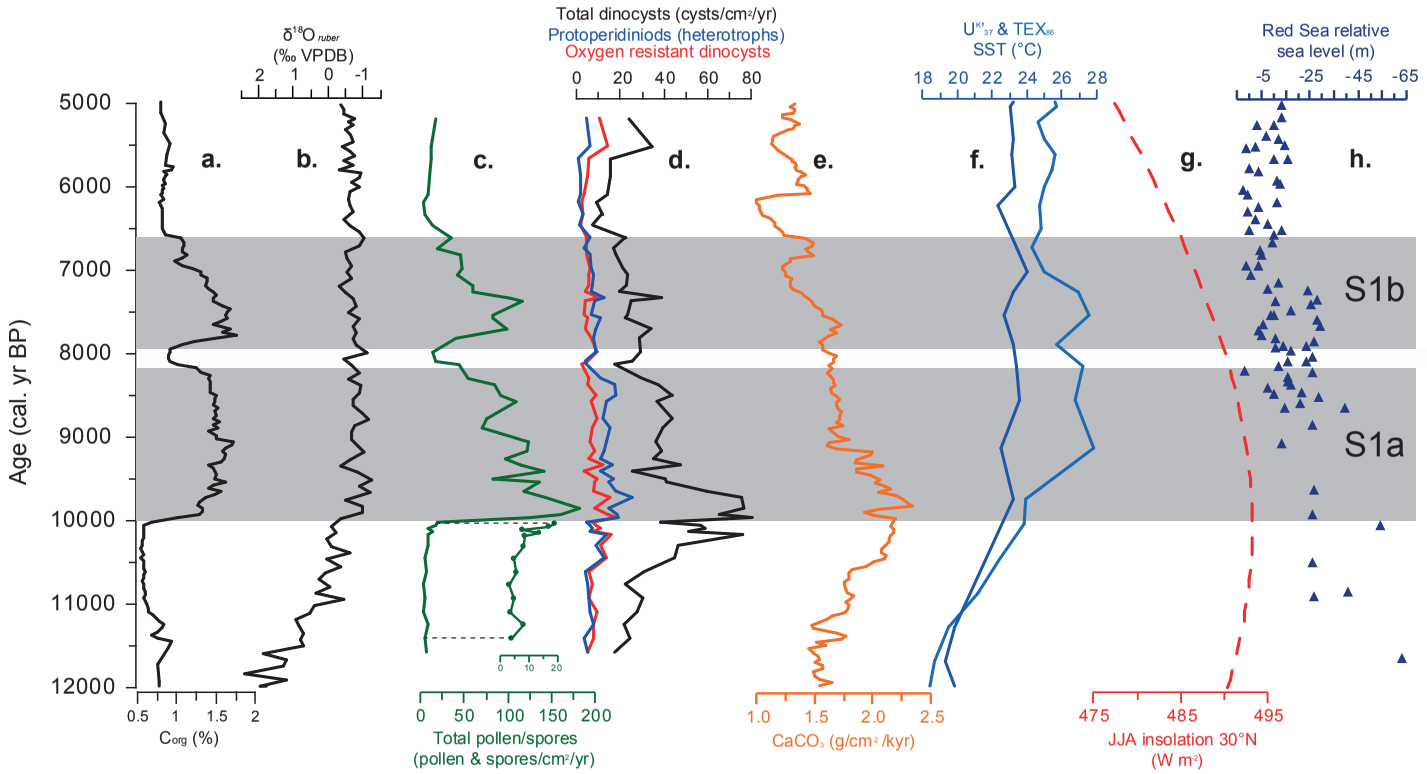

Figure 5. *Overview of different paleoenvironmental parameters and $CaCO_3$ total pollen and spores and dinocyst accumulation rates (ARs) of core PS009PC (a) Organic carbon content (C_{org}), (b) $\delta^{18}O_{ruber}$ (Hennekam et al., 2014). (c) The total pollen and spores AR. (d) The total dinocyst AR (black), the AR of peridinioid cysts (blue) and the AR of oxygen resistant dinocysts (red; e.g., Zonneveld et al., 2001). (e) $CaCO_3$ AR. (f) Sea surface temperature (SST)reconstructions based on $U^{K'}_{37}$ and TEX_{86} for GeoB 7702-3 (Castañeda et al., 2010). (g) June-July-August insolation at 30°N (Laskar et al., 2004). (h) Red Sea relative sea level record (Grant et al., 2012). Gray zones indicate the two sapropel phases S1a and S1b, respectively. The plotted age is derived from the age model for PS009PC by Hennekam et al. (2014).*

induced preservation alone was not sufficient during the early stages of sapropel S1. Moreover, sluggish circulation and water stratification also promotes the accumulation and availability of regenerated nutrients (e.g., Slomp et al., 2002), which in turn positively feedback on productivity.

The comparable increase in the relative abundance of heterotrophic protoperidinioids (Fig. 2c) during S1a and S1b may represent a mixed signal of both enhanced marine productivity and higher preservation (Zonneveld et al., 1997, 2001; Versteegh and Zonneveld, 2002). However, S1a has a much higher total dinocyst AR, together with rather elevated protoperidinioid ARs, than S1b. We infer that at least for the first half of unit S1a, marine productivity worked in tandem with preservation. During sapropel interruption and unit S1b the dinocyst ARs, including that of protoperidinioids, are much lower, implying lower productivity than in S1a. In this context the high relative abundance of protoperidinioids in S1b is probably due to enhanced preservation.

Total pollen and spores ARs seem to be closely associated with $C_{org,}$ which may lead to the conclusion that their occurrence is purely the result of preservation as previously suggested by terrestrial palynological studies in the same region (e.g., Cheddadi and Rossignol-Strick, 1995, and references therein). However, a mild oxidation (acetolysis; Erdtman, 1960) is standard practice in pollen preparation. Experiments on processing (with and without acetolysis), and pollen grazing by marine microorganisms show some but no significant alteration of pollen preservation (Mudie and McCarthy, 2006). The gradual change in pollen assemblages and absence of signs of selective or partial decomposition of terrestrial palynomorphs suggest that, rather than enhanced preservation of pollen and spores, other processes, i.e. enhanced vegetation cover (pollen production), increased transport, and geomorphological changes in the Nile delta, have played a significant role. The geomorphology of the Nile delta during the studied period was mainly influenced by long-term marine transgression up to ~8 cal. kyr BP (Stanley and Warne, 1993; Butzer, 2002). Hence, no abrupt changes that might explain the abrupt shift in the pollen AR occurred. An increase in pollen production is expected to have occurred as vegetation cover gradually increased during the "Green Sahara" period (e.g., Claussen and Gayler, 1997), but this again cannot explain the recorded rapid changes. The final option would then be increased transport. We suggest that due to the rapid development of stratification and coinciding sluggish circulation, the freshwater plume of the Nile expanded across the Eastern Mediterranean surface waters. The extension of the freshwater plume would then have transported pollen and spores much further away from the Nile outflow. Based on the previously discussed SSS reconstructions, this likely explains part of the rapid and large increase in the pollen AR at sapropel S1 onset.

The pollen assemblages show that during sapropel deposition the terrestrial hinterland ecosystem developed from semi-arid savanna to open woodlands, exhibited by decreasing herb pollen and increasing tree pollen, particularly *Quercus*, which is consistent with a more direct Nile-derived signal. Further supported by a somewhat higher taxa richness during S1a, indicating a higher proportion of river transported pollen. The relatively high abundance, during S1a, of *Rumex acetosella* is often attributed to human influence

(e.g., Tinner et al., 2009), but predates large-scale ancient Egyptian and Middle Eastern agricultural practice. However, in this region it is consistent with natural semi-open woodland with patches of grassland and herbs where *Rumex acetosella* typically occupies floodplains and moist soils, supporting increased Nile influence. The gradually increased *Pinus* pollen and decreased rarefaction diversity during S1b are indicative for increased distance of the core site to the coast due to sea level rise and a relatively gradual drying of the continent, in line with decreasing summer insolation (Fig. 5h), promoting a southward shift of the Intertropical Convergence Zone (ITCZ).

The rapid shifts in Mo and C_{org}/P_{tot} at sapropel onset and in V slightly after, support the relatively rapid establishment of anoxia and even some euxinia in bottom and pore waters (Helz et al., 1996). This is consistent with a previous report on anoxia in the Nile plume (Bayon et al., 2013). Anoxia at sapropel onset most likely resulted from the combined effects of degrading organic matter, resulting from high marine productivity, and freshwater forced stratification of the water column. During the sapropel interruption, overlaying waters became reoxygenated, as indicated by a drop to (or close to) background values in all three redox-parameters. Right after the onset of S1b, V and C_{org}/P_{tot} reach a maximum concentration and value, respectively, suggesting a return to anoxic conditions even stronger than during S1a. The absence of Mo, however, suggest that bottom and pore waters did not become euxinic again (Helz et al., 1996).

4.4. Post-sapropel: 6.6-5 kyr BP

After sapropel termination marine primary productivity generally reaches minimum values for the studied record, as reflected by low dinocyst and biogenic $CaCO_3$ ARs. Beside low marine productivity, this interval is characterized by a reduced extension of the freshwater plume as suggested by low ARs of *L. machaerophorum* and *P. dalei* and by low transport of pollen and spores to the studied site. Low productivity and a well-oxygenated water mass are expressed in the low C_{org} content, low V and Mo concentrations and low C_{org}/P_{tot} ratio. The ITCZ shifts back to a more southern position, which leads to the termination of the African Humid Period and its relatively rich vegetation (Gasse et al., 2000; Renssen et al., 2003), gradually causing decreased pollen production and drier conditions.

Notably, this interval is characterized by an increase in the AR of *Operculodinium israelianum*. Cysts of *O. israelianum* are restricted to (sub)-tropical regions, and have their highest abundance in regions with well-ventilated bottom waters where high SSS prevail (Bradford and Wall, 1984; Zonneveld et al., 2013). Highly saline surface waters and well-ventilated bottom waters occurred, a situation comparable to the present-day one.

The post-sapropel pollen assemblages, with relatively high abundances of spores and aquatic pollen types, typically point to a disturbed, erosional signal, which may be linked to human activity, e.g., deforestation.

5. Conclusion

A marine and terrestrial palynological approach was employed within a multi-proxy study on a core collected in a region of the eastern Mediterranean under strong influence of Nile discharge. In order to understand the roles of productivity and preservation in sapropel S1 formation. We found that marine productivity started to increase ~1 kyr prior to the onset of sapropel S1 at 10.8 cal. kyr BP. Such increase in productivity is due to enhanced nutrient input. Nutrients likely derive from increased Nile River discharge, as inferred from a coinciding decrease in $\delta^{18}O_{ruber}$, but may also partly originate from flooded shelves during marine transgression and subsequent expansion of the coastal marsh habitat as indicated by an increase in Chenopodiaceae pollen. Additionally shoaling of the nutricline may have played a role.

At sapropel onset, high ARs of the dinocysts *L. machaerophorum* and *P. dalei,* together with high pollen ARs, indicate maximum Nile discharge, which resulted in (seasonal) stratification of surface waters, all occurring exactly at a maximum in the Northern Hemisphere summer insolation. Persistent stratification led to reduced or shutdown of bottom water ventilation, promoting enhanced carbon sequestration at the sediment-water interface, all within one century. The abrupt increase in the total pollen and spores AR at sapropel onset largely results from increased surface transport, which is most consistent with a slowdown in the water circulation and greater extension of the freshwater plume of the Nile. While stratification-induced preservation seems to have played a minor role based on the generally well-preserved pollen prior to sapropel deposition and the absence of large turnovers in the assemblages. Pollen assemblages do, however, exhibit a gradual shift from a savanna-like ecosystem to moist open woodland during sapropel deposition.

In conclusion, a combination of high marine productivity and stratification-induced preservation were critical for triggering sapropel formation. Marine productivity, as derived from the ARs of dinocysts and $CaCO_3$, played a secondary role during the remainder of sapropel deposition. Pollen assemblages in the second part of the sapropel (S1b) and after sapropel are indicative of gradual aridification and disturbance of the natural landscape. While dinocyst assemblages after sapropel termination point to environmental conditions comparable with the present-day situation.

3

A perturbed hydrological cycle during Oceanic Anoxic Event 2

"The more difficult the victory, the greater the happiness in winning."

Pelé

Abstract

The Late Cretaceous Oceanic Anoxic Event 2 (OAE2; ~94 Ma) represents one of the largest global carbon cycle perturbations during the Phanerozoic. OAE2 represents an important, although extreme case study, for modern trends because widespread anoxia and enhanced organic carbon burial during OAE2 were linked to exceptionally warm climates and high atmospheric CO_2 concentrations. However, potential consequences of this warmth for the hydrological cycle remain poorly understood, hampering our understanding of its impact on biogeochemical cycles, and climate during this greenhouse episode. Here, we show evidence for changes in the hydrological cycle during OAE2 based on combined geochemical and palynological data for the stratigraphically expanded coastal OAE2 succession at Bass River, located on the New Jersey Shelf (Ocean Drilling Program Leg 174AX), eastern United States. Paleothermometry, based on TEX_{86}, indicates sea-surface warming at the onset of OAE2 and a subsequent pronounced cooling event. Palynological data show that these changes in temperature were associated with strong variations in precipitation and runoff. We suggest that an acceleration of the hydrological cycle during OAE2 played a key role in supplying nutrients to coastal waters and enhancing stratification, thus contributing to the development of ocean anoxia.

1. Introduction

Throughout the Mesozoic, several episodes of widespread deposition of organic matter occurred, associated with dysoxic or even anoxic bottom waters, termed Oceanic Anoxic Events (OAEs; Schlanger and Jenkyns, 1976). The most pronounced is the extensively studied OAE2, which occurred near the Cenomanian-Turonian boundary (93.9 Ma; Meyers et al., 2012a). Excess organic carbon burial during OAE2 resulted in a >2‰ positive carbon isotope excursion (CIE) in both marine and terrestrial carbon reservoirs (e.g., Arthur et al., 1988). Several, not mutually exclusive, hypotheses have been proposed for the widespread ocean dysoxia during OAE2. Many authors have linked high levels of atmospheric CO_2 (Schouten et al., 2003; Bice et al., 2006; Sinninghe Damsté et al., 2008; Barclay et al., 2010), resulting from massive igneous activity (Snow et al., 2005; Kuroda et al., 2007; Turgeon and Creaser, 2008), to exceptional warming of the ocean during the late Cenomanian (Bice et al., 2006; Forster et al., 2007b; Sinninghe Damsté et al., 2010), decreasing oxygen solubility. This warmth was likely associated with a more stratified water column, which resulted in poor atmosphere-ocean gas exchange, photic zone euxinia (Sinninghe Damsté and Köster, 1998), and enhanced organic matter preservation at the sediment water interface. Moreover, enhanced recycling of phosphorus (P) from anoxic sediments (Kuypers et al., 2004b; Mort et al., 2007; Kraal et al., 2010) likely provided a powerful feedback, whereby abundant N_2-fixing cyanobacteria (Kuypers et al., 2004b) added nutrients to boost primary production and export production, leading to further deep water oxygen depletion (Kuypers et al., 2002; Tsandev and Slomp, 2009).

Recent work has suggested elevated productivity resulted from enhanced silicate weathering during OAE2 (Pogge von Strandmann et al., 2013). However, no data exist on a crucial factor fuelling silicate weathering, sea surface stratification and nutrient budgets in the proto-North Atlantic: hydrology, notably precipitation and runoff over evaporation. Typically, in restricted basins, an excess basin-wide fresh water budget results in nutrient trapping, while excess evaporation results in a nutrient desert, as observed, for example, in the present-day Mediterranean Sea (Krom et al., 1991). Moreover, in the modern ocean runoff acts as a nutrient source and, therefore, partly determines sub-thermocline oxygen content (e.g., Middelburg and Levin, 2009). In concert with warm climates and nutrient feedbacks, changes in the intensity of the hydrological cycle may have contributed to the occurrence of OAE2 in the proto-North Atlantic. Because such changes are most obvious in coastal settings, we conducted a high-resolution multidisciplinary geochemical and palynological study on immature New Jersey shallow shelf sediments from the Bass River borehole (Ocean Drilling Program [ODP] Leg 174AX, New Jersey Shelf, eastern United States; Fig. 1), which yields remarkably well-preserved palynomorphs and high concentrations of organic molecules, suitable to reconstruct regional climate evolution, with a focus on sea-surface temperature (SST), and the hydrological cycle.

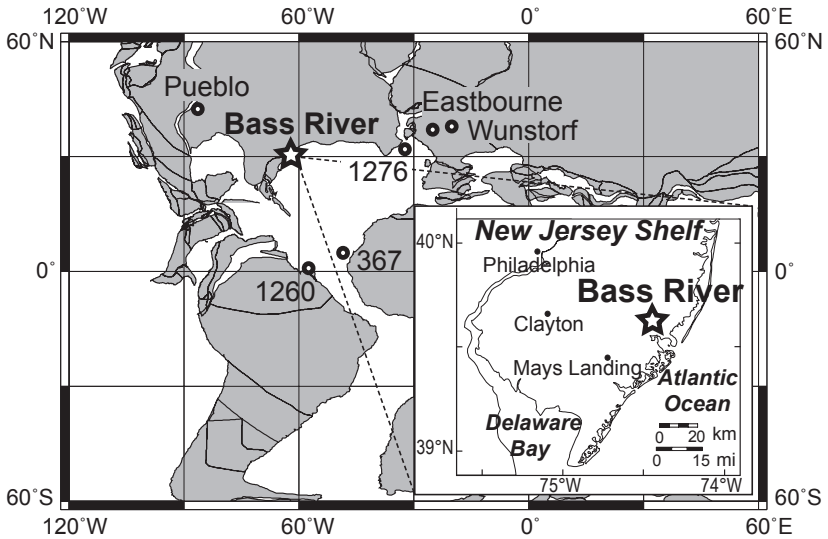

Figure 1. *Paleogeographic map for the Cenomanian-Turonian boundary time interval, indicating locations of the Bass River borehole (New Jersey, USA) and sections mentioned in the text: Pueblo (Colorado, USA), Eastbourne (UK), Wunstorf (Germany), Deep Sea Drilling Project (DSDP) Site 367, and Ocean Drilling Program (ODP) Sites 1260 and 1276 in a plate tectonic reconstruction. Map generated at http://www.odsn.de/odsn/services/paleomap/paleomap.html. Insert map (modified from Sluijs et al., 2007b) indicates the present-day drill location of the Bass River borehole.*

2. Material and Methods

The Bass River borehole (39°36'42"N, 74°26'12"W; Fig. 1; Miller et al., 1998) contains ~46 m of upper Cenomanian to lower Turonian strata consisting of dark gray, fossiliferous, micaceous (chloritic), silty clays to clayey silts, deposited in an inner neritic setting (water depth <30 m; Sugarman et al., 1999). OAE2 was previously identified based on ~2.5‰ positive shifts in the stable carbon isotopic composition ($\delta^{13}C$) of benthic foraminifera taxa *Gavelinella* and *Epistomina* and of bulk organic carbon ($\delta^{13}C_{org}$), combined with nannofossil biostratigraphy (Sugarman et al., 1999; Bowman and Bralower, 2005). Weight per cent total organic carbon (TOC) values are low (on average ~1%; Bowman and Bralower, 2005), compared to most other OAE2 sections in the proto-North Atlantic. We expanded (i.e., a broader interval with lower resolution) the data set of Bowman and Bralower (2005) on TOC contents and $\delta^{13}C_{org}$ (see supplements for detailed methods). Bulk sediment elemental compositions were measured using inductively coupled plasma – optical emission spectrometry (ICP-OES) of sediment extracts upon total digestion, followed by calculation of the ratio of titanium over aluminum (Ti/Al-ratio). We extracted branched and isoprenoid glycerol dialkyl glycerol tetraethers (GDGTs),

using organic solvents, and quantified the various GDGTs using high-performance liquid chromatography/atmospheric pressure positive ion chemical ionization – mass spectrometry (HPLC/APCI-MS). The Branched and Isoprenoid Tetraether (BIT) index, based on the amount of terrestrially derived GDGTs in marine sediments relative to the isoprenoid GDGT crenarchaeol, which is predominantly derived from marine Thaumarchaeota, was calculated to assess the relative abundance of soil organic matter versus marine organic matter (Hopmans et al., 2004). TEX_{86}^{H}, based on the isoprenoid GDGT distribution, was used to estimate absolute SSTs using the modern core top calibration by Kim et al. (2010), which has a calibration error of 2.5°C. The analytical error of TEX_{86}^{H}-based SSTs was 0.07°C ($1\sigma = 0.04$°C). Finally, we studied assemblages of organic dinoflagellate cysts (dinocysts), as well as the abundance of the main groups of pollen and spores derived from land plants, to assess surface water and continental ecology across OAE2. The ratio of terrestrial (T; pollen and spores) over marine (M; dinocysts) palynomorphs (T/M-ratio) was calculated dividing terrestrial palynomorphs by total encountered palynomorphs (T/T+M). Where possible, data were generated on the same samples to optimize comparability of the signals.

3. Results and Discussion

3.1. Updated Age Model

The encountered dinocyst taxa support the presence of OAE2 at Bass River but do not provide additional constraints on the existing age model based on calcareous macro- and microfossils and the characteristic positive CIE (Sugarman et al., 1999; Bowman and Bralower, 2005). The combined high-resolution $\delta^{13}C_{org}$ data set (Bowman and Bralower, 2005; this study; Fig. 2a), however, can be used to correlate confidently to global reference sections the of U.S. Geological Survey #1 Portland core, close to the Global Boundary Stratotype Section and Point (GSSP) at Pueblo, Colorado (Sageman et al., 2006), Eastbourne (Paul et al., 1999) and the Wunstorf core, North Germany (Voigt et al., 2008; supplements). Based on a duration of 430 – 445 kyr for OAE2 (Voigt et al., 2008), average sedimentation rates were around ~3 cm/kyr for upper Cenomanian to lower Turonian strata, similar to the estimate by Sugarman et al. (1999).

3.2. Paleo-Redox Conditions

Sediments for the Bass River borehole are not laminated and signs of bioturbation are present throughout the OAE2-interval. Together with the persistent presence of benthic foraminifera, this indicates that the sediment-water interface remained oxygenated at Bass River to some degree. Presumably, the sea floor at Bass River was above storm base (water depth <30 m; Sugarman et al., 1999) and, therefore, at least seasonally ventilated. This is in accordance with the relatively low organic carbon/total phosphorus ratio (C_{org}/P_{tot} ratios; Algeo and Ingall, 2007; Fig. 2b), which increases from ~70 mol/mol for the pre-OAE2-interval to average values of 100 mol/mol during OAE2. Although this suggests slightly enhanced P-regeneration resulting from low oxygen conditions, C_{org}/P_{tot} ratios at other

sites, predominantly located in the euxinic southern North Atlantic (Sinninghe Damsté and Köster, 1998), are >300 mol/mol (Mort et al., 2007; Kraal et al., 2010), indicating that P-regeneration on the New Jersey shelf during OAE2 was relatively modest.

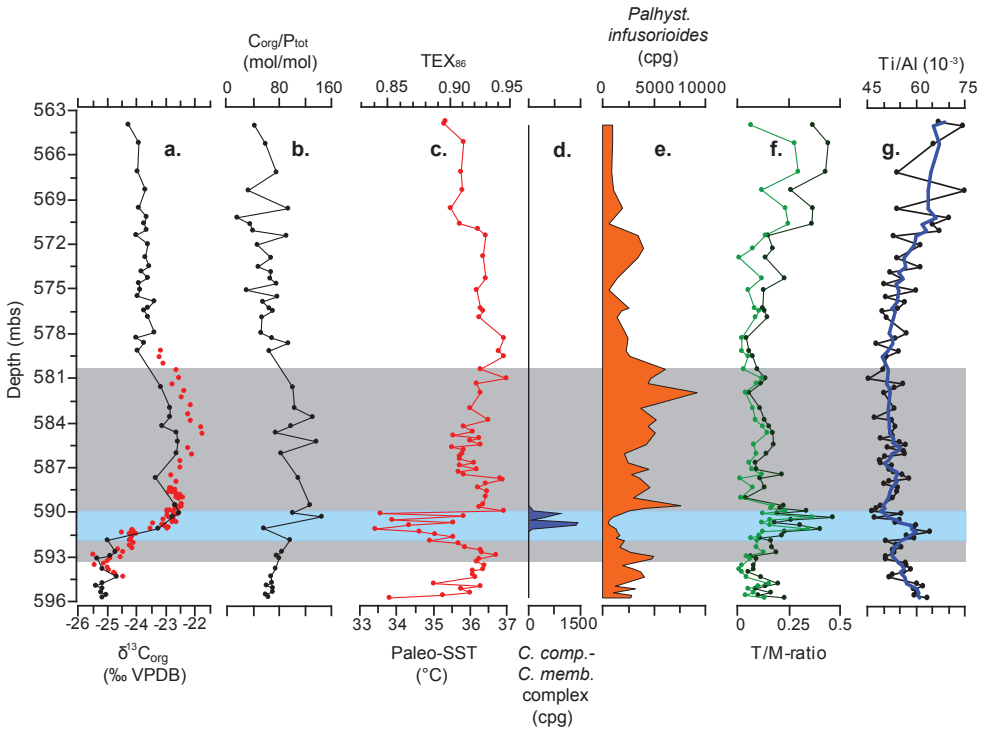

Figure 2. *Palynological and geochemical results across Oceanic Anoxic Event 2 (OAE2) at Bass River, New Jersey (USA). (a) $\delta^{13}C_{org}$, this study (black) and data adopted from Bowman and Bralower (2005; red). (b) Total organic carbon/total phosphorus ratio (C_{org}/P_{tot} ratio). (c) TEX_{86} and sea-surface temperature (SST) reconstruction based on TEX_{86}^{H} (Kim et al., 2010). Blue bar depicts the cold event. (d) dinocyst species Cyclonephelium compactum-membraniphorum complex in cysts per dry gram of sediment (cpg). (e) Dinocyst species Paleohystrichophora infusorioides (cpg). (f) Dark green data depict ratio of terrestrial versus marine palynomorphs (T/M-ratio); data in light green depict saccate gymnosperm pollen versus marine palynomorps. (g) Titanium over aluminum ratio (Ti/Al-ratio; black) and five-point moving average (blue). Gray zone indicates the OAE2 interval, based on correlation to global reference sections (see text). mbs is meters below surface.*

3.3. SST Reconstructions

For the studied interval BIT values are always <0.1, indicative for a predominant marine origin of the GDGTs. A bias from GDGTs derived from soil organic matter on TEX_{86}^{H}-based SSTs is, therefore, unlikely (Weijers et al., 2006). During OAE2 TEX_{86}^{H}-based

SST reconstructions indicate 36–37°C (Fig. 2c), generally somewhat higher than the reconstructed values prior to and after OAE2. Immediately after the onset of the CIE, SSTs drop by ~2.5°C to minima around 33–34°C (Fig. 2c). A t-test confirms that this cooling is significant in our data set ($p < 0.0005$). Although independent age constraints are limited, the stratigraphic position of the cooling seems to be consistent with the Plenus Cold Event, previously recorded throughout the North Atlantic (Jefferies, 1962, Gale and Christensen, 1996, Forster et al., 2007b; Sinninghe Damsté et al., 2010; Fig. S1). Indeed, both the trends in, and absolute values of reconstructed SSTs at Bass River are similar to previous TEX_{86}^{H}-based SST reconstructions for the OAE2-interval in the Equatorial Atlantic (Deep Sea Drilling Project (DSDP) Site 367 and ODP Site 1260; Forster et al., 2007b) and mid-latitudinal northwest Atlantic (ODP Site 1276; Sinninghe Damsté et al., 2010; Fig. 1), although the cooling was stronger at Site 1276. This cooling has been attributed to decreased atmospheric CO_2 levels as a result of enhanced global organic carbon burial (Sinninghe Damsté et al., 2010; Jarvis et al., 2011).

Within this cooler interval, we observed the influx of the typically boreal dinocyst species-"complex" (morphologically closely related species) *Cyclonephelium compactum-membraniphorum* (Fig. 2d; Marshall and Batten, 1988), indicating that this cooling resulted in plankton species migrating from high to low latitudes. A second cooling pulse, although much less pronounced (~1°C), is observed between 587 and 585.5 mbs (meters below surface). Because this phase is still within OAE2 this may be linked to decreased atmospheric CO_2 levels as well, because of continued enhanced global organic carbon burial during OAE2.

3.4. Hydrology

The recorded variations in SST, dinocyst assemblages and geochemistry provide insight in the relation between temperature and hydrology across OAE2. The dinocyst assemblages are characteristic of shallow shelf settings. Assemblages up to ~590 mbs are mainly composed of cosmopolitan species (e.g., *Spiniferites ramosus*, *Circulodinium distinctum*, and *Canningia* spp.; Tocher and Jarvis, 1995). From 590 mbs onward, *Palaeohystrichophora infusorioides* increase in absolute abundance per gram of sediment and start dominating dinocyst assemblages (Fig. 2e). This species is part of a group of morphologically closely related dinocysts produced by dinoflagellates that were tolerant to low sea-surface salinities (SSS), following previous Cretaceous and early Paleogene work also on the Bass River core, based on empirical relations (e.g., Harland, 1973; Brinkhuis et al. 2006; Sluijs and Brinkhuis, 2009). We, therefore, interpret the increase in *P. infusorioides* (Fig. 2e) to result from decreased SSS during OAE2 due to fresh water forcing by precipitation, resulting in increased stratification along the continental margin, contributing to water column deoxygenation.

Pollen and spore assemblages for the Bass River borehole are dominated by saccate gymnosperm pollen (Fig. 2f) of which modern relatives, Pinus and Picea (pine and spruce), are initially dispersed by wind (e.g., Mudie and McCarthy, 1994). Despite exceptions, modern trees producing saccate pollen, e.g., pines, are generally associated

with relatively dry conditions. (Willis et al., 1998). High values of the T/M-ratio during the cold event (Fig. 2f) may therefore in this case reflect relatively dry conditions. This is consistent with trends in the Ti/Al-ratio (Fig. 2g), which shows a statistically significant ($P<0.05$) rise during the cold event with a slight stratigraphic offset with the drop in TEX_{86} and peak in T/M ratios, despite the scatter in individual Ti/Al data points. Increasing Ti/Al-ratios of marine sediments may be interpreted as increased input of wind transported dust, as titanium concentrates in heavy minerals that are mainly transported by wind (Shimmield and Mowbray, 1991; Beckmann et al., 2005). We interpret the combination of increased saccate pollen and Ti/Al values to reflect relatively dry conditions for the cold event. Collectively, both palynology and inorganic geochemical proxies show that prior to OAE2 and during the large cooling event conditions were relatively dry. Within OAE2, conditions shifted to a more humid climate, with enhanced runoff. Post-OAE2 climate generally shifted back to drier conditions again. This general pattern is consistent with an intensified hydrological cycle during warmer climates (e.g., Pierrehumbert, 2002).

Our results show that temperature and hydrology changed consistently across OAE2. These coupled changes seem to be the result of enhanced evaporation that lead to increased precipitation and runoff at times of peak warmth, perhaps enforced by decreased plant transpiration feedbacks (e.g., Betts et al., 2007). Consequently, during relatively cooler episodes evaporation was less and precipitation and runoff decreased. Particularly because some sections in the proto-North Atlantic show relatively low TOC contents during the large cooling phase (Forster et al., 2007b; Sinninghe Damsté et al., 2010), hydrology was likely an important factor determining nutrient budgets, stratification, and seafloor oxygenation on at least a regional scale, and therefore was potentially a critical player in the carbon cycle. Future studies combining high-resolution hydrology and weathering proxy records combined with better resolved age models and site-to-site correlations will allow better quantification and determination of the sequence of events on a larger geographic scale.

4. Conclusion

Toward OAE2, SST rapidly increased and both palynological and inorganic geochemical records suggest enhanced runoff. During the "Plenus Cold Event," climate temporarily became drier and equatorward migration of plankton species occurred. For the remainder of OAE2, SSTs were high, and humid conditions prevailed. After OAE2, SSTs gradually returned to pre-OAE values and climate became drier. Our results provide evidence for changes in the hydrological cycle during OAE2, coupled to temperature changes, which impacted on nutrient supply and stratification, thereby contributing to basin wide oxygen depletion and associated enhanced burial of organic matter.

Supplements to Chapter 3

Total organic carbon and stable isotope analysis on bulk organic carbon

About 0.3 g of freeze-dried and powdered sediment sample was decalcified using HCl. Subsequently Total Organic Carbon (TOC) and $\delta^{13}C_{org}$ concentrations were measured using a Fisons Instruments CNS NA 1500 analyzer coupled to a Thermo Delta Plus isotope ratio spectrometer. Results were normalized to international standards. Average analytical uncertainty based on duplicate analyses of sediment samples was 0.03 wt. % for TOC and 0.12 ‰ for $\delta^{13}C_{org}$.

Bulk sediment elemental composition

Approximately 125 mg of freeze-dried and powdered sediment sample was dissolved in 2.5 ml mix acid ($HClO_4$:HNO_3; 3:2) and 2.5 ml 40% HF, heated to 90°C and left overnight. The acids were evaporated at 160°C after which the residue was dissolved in 25 ml 4.5% HNO_3. Bulk sediment elemental compositions were measured using Inductively Coupled Plasma-Optical Emission Spectrometry (ICP-OES; Perkin Elmer Optima 3000); the error calculated from standards and duplicates for aluminum (Al), titanium (Ti) and phosphorus (P) was generally <5% and never exceeded 15%.

Palynological treatment

Palynological processing followed standardized quantitative methods used at the Laboratory of Palaeobotany and Palynology, Utrecht University, the Netherlands. Between 3 and 13 g of freeze-dried sediment sample was slightly crushed (<5 mm), and a known amount of *Lycopodium clavatum* marker spores was added to enable palynomorph quantification per gram of sediment (Stockmarr, 1971). HCl (~30%) and HF (~38%) was added to dissolve carbonates, and silicates, respectively. Residues were sieved over a 15 μm nylon mesh and the >15 um fraction mounted on microscope. Samples were counted to a minimum of 200 dinocysts, which were identified to genus, or species level at 500x magnification, following the taxonomy of Fensome and Williams (2004). All samples and slides are stored in the collection of the Laboratory of Palaeobotany and Palynology, Utrecht University, the Netherlands.

TEX_{86} paleothermometry

Between 10 and 13 g of freeze-dried sediment sample was powdered using pestle and mortar. The sediments were extracted with a dichloromethane (DCM): methanol (MeOH) solvent mixture (9:1, v/v, 3 times for 5 minutes each) using an Accelerated Solvent Extractor (ASE 200, DIONEX) at 100°C and ca. 7.6 x 10^6 Pa. Total Lipid Extracts (TLE) were evaporated to near dryness using rotary evaporation under near vacuum, remaining solvents were subsequently removed under a nitrogen flow. TLEs were separated, using Al_2O_3 column chromatography, into apolar fractions (hexane:DCM, 9:1, v/v), ketone fractions (ethyl acetate (EtOAc), v), glycerol dialkyl glycerol tetraether (GDGT) fractions (DCM:MeOH, 95:5, v/v) and polar fractions (DCM:MeOH, 1:1, v/v). The GDGT fractions

were dried under a nitrogen flow after which 250 ng of the C_{46} GDGT internal standard was added. The GDGT fractions were ultrasonically dissolved in hexane:propanol (99:1, v/v) and filtered over a 0.45 µm mesh PTFE filter (ø 4mm) prior to analysis. GDGTs were analyzed using high performance liquid chromatography/atmospheric pressure positive ion chemical ionization mass spectrometry (HPLC/APCI-MS). HPLC/APCI-MS analyses were performed according to Schouten et al. (2007) on an Agilent 1100 series/Hewlett-Packard 1100 MSD SL series instrument, equipped with auto-injection system and HP-Chemstation software. Separation was achieved on a Prevail Cyano column (150 mm x 2.1 mm, 3 µm; Alltech). The flow rate of the hexane:propanol (90:10, v/v) eluent was 0.2 ml min-1, isocratically for the first 5 min, thereafter with a linear gradient to 18% propanol in 45 min. Injection volume of the samples was 10 µl. To increase sensitivity, selective ion monitoring (SIM) of the protonated molecular ions of the GDGTs was used. TEX_{86} values (Schouten et al., 2002) were used to estimate mean annual sea surface temperatures (SSTs) using the TEX_{86}^{H} calibration by Kim et al. (2010).

All data are listed in tables S1 and S2.

Updated age model

Sugarman et al. (1999), presented a bio-chemostratigraphic framework for the Cenomanian-Turonian boundary time interval (CTB) sediments of the Bass River core, based on calcareous nannofossil and planktonic foraminifera zonation and the $\delta^{13}C$ of two benthic foraminifera genera, *Gavelinella* spp. and *Epistomina* spp. The $\delta^{13}C$ profiles exhibit the characteristic positive carbon isotope excursion and the encountered species and genera of nannofossils and planktonic foraminifera support the presence of OAE2. However, the typical CTB marker species, notably the planktonic foraminifer *Rotaliphora cushmani* and the nannofossil *Microstaurus chiastius*, were not recorded. The CTB itself was placed at 589.9 mbs based on the last occurrence of the foraminiferal genus *Rotalipora* and the contact of nannofossil *Microstaurus chiastius* and *Eiffellithus eximius*, subzones of the *Parhabdolithus asper* zone. Bowman and Bralower (2005) published a high-resolution bulk organic carbon $\delta^{13}C_{org}$ curve, which after expansion (broadened interval) in this study, was used to correlate as reliable as possible to global reference sections (Fig. S1). Based on the correlation of the new high-resolution $\delta^{13}C_{org}$ data set (Bowman and Bralower, 2005 and this study) to global reference sections with a more robust biostratigraphic framework, we suggest modifying the placement of the CTB, to 581.5 mbs.

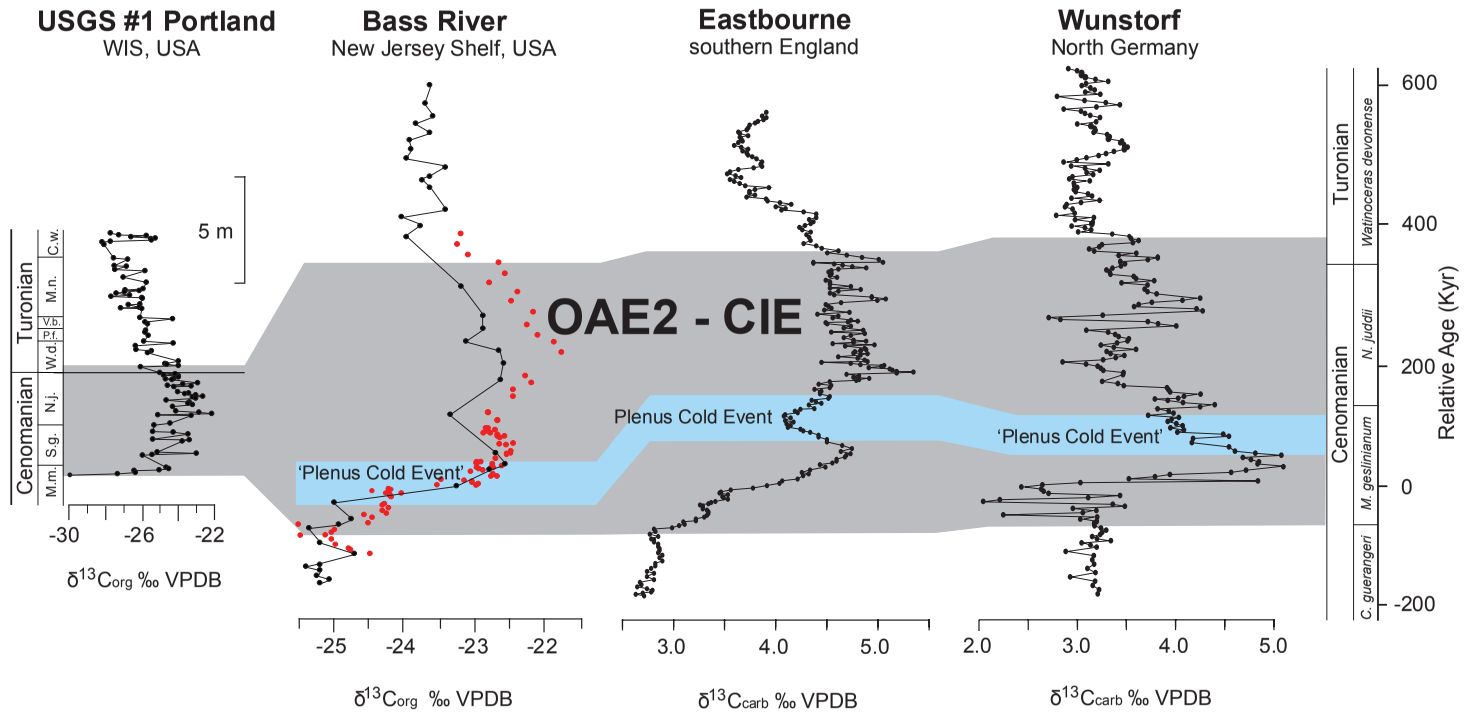

Figure S1. *Correlation scheme of Cenomanian-Turonian boundary time interval carbon isotope stratigraphies of four shelf sites, linking the Bass River borehole (this study) to the USGS #1 Portland core, located close to the GSSP at Pueblo (Sageman et al., 2006), Eastbourne (Paul et al., 1999) and the Wunstorf core (Voigt et al., 2008). Placement of the gray area, representing OAE2, and relative age scale are after Voigt et al. (2008). For the carbon isotope curve of Bass River, $\delta^{13}C_{org}$ data in black are generated in this study, data in red are adopted from Bowman and Bralower (2005). The blue bar depicts the 'Plenus Cold Event' recognized in the Bass River borehole through severe cooling in TEX_{86}^{H} -based SST reconstructions.*

Table S1. *Bulk geochemical, TEX_{86} and BIT data for the Bass River borehole ODP Leg 174AX. Ftbs = feet below surface, mbs = meters below surface, n.d. = not determined, ppm = parts per million, *calibration according to Kim et al. (2010).*

Depth (ftbs)	Depth (mbs)	TOC (%)	$\delta^{13}C_{TOC}$ (‰VPDB)	C_{org}/P_{tot} (mol/mol)	TEX_{86}	SST (°C)*	BIT-index	Al (%)	Ti (ppm)	Ti/Al-ratio
1849.35	563.68	n.d.	n.d.	n.d.	0.896	35.3	0.08	7.87	5248	0.067
1850.15	563.93	0.63	-24.28	42	0.895	35.3	0.08	7.72	5728	0.074
1854.15	565.14	0.86	-23.94	59	0.912	35.8	0.07	8.37	5463	0.065
1860.65	567.13	1.10	-23.97	76	0.909	35.8	0.08	10.35	5607	0.054
1864.65	568.35	0.47	-23.69	33	0.910	35.8	0.06	6.85	5116	0.075
1868.65	569.56	1.28	-23.93	95	0.900	35.5	0.08	10.56	5710	0.054
1870.65	570.17	0.43	-23.65	16	n.d.	n.d.	n.d.	5.33	3725	0.070
1872.05	570.60	0.65	-23.73	35	0.908	35.7	0.06	8.50	5509	0.065
1873.35	571.00	0.63	-23.63	39	0.923	36.2	0.04	8.12	5434	0.067
1874.65	571.39	1.10	-24.00	91	0.929	36.4	0.05	10.36	5498	0.053
1876.65	572.00	0.66	-23.59	47	n.d.	n.d.	n.d.	7.79	4758	0.061
1877.35	572.22	n.d.	n.d.	n.d.	n.d.	n.d.	n.d.	n.d.	n.d	n.d.
1879.35	572.83	0.84	-23.70	67	0.928	36.4	0.05	10.18	5501	0.054
1881.35	573.44	0.67	-23.58	48	n.d.	n.d.	n.d.	8.21	5021	0.061
1882.65	573.83	1.01	-23.83	68	n.d.	n.d.	n.d.	9.92	5159	0.052
1884.05	574.26	0.88	-23.60	66	0.929	36.4	0.05	10.18	5672	0.056
1885.35	574.65	1.04	-23.94	76	n.d.	n.d.	n.d.	9.77	4893	0.050
1886.65	575.05	0.70	-23.86	29	0.922	36.2	0.07	8.41	5047	0.060
1888.05	575.48	0.83	-23.98	77	n.d.	n.d.	n.d.	9.52	4818	0.051
1890.65	576.27	0.88	-23.60	64	0.926	36.3	0.04	10.00	5429	0.054
1891.35	576.48	1.02	-23.75	70	0.928	36.4	0.04	10.19	5041	0.049
1892.65	576.88	0.75	-23.60	53	0.924	36.2	0.04	10.04	5110	0.051
1896.05	577.92	0.59	-23.41	51	n.d.	n.d.	n.d.	8.29	4728	0.057
1897.35	578.31	0.86	-24.00	69	0.945	36.9	0.04	10.06	5369	0.053
1898.35	578.62	1.06	-23.76	94	n.d.	n.d.	n.d.	11.27	5369	0.048
1900.1	579.15	0.93	-23.94	64	0.941	36.8	0.04	9.76	5318	0.054
1901.35	579.53	n.d.	n.d.	n.d.	0.945	36.9	0.04	10.39	5273	0.051
1904.05	580.35	n.d.	n.d.	n.d.	0.926	36.3	0.05	11.32	5647	0.050
1906.05	580.96	n.d.	n.d.	n.d.	0.947	37.0	0.04	10.61	4796	0.045
1907.35	581.36	n.d.	n.d.	n.d.	0.922	36.2	0.04	8.95	5004	0.056
1908.05	581.57	1.13	-23.18	102	n.d.	n.d.	n.d.	9.75	5197	0.053
1909.35	581.97	n.d.	n.d.	n.d.	0.926	36.3	0.05	10.34	5184	0.050
1912.65	582.98	0.97	-22.85	104	0.916	36.0	0.05	8.46	4500	0.053
1914.65	583.59	1.22	-22.86	132	n.d.	n.d.	n.d.	10.03	4737	0.047
1915.35	583.80	n.d.	n.d.	n.d.	0.932	36.5	0.04	8.45	4438	0.053
1916.65	584.19	0.88	-23.10	99	0.911	35.8	0.05	8.94	4784	0.054
1918.05	584.62	1.09	-22.63	75	0.919	36.1	0.04	8.44	4415	0.052
1918.65	584.80	n.d.	n.d.	n.d.	0.903	35.6	0.05	6.14	3230	0.053
1919.35	585.02	n.d.	n.d.	n.d.	0.924	36.2	0.04	8.66	4231	0.049
1920.05	585.23	1.29	-22.60	138	0.917	36.0	0.05	9.67	5290	0.055
1920.65	585.41	n.d.	n.d.	n.d.	0.926	36.3	0.04	9.73	5518	0.057
1921.35	585.63	n.d.	n.d.	n.d.	0.902	35.5	0.04	8.13	4148	0.051
1922.05	585.84	n.d.	n.d.	n.d.	0.911	35.8	0.05	9.56	5362	0.056
1922.65	586.02	1.13	-22.63	82	0.910	35.8	0.05	9.24	5204	0.056
1923.35	586.24	n.d.	n.d.	n.d.	0.908	35.7	0.05	9.40	4737	0.050

Depth (ftbs)	Depth (mbs)	TOC (%)	$\delta^{13}C_{TOC}$ (‰VPDB)	C_{org}/P_{tot} (mol/mol)	TEX_{86}	SST (°C)*	BIT-index	Al (%)	Ti (ppm)	Ti/Al-ratio
1924.05	586.45	n.d.	n.d.	n.d.	0.907	35.7	0.05	9.38	4568	0.049
1924.65	586.63	n.d.	n.d.	n.d.	0.920	36.1	0.05	8.64	4238	0.049
1925.35	586.85	n.d.	n.d.	n.d.	0.908	35.7	0.05	9.01	4716	0.052
1926.15	587.09	n.d.	n.d.	n.d.	0.922	36.2	0.04	8.82	4547	0.052
1926.65	587.24	n.d.	n.d.	n.d.	0.907	35.7	0.04	8.58	4543	0.053
1927.35	587.46	n.d.	n.d.	n.d.	0.911	35.8	0.04	8.38	4666	0.056
1928.1	587.68	1.07	-23.36	109	0.942	36.8	0.04	9.78	5643	0.058
1928.65	587.85	n.d.	n.d.	n.d.	0.944	36.9	0.04	10.91	5645	0.052
1929.35	588.07	n.d.	n.d.	n.d.	0.930	36.4	0.04	10.60	5306	0.050
1930.15	588.31	n.d.	n.d.	n.d.	0.923	36.2	0.04	14.83	8059	0.054
1931.05	588.58	n.d.	n.d.	n.d.	0.931	36.5	0.03	9.99	5394	0.054
1932.35	588.98	n.d.	n.d.	n.d.	0.930	36.4	0.04	14.05	7386	0.053
1934.05	589.50	1.41	-22.70	128	0.927	36.4	0.03	10.13	4949	0.049
1934.65	589.68	n.d.	n.d.	n.d.	0.925	36.3	0.03	10.14	4833	0.048
1935.35	589.89	n.d.	n.d.	n.d.	0.946	36.9	0.05	9.57	4448	0.046
1935.95	590.08	1.12	-22.54	101	0.844	33.6	0.04	8.81	4877	0.055
1936.65	590.29	1.51	-22.76	146	0.912	35.8	0.03	8.38	3953	0.047
1937.35	590.50	n.d.	n.d.	n.d.	0.853	33.9	0.05	7.52	4119	0.055
1938.55	590.87	n.d.	n.d.	n.d.	0.867	34.4	0.04	7.04	4205	0.060
1939.35	591.11	0.61	-23.27	56	0.841	33.4	0.06	5.96	3523	0.059
1940.05	591.33	n.d.	n.d.	n.d.	0.875	34.6	0.04	7.18	4597	0.064
1940.65	591.51	n.d.	n.d.	n.d.	0.887	35.0	0.06	8.63	4911	0.057
1941.25	591.69	n.d.	n.d.	n.d.	0.902	35.5	0.06	9.23	5471	0.059
1942.05	591.94	1.06	-25.00	97	0.883	34.9	0.05	10.23	5178	0.051
1942.65	592.12	n.d.	n.d.	n.d.	0.907	35.7	0.05	9.36	5022	0.054
1943.35	592.33	n.d.	n.d.	n.d.	0.912	35.9	0.05	8.48	4697	0.055
1944.05	592.55	n.d.	n.d.	n.d.	0.925	36.3	0.05	10.18	5366	0.053
1944.55	592.70	1.14	-24.73	84	0.927	36.3	0.04	10.07	5350	0.053
1945.25	592.91	1.04	-24.88	76	0.938	36.7	0.04	10.96	5533	0.050
1946.05	593.16	1.10	-25.33	80	0.925	36.3	0.04	11.19	5665	0.051
1946.65	593.34	n.d.	n.d.	n.d.	0.922	36.2	0.03	9.60	5436	0.057
1947.35	593.55	n.d.	n.d.	n.d.	0.928	36.4	0.03	9.84	5615	0.057
1948.15	593.80	0.83	-25.16	74	0.928	36.4	0.03	9.99	5817	0.058
1948.65	593.95	n.d.	n.d.	n.d.	0.919	36.1	0.04	10.05	5632	0.056
1949.35	594.16	n.d.	n.d.	n.d.	0.919	36.1	0.04	10.04	5281	0.053
1950.05	594.38	0.98	-24.69	68	0.921	36.2	0.04	9.70	5016	0.052
1951.35	594.77	0.79	-25.17	69	0.886	35.0	0.04	8.32	4996	0.060
1952.05	594.98	0.76	-25.39	60	0.926	36.3	0.05	8.83	5467	0.062
1952.55	595.14	0.88	-25.16	70	0.909	35.8	0.04	9.65	5695	0.059
1953.35	595.38	0.86	-25.22	69	0.917	36.0	0.04	9.67	5810	0.060
1954.05	595.59	0.76	-25.02	60	0.894	35.3	0.04	8.61	5116	0.059
1954.65	595.78	0.68	-25.15	63	0.851	33.8	0.06	7.54	4782	0.063

Table S2. *Summarized palynological results for the Bass River borehole ODP Leg 174AX. P. hyst. = Paleohystrichophora infusorioides, cpg = cysts per dry gram of sediment, ppg = palynomorphs per dry gram of sediment.*

Depth (ftbs)	Depth (mbs)	Total dinocysts (cpg)	*C. comp.*-*C. memb.* complex (cpg)	*P. hyst.* (cpg)	Total ter. pal. (ppg)	Saccate gymnosperm pollen (ppg)	T/M-ratio	T/M-ratio T = saccate gymnosperms exclusively
1849.35	563.68	n.d.	n.d.	n.d.	n.d.	n.d.	n.d.	n.d.
1850.15	563.93	2966	0	990	1951	347	0.37	0.06
1854.15	565.14	3147	0	986	2659	1674	0.44	0.28
1860.65	567.13	5199	0	878	4181	2881	0.43	0.3
1864.65	568.35	3337	0	1059	1223	551	0.26	0.12
1868.65	569.56	6973	0	1978	4244	2719	0.37	0.24
1870.65	570.17	n.d.	n.d.	n.d.	n.d.	n.d.	n.d.	n.d.
1872.05	570.60	2062	0	635	1211	831	0.36	0.25
1873.35	571.00	n.d.	n.d.	n.d.	n.d.	n.d.	n.d.	n.d.
1874.65	571.39	10085	0	3437	1809	1628	n.d.	n.d.
1876.65	572.00	n.d.	n.d.	n.d.	n.d.	n.d.	n.d.	n.d.
1877.35	572.22	10037	0	3990	2095	898	0.17	0.07
1879.35	572.83	8780	0	3477	1391	77	0.14	0.01
1882.65	573.83	n.d.	n.d.	n.d.	n.d.	n.d.	n.d.	n.d.
1884.05	574.26	4304	0	1428	1281	672	0.23	0.12
1885.35	574.65	n.d.	n.d.	n.d.	n.d.	n.d.	n.d.	n.d.
1886.65	575.05	2323	0	663	358	144	0.13	0.05
1888.05	575.48	n.d.	n.d.	n.d.	n.d.	n.d.	n.d.	n.d.
1889.35	575.87	n.d.	n.d.	n.d.	n.d.	n.d.	n.d.	n.d.
1890.65	576.27	7931	0	2585	1125	755	0.12	0.08
1891.35	576.48	8123	0	1841	1261	989	0.13	0.1
1892.65	576.88	6276	0	1402	1094	673	0.15	0.09
1896.05	577.92	n.d.	n.d.	n.d.	n.d.	n.d.	n.d.	n.d.
1897.35	578.31	9326	0	2447	414	217	0.04	0.02
1898.35	578.62	n.d.	n.d.	n.d.	n.d.	n.d.	n.d.	n.d.
1900.1	579.15	9718	0	2302	575	234	0.06	0.02
1901.35	579.53	8768	0	2628	719	513	0.08	0.05
1904.05	580.35	23277	0	6070	2521	772	0.1	0.03
1906.05	580.96	14850	0	4680	2371	2059	0.14	0.12
1907.35	581.36	12396	0	4468	1635	1308	0.12	0.09
1908.05	581.57	23380	0	9235	1410	1021	0.06	0.04
1909.35	581.97	10430	0	3675	1340	908	0.11	0.08
1912.65	582.98	n.d.	n.d.	n.d.	n.d.	n.d.	n.d.	n.d.
1914.65	583.59	n.d.	n.d.	n.d.	n.d.	n.d.	n.d.	n.d.
1915.35	583.80	13590	0	5180	2066	1368	0.13	0.09
1916.65	584.19	13011	0	4451	2390	1912	0.15	0.12
1918.05	584.62	24327	0	5098	5041	4248	0.17	0.14
1918.65	584.80	n.d.	n.d.	n.d.	n.d.	n.d.	n.d.	n.d.
1919.35	585.02	n.d.	n.d.	n.d.	n.d.	n.d.	n.d.	n.d.
1920.05	585.23	n.d.	n.d.	n.d.	n.d.	n.d.	n.d.	n.d.
1920.65	585.41	17865	0	4222	3864	1713	0.18	0.08
1921.35	585.63	n.d.	n.d.	n.d.	n.d.	n.d.	n.d.	n.d.
1922.05	585.84	n.d.	n.d.	n.d.	n.d.	n.d.	n.d.	n.d.
1922.65	586.02	11791	0	2099	1967	1285	0.14	0.09

Depth (ftbs)	Depth (mbs)	Total dinocysts (cpg)	*C. comp.*-*C. memb.* complex (cpg)	*P. hyst.* (cpg)	Total ter. pal. (ppg)	Saccate gymnosperm pollen (ppg)	T/M-ratio	T/M-ratio T = saccate gymnosperms exclusively
1924.65	586.63	12209	0	2468	1186	799	0.09	0.06
1925.35	586.85	n.d.	n.d.	n.d.	n.d.	n.d.	n.d.	n.d.
1926.15	587.09	16202	0	4553	1707	1306	0.09	0.07
1926.65	587.24	n.d.	n.d.	n.d.	n.d.	n.d.	n.d.	n.d.
1927.35	587.46	10232	0	2846	2898	1604	0.22	0.12
1928.1	587.68	14706	0	3602	1832	253	0.11	0.02
1928.65	587.85	n.d.	n.d.	n.d.	n.d.	n.d.	n.d.	n.d.
1929.35	588.07	n.d.	n.d.	n.d.	n.d.	n.d.	n.d.	n.d.
1930.15	588.31	15598	0	4593	2402	1343	0.13	0.07
1931.05	588.58	n.d.	n.d.	n.d.	n.d.	n.d.	n.d.	n.d.
1934.05	589.50	29472	0	7575	8745	6679	0.23	0.17
1934.65	589.68	18387	89	4175	5152	3997	0.21	0.16
1935.35	589.89	21690	124	2606	11171	7695	0.34	0.23
1935.95	590.08	14870	932	1935	3583	2293	0.19	0.12
1936.65	590.29	8109	474	947	7281	5742	0.46	0.36
1937.35	590.50	4959	102	741	1587	1086	0.26	0.16
1937.95	590.69	7042	1421	490	1585	1029	0.18	0.12
1938.55	590.87	8574	1357	679	3869	2013	0.31	0.16
1939.35	591.11	5079	112	1310	3497	2986	0.4	0.35
1940.05	591.33	8635	0	1439	2693	1460	0.23	0.13
1940.65	591.51	9539	0	1698	2703	1318	0.22	0.11
1941.25	591.69	16776	0	1352	2099	1316	0.11	0.07
1942.05	591.94	13079	0	2138	2588	1519	0.16	0.1
1942.65	592.12	12235	0	1670	2533	1382	0.17	0.09
1943.35	592.33	n.d.	n.d.	n.d.	n.d.	n.d.	n.d.	n.d.
1944.05	592.55	n.d.	n.d.	n.d.	n.d.	n.d.	n.d.	n.d.
1944.55	592.70	12668	0	2749	6158	2062	0.19	0.13
1945.25	592.91	15217	0	4976	1163	775	0.07	0.05
1946.05	593.16	16866	0	4739	706	1150	0.09	0.06
1946.65	593.34	n.d.	n.d.	n.d.	n.d.	n.d.	n.d.	n.d.
1947.35	593.55	10362	0	1961	914	245	0.08	0.02
1948.15	593.80	15576	0	3092	1338	149	0.08	0.01
1948.65	593.95	17164	0	3691	997	406	0.05	0.02
1949.35	594.16	n.d.	n.d.	n.d.	n.d.	n.d.	n.d.	n.d.
1950.05	594.38	27540	0	4105	3763	1482	0.12	0.05
1951.35	594.77	9749	0	2029	2489	1957	0.2	0.16
1952.05	594.98	5621	0	1207	924	677	0.14	0.1
1952.55	595.14	13069	0	3144	1320	758	0.09	0.05
1953.35	595.38	10053	0	1104	2116	1058	0.16	0.08
1954.05	595.59	15280	0	2867	1792	684	0.1	0.04
1954.65	595.78	6645	0	2732	2041	1197	0.23	0.13

4

Freshwater discharge controlled deposition of Cenomanian-Turonian black shales on the NW European epicontinental shelf (Wunstorf, North Germany)

"Pain is temporary. It may last a minute, or an hour, or a day, or a year, but eventually it will subside and something else will take its place. If I quit, however, it lasts forever. That surrender, even the smallest act of giving up, stays with me. So when I feel like quitting, I ask myself, which would I rather live with?"

Lance Armstrong, in: *It's Not About the Bike: My Journey Back to Life (2000)*

Abstract

Global warming, changes in the hydrological cycle and enhanced marine primary productivity all have been invoked to have contributed to the occurrence of widespread ocean anoxia during the Cenomanian-Turonian Oceanic Anoxic Event (OAE2; ~94 Ma), but disentangling these factors on a regional scale has remained problematic. We generated palynological and organic geochemical records that allow the separation of these forcing factors in a core spanning the OAE2 from Wunstorf, Lower Saxony Basin (LSB; North Gemany), which exhibits cyclic black shale – marl alternations related to the orbital precession cycle.

Despite the widely varying depositional conditions complicating the interpretation of the obtained records, TEX_{86}^{H} indicates that sea-surface temperature (SST) evolution in the LSB during OAE2 resembles that of previously studied sites throughout the proto-North Atlantic. Cooling during the so-called Plenus Cold Event interrupted black shale deposition during the early stages of OAE2. However, TEX_{86} does not vary significantly across marl-black shale alternations, suggesting that temperature variations did not force the formation of the cyclic black shale horizons. Relative (i.e., with respect to marine palynomorphs) and absolute abundances of pollen and spores are elevated during phases of black shale deposition, indicative of enhanced precipitation and run-off. High abundances of cysts from inferred heterotrophic and euryhaline dinoflagellates supports high run-off, which likely introduced additional nutrients to the epicontinental shelf resulting in elevated marine primary productivity.

We conclude that orbitally-forced enhanced precipitation and run-off, in tandem with elevated marine primary productivity, were critical in cyclic black shale formation on the northwest European epicontinental shelf and potentially for other OAE2 sections in the proto-Atlantic and Western Interior Seaway at similar latitudes as well.

1. Introduction

Dark, often laminated marine sediments that are usually devoid of fossil traces of benthic life and exhibit a total organic carbon (TOC) content of >1% (Creaney and Passey, 1993), were episodically deposited during Jurassic and Cretaceous times. The deposition of these sediments, generally referred to as black shales, has typically been taken to indicate ancient episodes of dys- or anoxic bottom water conditions (Schlanger and Jenkyns, 1976). During some of these episodes, anoxia developed widespread in one or more ocean basins; such episodes were termed Oceanic Anoxic Events (OAEs; Schlanger and Jenkyns, 1976). One of the most prominent, best-constrained and best-studied of these OAEs formed across the Cenomanian-Turonian boundary (CTB; ~94 Ma) and became known as OAE2 (e.g., Jenkyns, 2010). The widespread enhanced organic carbon burial in marine sediments during OAE2 is expressed by a worldwide documented >2‰ positive excursion in the carbon isotopic composition of carbonate ($\delta^{13}C_{carb}$) and organic matter ($\delta^{13}C_{org}$), with an estimated duration of 450-600 kyr (e.g., Voigt et al., 2008; Meyers et al., 2012b). This excursion likely resulted from enhanced burial of $\delta^{13}C$-depleted organic matter (Arthur et al., 1988; Tsikos et al., 2004) and therefore provides a C-isotopic signature of the global exogenic carbon pool, making it a proper tool to confidently correlate OAE2 sections.

Over the past decades, many studies have been conducted to unravel the processes responsible for this massive burial of organic carbon during OAEs, and OAE2 in particular. Extensive volcanism close to the CTB (e.g. Snow et al., 2005; Kuroda et al., 2007; Turgeon and Craser, 2008) has been linked to high levels of atmospheric CO_2 (e.g., Schouten et al., 2003; Sinninghe Damsté et al., 2008; Barclay et al., 2010), raising the temperatures of already warm oceans towards a maximum at the onset of OAE2 (e.g., Bice et al., 2006; Forster et al., 2007a, b), thereby diminishing oxygen solubility in the surface waters. This warming caused an enhanced hydrological cycle (Chapter 3), which would likely have contributed to increased rates of continental weathering and runoff (Blätter et al., 2011; Pogge von Strandmann et al., 2013). This, in turn would have led to at least seasonal stratification and enhanced nutrient supply to continental margins and epicontinental seas. Extensive volcanism may also have directly contributed to ocean fertilization (Kerr et al., 1998; Snow et al., 2005), while changes in proto-Atlantic circulation may have increased the strength of upwelling (e.g., Poulsen et al., 2001; Junium and Arthur, 2007). Enhanced regeneration of sedimentary phosphorus from dysoxic and anoxic sediments (e.g., Kuypers et al., 2004b; Mort et al., 2007) combined with abundant nitrogen-fixing cyanobacteria (Kuypers et al., 2004b) may have sustained high levels of primary productivity. All of the above factors would conspire to expansion of oxygen minimum zones and oxygen depletion of bottom waters, leading to enhanced organic carbon burial.

As a result of late Cenomanian sea level rise (e.g., Erbacher et al., 1996; Voigt et al., 2006), large parts of continents became flooded, greatly expanding the extent of epicontinental shelf seas where sediments recording the OAE2 were deposited. Particularly the Lower Saxony Basin (LSB; northwest Germany) exhibits expanded and

complete OAE2-succesions (Wilmsen, 2003) containing several cyclic alternations of organic-poor marls, limestones and organic-rich black shales (Voigt et al., 2008). Organic matter accumulation on the European shelf was relatively modest, however, compared with other cyclic OAE2-sections in the proto-Atlantic (Kuypers et al, 2004a; Forster et al., 2008).

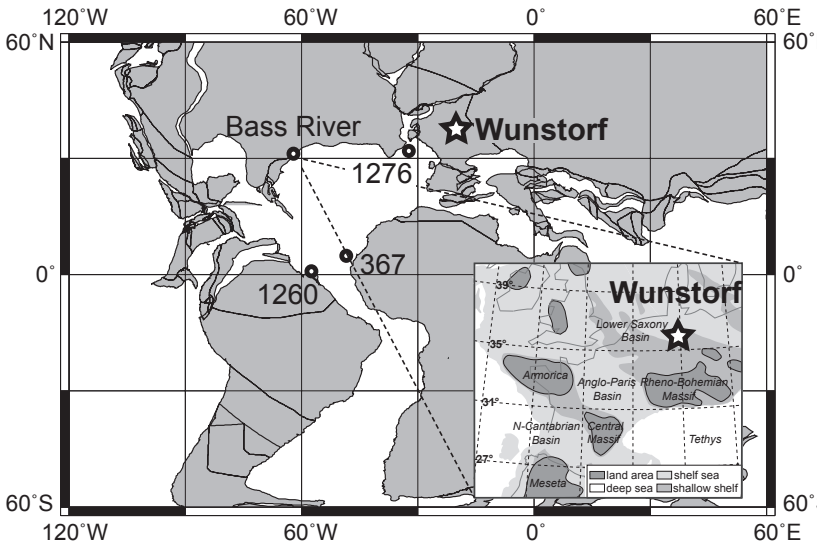

Figure 1. *Paleotectonic reconstruction for the Cenomanian-Turonian boundary time interval, with the location of the Wunstorf core and sections with previously published TEX_{86}-based SST-records: Bass River, DSDP site 367, ODP sites 1260 and 1276 indicated (map generated at http://www.odsn.de/odsn/services/paleomap/paleomap.html). Inset map shows a detailed paleogeographic reconstruction of central and western Europe, including the location of the Wunstorf core (modified from Voigt et al., 2004).*

The complete OAE2-interval has been recovered from the LSB through coring at Wunstorf (Erbacher et al., 2007; North Germany; Fig. 1). Application of an orbital cycle-based age model has shown that black shale deposition in the Wunstorf core sediments is consistent with precession forcing (Voigt et al., 2008). This implies that climate change resulting from orbital fluctuations was directly related to phases of black shale deposition. The robust cyclostratigraphy and biostratigraphic zonation of the Wunstorf core allows for a high-resolution study of astronomically-induced climate change. Here we aim to reconstruct mean annual sea surface temperature (SST), hydrological changes and marine primary productivity, to determine the dominant control on decreasing oxygen concentrations during OAE2 on the European shelf. To this end, we combined organic geochemical (TEX_{86}; BIT index) and palynological proxies, notably organic-walled dinoflagellate cysts (dinocysts) and pollen and spore abundances, across the CTB for the Wunstorf core.

2. Material and Methods

2.1. Site description, depositional setting and age model

The Wunstorf core was drilled in 2006 ~25 km west of Hannover, Germany (TK 25 Wunstorf, no. 3522, 52°23.942'N, 9°28.824'E; Fig. 1). Approximately 76 m of middle Cenomanian to middle Turonian sediments, comprising a ~13.5 m thick CTB succession, were retrieved. During the Late Cretaceous, the drill site was located in the LSB, which was part of the expanded epicontinental shelf sea that covered most of Eurasia after the Cenomanian transgression (Hancock and Kauffman, 1979). The sediments at Wunstorf were deposited at an estimated water depth of 100-150 m based on sequence stratigraphy, sedimentological analysis and (micro)fossil content (Wilmsen, 2003). The most proximal exposed land, the Rheno-Bohemian Massif, was located ~150 km to the south and formed a barrier towards the Western Tethys. The Armorican and British massifs formed a barrier towards the Atlantic, while the Fennoscandian Shield formed a barrier to the open ocean in the north (Fig. 1; Wilmsen, 2003).

The OAE2-interval at Wunstorf is part of the Hesseltal Formation and occurs between 49.6 and 23.1 meters below surface (mbs). The Hesseltal Formation consists of rhythmically alternating couplets of finely laminated black shales relatively rich in total organic carbon (TOC; max. 2.8%; Hetzel et al., 2011; Fig. 2b), gray to green marls, and light-gray (marly) limestones (Fig. 2; Erbacher et al., 2007; Voigt et al., 2008). The cyclic lithology results from a depositional system greatly influenced by precession (Voigt et al., 2008). Biostratigraphic zonation for the Hesseltal Formation relies on inoceramids, ammonites, acme occurrences of macrofossils and planktonic foraminifera that can be reliably correlated regionally and globally (Ernst et al., 1984; Voigt et al., 2008, and references therein).

The onset of the OAE2-interval is primarily based on the first occurrence (FO) of the ammonite *Metoicoceras geslinianum* at 49.6 mbs, consistent with the English Chalk (Voigt et al., 2008). At 47.8 mbs, the onset of the characteristic positive shift in $\delta^{13}C_{carb}$ (~2‰) and $\delta^{13}C_{org}$ (~2.5‰) was recognized (Voigt et al., 2008; Du Vivier et al., 2014; Fig. 2a). The termination of the OAE2-interval at Wunstorf was placed at 36 mbs (Voigt et al., 2008). The duration of the OAE2 for the Wunstorf core was estimated at ~435 kyr or ~500 kyr based on spectral analyses of the lithological cyclicity and $\delta^{13}C_{org}$, respectively (Voigt et al., 2008; Du Vivier et al., 2014).

2.2. Total organic carbon analysis

About 0.3 g of freeze-dried and powdered sediment sample was decalcified using 1M HCl, followed by rinsing with demineralized water and drying again. Total organic carbon (TOC) concentrations were measured using a Fisons Instruments CNS NA 1500 analyzer and corrected for weight loss during decalcification. Results were normalized to in-house standards, acetanilide, atropine and nicotinamide. The average analytical uncertainty based on duplicate analyses of sediment samples was 0.04 weight percent (wt.%).

2.3. *Organic geochemistry*

For 48 samples, organic molecules were extracted from 10-15 g of powdered and freeze-dried sediments with a Dionex accelerated solvent extractor (ASE) using dichloromethane (DCM)/methanol mixture (9:1, v/v). Total lipid extracts (TLEs) were evaporated to near dryness using rotary evaporation. Subsequently, remaining solvents were removed under a nitrogen flow. The TLEs were separated by Al_2O_3 column chromatography, into apolar, ketone, glycerol dialkyl glycerol tetraether (GDGT) and polar fractions using the eluents hexane/DCM (9:1, v/v), ethyl acetate (v), DCM/methanol (95:5, v/v) and DCM/methanol (1:1, v/v), respectively. The apolar and GDGT fractions were dried under a nitrogen flow and weighed. Selected apolar fractions were measured using gas chromatography-mass spectrometry (GC – MS), to determine the thermal maturity of the sediments based on the degree of isomerisation of hopanes. Analyses were performed on a Thermo Finnigan Trace gas chromatograph (GC) Ultra connected to a Thermo Finnigan DSQ mass spectrometer operated at 70 eV, with a range of m/z 50 – 800 and a cycle time of 3 scans s^{-1}. The temperature program and column conditions resemble that of Sinninghe Damsté et al. (2008). To quantify the GDGT abundances a known amount of C_{46} GDGT-standard was added (Huguet et al., 2006), after which the GDGT-fractions were re-dissolved in hexane/propanol (99:1, v/v) and filtered over a 0.45 μm mesh PTFE filter. The filtered GDGT fractions were analysed using high performance liquid chromatography – atmospheric pressure chemical ionization/mass spectrometry (HPLC-APCI/MS) according to the method described in Schouten et al. (2007). Analysis were performed on an Agilent 1290 infinity series coupled to a 6130 single quadrupole MSD, equipped with auto-injection system and HP-Chemstation software. Separation was achieved on a Prevail Cyano column (150 mm x 2.1 mm, 3 μm; Alltech). Selective ion monitoring was used to detect the GDGTs, for which it was exhibited that for samples with a high TEX_{86} value, a concentration of 0.1 ng of injected GDGTs on the LC column was still sufficient to yield trustworthy TEX_{86} values (Schouten et al., 2007). The minimum GDGT concentration injected on the LC column per measurement in this study was ~0.3 ng. TEX_{86}-index values were calculated after Schouten et al. (2002), and converted to absolute annual average sea surface temperatures (SSTs) using the TEX_{86}^{H} Kim et al. (2010) modern core top calibration, which has a calibration error of 2.5°C. Analytical reproducibility was generally better than 0.3°C.

The Branched and Isoprenoid Tetraether (BIT) index was used to estimate the relative abundance of soil organic matter in marine sediments (Hopmans et al., 2004). The BIT index is based on the amount of predominantly soil-derived branched GDGTs (brGDGTs) relative to the isoprenoid GDGT (iGDGT) crenarchaeol, which is chiefly derived from marine Thaumarchaeota.

2.4. *Palynology*

In total 51 samples were prepared for quantitative palynological analysis. In general between 5 and 10 g, and for samples low in organic carbon up to ~20 g, of freeze-dried

sediment sample were crushed to pieces smaller than 5 mm. Subsequently a known amount of *Lycopodium clavatum* marker spores was added to allow for quantitative analysis. After reaction with ~30% HCl and twice with ~38% HF, to dissolve carbonates and silicates respectively, ultrasonic separation was employed. Finally, samples were sieved over a 15 μm nylon mesh. Residuals were mounted on slides for microscopic analysis. Approximately 250 dinocysts per sample were counted using a light microscope at 500x magnification. Taxonomy follows that of Fensome and Williams (2004). Pollen and spores were counted as one group, except for saccate gymnosperm pollen. All samples and slides are stored in the collection of the Laboratory of Palaeobotany and Palynology, Utrecht University, the Netherlands.

3. Results

3.1. Total organic carbon

Trends in, and absolute values of, TOC (Fig. 2) are generally in agreement with results reported by Hetzel et al. (2011), i.e., relatively high for black shales and low for marls and limestones. The background TOC content is <0.3%, somewhat higher than reported by Hetzel et al. (2011). Within the OAE2, four intervals with elevated TOC content are identified. The first interval is between 49 and 47.5 m and contains the first black shale, at the onset of the CIE. A second organic-rich cluster is recognized between ~44 and 42 mbs, with the maximum TOC content approaching 2%. The third organic-rich interval is from 41 to 39.5 mbs, with a maximum TOC content just over 2.5%. The last organic-rich cluster ranges from 37.5 to 35.5 mbs, with a maximum TOC content just above 2%. For the remainder of the record, only the youngest sample (26.51 mbs) has an elevated TOC content (close to 1.5%).

3.2. Thermal maturity

For the selected samples the hopane distribution was determined. $C_{31}17\beta,21\beta(H)$ hopane was the dominant hopane. No αβ-hopanes were encountered, so the (ββ/(ββ+βα+αα)) of hopane biomarkers was 1, in agreement with results on sediments from this core presented by Blumenberg and Wiese (2012). This indicates that the thermal maturity of the sedimentary organic matter was sufficiently low for the application of TEX_{86} paleothermometry (Schouten et al., 2004).

3.3. GDGT-based proxies

Except for Sample 41.45 mbs, all samples yielded quantifiable GDGT abundances, although with orders of magnitude differences in concentration (Fig. 2c). Total GDGT concentrations are in the range of 0.13-43 μg/g organic carbon (OC). Crenarchaeol concentrations vary by three orders of magnitude, whereas brGDGT concentrations vary by one to two orders of magnitude. High GDGT concentrations coincide with the organic carbon-rich black shales (Figs. 2b, c), while low GDGT concentrations coincide with organic-poor sediments (Figs. 2b, c). Values for the BIT-index range from 0.02, indicating

low relative abundances of soil-derived brGDGTs, to 0.56, evidencing substantial soil-derived input of brGDGTs. The BIT-index (Fig. 2d) is relatively high in the organic-poor intervals and generally low (i.e., <0.10) for the organic-rich black shale intervals. Values for TEX_{86} fluctuate between 0.71 and 0.99 (Fig. 2e).

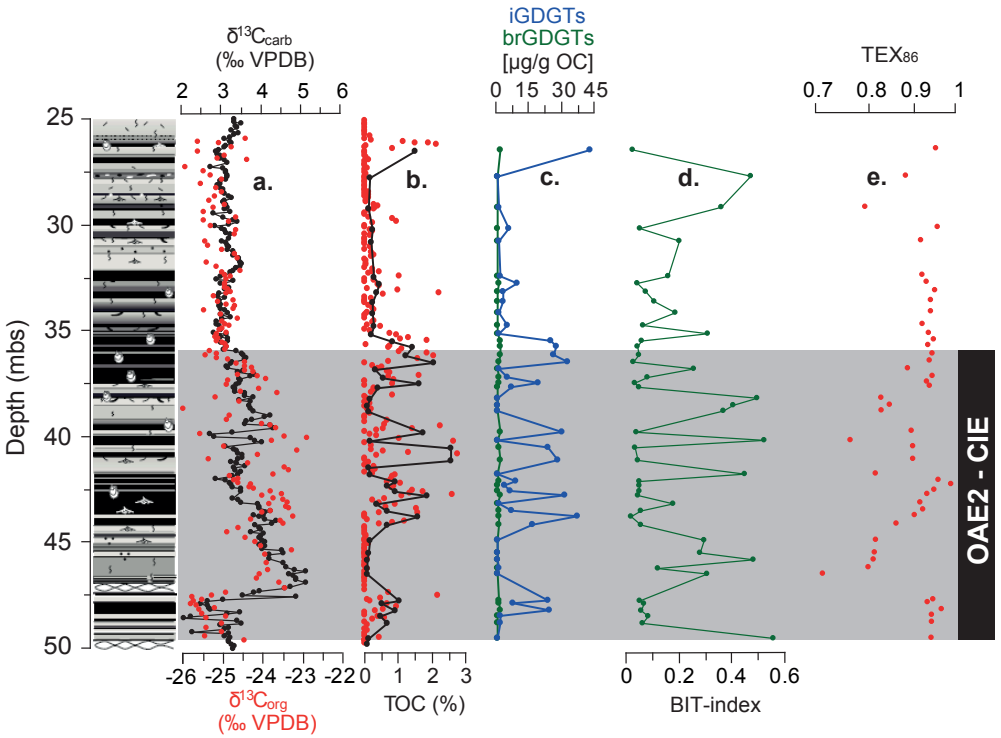

Figure 2. *Geochemical results for the Cenomanian-Turonian transition of the Wunstorf core. Stratigraphy from Voigt et al. (2008). (a) $\delta^{13}C_{carb}$ (Voigt et al., 2008) and $\delta^{13}C_{org}$ (Du Vivier et al., 2014; red). (b) Total organic carbon (TOC; black, this study; red, Hetzel et al., 2011). (c) concentrations of summed iGDGTs and summed brGDGTs [µg/g OC]. (d) BIT-index. (e) TEX_{86}-values. The gray zone indicates the OAE2-interval cf. Voigt et al. (2008). mbs = meters below surface.*

3.4. Palynology

Nine samples were barren of palynomorphs (Fig. 3c). For the remaining 42 samples, dinocyst concentrations range from ~35 to 15000 cysts per gram, and pollen and spores concentrations range from 10> to 5000 grains per gram, with highest concentrations in the organic-rich black shales (Fig. 3c).

Palynological assemblages are dominated by dinocysts, ~85% on average (max. >99%). Summed pollen and spores, and hence the terrestrially derived fraction, comprises on average ~15% of the assemblage (max. ~40%). The terrestrial over marine palynomorph ratio (T/M-ratio) was calculated by dividing terrestrial palynomorphs (pollen and spores)

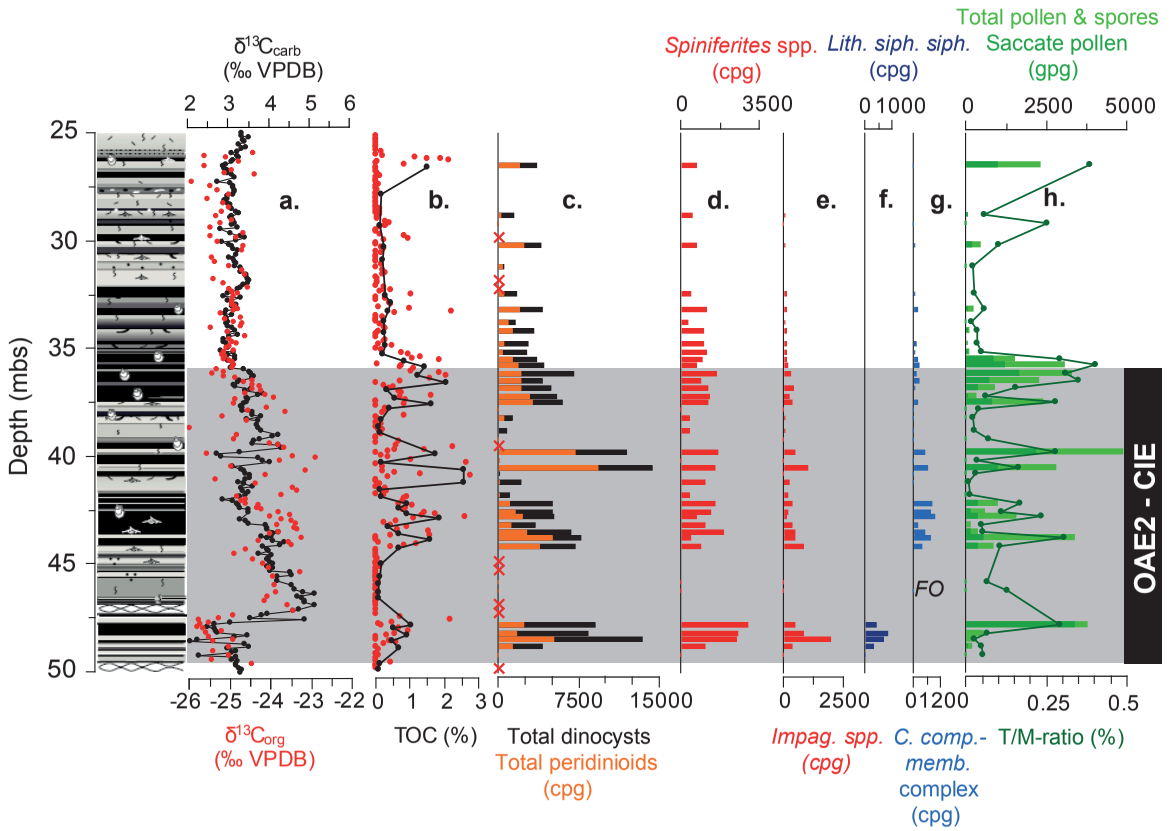

Figure 3. *Geochemical and palynological results for the Cenomanian-Turonian transition of the Wunstorf core. Stratigraphy from Voigt et al. (2008). (a) $\delta^{13}C_{carb}$ (Voigt et al., 2008) and $\delta^{13}C_{org}$ (Du Vivier et al., 2014; red). (b) Total organic carbon (TOC; black, this study; red, Hetzel et al., 2011). (c) Total dinocyst concentrations (black) and total peridinioidal cysts (orange) per gram sediment dry weight (cpg). (d) Dinocyst species Spiniferites spp. (cpg). (e) Dinocyst species Impagidinium spp. (cpg). (f) Dinocyst species Lithosphaeridium siphoniphorum siphoniphorum (cpg). (g) Dinocyst species Cyclonephelium compactum – membraniphorum complex (cpg). (h). Terrestrial vs. marine palynomorphs (T/M-ratio) and total pollen and spores in grains per dry gram of sediment (gpg), saccate gymnosperm pollen in dark green. The gray zone indicates the OAE2 interval cf. Voigt et al. (2008). mbs = meters below surface.*

by aquatic palynomorphs (dinocysts and acritarchs). In general T/M-values are elevated in the organic-rich intervals (Fig. 3h), while minima in the T/M-ratio correspond to organic-poor intervals.

Age-diagnostic dinocyst species include *Lithosphaeridium siphoniphorum siphoniphorum*, a marker species for the CTB-interval in the northwest European reference section at Eastbourne (Pearce et al., 2009). The last occurrence of *L. siphoniphorum siphoniphorum* is at 47.81 mbs (Fig. 3f), confirming a latest Cenomanian age.

Dinocyst assemblages are dominated by multiple species of the Peridiniaceae family, i.e., *Paleohystrichophora infusorioides*, *Subtilisphaera pontis-mariae*, *Eurydinium saxoniense*, *Isabelidinium* spp., and *Ginginodinium* spp.. Members of this family have repeatedly been shown to be derived of low-salinity tolerant dinoflagellates in Late Cretaceous and Paleogene successions and likely represent heterotrophic, euryhaline dinoflagellates (e.g., Harland, 1973; Sluijs and Brinkhuis, 2009; Powell et al., 1990; Lewis et al., 1990; Fig. 3c). Other quantitatively important taxa include *Spiniferites* spp. (Fig. 3d) and *Impagidinium* spp. (Fig. 3e), which are generally associated with outer shelf to oceanic environments (e.g., Wall et al., 1977; Harland, 1983; Brinkhuis, 1994). Commonly present are representatives of *Odontochitina*, *Oligosphaeridium*, *Exochosphaeridium*, *Downiesphaeridium*, *Cyclonephelium*, *Lithosphaeridium*, *Achomosphaera*, and *Florentinia* spp., which are, like most encountered pollen and spores, typical for Late Cretaceous dinocyst shelf to bathyal assemblages (e.g., Dodsworth, 2004a, b; Pearce et al., 2009; Peyrot et al., 2012).

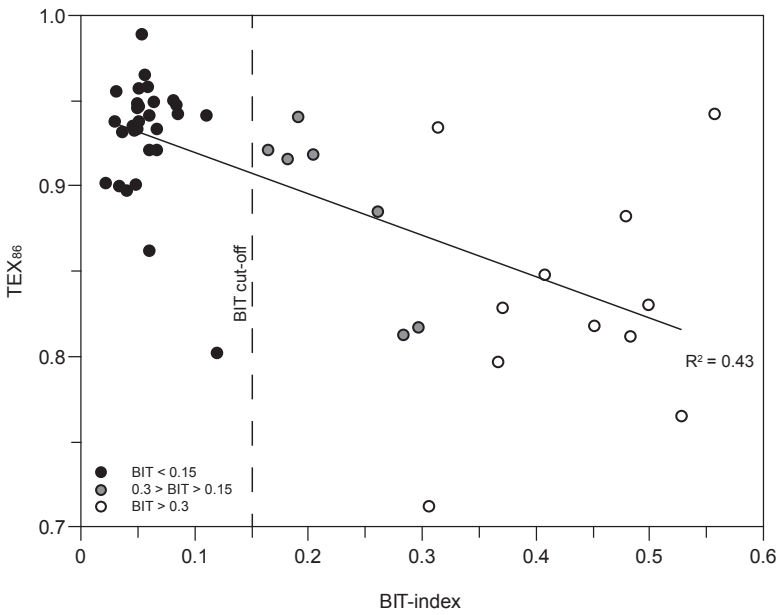

Figure 4. *Cross plot of TEX_{86} versus BIT-index values.*

4. Discussion

4.1. SST reconstruction

4.1.1. Input of terrestrially derived GDGTs and post-depositional oxidation

Small quantities of iGDGTs as used for determination of TEX_{86} values, are also produced in soils. High input of soil-derived iGDGTs, reflected by elevated BIT index values, might therefore bias TEX_{86}-derived SST reconstructions (Weijers et al., 2006). TEX_{86} and BIT index values for the OAE2-record of the Wunstorf core exhibit a negative linear relation (R^2-value of 0.43; Fig. 4), which may be the result of relatively high input of soil-derived iGDGTs, potentially affecting TEX_{86} values. Previous work has recommended a cut-off value of the BIT index to exclude this effect from TEX_{86}-based paleo-SST reconstructions (Weijers et al., 2006).

Low-TOC sediments have high BIT index values and low TOC-normalized concentrations for brGDGTs and, to a larger extent, iGDGTs (Fig. 5). This is similar to results from TOC-rich turbidites that are affected by post-depositional oxidation (e.g., Huguet et al., 2008; Lengger et al., 2013). This was explained by preferential preservation of soil-derived brGDGTs over marine-derived iGDGTs upon post-depositional oxidation of the turbidites. For the Wunstorf section, the marls and limestones represent depositional phases during which the water column and pore waters of surface sediments contained relatively high concentrations of oxygen, as is evident from bioturbation, low TOC content (Fig. 2b), and low levels of redox-sensitive trace elements (Hetzel et al., 2011). Diagenetic effects caused by the oxidation of biomarkers in the water column and pore waters most likely played a substantial role in this depositional setting. Preferential preservation of brGDGTs is therefore likely responsible for the observed pattern in the BIT-index. Although Lengger et al. (2013) did not find a bias in TEX_{86} values for sediments that suffered post-depositional oxidation, other studies have shown that there can be a considerable post-depositional oxidation effect on TEX_{86} values and thus the paleo-SST reconstructions derived from it (e.g., Huguet et al., 2009). The linear correlation between TEX_{86} and BIT-index values for the analyzed sediments of the Wunstorf core, is in line with the latter.

Based on the relation between TOC and the BIT-index (Fig. 5a) and the concentrations of the sum of the brGDGTs and crenarcheol (Fig. 5b), we decided to remove reconstructed paleo-SST data with a BIT-index >0.15. This changes the linear correlation between TEX_{86} and BIT-index, suggesting that samples with a BIT-index >0.15 are affected by post-depositional oxidation. This results in a dataset in which samples with a BIT-index value between 0.02 and 0.12 are considered for paleo-SST reconstructions, removing the impact of soil-derived iGDGTs on the paleo-SST reconstructions.

4.1.2. Trends and absolute values

Trends and values of the reconstructed SSTs at Wunstorf using the TEX_{86}^{H}-calibration of Kim et al. (2010; Fig. 6c) are similar to previous TEX_{86}-based SST reconstructions for OAE2. Previously studied sites were located in the equatorial Atlantic (DSDP Site 367 and

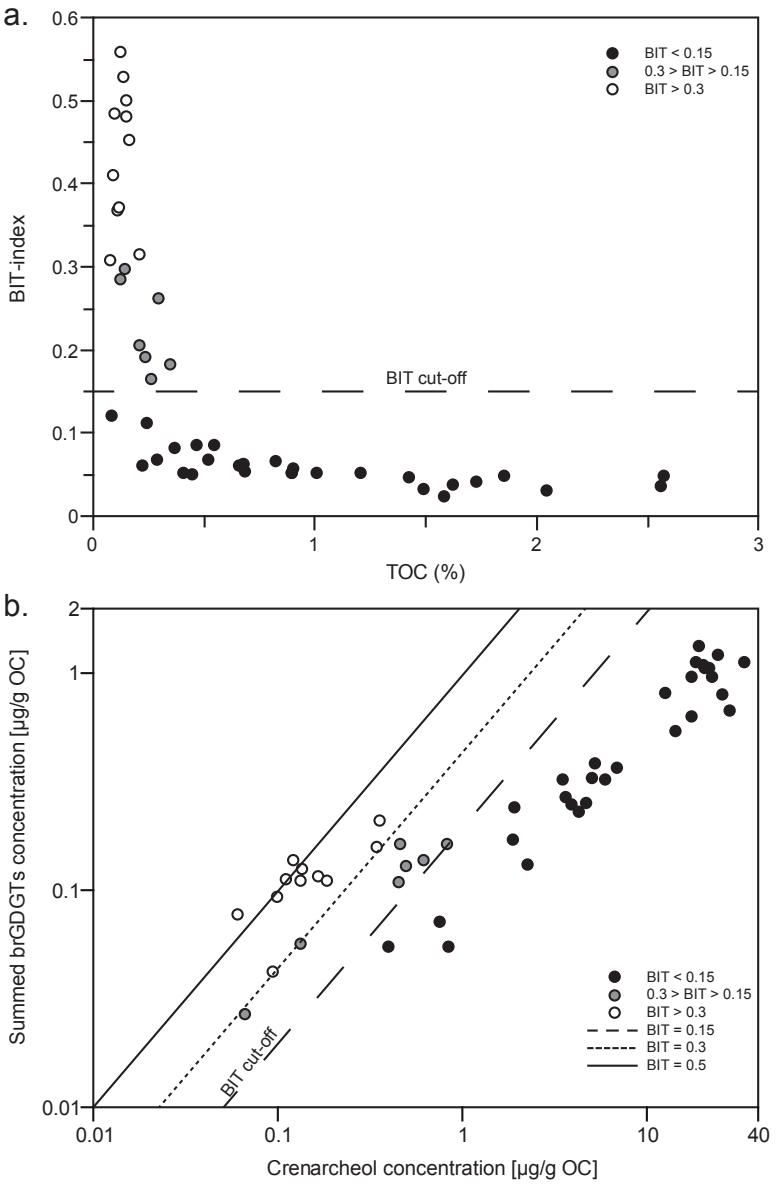

Figure 5. *(a) Cross plot of summed brGDGTs [µg/g OC] versus crenarcheol [µg/g OC] on a logarithmic axis. (b) Cross plot of BIT-index values versus total organic carbon (TOC).*

ODP Site 1260 – Forster et al., 2007b) and the mid-latitudes (ODP Site 1276 – Sinninghe Damsté et al., 2010; Bass River – Chapter 3; Fig. 1). Potentially due to a lack of reliable TEX_{86} values at the onset of the OAE2-interval (Fig. 6b) the Wunstorf SST-record does

not capture the rapid warming in SST at the onset of OAE2, previously attributed to a rise in atmospheric CO_2 released by extensive volcanism (e.g., Forster et al., 2007b). The Wunstorf SST-record does show, however, a ~5°C cooling pulse during the early stages of OAE2 (Fig. 6c). Based on its stratigraphic position within the carbon isotope excursion, we attribute this pulse to the Plenus Cold Event (Gale and Christensen, 1996). The Plenus Cold Event, previously recognized as an incursion of boreal fauna in the shelf seas of NW Europe (e.g., Jefferies, 1962; Gale and Christensen, 1996; Voigt et al., 2004), has by now been identified as a substantial cooling event in TEX_{86}-based paleo-SST records at DSDP Site 367, ODP Site 1260, ODP Site 1276, Bass River (all proto-North Atlantic Basin; Forster et al., 2007b; Sinninghe Damsté et al., 2010; Chapter 3) and Wunstorf, suggesting that it was a hemisphere-wide and perhaps even a global signal. This supports the hypothesis that enhanced global carbon burial temporary suppressed atmospheric CO_2 levels during OAE2 (Sinninghe Damsté et al., 2010).

Interestingly, this interval marks the occurrence of the *Cyclonephelium compactum-membraniphorum* complex (*Ccm*) within the OAE2-interval in the Wunstorf core (Fig. 6c,d). This is in accordance with previous records from the Bass River section (Chapter 3). Although the biogeographic distribution of this complex is still partly unclear, this suggests that the introduction of *Ccm* at mid-latitude sites in both northwest Europe and the east coast of North-America was quasi-instantaneous and linked to the Plenus Cold Event

Site	Estimated paleolatitude	TEX_{86} range (average)	Reconstructed paleo-SST[a] range (average)
ODP Site 367 [b]	5°N	0.84-0.95 (0.90)	33-37°C (36°C)
ODP Site 1260 [b]	0°	0.85-0.95 (0.92)	34-37°C (36°C)
ODP Site 1276 [c]	30°N	0.74-0.96 (0.90)	30-37°C (36°C)
Bass River [d]	30°N	0.84-0.95 (0.91)	33-37°C (36°C)
Wunstorf	40°N	0.80-0.99 (0.93)	32-38°C (36°C)

Table 1. *Overview of the different sites for which TEX_{86}-paleothermometry was applied over the OAE2-interval, and TEX_{86} values and paleo-SST ranges and averages. [a]Based on the TEX_{86}^{H} calibration by Kim et al. (2010), [b]Forster et al. (2007b), [c]Sinninghe Damsté et al. (2010), [d]Chapter 3.*

No significant difference in the reconstructed SSTs is recorded between the black shales and the more TOC-lean marls and limestones. This suggests that the cyclic deposition of black shales during OAE2 in the LSB was not primarily driven by changes in SST.

Average SSTs for the OAE2-interval at Wunstorf are higher than at Bass River (New Jersey Shelf), DSDP Site 367 (Cape Verde Basin), ODP Site 1260 (Demarara Rise), and Site 1276 (North Atlantic; Table 1), which may perhaps be an artefact of the low resolution achieved for the Plenus Cold Event at Wunstorf. Reconstructions of absolute temperatures based on TEX_{86} at values significantly exceeding the modern calibration may yield significant errors. Nonetheless, the warm and relatively stable background SSTs for Wunstorf (~37°C) suggest that SSTs on the European shelf were exceptionally high and

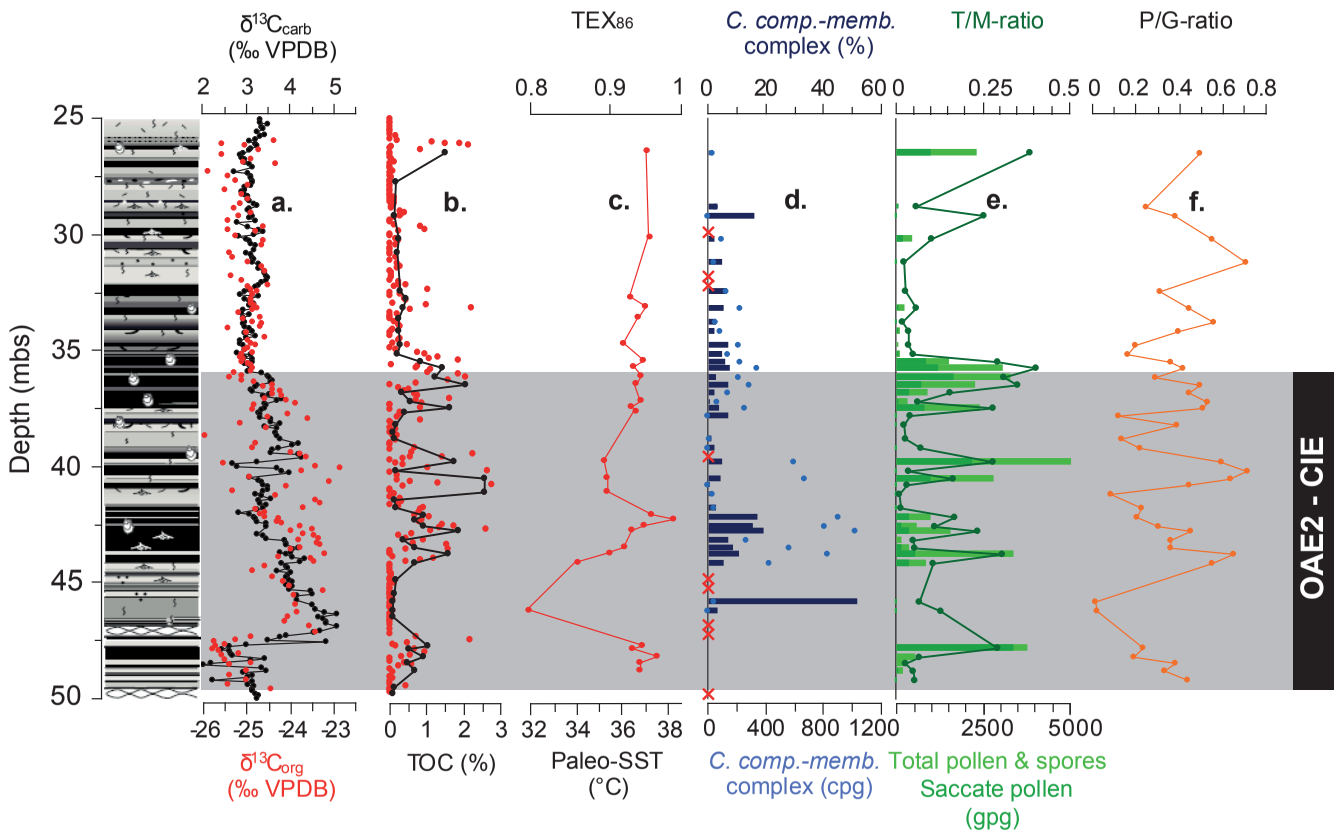

Figure 6. *Geochemical and palynological results for the Cenomanian-Turonian transition of the Wunstorf core. Stratigraphy from Voigt et al. (2008). (a) $\delta^{13}C_{carb}$ (Voigt et al., 2008) and $\delta^{13}C_{org}$ (Du Vivier et al., 2014; red). (b) Total organic carbon (TOC; black, this study; red, Hetzel et al., 2011). (c) TEX_{86}-values and TEX_{86}^{H}-based SST reconstructions (Kim et al., 2010). (d) Relative and absolute abundance in cysts per dry gram of sediment (cpg), of the dinocyst species Cyclonephelium compactum-membraniphorum complex, 'X' represents barren samples. (e) Terrestrial vs. marine palynomorphs (T/M-ratio) and total pollen and spores in grains per dry gram of sediment (gpg), saccate gymnosperm pollen in dark green. (f) Peridiniod vs. gonyaulacoid dinocysts (P/G-ratio). The gray zone indicates the OAE2 interval cf. Voigt et al. (2008). mbs = meters below surface.*

supports the notion that thermal gradients were substantially reduced during the Late Cretaceous greenhouse world (e.g., Baron, 1983; Huber et al., 1995).

4.2. Hydrology

Although pollen rank among the most resistant groups of palynomorphs (Traverse, 1994), there is evidence that pollen grains are degraded relatively rapidly (<10 kyr) in the presence of diffusively introduced oxygen (e.g., Keil et al., 1994). This may perhaps explain why absolute pollen and spores concentrations are higher in the black shales, deposited under anoxic conditions. This contrasts with the organic lean marls and limestones deposited in phases in which pore waters of surface sediments contained relatively high concentrations of oxygen. Despite evidence for some preferential preservation of some groups of dinocysts in Quaternary sediments (e.g., Zonneveld, et al., 1997; Versteegh and Zonneveld, 2002), in general the same holds for dinocysts, explaining higher dinocyst concentrations in the black shales. Thin-walled dinocysts, e.g., *Paleohystrichophora infusorioides*, which would be expected to be lost from sediments upon oxidation most rapidly, are, however, commonly present in the organic lean marls and limestones. This shows that the preferential preservation of palynomorphs, and dinocysts in particular, may not be so straightforward in older sediments, e.g., the Cretaceous, as previously reported for some Quaternary sediments (e.g., Zonneveld, et al., 1997; Versteegh and Zonneveld, 2002).

Pollen and spores are transported to the marine environment by a wide range of processes ranging from river discharge, wind, to birds and insects (e.g., Traverse and Ginsburg, 1966; Thomson, 1986; Feinsinger and Busby, 1987). Particularly saccate gymnosperm pollen (bisaccates) may be transported by eolian pathways (e.g., Heusser, 1988). Palynological assemblages at Wunstorf contain relatively low amounts of saccate gymnosperm pollen (Fig. 6e; Prauss, 2006), suggesting that most pollen and spores encountered at Wunstorf were transported to the ocean by fluvial processes. The relatively high amounts of pollen and spores in the black shales at Wunstorf are therefore interpreted to represent phases of enhanced run-off. Enhanced run-off most likely resulted from increased (seasonal) precipitation over north and mid-European landmasses, assuming that these yielded significant vegetation cover. Regarding the distance to the coring site, non-saccate pollen and spores most likely originated from the Rheno-Bohemian Massif, which is in accordance with the prevailing paleo-wind directions (Hay and Floegel, 2012). Enhanced (seasonal) influx of fresh, low-density, surface waters could well have stratified the water column, leading to low-oxygen levels in bottom waters. This is also indicated by high abundances of bacterivorous ciliates (Blumenberg and Wiese, 2012), which graze on the interfaces of stratified water bodies (Sinninghe Damsté et al., 1995), supporting the presence of a chemocline in the water column. A persistent stratification of the water column ultimately leads to bottom water anoxia and the formation of black shales. The coupling of the rhythmical occurrence of the black shale layers to the precession cycle (Voigt et al., 2008) suggests that changes in the hydrological cycle were controlled by Earth's orbital parameters.

4.3. Marine Productivity

High abundances of dinocysts and organic matter in general may result from both enhanced marine primary productivity and an improved preservation potential for organic matter during black shale deposition. In modern oceans, most peridinioid dinocysts are produced by heterotrophic dinoflagellates, whilst most gonyaulacoid dinocysts are derived from autotrophic taxa (Lewis et al., 1990). As a consequence, the ratio between peridinioids and gonyaulacoids (P/G-ratio) has been employed widely as a proxy for paleoproductivity (Sluijs et al., 2005). In the Wunstorf OAE2-section, the P/G-ratio reaches maximum values within the different black shale couplets, implying that productivity was elevated during their deposition (Fig. 6f). Furthermore the peridinioids encountered at Wunstorf belong to the Peridiniaceae family, which has been shown to be low-salinity tolerant (e.g., Harland, 1973; Sluijs and Brinkhuis, 2009). Together, this suggests that during seasons of high precipitation and run-off that introduced nutrients a low-salinity, high-productivity surface layer existed in the Lower Saxony Basin. This hypothesis is supported by assemblages of calcareous nannofossils, showing a shift from a generally oligotrophic ecosystem to more mesotrophic or even eutrophic conditions during black shale deposition (Linnert et al., 2010).

Enhanced marine primary productivity likely contributed to the establishment of bottom water anoxia by increasing the flux of organic matter to the seafloor, depleting bottom water oxygen concentrations upon decay.

5. Conclusions

Despite differences in the preservation of organic matter throughout the OAE2-interval at Wunstorf, the general trend in reconstructed SSTs, including the cooling phase associated with the Plenus Cold Event, is consistent with the results of previous studies that targeted the proto-North Atlantic. Hence, the SST trend recorded at Wunstorf and the other sites was of at least hemispheric significance. Reconstructed SSTs do not substantially differ between black shales and less organic-rich deposits, implying that temperature was not the critical factor for the cyclic deposition of organic matter. Absolute SSTs for the Wunstorf OAE2-section show little or no difference in comparison with SST reconstructions for sites located at lower latitudes, which were evaluated using the same proxy and the same methodology. This confirms that thermal gradients were much reduced during the Late Cretaceous (Barron, 1983; Huber et al., 1995).

The dinocyst complex *Cyclonephelium compactum–membraniphorum*, previously linked to the Plenus Cold Event (Chapter 3), was encountered at the respective level at Wunstorf, suggesting that its occurrence is indeed linked to this cooling. Its continued presence in the remainder of the record suggests, however, that other paleoenviromental factors were also critical in controlling its distribution.

Black shale deposition for the OAE2-interval at Wunstorf relied on precession-driven changes (Voigt et al., 2008). We conclude, based on relatively high numbers of terrestrially

derived pollen and spores and freshwater tolerating dinocysts in the black shale intervals, that precession drove variations in the hydrological cycle. This caused (seasonal) freshwater stratification of the water column and likely enhanced primary production, ultimately culminating in bottom water anoxia and black shale formation. An orbitally controlled hydrological cycle may have been a critical factor triggering mechanism for other cyclic OAE2 sites located in the proto-Atlantic and Western Interior Seaway at similar latitudes as well.

Supplements to Chapter 4

Table S1. *Total organic carbon (TOC), summed iGDGT and brGDGT concentrations in [µg/g organic carbon (OC)], BIT-index, TEX_{86} values and SSTs reconstructed using the TEX_{86}^{H} calibration by Kim et al. (2010). mbs = meters below surface. n.d. = not determined.*

Sample depth (mbs)	TOC (%)	summed iGDGTs [µg/g OC]	summed brGDGTs [µg/g OC]	BIT-index	TEX_{86}	SST (°C)
26.51	1.49	42.34	1.13	0.03	0.955	37.2
27.75	0.15	0.21	0.13	0.48	0.882	n.d.
29.21	0.12	0.56	0.21	0.37	0.796	n.d.
30.21	0.23	5.01	0.25	0.06	0.957	37.3
30.79	0.21	0.67	0.13	0.21	0.918	n.d.
32.47	0.27	1.10	0.16	0.16	0.921	n.d.
32.78	0.45	8.77	0.37	0.05	0.933	36.5
33.21	0.37	2.45	0.17	0.08	0.950	37.1
33.69	0.25	2.51	0.24	0.11	0.941	36.8
34.21	0.24	0.62	0.11	0.19	0.940	n.d.
34.79	0.29	4.64	0.27	0.07	0.921	36.1
35.21	0.21	0.47	0.16	0.31	0.934	n.d.
35.51	0.83	24.04	1.34	0.06	0.949	37.0
35.81	1.43	27.17	1.06	0.05	0.935	36.6
36.21	1.21	25.80	1.09	0.05	0.945	36.9
36.51	2.05	31.94	0.80	0.03	0.937	36.7
36.81	0.30	0.64	0.16	0.26	0.885	n.d.
37.21	0.55	4.59	0.32	0.08	0.947	37.0
37.47	1.62	18.46	0.54	0.04	0.931	36.5
37.68	0.41	6.49	0.25	0.05	0.937	36.7
38.21	0.15	0.18	0.11	0.50	0.829	n.d.
38.53	0.09	0.25	0.12	0.41	0.847	n.d.
38.81	0.12	0.29	0.11	0.37	0.828	n.d.
39.81	1.73	29.75	0.97	0.04	0.896	35.3
40.21	0.14	0.22	0.14	0.53	0.764	n.d.
40.51	2.57	23.09	0.63	0.03	0.899	35.4
41.14	2.58	27.48	1.05	0.05	0.900	35.5
41.15	0.12	-	-	-	-	-
41.8	0.16	0.24	0.11	0.45	0.818	n.d.
42.16	0.90	8.04	0.32	0.05	0.957	37.3
42.34	0.69	2.93	0.13	0.05	0.989	38.3
42.61	0.90	5.61	0.23	0.05	0.948	37.0
42.81	1.86	30.79	1.21	0.05	0.932	36.5
43.21	0.35	0.85	0.14	0.18	0.916	n.d.
43.51	0.66	6.62	0.33	0.06	0.920	36.1
43.81	1.59	36.18	0.67	0.02	0.901	35.5
44.21	0.68	16.23	0.81	0.06	0.861	34.2
44.89	0.15	0.21	0.06	0.30	0.816	n.d.
46.21	0.08	0.64	0.05	0.12	0.802	32.0
46.51	0.08	0.21	0.04	0.31	0.712	n.d.
47.74	1.01	23.26	0.96	0.05	0.946	36.9

Sample depth (mbs)	TOC (%)	summed iGDGTs [µg/g OC]	summed brGDGTs [µg/g OC]	BIT-index	TEX_{86}	SST (°C)
47.91	0.52	6.99	0.38	0.07	0.933	36.5
48.21	0.90	23.59	1.12	0.06	0.964	37.5
48.51	0.47	1.02	0.07	0.09	0.942	36.8
48.82	0.68	1.13	0.05	0.06	0.941	36.8
49.51	0.13	0.10	0.08	0.56	0.941	n.d.

Table S2. *Total dinocyst concentrations and total peridinioidal cysts per gram sediment dry weight (cpg). Pollen and spores and saccate gymnosperm pollen in grains per dry gram of sediment (gpg). Peridiniod vs. gonyaulacoid dinocysts (P/G-ratio). Terrestrial vs. marine palynomorphs (T/M-ratio). Dinocyst species Spiniferites spp., Impagidinium spp., Lithosphaeridium siphoniphorum siphoniphorum and Cyclonephelium compactum – C. membraniphorum complex (cpg). mbs = meters below surface.*

Sample depth (mbs)	Dinocysts (cpg)	Total peridiniod cysts (cpg)	Pollen and spores (gpg)	Saccate pollen (gpg)	P/G-ratio	T/M-ratio	*Impag.* spp. (cpg)	*Spin.* spp. (cpg)	*L. siph. siph.* (cpg)	*C. comp.-C. memb.* complex (cpg)
26.51	3755	2158	2342	1022	0.50	0.39	85	767	0	28
28.81	1620	454	95	71	0.25	0.06	123	546	0	55
29.21	24	9	9	4	0.38	0.25	1	0	0	4
29.81	-	-	-	-	-	-	-	-	-	-
30.21	4115	2497	467	230	0.55	0.10	112	767	0	98
31.21	724	521	18	9	0.71	0.02	50	61	0	38
31.81	-	-	-	-	-	-	-	-	-	-
32.21	-	-	-	-	-	-	-	-	-	-
32.47	1893	645	50	36	0.31	0.02	194	531	0	129
33.21	4253	2127	278	103	0.45	0.06	190	1206	0	222
33.81	1759	999	35	16	0.56	0.02	148	387	0	52
34.21	3427	1462	122	73	0.40	0.03	208	1101	0	86
34.81	2902	696	110	37	0.20	0.04	167	1046	0	209
35.21	2755	521	149	74	0.16	0.05	149	1223	0	138
35.51	3774	1505	1540	874	0.36	0.29	180	1041	0	222
35.81	4415	1991	3093	1229	0.42	0.40	237	763	0	339
36.21	7200	2279	3298	1689	0.29	0.31	349	1663	0	215
36.51	4197	2239	2307	774	0.49	0.35	61	926	0	288
36.81	4982	2302	940	405	0.45	0.15	448	1293	0	138
37.21	5606	3064	374	96	0.53	0.06	299	1303	0	64
37.47	6133	3299	2439	836	0.51	0.28	395	1255	0	256
37.81	23	3	1	1	0.12	0.04	3	3	0	2
38.21	1513	616	31	14	0.39	0.02	142	460	0	11
39.21	156	34	12	1	0.22	0.07	6	53	0	4
39.5	-	-	-	-	-	-	-	-	-	-
39.81	12138	7347	4906	2234	0.59	0.28	507	1704	0	599
40.21	328	234	13	4	0.72	0.04	10	1	0	1
40.51	14419	9425	2817	1024	0.64	0.16	1076	1588	0	666
40.81	297	131	10	1	0.44	0.03	12	75	0	3

Sample depth (mbs)	Dinocysts (cpg)	Total peridiniod cysts (cpg)	Pollen and spores (gpg)	Saccate pollen (gpg)	P/G-ratio	T/M-ratio	*Impag.* spp. (cpg)	*Spin.* spp. (cpg)	*L. siph. siph.* (cpg)	*C. comp.-C. memb.* complex (cpg)
41.21	2305	201	18	18	0.08	0.01	313	1128	0	27
41.81	1254	298	20	15	0.23	0.02	235	445	0	39
42.21	5216	1165	1039	409	0.21	0.17	420	1574	0	903
42.61	5158	1662	639	192	0.30	0.11	256	1407	0	810
42.81	5251	2419	1603	403	0.45	0.23	157	767	0	1023
43.21	3587	1349	186	27	0.36	0.05	412	1156	0	266
43.51	6961	2818	386	180	0.36	0.05	540	1981	0	566
43.815	7768	5189	3408	583	0.65	0.30	522	522	0	829
44.21	7243	4047	881	398	0.55	0.11	909	966	0	426
44.81	-	-	-	-	-	-	-	-	-	-
45.21	-	-	-	-	-	-	-	-	-	-
45.81	81	1	6	2	0.01	0.06	11	2	0	42
46.21	31	1	5	2	0.02	0.13	5	5	0	1
46.81	-	-	-	-	-	-	-	-	-	-
47.21	-	-	-	-	-	-	-	-	-	-
47.81	9170	2552	3802	3415	0.24	0.29	528	3027	458	0
48.21	8475	1885	592	62	0.19	0.07	872	2617	872	0
48.51	13577	5277	359	51	0.38	0.03	2049	2510	717	0
48.81	4242	1443	223	96	0.33	0.05	391	1156	351	0
49.21	109	48	6	3	0.44	0.05	5	22	3	0
49.81	-	-	-	-	-	-	-	-	-	-

5

Equatorward migration of dinoflagellates during the Plenus Cold Event, Oceanic Anoxic Event 2

"You can't always get what you want
But if you try sometimes well you just might find
You get what you need"

The Rolling Stones, in: *You Can't Always Get What You Want (Let It Bleed, 1969)*

Abstract

We reconstruct migration patterns of dinoflagellates gathered in the dinoflagellate cysts (dinocysts) complex *Cyclonephelium compactum-membraniphorum* (*Ccm*), across the Cenomanian-Turonian Oceanic Anoxic Event 2 (OAE2; ~94 Ma). To this end, dinocyst assemblages for Pratt's Landing (northwest Alberta, Canada), a site located in the northern part of the former Western Interior Seaway are analyzed, and the global biogeographical distribution of *Ccm* is compiled for records spanning OAE2. Our results indicate that *Ccm* had a ubiquitous bi-hemispheric high-latitude distribution, prior to, during, and after OAE2, whereas *Ccm* was only sporadically present in the mid-latitudes prior to OAE2. The first consistent presence (FCP) of *Ccm* in Northern Hemisphere mid-latitudes coincides with the first positive carbon isotope excursion during OAE2 and was a response to pronounced cooling associated with the Plenus Cold Event. The stratigraphic distribution of *Ccm* is also mirrored in other marine faunal elements, and indicates that this climatic cooling during the Plenus Cold Event induced marine biogeographic reorganization.

1. Introduction

The Cenomanian-Turonian boundary (93.9 Ma; Meyers et al., 2012a) was probably the warmest interval of the Phanerozoic (Huber et al., 2002; Forster et al., 2007a), and corresponds with a major Oceanic Anoxic Event (OAE2), that led to widespread deposition of black mud in ocean basins (Schlanger and Jenkyns, 1976), and to a distinct positive carbon isotope ($\delta^{13}C$) excursion in all active carbon reservoirs (e.g., Tsikos et al., 2004). Earlier work indicated that OAE2 is marked by the incursion of a boreal group of faunal elements into mid-latitude shelf sites in Europe (Jefferies, 1962; Gale and Christensen, 1996; Voigt et al., 2004). In the proto-North Atlantic, this interval is characterized by 3-5°C cooling of sea surface temperatures (SSTs), as recognized in TEX_{86}^{H} records from equatorial regions (Deep Sea Drilling Project [DSDP] Site 367, Ocean Drilling Program [ODP] Site 1260 - Forster et al., 2007b) and mid latitudes (ODP Site 1276 - Sinninghe Damsté et al., 2010; Bass River - Chapter 3). In several regions, such as the Western Interior Seaway (WIS; Eldrett et al., 2014) and proto-North Atlantic (e.g., Forster et al., 2007b), this intervals marks a drop in the concentration of sedimentary organic carbon and changes in redox-sensitive element concentrations, indicative of temporary (re)oxygenation of bottom waters. This episode is informally termed the 'Plenus Cold Event' (PCE), after the belemnite *Actinocamax plenus*, a Boreal faunal element associated with this event (Jefferies, 1962; Gale and Christensen, 1996). The stratigraphic position of the PCE is consistent with a rapid drop in atmospheric pCO_2 proxy records (Freeman and Hayes, 1992; Kuypers et al., 1999; Sinninghe Damsté et al., 2008; Barclay et al., 2010). This event has generally been attributed to globally enhanced sequestration of carbon during the early stages of OAE2 (Kuypers et al., 1999; Barclay et al., 2010). Although paleotemperature reconstructions and the related biotic response have only been documented for the proto-North Atlantic, a causal relation between pCO_2 drawdown, biogeographic reorganisation, and the PCE has previously been proposed (Forster et al., 2007b; Sinninghe Damsté et al., 2010; Jarvis et al., 2011).

To further assess migrations of phytoplankton in response to the PCE we have compiled both new and published biogeographical data on dinoflagellate cysts (dinocysts). Recently, the first consistent presence (FCP), i.e., presence of multiple specimens in consecutive samples, of both *Cyclonephelium compactum* and *C. membraniphorum* (mid- to high-latitude species) was shown to coincide with the PCE and the first maximum in the broad positive excursion in $\delta^{13}C$ (point "A" - cf. Voigt et al., 2008) from sections in the proto-North Atlantic and on the European shelf (Chapters 3 and 4). Presumably the dinoflagellates that produced these cysts migrated from higher northern latitudes. To test whether equatorward migration of these dinoflagellates occurred during the PCE, dinocyst assemblages of a high-latitude end-member site, located in the northern part of the WIS have been stratigraphically analysed. Additionally, a global distribution of the *C. compactum-membraniphorum* morphological plexus (*Ccm*) has been compiled (see supplements for detailed discussion on the taxonomic status of *Ccm* and methods), prior

to, during and after OAE2, using a common stratigraphic framework primarily based on carbon isotope stratigraphy.

2. Material and Methods

Pratt's Landing is located in the Peace River valley in northwest Alberta, Canada (56°01'14"N, 118°48'47"W). During the Late Cretaceous, the study site was located on the eastern flank of the foredeep in the northern part of the WIS (Fig. 1; number 1), about 160 km from the contemporaneous shoreline in the west (Varban and Plint, 2008). The section exposes about 23 m of upper Cenomanian to lower Turonian strata that consist predominantly of thinly bedded silt- and claystones. The carbon isotope composition of bulk organic carbon ($\delta^{13}C_{org}$) was measured at 20 cm intervals in order to constrain the position of OAE2, and to allow interbasinal correlation. Dinocyst abundances were determined using standard palynological methods, including HCl and HF treatment (see Supplement for details).

For the compilation of the global biogeographical distribution of *Ccm* prior to, during and after OAE2, an extensive literature survey was conducted. In addition to this compilation, five Northern Hemisphere shelf sites in Europe and North America, notably Pratt's Landing, Iona-1 (southwest Texas, USA), Bass River (New Jersey, USA), Eastbourne (East Sussex, UK) and Wunstorf (Lower Saxony, Germany), were selected in order to make detailed comparison between established high-resolution records of both $\delta^{13}C$ and the relative abundances of *Ccm* (Pearce et al., 2009; Eldrett et al., 2014; Chapters 3 and 4; Fig. 1).

3. Results and Discussion

3.1. Migration

The interval spanning OAE2 at Pratt's Landing is recorded between 10.2 m and 16.8 m, based on a ~2‰ positive carbon isotope excursion (CIE; Fig. 2a). The Cenomanian-Turonian boundary has been placed at 15.5 m, based on inoceramid biostratigraphy (Fig. 2a; Varban and Plint, 2008). Sedimentation rates average ~12 m/Myr, assuming a duration of the buildup and plateau phases of the CIE of ~550 kyr (Meyers et al., 2012b). *Ccm* is a common constituent (1-4%) of the dinocyst assemblage at Pratt's Landing starting ~6 m below the onset of the CIE (Fig. 2a), which represents at least a few hundreds of thousands of years.

The global biogeographic distribution of *Ccm* is illustrated in Figure 1. Recent dinoflagellate biostratigrapic studies from the East Coast Basin, New Zealand, show that the FCP of *Ccm* was at least ~500 kyr prior to OAE2 indicating a distinctly high latitude, bi-hemispheric distribution of this taxon (Schiøler and Crampton, 2014). For most Northern Hemisphere mid-latitude sites, *Ccm* has not been reported prior to OAE2, with the exception of a few sporadic occurrences in Eastbourne and Iona-1 (Pearce et al., 2009; Eldrett et al., 2014). Crucially, *Ccm* was never a common constituent of mid-latitude

dinocyst assemblages prior to OAE2. As a result, the records indicate that Ccm indeed was generally confined to high latitudes during the Late Cenomanian.

Maximum relative abundances of *Ccm* (i.e., >10%) are recorded during the first positive CIE within OAE2, point "A", at Pratt's Landing (Fig. 2a). At the same stratigraphic position, *Ccm* became abundant at several other Northern Hemisphere mid-latitude sites, for example, the southern WIS, New Jersey Shelf, Wunstorf, Poland and in the Vocontian Basin (Figs. 1, 2; Table S1). Despite a spot occurrence at point "A", the FCP of *Ccm* seems somewhat delayed in the English Chalk (Pearce et al., 2009; Fig. 2d). Spot occurrences of *Ccm* have been reported throughout the Cenomanian-Turonian interval from a low-latitude section at Tarfaya, Morocco, but its distribution is not related to OAE2, i.e., a few occurrences in a 30 cm wide interval >30 m below the onset of OAE2 (Prauss, 2012; M.L. Prauss, personal communication, 2014).

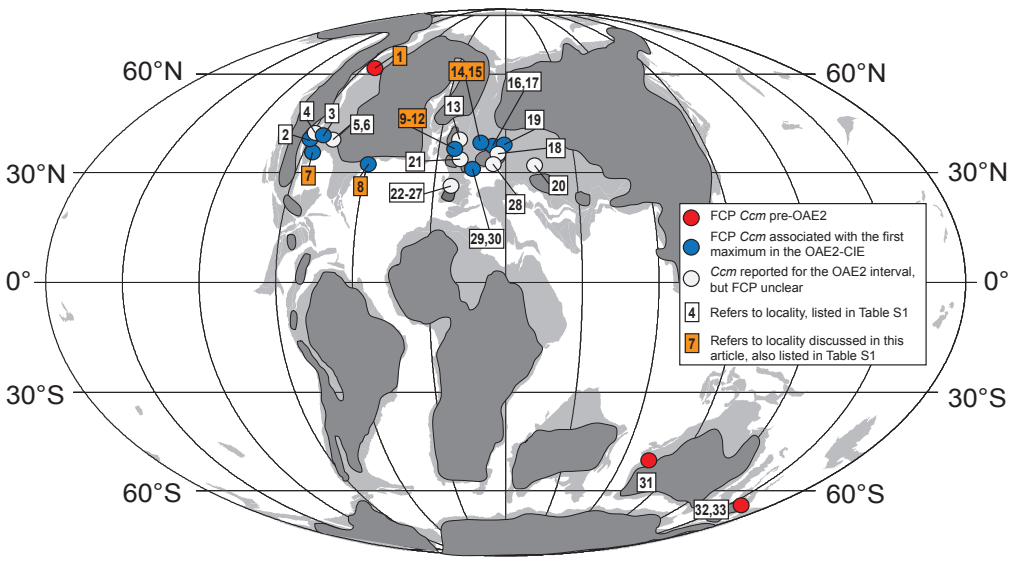

Figure 1. *Compilation of the first consistent presence (FCPs) of Cyclonephelium compactum-membraniphorum morphological plexus (Ccm) across the Cenomanian-Turonian boundary (including OAE2). Red dots indicate sites where the FCP of Ccm was prior to OAE2. Blue dots indicate sites where the FCP of Ccm was associated with the first positive carbon isotope excursion (CIE, 'point A'), characteristic of OAE2. Numbers in white boxes refer to localities compiled in Table S1. Numbers in orange boxes refer to the sites selected for detailed comparison of high-resolution $\delta^{13}C$ curves and the relative abundances of Ccm: 1. Pratt's Landing, northwest Alberta, Canada; 7. Shell Iona-1, Texas, USA; 8. Bass River, New Jersey, USA; 11. Eastbourne, southern UK; 14. Wunstorf, northwest Germany. The Mollweide projected paleogeographic map for the Cenomanian-Turonian boundary interval map generated at http://www.odsn.de/odsn/services/paleomap/paleomap.html. Continental plates are in light gray. Non-submerged landmasses in dark gray are after Scotese (2001).*

3.2. Ecology

At Bass River and Wunstorf the FCP of *Ccm* corresponds to a lowering of SSTs (Chapters 3 and 4), leading to the suggestion that the dinoflagellates that produced *Ccm* migrated to these sites in response to climatic cooling. We therefore presume that the biogeographic distribution of *Ccm* was principally controlled by SST. Sediments in the Shell Iona-1 core were unfortunately not suited for TEX_{86}-paleothermometry. However, at this site, the FCP of *Ccm* coincides with a period of (re)oxygenation of bottom waters, reflected by minima in sedimentary organic carbon, redox-sensitive elements and relatively high abundances of benthic foraminifera and ichnofossils (Eldrett et al., 2014), in accordance with previous findings for the PCE in the proto-North Atlantic (e.g., Forster et al., 2007b). This implies that the FCP of *Ccm* in the Iona-1 core is coincident with the PCE. The sustained presence of *Ccm* after the PCE at all sites, except Bass River (Fig. 2), suggests that, in addition to SST, other environmental and paleoceanographic factors became important in determining the distribution of *Ccm* once it had occupied niches at lower latitudes. For example, salinity and proximity to the shoreline may have been important (cf. Harris and Tocher, 2003).

The apparent migration of *Ccm* towards lower latitudes in response to global cooling strongly resembles previously recognized dinoflagellate migration events during other periods of marked climate change. Dinocysts referable to the Arctic Paleogene taxon, *Svalbardella*, were encountered in middle and lower paleolatitudes during the most pronounced Oligocene glaciations (ca. 30–25 Ma; van Simaeys et al., 2005). In contrast, during the Paleocene-Eocene Thermal Maximum (PETM), the situation was reversed, with tropical species of the dinocyst genus Apectodinium moving from low toward high latitudes in response to global peak warmth (e.g., Sluijs et al., 2007). In addition, studies across the Cretaceous-Paleogene boundary indicate initial high latitude to equatorial dinoflagellate migration at the boundary, followed rapidly by a reverse situation. This presumably took place in response to impact-related initial climatic cooling followed by a return to warmer conditions (Brinkhuis et al., 1998; Galeotti et al., 2004; Vellekoop et al., 2014).

The biogeographic expansion of *Ccm* towards the equator seems to be a relatively strong response to only a moderate change in SST (~3–5°C), and may be considered the opposite of the migration of *Apectodinium* during the PETM. The migration of *Ccm* over relatively large distances, i.e., 20° to 30° in latitude southwards, may have been amplified by the flat meridional temperature gradients during much of the mid-Cretaceous to early Paleogene (Barron, 1983; Huber et al., 1995). Compared to the present day, which has much steeper temperature-latitudinal gradients, relatively small changes in temperature in mid-Cretaceous and early Paleogene climates may have had a much larger impact on the distribution of marine organisms.

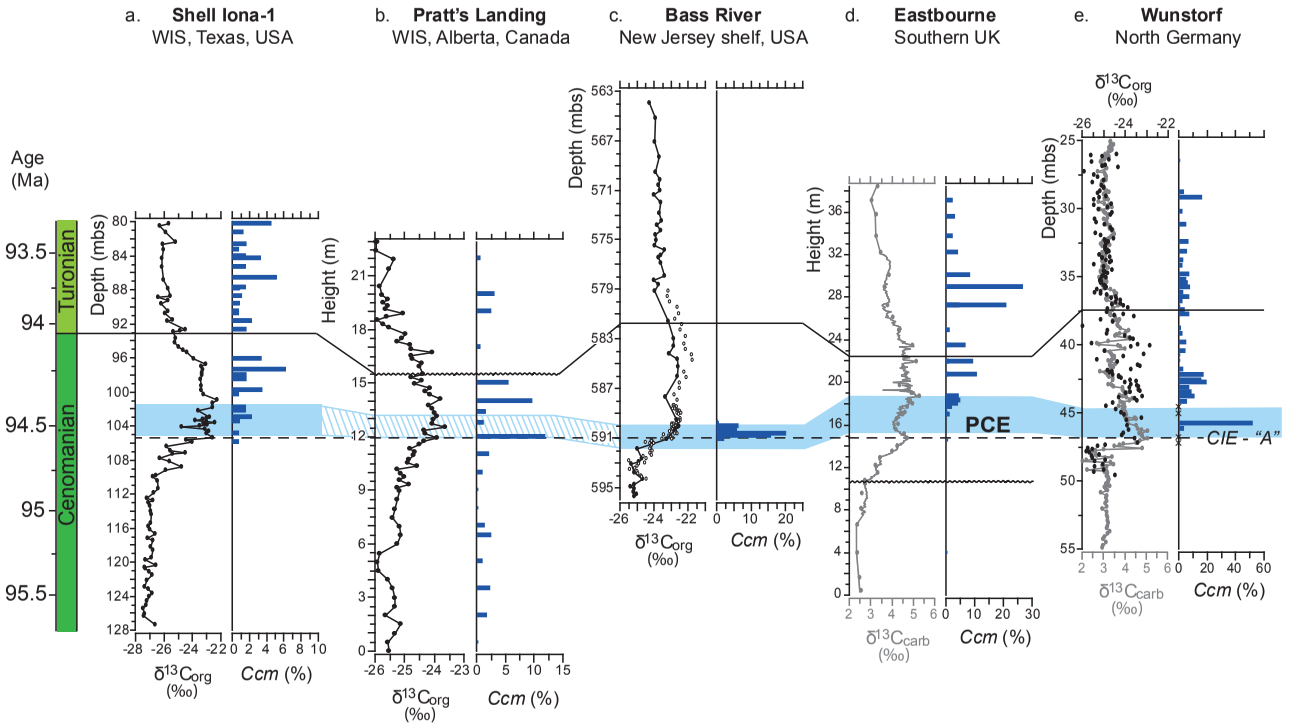

Figure 2. *Overview of $\delta^{13}C_{org}$ and/or $\delta^{13}C_{carb}$ and abundances of Cyclonephelium compactum-membraniphorum morphological plexus (Ccm) for the studied sections; a. Shell Iona-1 core (Eldrett et al., 2014); b. Pratt's Landing (this study); c. Bass River – (Chapter 3) open symbols is $\delta^{13}C_{org}$ derived from Bowman and Bralower (2005); d. Eastbourne – (Pearce et al., 2009), high-resolution $\delta^{13}C_{carb}$ data derived from (Paul et al., 1999); e. Wunstorf – relative abundances of Ccm from van Chapter 4 $\delta^{13}C_{org}$ from Du Vivier et al. (2014) and $\delta^{13}C_{carb}$ from Voigt et al. (2008). Red crosses in the Wunstorf record mark barren samples. Age is from the astronomically tuned age model for the Shell Iona-1 core (Eldrett et al., 2014). Dashed line represents the first maximum in the CIE, point "A" (cf. Voigt et al., 2008). The solid line represents the Cenomanian-Turonian boundary. The blue shaded area represents the Plenus Cold Event as defined by the presence of boreal fauna at Eastbourne, the cooling in TEX_{86}-based SST reconstructions at Bass River and Wunstorf (Chapters 3 and 4), and the (re) oxygenation of bottom waters in the Shell Iona-1 core (Eldrett et al., 2014).*

3.3. A new stratigraphic marker

Because the mid-Cretaceous marks the Cretaceous Normal Superchron C34n from ~126 to ~84 Ma (Gradstein et al., 2012), stratigraphy relies on biostratigraphy and carbon isotope stratigraphy (Gale et al., 2005) and recent advances in chronostratigraphy, e.g., astrochronology (Meyers et al., 2012a, b). In many depositional settings, and in particular cored sections, macrofossils often have limited availability (Sugarman et al., 1999), and sediments deposited during OAEs are typically relatively poor in carbonates, complicating planktonic foraminifer and calcareous nannofossil biostratigraphy (Erba, 2004). Consequently, carbon isotope stratigraphy is the dominant stratigraphic tool for OAEs since the CIE is recognized in all active carbon reservoirs (Tsikos et al., 2004). However, all carbon isotope records are impacted by factors relating to biology, carbon cycling and sedimentology, leading to offsets from the global exogenic signatures (Sluijs and Dickens, 2012; Wendler, 2013). Therefore, calibration of carbon isotope stratigraphy with bioevents is essential for the establishment of detailed stratigraphic frameworks. The coincidence of the FCP of *Ccm* with the first positive CIE (point "A") associated with OAE2 in Northern Hemisphere mid-latitude sites (Fig. 2), suggests that dinoflagellate migration likely occurred on time scales of 10^4 years. The FCP of *Ccm* thus represents a useful biostratigraphic marker, being the sole microfossil to date marking the PCE, at least in the proto-North Atlantic and WIS.

4. Conclusions

Chronostratigraphic analyses of dinocyst assemblages of a high-latitude WIS site across OAE2, and a literature survey documenting dinocyst biogeography have illustrated the migration of the dinocyst morphological complex *Cyclonephelium compactum-membraniphorum* from high-latitudes into mid-latitude regions during the early stages of OAE2 (latest Cenomanian). Crucially, the FCP of this taxon correlates with the first positive CIE associated with OAE2 for mid-latitude sites from North America and Europe. This interval marks the stratigraphic position of the Plenus Cold Event, a 3–5°C cooling episode, implying reorganization of phytoplankton biogeography in response to transient climate change during the mid-Cretaceous supergreenhouse.

Supplements to Chapter 5

Taxonomic notes regarding Ccm

Originally the cysts of *Cyclonephelium membraniphorum* (Cookson and Eisenack, 1962), which was recombined to *Cauveridinium membraniphorum* (Masure in Fauconnier and Masure, 2004), were described apart from *C. compactum* (Deflandre and Cookson, 1955), based on the generally higher and structurally ordered crests and membranes of *C. membraniphorum*. Additionally, cysts of *C. membraniphorum* form a series of funnel-shaped structures bordering unornamented mid-dorsal and mid-ventral areas. However, the apparent morphological variation regarding ornamentation within the two species exceeds the defined difference between the two species. Therefore it was proposed to refer to the dinocyst morphological complex *Cyclonephelium compactum-membraniphorum*, rather than separating both species (Marshall and Batten, 1988). We agree that the two species are members of a morphological continuum and therefore group all these morphotypes of this continuum from our study site and the literature under the *Cyclonephelium compactum-membraniphorum* morphological plexus (*Ccm*) (Fig. S1; Table S1).

Stable carbon isotopic composition of organic matter

Analyses were performed in the Stable-Isotope Biogeochemistry Laboratory of the School of Geography and Earth Sciences, McMaster University, Hamilton, Ontario, Canada. In total, 77 samples were treated with 3N HCl to remove carbonates, rinsed with demineralised water, freeze-dried and powdered. Between 1 and 3 mg of powdered sediment sample was weighed in tin capsules, and put in a rotating carousel for subsequent combustion in an elemental analyser. After purification of the gas sample it was passed through a SIRA II Series 2 dual-inlet isotope-ratio mass-spectrometer to determine the stable carbon isotopic composition of organic matter. Carbon isotope ratios were measured against an international standard, NBS-21. The analytical reproducibility, based on replicate samples, was better than 0.1‰.

Palynological treatment

For 21 samples, about 5 grams of freeze-dried sediment was processed following standardized quantitative methods, which involve the addition of a known amount of *Lycopodium clavatum* marker spores. To dissolve carbonates and silicates, HCl (~30%) and HF (~38%) were added, respectively. Residues were sieved over a 15 µm nylon mesh and the >15 µm fraction was mounted on slides for analysis by light microscopy. Samples were counted to a minimum of 250 dinocysts, which were identified to genus, or species level at 500x magnification, following the taxonomy of Fensome and Williams (2004). All samples and slides are stored in the collection of the Laboratory of Palaeobotany and Palynology, Utrecht University, the Netherlands.

Compilation of the presence of Ccm

For the compilation of the global biogeographical distribution of *Ccm* prior to, during and after OAE2, an extensive literature survey was conducted. In this survey all localities (n=33) where cysts of *Ccm* (i.e., *Cauverodinium membraniphorum*, *Cyclonephelium membraniphorum*, *Cyclonephelium compactum* and/or *Cyclonephelium compactum-membraniphorum*) have been reported were listed (Table S1). The first common presence (FCP) of *Ccm* could only be determined for a limited amount of localities (n=18) due to lacking stratigraphic information and unquantified abundances of *Ccm*.

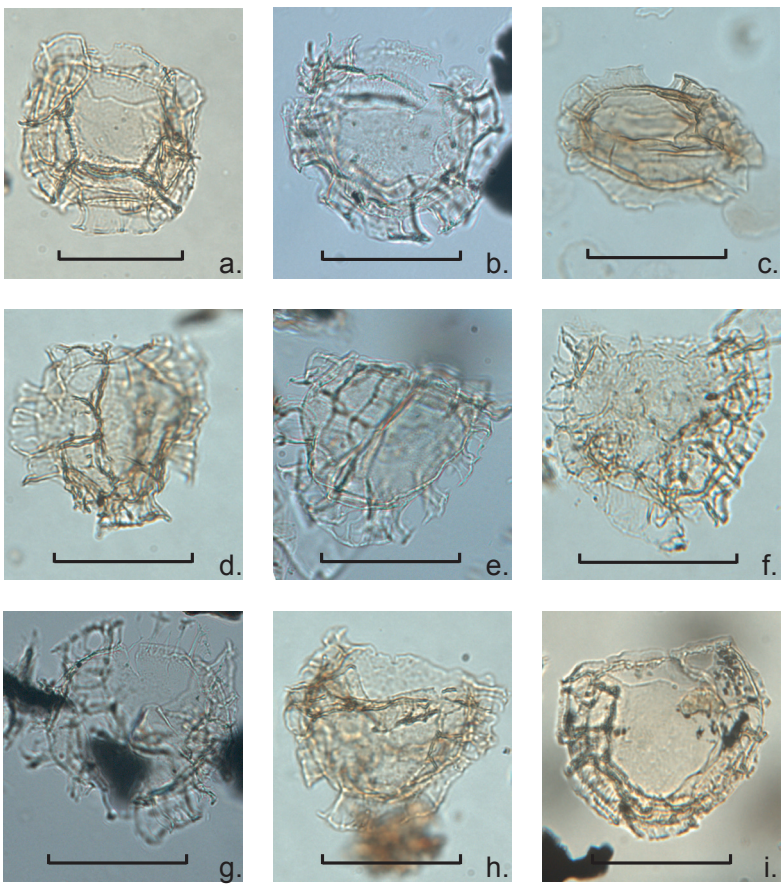

Figure S1. *Various specimens of the Cyclonephelium compactum-membraniphorum morphological plexus (Ccm), moving from the C. membraniphorum end-member (a-c) to the C. compactum end-member (g-i). Specimens a and i are from Wunstorf sample 42.21 mbs, specimen b is from Bass River sample 590.69 mbs, specimen c is from Wunstorf sample 45.81 mbs, specimens d and h are from Pratt's Landing sample 6.5 m, specimens e and g are from Bass River sample 590.08 mbs and specimen f is from Pratt's Landing sample 12 m. Scale bars represent 50 µm.*

Table S1. *Overview of the localities where cysts of Cyclonephelium compactum-membraniphorum morphological plexus (Ccm) have been reported across the Cenomanian-Turonian boundary interval. In the fifth and sixth column an "X" marks whether the first common presence (FCP) of Ccm was associated with the first maximum in the positive carbon isotopic excursion (CIE), point "A" (cf. Voigt et al., 2008). Question marks indicate that FCP could not be determined accurately, resulting from insufficient supporting information (e.g., high-resolution carbon isotope stratigraphy or unquantified abundances of Ccm). Localities discussed in this chapter are in bold.*

Continent	Site Number	Region	Locality	FCP of *Ccm* prior to OAE2	FCP of *Ccm* associated with CIE-"A"	References
North America	1	**Boreal WIS**	**Pratt's Landing, Alberta, Canada**	**X**		**This study**
	2	WIS	Blue Point, Arizona, USA		**X**	Li and Habib, 1996
		WIS	Blue Point, Arizona, USA	?	?	Harris and Tocher, 2003
	3	WIS	Pueblo, Colorado, USA		**X**	Dodsworth, 2000
		WIS	Pueblo, Colorado, USA	?	?	Harris and Tocher, 2003
	4	WIS	Wahweap Wash, Utah, USA	?	?	Harris and Tocher, 2003
	5	WIS	Bunker Hill, Kansas, USA	?	?	Harris and Tocher, 2003
	6	WIS	Rebecca K. Bounds Core, Kansas, USA	?	?	Harris and Tocher, 2003
	7	**WIS**	**Shell Iona-1, Texas, USA**		**X**	**Eldrett et al., 2014**
	8	**proto-N. Atlantic shelf**	**Bass River, New Jersey, USA**		**X**	**Chapter 3**
Europe	9	European shelf	Lulworth, Dorset, UK		**X**	Dodsworth, 2000
	10	European shelf	Culver Cliff, Isle of Wight, UK		**X**	Lignum, 2009
	11	European shelf	**Eastbourne, East-Sussex, UK**		**X**	**Pearce et al., 2009**
	12	European shelf	Folkstone, Kent, UK	?	?	Jarvis et al., 1988
	13	European shelf	Eastern UK	?	?	Dodsworth, 1996
	14	European shelf	**Wunstorf, Lower Saxony, Germany**		**X**	Marshall and Batten, 1988; Prauss, 2006; Lignum, 2009; **Chapter 4**
	15	European shelf	Misburg, Lower Saxony, Germany		**X**	Marshall and Batten, 1988
	16	European shelf	Gröbern, Saxony Anhalt, Germany		**X**	Lignum, 2009

Continent	Site Number	Region	Locality	FCP of *Ccm* prior to OAE2	FCP of *Ccm* associated with CIE-"A"	References
Europe	17	European shelf	Ratssteinbruch, Saxony, Germany		X	Lignum, 2009
	18	European shelf	Nymburk, Central Bohemia, Czech Republic	?	?	Čech et al., 2005
	19	European shelf	Pulawy, central Poland		X	Dodsworth, 2004a
	20	European shelf	Aksudere, Crimea, Ukraine	?	?	Dodsworth, 2004b
	21	European shelf	Bois du Gallet, St.-Sylvestre-de-Cormeilles, Haute-Normandie, France	?	?	Tocher and Jarvis, 1995
	22	European shelf	Les Fosses Blanches, Duneau, Maine, France	?	?	Tocher and Jarvis, 1995
	23	European shelf	Ganuza, Castilian Platform, Spain	?	?	Lamolda and Mao, 1999
	24	European shelf	Puentedey, Castillian Platform, Spain	?	?	Peyrot er al., 2011
	25	European shelf	Fuentetoba, Castillian Platform, Spain	?	?	Peyrot er al., 2011
	26	European shelf	Tamajon, Castillian Platform, Spain	?	?	Peyrot er al., 2011
	27	European shelf	Condemios, Castillian Platform, Spain	?	?	Peyrot er al., 2012
	28	Tethys	Ultrahelvetic Rehkogelgraben, Austria	?	?	Pavlishina and Wagreich, 2012
	29	Tethys	Pont d'Issole, Provence-Alpes-Côte d'Azur, France		X	Lignum, 2009
	30	Tethys	Vergons. Provence-Alpes-Côte d'Azur, France		X	Lignum, 2009
		Tethys	Vergons, Provence-Alpes-Côte d'Azur, France	?	?	Courtinat et al., 1991
Oceania	31	Boreal S. Hemisphere	Northwestern Australia	X		McMinn, 1988
	32	Boreal S. Hemisphere	East Coast Basin, New Zealand	X		Hasegawa et al., 2013; Schiøler and Crampton, 2014
	33	Boreal S. Hemisphere	Mangaotane Stream, Raukumara Peninsula, New Zealand	X		Crampton et al., 2001

6

Spatial extent and degree of oxygen depletion in the deep proto-North Atlantic Basin during Oceanic Anoxic Event 2

"What we know is a drop, what we don't know is an ocean."

Sir Isaac Newton

Abstract

Massive organic matter burial due to widespread ocean anoxia across the Cenomanian-Turonian boundary event (~94 Ma), resulted in a major perturbation of the global carbon cycle: the so-called Oceanic Anoxic Event 2 (OAE2). The characteristics and spatial distribution of the OAE2 deposits that formed in the deep part of the proto-North Atlantic Basin remain poorly described, however. Here, we present proxy data of redox sensitive (trace) elements (e.g., Mo, Fe/Al, Corg/Ptot and Mn) for OAE2 sediments from five Deep Sea Drilling Project and Ocean Drilling Program sites located in the deep proto-North Atlantic Basin. Our results highlight that bottom waters in the entire deep proto-North Atlantic were anoxic during most of OAE2. Furthermore, regressions of Mo with total organic carbon content (TOC), previously shown to document the degree of water mass restriction, confirm that the water circulation in the proto-North Atlantic basin was severely restricted during OAE2. Comparison of these values to Mo/TOC ratios in the present-day Black Sea suggests a renewal frequency of the deep proto-North Atlantic water mass of between 0.5 and 4 ka, compared to a maximum of ~200 years for the present-day northern Atlantic. The Plenus Cold Event, a cooler episode during the early stages of OAE2 hypothesized to be caused by declining pCO_2 due to extensive burial of organic matter, appears to have led to temporary re-oxygenation of the bottom water in the deep proto-North Atlantic Basin during OAE2.

1. Introduction

The mid-Cretaceous Cenomanian-Turonian boundary event (93.9 Ma; Meyers et al., 2012a) marks the widespread deposition of organic-rich marine sediments associated with large-scale ocean anoxia (Schlanger and Jenkyns, 1976; Arthur and Sageman, 1994). Oceanic Anoxic Event 2 (OAE2), is characterized by a positive >2‰ excursion in the stable carbon isotopic composition ($\delta^{13}C$) of the global exogenic carbon pool, recognized in sedimentary organic matter ($\delta^{13}C_{org}$) and carbonate ($\delta^{13}C_{carb}$) (e.g., Kuypers et al., 2002; Tsikos et al., 2004). The ~550 kyr long (e.g., Meyers et al., 2012b) positive carbon isotopic excursion (CIE) typically encompasses three phases, the onset (phase A), a plateau phase with relatively stable values (phase B), and a recovery phase to pre-event values (phase C) (e.g., Kuypers et al., 2004). The onset and presumably the plateau phases are most likely the result of enhanced burial of $\delta^{13}C$-depleted organic matter (Schlanger and Jenkyns, 1976; Arthur et al., 1988; Sinninghe Damsté and Köster, 1998; Kuypers et al., 2002; Tsikos et al., 2004).

OAE2 has been linked to the emplacement of the large igneous province (LIP) of the Caribbean Plateau (Leckie et al., 2002). The associated release of trace metals to the marine environment, as deduced from enrichments of a wide range of trace metals in sediments (Snow et al., 2005), has been suggested to have fueled primary production in the proto-North Atlantic by reducing trace-metal limitation of nitrogen fixers (Morel and Price, 2003; Trabucho-Alexandre et al., 2010). The increased igneous activity (e.g., Kuroda et al., 2007; Turgeon and Creaser, 2008) also led to high levels of atmospheric CO_2 (e.g., Bice et al., 2006; Sinninghe Damsté et al., 2008; Barclay et al., 2010), and extreme warmth during OAE2 (e.g., Forster et al., 2007b; Sinninghe Damsté et al., 2010). As a consequence of the warming, oxygen solubility in seawater decreased. In combination with a more stratified water column, this led to a reduced ventilation of the ocean and an expansion of areas of anoxia, and even photic-zone euxinia, i.e., free H_2S in the water column (Sinninghe Damsté and Köster, 1998; Kuypers et al., 2002). The prevailing extreme greenhouse conditions also enhanced the hydrological cycle, which induced freshwater stratification on shelves and in epicontinental seas and led to enhanced weathering, increasing continentally derived nutrient input and primary productivity (Pogge von Strandmann et al., 2013; Chapter 3). Once anoxia was established, recycling and upwelling of phosphorus (P) and nitrogen (mostly as NH_4) and fixation of N_2 from the atmosphere further boosted primary productivity (Kuypers et al., 2004b; Mort et al., 2007; Kraal et al., 2010; Higgins et al., 2012).

A wide range of proxies can be employed for the reconstruction of redox conditions. The simplest one is the total organic carbon content (TOC) of sediments. However, along with bottom-water oxygen conditions, TOC content is also a function of the organic matter flux to the seafloor, degradation of organic matter and dilution with inorganic matter (e.g., Reed et al., 2011). Concentrations of trace metals in sediments, e.g., V, Cr, Cu, Zn, Ni, and in particular Mo (Brumsack, 1980; Emerson and Huested, 1991; Scott and Lyons, 2012) have been shown to be excellent proxies for paleoredox conditions in

bottom waters. They are actively scavenged from oxygen-depleted marine environments, and therefore enriched in the sediments. Mn and P, in contrast, are mobilized under reducing conditions. Therefore, depletions in sedimentary Mn (e.g., Thomson et al., 1995; Lenz et al., 2014) and the ratio of organic carbon over total phosphorus (C_{org}/P_{tot}) (Algeo and Ingall, 2007) can be used as an indicator for sea floor deoxygenation. Corg/Ptot ratios also provide insight in the degree of P recycling (Mort et al., 2007; Kraal et al., 2010). An elevated value of Fe/Al ratios is indicative of a sedimentary enrichment of Fe relative to a detrital background. Such enrichments are assumed to be the result of enhanced Fe-shuttling from continental margins to the deep-sea, driven by the expansion of low-oxygen zones, thus providing a proxy for more widespread anoxia (e.g., Canfield et al., 1996; Lyons and Severmann, 2006; Eckert et al., 2013). Additionally, regressions between Mo and TOC can provide insight into the degree of restriction of the subchemoclinical water mass (Algeo and Lyons, 2006).

Most sedimentary records for OAE2 have been obtained from continental margins. These records indicate significant temporal and spatial differences in primary productivity and bottom-water redox conditions in the coastal zone during the event (e.g., Tsikos et al., 2004; Hetzel et al., 2011; Chapter 3). For example, high total organic carbon (TOC) contents (generally >10%), organic carbon over phosphorus ratios (C_{org}/P_{tot}; generally >600) and trace-metal contents (e.g., molybdenum; Mo >40 parts per million; ppm) are observed on the Moroccan shelf (Tsikos et al., 2004; Kraal et al., 2010). In contrast, the European and North American shelves (e.g., New Jersey) are characterized by a low TOC content (generally <1%), a low C_{org}/P_{tot} ratio (generally <100) and a low trace-metal content (e.g., Mo <5 ppm) (Hetzel et al., 2011; Chapter 3). Bottom-water redox conditions in the deep central part of the proto-North Atlantic Basin, i.e., at estimated water depths >2000m, during OAE2 are less well constrained than at continental margins. Datasets, including TOC content, trace-metal concentrations and C_{org}/P_{tot} ratio are only available for two Deep Sea Drilling Project (DSDP) sites: 367 and 603. DSDP Site 367, which is located in the southern deep part of the proto-North Atlantic, is characterized by an extremely high (i.e., 20-40%) and relatively stable TOC content, high (i.e., 400-1500) C_{org}/P_{tot} ratios, high trace-metal contents (e.g., Mo >50 ppm) and high Fe/Al ratios (i.e., 1-3; Kuypers et al., 2002; Kraal et al., 2010; Owens et al., 2012). At DSDP Site 603 in the northern deep part of the proto-North Atlantic, in contrast, concentrations and ratios of the same elements for OAE2 are significantly lower and much more variable (Kuypers et al., 2004b; Kraal et al., 2010; Owens et al., 2012). The lack of further insight in the spatial extent and temporal variability in bottom-water anoxia in the deep part of the basin hampers a correct understanding of the causes and consequences of OAE2.

Two recent model studies of ocean biogeochemistry during OAE2 suggest that extensive anoxia in the central deep part of the proto-North Atlantic Basin required low oxygen concentrations in the Pacific Ocean (Monteiro et al., 2012; Ruvalcaba Baroni et al., 2014a). This is because inflow of oxygen-rich waters from the Pacific would not have allowed for the development of full anoxia. Unfortunately, sediments capturing the OAE2-interval in the Pacific Ocean are scarce, and at present only a few continental margin sites

have been studied (Takashima et al., 2011). Validation of these model results therefore requires a dataset that provides insight into the regional and temporal variability of redox conditions in the bottom waters of the deep part of the proto-North Atlantic Basin during OAE2.

Here, we assess the spatial and temporal trends in bottom-water redox conditions during OAE2 in the deep proto-North Atlantic. For that purpose, we combine the existing geochemical data for DSDP Sites 367 and 603 with newly generated data for DSDP Site 386 and Ocean Drilling Program (ODP) Sites 641 and 1276 (Fig. 1). Our redox proxies include ratios of C_{org}/P_{tot}, Fe/Al and Mo/TOC and concentrations of various trace elements such as Mo and Mn. Our results highlight that water circulation in the proto-North Atlantic was severely restricted during OAE2. The deep part of the basin was fully anoxic for most of OAE2, except for what appears to have been a basinwide oxygenation event within OAE2, associated with the "Plenus Cold Event" (PCE; Gale and Christensen, 1996;

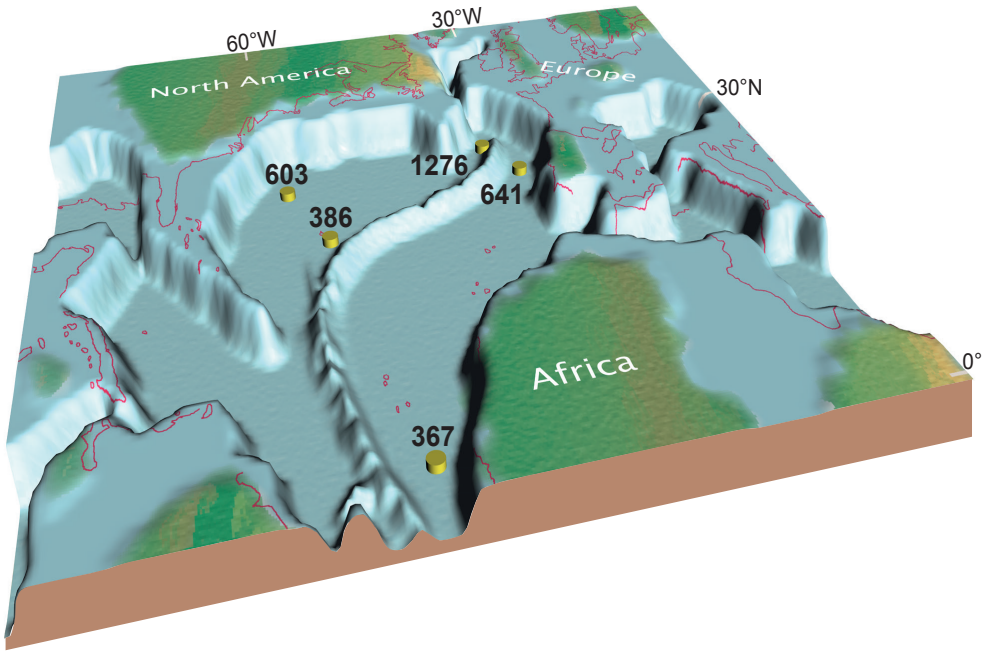

Figure 1. *Three-dimensional paleogeographic map of the proto-North Atlantic basin for the Cenomanian Turonian boundary time interval, indicating the locations of the cores used in this study. Map adjusted from the map created at http://www.odsn.de/odsn/services/paleomap/paleomap.html. Non-submerged land masses in green are after Scotese (2001).*

Forster et al., 2007b; Sinninghe Damsté et al., 2010).

2. Materials and Methods

2.1. Study sites

All five sites in this study were located in the deep proto-North Atlantic during OAE2 (Fig. 1). Estimated water depths, available from the literature (Table 1), range from 2000 to 3800 m and sediments over the OAE2-interval are pelagic or hemi-pelagic (Table 1). The sources of existing geochemical data for all DSDP and ODP sites and the newly generated data are listed in Table 2. Below, we describe the locations of the study sites and the lithology of the sediments covering the OAE2-interval.

Site	Estimated water depth (m)	Type of sediment
DSDP 367	3700 [a]	Pelagic [b]
DSDP 386	2000-3800 [a]	Pelagic [c]
DSDP 603	4000 [a]	Hemipelagic [d]
ODP 641	3500 [e]	Pelagic [e]
ODP 1276	>2000 [f]	(Hemi)pelagic [f]

Table 1. *Estimated water depth and type of sediment during OAE2.[a]Chénet and Francheteau (1979), [b]Shipboard Scientific Party (1977), [c]Tucholke and Vogt et al. (1979), [d]Herbin et al. (1987), [e]Shipboard Scientific Party (1987b), [f]Urquhart et al. (2007).*

2.1.1. Site 367: Cape Verde Basin, DSDP Leg 41

The southernmost site in this study is located offshore Senegal in the eastern equatorial Atlantic, on the abyssal plain in the vicinity of the mid-oceanic ridge (12°29.2'N, 20°02.8'W, 4748 m water depth). A minor component of the OAE2 sediments at Site 367 is composed of turbidities (Shipboard Scientific Party, 1977). However, no direct evidence exists for a turbiditic origin for the OAE2-related black shales, which have been interpreted to reflect in-situ pelagic sediments (Kuypers et al., 2002).

2.1.2. Site 386: Central Bermuda Rise, DSDP Leg 43

This site is the most centrally located site in this study, at ~140 km south-southeast of Bermuda (31°11.21'N, 64°14.94'W, 4793 m water depth). The OAE2 sediments predominantly consist of multicolored, i.e., green, gray and black, clay- and mudstones that are interpreted as deep marine sediments (Tucholke and Vogt, 1979).

2.1.3. Site 603 (Hole B): Off Cape Hatteras, DSDP Leg 93

Site 603 was located in the northern part of the deep proto-North Atlantic. The site is located on the western edge of the Hatteras Abyssal Plain, part of the North American Basin, 435 km west of Cape Hatteras (35°29.66'N, 70°01.70'W, 4644 m water depth) (Shipboard Scientific Party, 1987a). The OAE2 sediments consist of an alternation of organic-poor, often bioturbated green claystones, and organic-rich black shales (Herbin

et al., 1987). Sedimentation at Site 603 was hemipelagic with some influence of coastal oceanic events (Kuypers et al., 2004a).

2.1.4. Site 641 (Hole A): Galicia Bank, ODP Leg 103

The core at Site 641 was retrieved from the western margin of the Galicia Bank, offshore northwestern Spain (42°09.3'N, 12°10.9'W, 4646 m water depth). The Late Cenomanian-Early Turonian sediments consist of green and gray claystones. The OAE2-interval itself is represented by ~30 cm of dark green and black shales (Shipboard Scientific Party, 1987b).

2.1.5. Site 1276: Newfoundland Basin, ODP Leg 210

Site 1276, our most northerly site, is located in the Newfoundland Basin, offshore Canada (45°24.31980'N, 44°47.14960'W, 4565 m water depth). The mid-Cretaceous sequence predominantly consists of mud-dominated gravity flow deposits (Shipboard Scientific Party, 2004). OAE2 itself is represented by a 3.5 m thick stack of mainly pelagic sediments (Urquhart et al., 2007), concurrent with a drastic drop in the relative abundance of terrestrially derived palynomorphs (pollen and spores; Sinninghe Damsté et al., 2010).

Site	Original publication: type of data
DSDP 367	Kuypers et al. (2002): $\delta^{13}C_{org}$, TOC, trace elements (ICP-AES)
	Kuypers unpublished: molar C_{org}/P_{tot}
	Owens et al. (2012): Fe/Al
DSDP 386	This study: all data
DSDP 603	Herbin et al. (1987): TOC
	Selection of Kuypers et al. (2004a): $\delta^{13}C_{org}$, TOC, trace elements (ICP-AES)
	Kraal et al. (2010): molar C_{org}/P_{tot}
	Owens et al. (2012): Fe/Al
ODP 641	This study: all data
ODP 1276	Sinninghe Damsté et al. (2010): $\delta^{13}C_{TOC}$, TOC
	This study: trace elements (ICP-OES), molar C_{org}/P_{tot} an Fe/Al

Table 2. *Overview of data sources and original publications.*

2.2. Total organic carbon and isotopes of organic carbon

Surfaces of selected sediment samples were scraped clean with a knife, freeze-dried and powdered and homogenized using a ceramic mortar and pestle. About 0.3 g of powdered sample was decalcified using 1M HCl. Subsequently sediment residues were analyzed for organic carbon content, from which TOC content was calculated after compensation for carbonate loss, and $\delta^{13}C_{TOC}$ (Table S1) using a Fisons Instruments CNS NA 1500 analyzer coupled to a Thermo Delta Plus isotope ratio spectrometer. Results were normalized to international standards. Average analytical uncertainty based on duplicate analyses of sediment samples was 0.01 wt. % for TOC and 0.02 ‰ for $\delta^{13}C_{TOC}$.

2.3. *Major and minor element compositions*

Approximately 125 mg of freeze dried and powdered sample was dissolved in 2.5 ml mixed acid ($HClO_4$:HNO_3; 3:2) and 2.5 ml 40% HF, heated to 90°C and left overnight. The acids were evaporated at 160°C after which the residue was dissolved in 25 ml 4.5% HNO_3. Sediment elemental compositions were measured using Inductively Coupled Plasma-Optical Emission Spectrometry (ICP-OES; Perkin Elmer Optima 3000); the error calculated from standards and duplicates of the trace elements generally was <5% and never exceeded 15% for the elements used in this study, i.e. Mo, P, Fe, Al, Mn, Cr, V, Cu, Zn, Ni and S (Table S1). Molybdenum values <20 ppm were below the background emission signal, and therefore have an error of >10%; these should, hence, be regarded as approximate values.

3. Results

3.1. *Stratigraphy*

At all five sites, the OAE2-interval was identified chemostratigraphically based on an increase in TOC content combined with the characteristic positive carbon isotope excursion of C_{org} (Fig. 2a). For Site 367, phases A and B of the CIE (isotopic "increase" and "plateau" phases respectively), were identified based on a positive CIE of ~6‰ in both TOC, S-bound phytane (Kuypers et al., 2002) and other biomarkers (Sinninghe Damsté et al., 2008). The isotopic "recovery", phase C, was not captured due to a coring gap. For DSDP Site 386, phase A of the OAE2-interval is absent due to a coring gap. A distinct 2.5‰ increase in $\delta^{13}C_{TOC}$ occurs right above the coring gap at 742.11 m below seafloor (mbsf) marking phase B of the event (Fig. 2b). From 738.76 mbsf onwards, isotopic values rapidly drop towards pre-OAE2 levels, indicating the start of phase C.

For DSDP Site 603, phases A and B were identified based on a ~2.5‰ positive CIE in TOC (Fig. 2c) and a 4-5‰ positive shift in stable carbon isotopes of S-bound phytane (Kuypers et al., 2004a). Similar to Site 367, phase C was not recovered at Site 603 due to a coring gap. Encountered dinocyst assemblages confirm a Cenomanian age for the studied sediments (Habib and Drugg, 1987; Fig. 2c).

For ODP Site 641 the OAE2-interval was previously identified based on stable carbon isotope stratigraphy (Thurow et al., 1988). Here, we determined a similar $\delta^{13}C_{TOC}$ profile, showing the isotopic "increase", phase A, from -26.0‰ at 54.10 mbsf to -23.6‰ at 53.98 mbsf, after a short plateau phase of ~20 cm, values drop back to the pre-excursion level (Fig. 2d). Identification of the OAE2-interval at Site 641 was further confirmed by calcareous nannofossil biostratigraphy (Shipboard Scientific Party, 1987b). The occurrence of Lithraphidites acutum and Microstaurus chiastus from ~54.1 to 54 mbsf (Fig. 2d) are indicative for the Cenomanian-Turonian boundary (e.g., Bralower et al., 1997; Luciani and Cobianchi, 1999).

The OAE2-interval of ODP Site 1276 was identified based on a positive CIE of ~4.5‰ in TOC (Fig. 2e) and a >5‰ in the stable isotopes of the bacterial biomarker C_{31} 17β,21β(H)-hopane (Sinninghe Damsté et al., 2010), and other biomarkers (van Bentum

et al., 2012), clearly identifying all three phases of the CIE. Calcareous nannofossil and planktonic foraminifer biostratigraphy confirmed this age assignment (Urquhart et al., 2007; Fig. 2e).

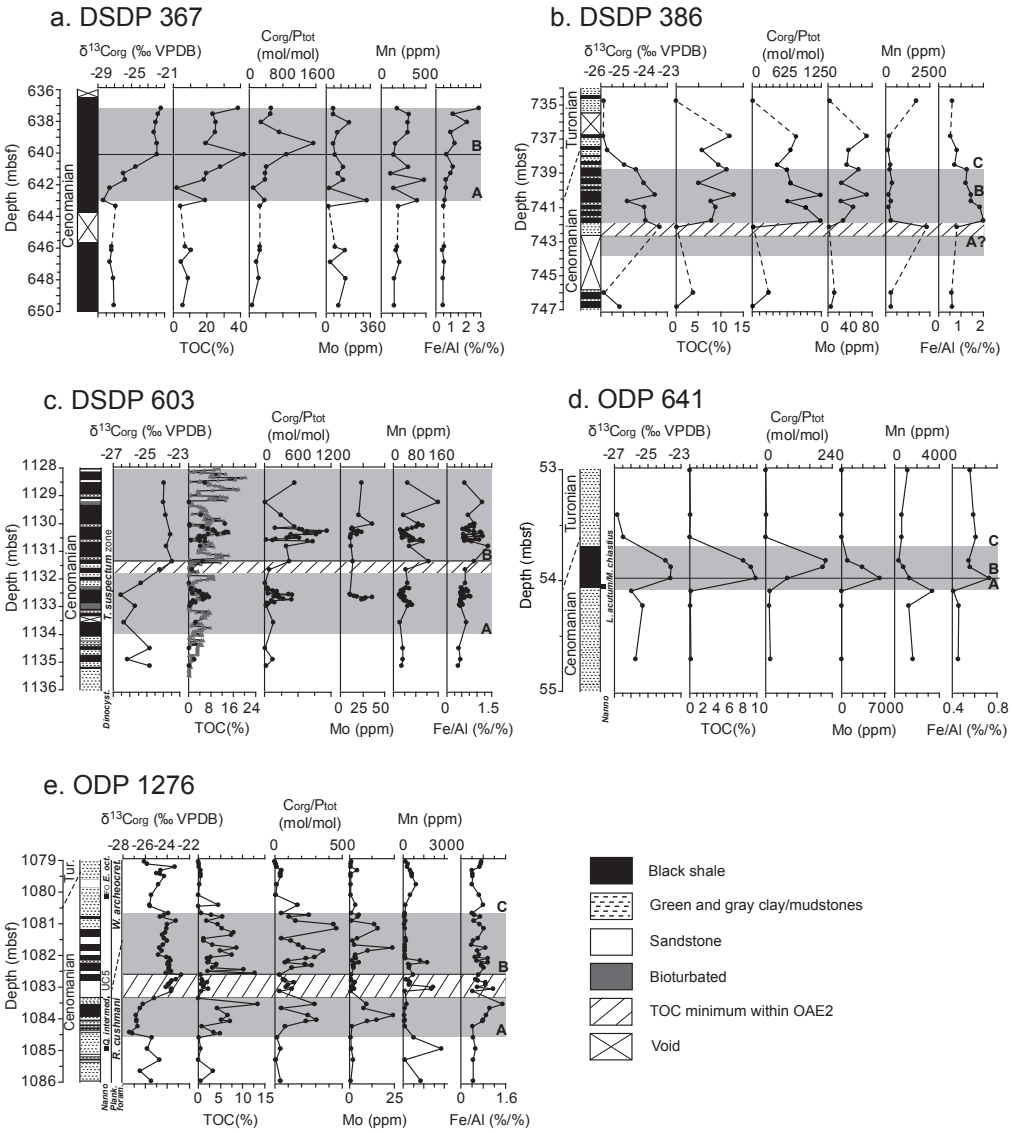

Figure 2. *Lithology, biostratigraphy, chemostratigraphy ($\delta^{13}C_{org}$/$\delta^{13}C_{TOC}$ and TOC), C_{org}/P_{tot}, Mo, Mn and Fe/Al for Sites 367 (a), 386 (b), 603 (c), 641 (d) and 1276 (e). Gray shades highlight the OAE2-interval, based on the positive excursion in $\delta^{13}C_{org}$/$\delta^{13}C_{TOC}$ and elevated TOC content, with the subdivision into different phases of the CIE marked by an "A", "B" or "C" after Kuypers et al. (2002). Data sources are listed in Table 2. mbsf: meters below seafloor.*

3.2. *TOC and C_{org}/P_{tot}*

Site 367 exhibits the highest TOC concentrations during OAE2, with average values >15% and maximum values exceeding 30% (Fig. 2a). For Sites 386, 603, 641 and 1276, TOC concentrations are elevated during OAE2, with average values ranging from 3 to 9% and maximum values between 10 and 19% (Fig. 2; Table 3). Downcore variations in the TOC profile is high, particularly for Sites 603 and 1276. Intriguingly, the TOC profiles for Sites 386, 603 and 1276, show a distinct minimum within OAE2, with TOC <1%., close to the transition from the A phase to the B phase of the CIE (Fig. 2).

At all five sites, C_{org}/P_{tot} ratios are high (above the Redfield ratio of 106 associated with organic matter production) during OAE2 (Fig. 2). Average and maximum values are, however, much higher for the three most western Sites 367, 386 and 603. Average values for phase B range from 500 to 800 with maxima up to ~1500, compared to values of around 200 (maxima up to ~450) for Sites 641 and 1276 (Fig. 2; Table 3). Again, a minimum in C_{org}/P_{tot} ratios is observed within OAE2 for Sites 386, 603 and 1276, at the same stratigraphic interval as the TOC minimum mentioned above.

Site		TOC (%)		C_{org}/P_{tot} (mol/mol)		Mo (ppm)		Mn (ppm)		Fe/Al (%/%)	
		avg.	max.	avg.	max.	avg.	max.	avg.	max.	avg.	max.
DSDP 367	phase A	17	28	328	405	146	332	284	481	0.8	1.1
	phase B	27	39	709	1536	86	185	230	308	1.5	2.9
DSDP 386	phase A[a]	-	-	-	-	-	-	-	-	-	-
	phase B	8	13	778	1244	35	70	550	2320	1.4	2.0
DSDP 603	phase A	3	11	173	501	21	36	45	126	0.6	0.9
	phase B	7	19	539	1130	19	49	61	159	0.8	1.4
ODP 641	phase A[b]	-	-	-	-	-	-	-	-	-	-
	phase B	9	10	167	216	3494	6206	824	1320	0.6	0.7
ODP 1276	phase A	3	13	135	313	6	24	530	2161	0.8	1.5
	phase B	5	13	198	457	6	24	322	1731	0.7	1.0

Table 3. *Average (avg) and maximum (max) values for TOC, C_{org}/P_{tot}, Mo, Mn and Fe/Al, for phases A and B of OAE2. [a]At DSDP Site 386 phase A of OAE2 was not recovered/identified. [b]Regarding the condensed nature of OAE2 at ODP Site 641, no values for phase A were derived.*

3.3. *Trace elements and trace elemental ratios*

Concentrations of the trace metals Mo (Fig. 2; Table 3), V, Cr, Ni, Zn and Cu (Fig. S1) generally increase within the OAE2-interval for Sites 386, 603 and 1276, although downcore variability ranges up to one order of magnitude for some trace metals, particularly for the latter two sites. For Site 367, no distinct increase in the concentration of trace metals was recorded across the transition to OAE2, except for Ni concentrations, which more than double. In terms of absolute values, there is great diversity between sites and all trace elements. Extreme enrichments in trace metals are observed (e.g., up to 6000 ppm for Mo) in the condensed OAE2 section at Site 641 (Fig. 2; Fig. S1). In contrast with

the elements listed above, Mn decreases within the OAE2 or remains low (Sites 367 and 603).

3.3.1. Fe/Al ratios

Ratios of Fe/Al are near the crustal average of ~0.5 (Taylor and McLennan, 1995) at all sites prior to and after OAE2 (Fig. 2; Table 3). During OAE2, values are typically >1 for Sites 367 and 386, with maximum values around 2.9 and 2.0 respectively. At Sites 603 and 1276 pre-event average Fe/Al values of ~0.7 increase to maximum values close to 1.5 during the CIE, indicating a modest increase. At Site 641 only one datapoint shows a distinct increase relative to background crustal values, with a value of 0.7 (Fig. 2; Table 3). For all sites the S contents follow the trends in Fe/Al-ratios (Fig. S1).

3.3.2. Mo/TOC ratios

Ratios of Mo/TOC (Table S1) for the OAE2-interval of Sites 367 and 386 are quite similar, and generally range between 3 to 5. Average Mo/TOC ratios for Sites 603 and 1276 are lower at ~3 and ~2, respectively. Site 641 shows values >100, resulting from the unusually high Mo concentrations measured at this site.

4. Discussion

4.1. Distribution and degree of oxygen depletion

The southern part of the proto-North Atlantic, which was located in the equatorial zone during the Late Cretaceous, was highly productive prior to and during OAE2, based on bulk geochemical data and calcareous nannofossil assemblages (e.g., Kuypers et al., 2002; Hardas and Mutterlose, 2007). Furthermore, multiple studies provide evidence for euxinia extending into the photic zone, based on high concentrations of the biomarkers isorenieratane, chlorobactane and maleimide, molecular remains of the brown strain of green sulfur bacteria, that require both light and free sulfide (Sinninghe Damsté and Köster, 1998; Kuypers et al., 2002; Pancost et al., 2004; van Bentum et al., 2009). The high TOC and C_{org}/P_{tot} contents for Site 367 are the result of high export productivity and anoxic conditions, as P is regenerated from the sediments under anoxic conditions (Ingall et al., 1993; Ingall and Jahnke, 1994), resulting in an elevated C_{org}/P_{tot} ratio. Low Mn concentrations, elevated Mo and increasing Fe/Al confirm the reducing conditions in the bottom waters at this site and in the surrounding area (Fig. 2a; Table 3). However, the maximum concentrations for Mo, V, Zn, Cr and Cu are observed prior to OAE2 (Fig. 2a; Fig. S1). This was previously documented for ODP Sites 1258 and 1260, which are also located in the southern part of the proto-North Atlantic (Hetzel et al., 2009), and was attributed to a shift from regional, southern proto-North Atlantic anoxia, to basin scale anoxia, ultimately leading to a drawdown of the seawater trace metal reservoir (Hetzel et al., 2009). The combined existing and newly generated data for our sites, distributed throughout the proto-North Atlantic, highlight the temporal and spatial variability in redox conditions in the deep part of the proto-North Atlantic Basin during OAE2.

At Site 386, in the central part of the proto-North Atlantic, high TOC values and extremely high C_{org}/P_{tot} values in combination with elevated trace-metal concentrations and a minimum in Mn concentrations, indicate that bottom waters were anoxic and sulfidic during OAE2 (Fig. 2b; Fig. S1). Sediment Fe/Al ratios increased across the OAE2-interval, suggesting an expanding oxygen-depleted zone. In phase C of the CIE, TOC, C_{org}/P_{tot} and trace-metal concentrations remained high, suggesting that anoxia persisted at this site in the central part of the proto-North Atlantic. During this phase, Fe/Al ratios declined, however, indicating either a smaller oxygen-depleted zone or more sulfidic conditions (Scholz et al., 2014). Although anoxia seems to have continued locally after OAE2 at Site 386, the decline of the Fe/Al ratio most likely reflects a reduction in oxygen depletion in the surrounding area.

The northerly Sites 603 and 1276, both show very distinctive TOC, C_{org}/P_{tot} and trace-metal enrichments for the OAE2-interval (Fig. 2c, e; Fig. S1). In comparison to Sites 367, 386 and 641, average concentrations (Table 3) remained relatively low, however, with exception of the Mn concentrations at Site 1276. We interpret this to reflect comparatively less severe oxygen depletion in the northern part of the deep proto-North Atlantic Basin. The repeated fluctuations in TOC with values that are frequently close to zero, and variations in lithology, i.e., variations between laminated organic-rich black shales and organic-poor sand-, clay-, and mudstones (Fig. 2c, e), i.e., even suggest temporary oxygenation. For both sites the presence of the biomarker for photic-zone euxinia, isorenieratane, has been demonstrated (Kuypers et al., 2004; van Bentum et al., 2012). Isorenieratane was, however, only present in very low quantities and only in the most organic-rich parts of the section. This supports sporadic occurrences of photic-zone euxinia at these sites, but excludes persistent photic-zone euxinia as reported for the southern, equatorial part of the proto-North Atlantic (Sinninghe Damsté and Köster, 1998; Kuypers et al., 2002; van Bentum et al., 2009). For both sites, Mn concentrations are low during OAE2, supporting anoxic conditions at the sediment-water interface. At the same time Fe/Al is elevated, suggesting expansion of the area with oxygen-depleted bottom waters in the surrounding part of the basin.

Site 641 clearly had anoxic bottom waters during OAE2, reflected in the distinct black shale layer with a TOC content of ~10%. Isorenieratane was reported (Sinninghe Damsté and Köster, 1998), but again in low quantities. Trace-metal enrichments are, however, extreme, e.g., Mo concentrations up to 6000 ppm (Thurow et al., 1988; this study; Fig. 2d; Fig. S1). Such extreme enrichments might result from proximity to the mid-ocean ridge. The mid-ocean ridge was very active during the mid-Cretaceous (e.g., Hays and Pitman, 1973; Larson, 1991; Cogné and Humler, 2004), and associated vent systems most likely introduced large amounts of trace metals into bottom waters (e.g., Douville et al., 2002). During periods of anoxia, these trace metals would be scavenged from the water column directly, resulting in the observed extreme enrichments in the sediment. However, ratios of Fe/Al do not show a large increase at Site 641, conflicting with this hydrothermal input scenario (e.g., Owens et al., 2012). Furthermore, Sites 386 and 1276 are also positioned close to the mid-ocean ridge and do not show such extreme enrichments.

The most straightforward explanation for the extreme trace-metal concentrations is that they did not result from high fluxes but rather from very low sedimentation rates at Site 641. A similar relationship between low sedimentation rates and high authigenic trace-metal concentrations was inferred for Pennsylvanian black shales (Algeo and Maynard, 2004; Algeo and Heckel, 2008). Average sedimentation rates during OAE2 at Site 641 would have been in the order of 0.25 cm kyr^{-1}, when assuming a constant rate of sedimentation, 80% compaction of clays after deposition (Hedberg, 1936) and a ~600 kyr long duration for the positive CIE (e.g., Meyers et al., 2012). These sedimentation rates are common for seamounts (Kukal, 1990). It is unclear, however, whether Site 641 was located on such a height. Periods of typical pelagic sedimentation at rates of 2-4 cm kyr^{-1} (Kukal, 1990), may also have alternated with periods without net sediment deposition.

The supply of trace metals at the site could have been augmented by input from relatively oxic water masses, for example originating from the intermittent (sub)oxic northern Tethyan realm (e.g., Westermann et al., 2010; Hetzel et al., 2011). Unfortunately our knowledge of mid-Cretaceous ocean and bottom-water currents is not sufficient to prove or disprove the latter suggestion.

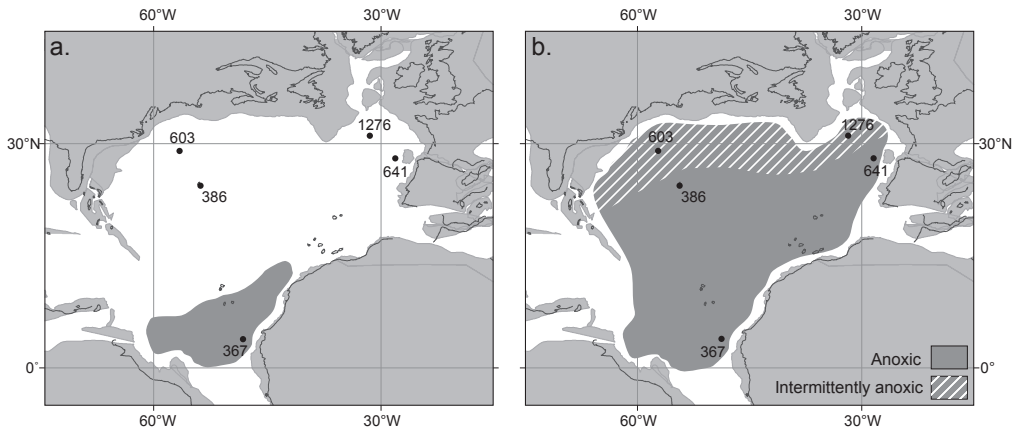

Figure 3. *Schematic, showing the progressive change in oxygenation of bottom waters across the basin from the situation prior to OAE2 (a.) to the situation during OAE2 (b.). Maps were created at http://www.odsn.de/odsn/services/paleomap/paleomap.html.*

Our results suggest that the entire deep proto-North Atlantic Basin was anoxic during a major part of OAE2. Based on our paleoredox proxies, we conclude that there were large spatial differences in the degree of oxygen depletion during the event (Fig. 3). Anoxia and euxinia were particularly severe in the southern part of the basin, where bottom waters were already euxinic before OAE2 (Fig. 3), in perfect agreement with the isorenieratene derivatives and other biomarker proxies (Sinninghe Damsté et al., 2014). In contrast, the bottom waters of the northern part of the deep proto-North Atlantic were not anoxic prior to and after OAE2, and were intermittently anoxic during a major part of the event (Fig.

3). Bottom waters in the central, deep basin were likely anoxic and sulfidic throughout the event, but may have been overlain by oxic/suboxic intermediate waters (Ruvalcaba Baroni et al., 2014a). Crucially, according to modeling experiments, the inflow of low-oxygen waters from the Pacific Ocean is required to have maintained widespread anoxia in the central, deep proto-North Atlantic Basin throughout OAE2 (Monteiro et al., 2012; Ruvalcaba Baroni et al., 2014a).

4.2. Water mass renewal rates

Under euxinic conditions molybdate anions are converted to particle-reactive thiomolybdates, hence allowing for burial of Mo in the sediments (Helz et al., 1996). As a result of this more rapid burial of Mo, it was shown for modern euxinic basins that the renewal time of the deep water mass, which is a function of multiple factors ranging from tectonic restriction of a basin to the rates of overturning, mixing and circulation in a basin, can be estimated from the regression slope of Mo with TOC (Algeo and Lyons, 2006). This proxy was successfully applied to Mesozoic sediments (McArthur et al., 2008; Westermann et al., 2013). For the Early Toarcian OAE, the degree of water mass restriction was shown to be strongest at greater water depth (McArthur et al., 2008). Very low Mo/TOC ratios in sediments deposited during OAE2 in the Tethys Ocean, have been suggested to reflect extreme restriction of the water mass, i.e., a long renewal period of deep water (Westermann et al., 2013). Low Mo/TOC ratios for the equatorial sites at Demarara Rise (ODP Sites 1258 and 1260) during OAE2 have also been attributed to a restricted circulation (Hetzel et al., 2009; Algeo and Rowe, 2012).

At present, the Black Sea is the marine euxinic basin with the longest deep water renewal time, due to its tectonic restriction and lack of vertical mixing. This is reflected by ratios of Mo/TOC for Black Sea sediments, which plot at a regression slope of 4.5 ± 1 (Fig. 4), corresponding to a renewal period for Black Sea deep water in the range of 500 to 4000 years. For comparison, the regression slope for Saanich Inlet, which is a modern, relatively shallow, euxinic basin with only minor tectonic restriction, is 45 ± 5 (Fig. 4), corresponding to a renewal period of deep water of only ~1.5 years (Algeo and Lyons, 2006 and references therein; Fig. 4).

The Mo/TOC data for sediments deposited under anoxic bottom waters during the OAE2-interval, as compiled in this study, can be used to quantify the degree of restriction for proto-North Atlantic deep water. The Mo/TOC-data for Site 641 were excluded, because the extremely enriched values seem to be the result of the condensed OAE2-interval. Mo/TOC-data for the four remaining Sites 367, 386, 641 and 1276, are within the same range. The Mo/TOC data are characterized by a regression slope of ~4.1 with a R2 of 0.43 (Fig. 4).

The regression slope for Mo/TOC data of the OAE2-interval in the proto-North Atlantic thus almost equals the regression slope for Mo/TOC in the modern Black Sea, which suggests a similar renewal period for proto-North Atlantic deep water during OAE2, i.e., 500 to 4000 years. This renewal period is relatively short compared with the renewal period that could be calculated for the OAE2-interval at Demerara Rise, ODP

Sites 1258 and 1260 (Mo/TOC of 2-3; Hetzel et al., 2009) or the renewal period for the stagnant, i.e., very poor vertical mixing of the water column, Cleveland Basin during the Toarcian-OAE (Mo/TOC of ~0.5; McArthur et al., 2008). The renewal period for deep waters in the proto-North Atlantic during OAE2 is, however, still considerably longer when compared with the ~200 year period for the present-day northern Atlantic (Broecker, 1991).

Although the renewal period for deep waters during OAE2 was much longer then at present, we infer that deep waters in the proto-North Atlantic Basin were far from stagnant, in line with results from modelling studies (e.g., Monteiro et al., 2012; Ruvalcaba Baroni et al., 2014a).

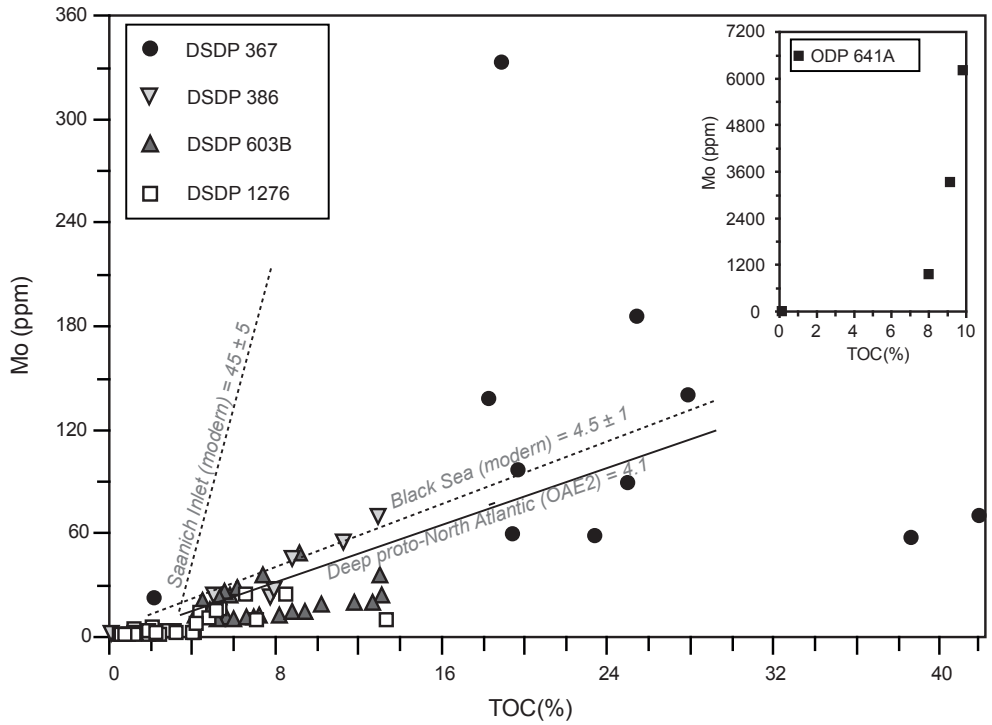

Figure 4. *Cross plot of sediment Mo versus TOC for the OAE2-interval at the studied sites. Dashed lines show regression slopes for Mo and TOC data of two modern anoxic marine environments, the minor restricted Saanich Inlet and the severely restricted Black Sea (Algeo and Lyons, 2006). The solid line is the combined regression slope of the four (DSDP 367, DSDP 386, DSDP 603 and ODP 1276) deep proto-North Atlantic sites during OAE2.*

4.3. A basin wide oxygenation event?

At Site 1276 the organic-rich deposits of OAE2 are interrupted by an organic-poor interval with a thickness of ca. 75 cm, between 1082.39 and 1083.13 mbsf (Fig. 2e). Along with low TOC concentrations (< 2.3 wt. %; Sinninghe Damsté et al., 2010), this interval is also characterized by low trace-metal concentrations (Fig. 2e). Both suggest that conditions at the sediment-water interface were less reducing during this period. Mean annual average sea surface temperature reconstructions, using TEX_{86} paleothermometry, show a concomitant 5-11°C cooling, attributed to a drop in atmospheric CO_2 resulting from the widespread burial of organic matter (Sinninghe Damsté et al., 2010). This cooling is synchronous with an incursion of boreal fauna in the shelf seas of NW Europe and was called the "Plenus Cold Event" (PCE; Jefferies, 1962; Gale and Christensen, 1996). The PCE-related cooling has now been recognized throughout the proto-North Atlantic in different paleoenvironmental settings, i.e., in the deep basin (DSDP Site 367) (Forster et al., 2007b), in intermediate waters (ODP Site 1260; Forster et al., 2007b), and in shallow-marine environments (Chapter 3), and coincident with minima in TOC and trace-metal concentrations at several sites, although not at Site 367.

The lowest data point within the recovered OAE2-interval at Site 386 shows that anoxia might not have persisted throughout the entire event at this site either, as concentrations of TOC, Mo, and other trace elements are close to zero and the Mn content increases. This is indicative of less reducing or even oxic conditions at the seafloor. Unfortunately the OAE2-interval at Site 386 is not complete and the stratigraphy lacks detail; therefore, it is impossible to confirm whether this data point represents the PCE. At Site 603, the OAE2-interval also contains a section with low TOC values between 1131.85 and 1131.4 mbsf. Although C_{org}/P_{tot}, Mo and other trace elements are low for this interval, similar values are recorded for organic-rich parts of the OAE2-interval. The stratigraphic position of the interval with TOC values at Site 603 relative to the CIE does, however, does match the organic-lean interval at Site 1276, where it was linked with the PCE. Therefore, we consider it likely that this interval also represents the PCE at Site 603.

Based on our findings, we suggest that the PCE led to substantial, temporary re-oxygenation of bottom waters during OAE2, throughout the proto-North Atlantic, including the deep part of the basin.

5. Conclusions

Newly generated and compiled existing redox proxy data for five deep-sea sites distributed over the proto-North Atlantic confirm that the entire deep proto-North Atlantic was anoxic during most of OAE2. Based on our data, however, spatial differences in redox conditions existed within the basin, with persistent severe anoxia and euxinia in the southern proto-North Atlantic, and only intermittently anoxic bottom waters in the northern proto-North Atlantic.

The regression slope of the Mo and TOC data for the OAE2-interval for the presented sites is similar to that of the modern euxinic Black Sea. This suggests that circulation in the proto-North Atlantic basin was severely restricted during OAE2.

Finally, a previously identified oxygenation event within OAE2, associated with the Plenus Cold Event, has been found in the sediments of multiple deep-sea sites as well. This implies that, during this event, bottom-water oxygenation not only occurred on the shelves and in epicontinental seas but also in the deep sea.

Supplements to Chapter 6

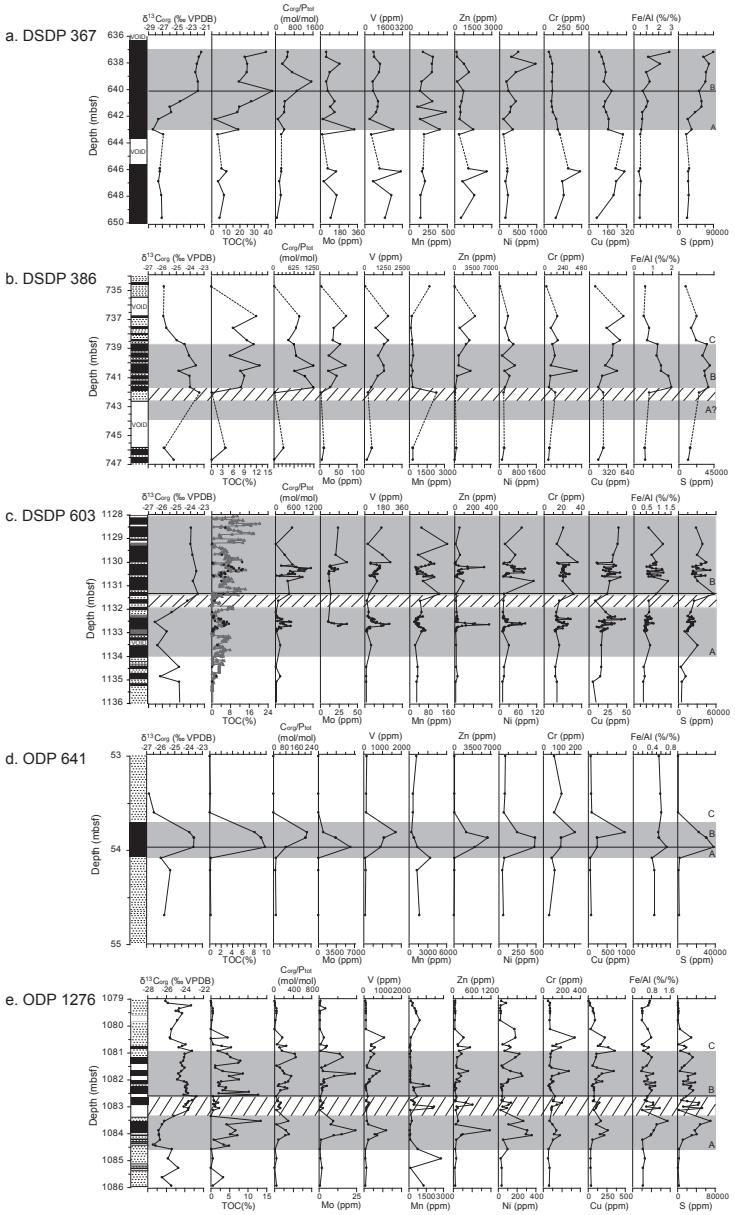

Figure S1. *Lithology, chemostratigraphy ($\delta^{13}C_{org}$, $\delta^{13}C_{TOC}$ and TOC), C_{org}/P_{tot}, Mo, V, Mn, Zn, Ni, Cr, Cu, Fe/Al and S for sites 367 (a), 386 (b), 603 (c), 641 (d) and 1276 (e). Gray shades highlight the OAE2-interval, based on the positive excursion in $\delta^{13}C_{org}$/$\delta^{13}C_{TOC}$ and elevated TOC content, with the subdivision into different phases of the CIE marked by an "A", "B" or "C" after Kuypers et al. (2002). mbsf: meters below seafloor.*

Table S1. *Overview of all geochemical data used in this study, listed per sample. Bold data generated in this study, other data originates from previous publications, which are listed in Table 2.*

Leg	Site	Hole	Core	Section	Top depth (cm)	Base depth (cm)	Sample depth (mbsf)	TOC (%)	$\delta^{13}C_{org/TOC}$ (‰ VPDB)	C_{org}/P_{tot} (mol/mol)	P (ppm)	Al (%)	Fe (%)	Mo (ppm)	V (ppm)	Mn (ppm)	Zn (ppm)	Ni (ppm)	Cu (ppm)	Cr (ppm)	S (%)	Fe/Al (%/%)	Mo(s)/ TOC
41	367		18	1	120	124	637.2	38.65	-21.45	531	1879	1.70	4.89	58	744	178	174	501	89	63	8.94	2.88	1
41	367		18	2	6	9	637.56	23.43	-21.8	515	1174	2.91	3.38	59	807	308	203	324	109	88	6.51	1.16	3
41	367		18	2	59	62	638.09	25.43	-22.05	286	2294	2.48	5.22	185	1294	299	773	973	124	110	7.82	2.10	7
41	367		18	2	121	125	638.71	25.06	-22.25	725	892	2.84	2.83	89	1217	298	1171	442	144	114	7.02	0.99	4
41	367		18	3	39	42	639.39	19.44	-21.95	1536	327	3.15	4.02	59	690	158	206	185	125	108	6.91	1.27	3
41	367		18	3	111	114	640.11	42.08	-21.95	865	1254	3.58	2.54	70	728	137	721	239	192	115	5.27	0.71	2
41	367		18	4	40	43	640.9	27.93	-24.5	405	1781	2.22	2.52	140	1146	302	551	438	140	99	5.87	1.13	5
41	367		18	4	79	83	641.29	19.75	-25.95	381	1336	3.26	3.25	97	1086	102	457	306	126	104	5.88	1.00	5
41	367		18	4	121	125	641.71	18.34	-25.75	378	1253	3.35	2.23	138	968	481	463	282	147	117	4.29	0.67	8
41	367		18	5	24	30	642.24	2.19	-27.55	101	557	5.88	4.01	22	436	136	409	110	170	163	2.39	0.68	10
41	367		18	5	100	106	643	18.95	-28.35	375	1305	3.74	2.19	332	2452	401	1516	357	162	184	3.45	0.59	18
41	367		18	5	137	142	643.37	4.07	-26.9	248	423	6.80	3.55	19	555	191	365	112	291	212	2.05	0.52	
41	367		19	1	143	147	645.93	7.06	-27.4	248	734	6.27	3.34	73	1263	178	1139	212	226	322	2.79	0.53	
41	367		19	2	14	18	646.14	10.45	-27.35	256	1055	6.42	2.68	154	3093	166	2590	211	304	483	2.55	0.42	
41	367		19	2	89	94	646.89	4.42	-27.6	168	678	7.03	4.00	36	731	202	626	156	232	243	2.51	0.57	
41	367		19	3	43	47	647.93	8.85	-27.15	230	995	6.09	2.82	160	2265	147	1613	222	209	265	2.61	0.46	
41	367		19	4	62	66	649.62	5.46	-27.1	65	2185	6.34	3.06	102	1739	146	504	166	66	161	2.28	0.48	
43	**386**		**42**	**CC**	**23**	**24.5**	**734.74**	**0.03**	**-25.87**	**3**	**302**	**3.65**	**2.20**	**3**	**63**	**1724**	**77**	**41**	**103**	**28**	**0.88**	**0.60**	
43	**386**		**43**	**1**	**46.5**	**48**	**736.77**	**12.00**	**-25.90**	**797**	**388**	**3.18**	**1.66**	**71**	**1579**	**216**	**4007**	**391**	**587**	**168**		**0.52**	
43	**386**		**43**	**1**	**131.5**	**133**	**737.62**	**5.73**	**-25.70**	**683**	**216**	**1.87**	**1.53**	**37**	**752**	**118**	**1099**	**265**	**300**	**80**	**1.56**	**0.82**	
43	**386**		**43**	**2**	**65**	**66.5**	**738.46**	**9.50**	**-24.94**	**450**	**544**	**2.55**	**1.83**	**34**	**1569**	**256**	**2970**	**435**	**527**	**170**	**2.24**	**0.72**	
43	**386**		**43**	**2**	**95**	**96.5**	**738.76**	**11.32**	**-24.39**	**631**	**463**	**2.25**	**2.83**	**55**	**1326**	**250**	**2337**	**609**	**406**	**101**	**3.58**	**1.26**	**5**
43	**386**		**43**	**3**	**23**	**24.5**	**739.54**	**4.98**	**-24.06**	**693**	**185**	**2.24**	**2.69**	**25**	**905**	**354**	**897**	**138**	**393**	**134**	**3.01**	**1.20**	**5**
43	**386**		**43**	**3**	**91.5**	**93**	**740.22**	**12.95**	**-23.56**	**1244**	**268**	**1.71**	**2.48**	**70**	**1297**	**170**	**867**	**692**	**273**	**85**	**4.01**	**1.45**	**5**
43	**386**		**43**	**3**	**128.5**	**130**	**740.59**	**7.79**	**-24.80**	**643**	**312**	**1.88**	**2.72**	**23**	**1316**	**301**	**3125**	**240**	**480**	**413**	**3.29**	**1.44**	**3**
43	**386**		**43**	**4**	**14**	**15.5**	**740.95**	**8.78**	**-24.03**	**974**	**233**	**1.25**	**2.29**	**46**	**877**	**153**	**618**	**448**	**220**	**77**	**3.37**	**1.83**	**5**
43	**386**		**43**	**4**	**93.5**	**95**	**741.74**	**7.92**	**-23.98**	**1241**	**165**	**1.35**	**2.68**	**27**	**447**	**301**	**168**	**251**	**151**	**55**	**3.82**	**1.99**	**3**
43	**386**		**43**	**4**	**130**	**131.5**	**742.11**	**0.12**	**-23.33**	**19**	**169**	**3.93**	**3.22**	**2**	**235**	**2320**	**175**	**197**	**241**	**138**	**2.61**	**0.82**	**17**
43	**386**		**44**	**1**	**15.5**	**17**	**745.96**	**3.75**	**-25.88**	**303**	**319**	**2.88**	**1.68**	**11**	**501**	**310**	**421**	**222**	**242**	**63**	**1.48**	**0.58**	
43	**386**		**44**	**1**	**98**	**99.5**	**746.79**	**0.09**	**-25.15**	**7**	**311**	**4.11**	**2.53**	**5**	**157**	**304**	**100**	**122**	**155**	**54**	**1.23**	**0.61**	
93	603	B	34	1	101	105	1128.51	5.85	-23.95	537	281	4.1	2.5	24	160	52	54	73	40	21	2.83	0.60	4

Leg	Site	Hole	Core	Section	Top depth (cm)	Base depth (cm)	Sample depth (mbsf)	TOC (%)	$\delta^{13}C_{org/TOC}$ (‰ VPDB)	C_{org}/P_{tot} (mol/mol)	P (ppm)	Al (%)	Fe (%)	Mo (ppm)	V (ppm)	Mn (ppm)	Zn (ppm)	Ni (ppm)	Cu (ppm)	Cr (ppm)	S (%)	Fe/Al (%/%)	Mo(s)/TOC
93	603	B	34	2	20	25	1129.2	0.23	-24.00	14	437	6.3	7.4		30	159	10	18	38	14	3.84	1.18	
93	603	B	34	2	68	72	1129.68	4.46	-23.85	294	391	5.0	3.6	21	170	35	58	51	32	25	2.96	0.72	
93	603	B	34	2	99	100	1129.99	13.08				4.8	4.4	36	247	87	13	33	31	36	4.46	0.92	3
93	603	B	34	2	102	103	1130.02	0.38				6.5	5.6		55	90	6	16	11	14	4.36	0.86	
93	603	B	34	2	106	107	1130.06	0.37				7.1	5.6		58	104	7	12	12	16	3.66	0.78	
93	603	B	34	2	110	111	1130.1	5.35		545	254	5.4	4.9		114	82	14	26	33	27	3.67	0.90	
93	603	B	34	2	114	115	1130.14	7.26		195	959	6.2	4.1	13	148	67	42	42	36	21	2.86	0.66	2
93	603	B	34	2	117	118	1130.17	8.19		622	340	4.0	2.1	13	142	51	136	50	32	23	2.31	0.53	2
93	603	B	34	2	121	122	1130.21	8.85		682	335	5.0	3.3	15	144	26	320	39	20	21	2.91	0.66	2
93	603	B	34	2	124	125	1130.24	11.80		1130	270	4.3	3.2	20	146	27	146	44	23	21	3.21	0.74	2
93	603	B	34	2	127	128	1130.27	9.46		773	316	3.1	2.8	15	126	38	142	84	27	20	2.96	0.90	2
93	603	B	34	2	129	130.5	1130.29	13.17		993	342	3.5	3.9	24	133	33	77	65	29	21	4.01	1.13	2
93	603	B	34	2	133	134	1130.33	12.70		736	445	5.2	6.1	20	118	29	47	48	19	20	5.15	1.17	2
93	603	B	34	2	137	138	1130.37	10.23		936	282	3.9	2.2	19	107	33	37	46	22	21	2.39	0.55	2
93	603	B	34	2	137	142	1130.37	6.93	-23.55	478	374	2.7	2.4	12	98	45	50	72	27	21	2.40	0.90	2
93	603	B	34	2	143	144	1130.43	4.04		569	183	1.9	2.3		91	57	92	79	42	19	2.41	1.20	
93	603	B	34	2	145	146	1130.45	5.51		557	255	6.5	4.1	11	85	32	57	24	28	22	2.87	0.63	2
93	603	B	34	2	147	148	1130.47	5.66		449	326	6.1	3.4	12	103	35	77	30	33	24	2.27	0.56	2
93	603	B	34	2	149	150	1130.49	4.31		405	275	6.3	3.9		94	32	51	23	25	28	2.33	0.62	
93	603	B	34	3	0	1.5	1130.5	5.98		625	247	4.8	2.6	11	124	68	39	22	35	26	2.19	0.55	2
93	603	B	34	3	3	4	1130.53	3.36		201	431	6.7	6.4		73	71	26	19	25	20	3.66	0.96	
93	603	B	34	3	6	7	1130.56	0.54		35	392	6.7	7.3		49	97	22	19	24	17	4.35	1.09	
93	603	B	34	3	8.5	9.5	1130.58	0.88		148	153	7.3	5.2		57	69	14	14	18	17	3.65	0.72	
93	603	B	34	3	11	12	1130.61	3.98		775	133	6.6	3.9		97	59	13	13	21	23	2.65	0.59	
93	603	B	34	3	12.5	13.5	1130.62	5.83		875	172	2.9	2.4		97	105	25	36	42	21	2.71	0.83	
93	603	B	34	3	30	34	1130.8	4.14	-23.80	388	275	2.5	3.4	12	116	58	95	111	28	20	3.11	1.37	3
93	603	B	34	3	85	90	1131.35	5.02	-23.45	442	293	6.9	6.3	14	43	126	17	15	24	32	5.67	0.91	3
93	603	B	34	3	114	120	1131.64	1.31	-24.20	87	387	8.6	5.3		18	45	14	13	9	17	2.50	0.61	
93	603	B	34	4	12	18	1132.12	0.24	-25.35	13	479	7.9	4.9		37	50	19	11	23	13	2.01	0.62	
93	603	B	34	4	29	30	1132.29	0.91		51	460	7.0	3.3		29	45	25	13	28	13	1.49	0.47	
93	603	B	34	4	32	33	1132.32	1.01		45	574	7.4	4.8		35	56	27	14	35	14	2.10	0.65	
93	603	B	34	4	35	36	1132.35	0.66		48	355	6.3	4.1		44	39	22	12	25	14	2.18	0.64	
93	603	B	34	4	37	38	1132.37	0.80		75	276	5.9	3.2		45	35	23	12	25	15	1.82	0.54	
93	603	B	34	4	40	41	1132.4	2.87		150	494	6.7	4.8		72	27	21	12	30	26	2.42	0.72	

Leg	Site	Hole	Core	Section	Top depth (cm)	Base depth (cm)	Sample depth (mbsf)	TOC (%)	$\delta^{13}C_{org/TOC}$ (‰ VPDB)	C_{org}/P_{tot} (mol/mol)	P (ppm)	Al (%)	Fe (%)	Mo (ppm)	V (ppm)	Mn (ppm)	Zn (ppm)	Ni (ppm)	Cu (ppm)	Cr (ppm)	S (%)	Fe/Al (%/%)	Mo(s)/TOC
93	603	B	34	4	44.5	45.5	1132.44	3.62		189	495	3.8	2.2		93	37	37	27	44	13	1.84	0.57	
93	603	B	34	4	47.5	48.5	1132.47				538	5.9	2.7		63	28	17	22	20	13	1.65	0.46	
93	603	B	34	4	50	51	1132.5	1.40		59	609	7.4	4.2		64	25	13	18	14	15	1.72	0.57	
93	603	B	34	4	53	54	1132.53	5.20		435	308	6.0	3.3	11	70	25	17	24	21	15	2.72	0.55	2
93	603	B	34	4	54	58	1132.54	6.59	-26.55	501	340	6.3	3.4	11	85	22	17	21	18	17	2.33	0.54	2
93	603	B	34	4	56	57.5	1132.56	5.01		248	521	6.9	3.2		118	21	32	23	20	21	1.44	0.47	
93	603	B	34	4	59	60	1132.59	4.86		225	557	3.7	2.7	16	102	34	115	65	30	19	2.34	0.73	3
93	603	B	34	4	61.5	62.5	1132.61	5.23		165	818	3.3	2.6	19	152	40	217	83	34	22	2.32	0.79	4
93	603	B	34	4	64	65	1132.64	7.40		258	741	6.1	3.0	36	239	28	195	39	21	25	2.07	0.49	5
93	603	B	34	4	66	67	1132.66	6.15		278	570	4.2	2.5	29	176	41	373	73	31	24	2.37	0.59	5
93	603	B	34	4	69.5	70.5	1132.69	5.54		342	419	6.1	3.0	26	178	33	121	34	18	24	2.40	0.49	5
93	603	B	34	4	72	73	1132.72	5.27		484	281	6.5	2.9	24	161	37	81	28	17	21	2.00	0.45	5
93	603	B	34	4	75.5	76.5	1132.76	1.67		126	343	8.7	4.1		52	40	41	18	11	16	1.93	0.48	
93	603	B	34	4	78	79	1132.78	1.68		131	332	9.0	4.1		40	49	26	14	13	15	1.75	0.45	
93	603	B	34	4	82	83	1132.82	2.54		184	355	7.0	3.4		50	59	22	15	25	20	1.67	0.48	
93	603	B	34	4	84	85	1132.84	0.68		47	371	8.5	4.2		25	59	17	13	21	14	1.54	0.50	
93	603	B	34	4	87	88	1132.87	1.05		73	375	7.3	3.4		25	60	16	13	22	13	1.62	0.46	
93	603	B	34	4	90	91	1132.9	0.66		45	381	7.2	3.0		19	64	16	12	20	11	1.45	0.42	
93	603	B	34	4	92	93	1132.92	0.49		28	449	8.7	4.6		19	67	15	12	19	12	1.52	0.53	
93	603	B	34	4	95.5	96.5	1132.95	0.45		34	342	7.2	3.4		18	53	12	11	16	12	1.49	0.48	
93	603	B	34	4	96	101	1132.96	0.34	-25.70	29	300	8.3	3.7		19	51	12	10	18	13	1.00	0.45	
93	603	B	34	5	4	10	1133.54	2.60	-26.35	159	421	5.8	3.8		60	23	16	30	17	16	3.07	0.66	
93	603	B	34	5	97	103	1134.47	0.18	-24.80	10	484	8.9	3.5		16	34	14	14	17	12	0.41	0.39	
93	603	B	34	5	137	140	1134.87	2.04	-26.14	151	349	8.7	3.9		14	34	34	14	15	12	1.20	0.45	
93	603	B	34	6	12	18	1135.12	0.30	-24.80	28	279	10.3	3.9		13	29	9	9	5	13	0.56	0.38	
103	**641**	**A**	**6X**	**6**	**100**	**101.5**	**53.01**	**0.01**		**0**	**786**	**10.47**	**5.83**	**7**	**156**	**1154**	**82**	**86**	**63**	**70**	**0.06**	**0.56**	
103	**641**	**A**	**6X**	**6**	**140**	**141.5**	**53.41**	**0.05**	**-26.84**	**1**	**945**	**9.87**	**5.81**	**5**	**141**	**634**	**106**	**78**	**73**	**116**		**0.59**	
103	**641**	**A**	**6X**	**7**	**9.5**	**12.5**	**53.61**	**0.03**	**-26.49**	**1**	**882**	**9.70**	**5.95**	**5**	**143**	**639**	**101**	**68**	**94**	**70**	**0.03**	**0.61**	
103	**641**	**A**	**6X**	**7**	**30**	**34**	**53.82**	**7.99**	**-23.91**	**216**	**954**	**6.94**	**3.78**	**945**	**1710**	**364**	**2373**	**244**	**975**	**203**	**2.26**	**0.54**	**118**
103	**641**	**A**	**6X**	**CC**	**4**	**8**	**53.88**	**9.14**	**-23.61**	**206**	**1149**	**6.34**	**3.52**	**3332**	**1070**	**787**	**6415**	**486**	**243**	**114**	**3.06**	**0.56**	**365**
103	**641**	**A**	**6X**	**CC**	**14**	**18**	**53.98**	**9.81**	**-23.63**	**79**	**3223**	**6.54**	**4.78**	**6206**	**885**	**1320**	**3991**	**477**	**241**	**109**	**3.86**	**0.73**	**632**
103	**641**	**A**	**6X**	**CC**	**26**	**29**	**54.10**	**0.17**	**-25.99**	**16**	**285**	**5.74**	**2.35**	**15**	**71**	**3393**	**94**	**72**	**58**	**53**	**2.18**	**0.41**	**85**
103	**641**	**A**	**7X**	**1**	**12**	**13.5**	**54.23**	**0.13**	**-25.29**	**13**	**250**	**7.12**	**3.27**	**3**	**97**	**1241**	**86**	**48**	**46**	**71**	**0.09**	**0.46**	
103	**641**	**A**	**7X**	**1**	**60**	**61.5**	**54.71**	**0.18**	**-25.73**	**17**	**341**	**6.00**	**2.73**	**31**	**74**	**1630**	**44**	**58**	**77**	**39**	**0.16**	**0.45**	

Leg	Site	Hole	Core	Section	Top depth (cm)	Base depth (cm)	Sample depth (mbsf)	TOC (%)	$\delta^{13}C_{org/TOC}$ (‰ VPDB)	C_{org}/P_{tot} (mol/mol)	P (ppm)	Al (%)	Fe (%)	Mo (ppm)	V (ppm)	Mn (ppm)	Zn (ppm)	Ni (ppm)	Cu (ppm)	Cr (ppm)	S (%)	Fe/Al (%/%)	Mo(s)/TOC
210	1276	A	31	1	4	5	1079.04	0.03	**-26.07**	**3**	**276**	**3.80**	**2.83**	**1**	**67**	**167**	**57**	**33**	**8**	**55**		**0.7**	
210	1276	A	31	1	11	12	1079.11	0.08	**-25.82**	**8**	**261**	**6.83**	**4.83**	**1**	**104**	**352**	**61**	**87**	**24**	**77**	**0.12**	**0.7**	
210	1276	A	31	1	20	21	1079.2	0.11	**-23.32**	**11**	**251**	**6.14**	**4.10**	**1**	**100**	**286**	**53**	**28**	**29**	**70**	**0.07**	**0.7**	
210	1276	A	31	1	32	33	1079.32	0.5	**-24.62**	**47**	**275**	**6.58**	**2.64**	**4**	**113**	**532**	**49**	**23**	**66**	**74**	**0.17**	**0.4**	
210	1276	A	31	1	40	41	1079.4	0.49	**-24.95**	**45**	**283**	**6.73**	**2.81**	**1**	**117**	**585**	**70**	**24**	**68**	**76**	**0.17**	**0.4**	
210	1276	A	31	1	42	43	1079.42	0.51	**-24.63**	**45**	**291**	**6.74**	**2.78**	**1**	**116**	**619**	**65**	**24**	**68**	**74**	**0.19**	**0.4**	
210	1276	A	31	1	50	51	1079.5	0.48	**-24.26**	**43**	**290**	**6.66**	**2.81**	**1**	**118**	**623**	**69**	**25**	**77**	**76**	**0.17**	**0.4**	
210	1276	A	31	1	75	76	1079.75	0.24	**-24.82**	**16**	**382**	**6.17**	**2.50**	**1**	**108**	**920**	**49**	**23**	**91**	**71**	**0.11**	**0.4**	
210	1276	A	31	1	110	111	1080.1	0.05	**-25.47**	**5**	**268**	**6.67**	**4.31**	**1**	**103**	**532**	**50**	**175**	**31**	**72**	**0.48**	**0.6**	
210	1276	A	31	1	140	141	1080.4	4.45	**-25.62**	**172**	**668**	**6.21**	**4.99**	**3**	**1087**	**150**	**325**	**186**	**229**	**340**	**2.98**	**0.8**	
210	1276	A	31	2	17	18	1080.67	0.64	**-23.92**	**52**	**318**	**7.54**	**3.04**	**1**	**405**	**125**	**140**	**48**	**167**	**146**	**0.19**	**0.4**	
210	1276	A	31	2	22	23	1080.72	2.89	**-24.29**	**258**	**289**	**7.01**	**3.42**	**5**	**390**	**130**	**157**	**118**	**130**	**104**	**1.46**	**0.5**	**1.8**
210	1276	A	31	2	27	28	1080.77	5.46	**-24.67**	**105**	**1342**	**5.59**	**3.83**	**5**	**592**	**99**	**544**	**133**	**273**	**191**	**1.94**	**0.7**	**0.8**
210	1276	A	31	2	41	42	1080.91	1.9	**-23.24**	**157**	**312**	**6.23**	**2.85**	**1**	**346**	**181**	**186**	**69**	**361**	**97**	**0.67**	**0.5**	**0.5**
210	1276	A	31	2	52	53	1081.02	4.37	**-24.01**	**436**	**259**	**5.35**	**3.57**	**14**	**549**	**104**	**275**	**229**	**114**	**79**	**2.51**	**0.7**	**3.2**
210	1276	A	31	2	64	65	1081.14	5.35	**-24.07**	**457**	**302**	**5.11**	**4.22**	**16**	**362**	**110**	**120**	**187**	**109**	**79**	**3.31**	**0.8**	**3.0**
210	1276	A	31	2	97	98	1081.47	1.23	**-24.28**	**47**	**679**	**5.11**	**3.08**	**4**	**154**	**155**	**88**	**39**	**60**	**70**	**1.50**	**0.6**	**3.4**
210	1276	A	31	2	104	105	1081.54	1.24	**-24.02**	**118**	**271**	**6.51**	**2.90**	**2**	**192**	**228**	**114**	**52**	**121**	**91**	**0.99**	**0.4**	**1.3**
210	1276	A	31	2	116	117	1081.66	3.2	**-24.4**	**177**	**465**	**6.21**	**2.39**	**3**	**830**	**115**	**478**	**134**	**349**	**276**	**0.58**	**0.4**	**0.8**
210	1276	A	31	2	126	127	1081.76	8.59	**-24.71**	**215**	**1033**	**5.33**	**4.71**	**24**	**668**	**124**	**181**	**244**	**185**	**172**	**3.80**	**0.9**	**2.8**
210	1276	A	31	2	135	136	1081.85	4.85	**-24.51**	**359**	**349**	**5.51**	**3.24**	**10**	**484**	**113**	**259**	**259**	**148**	**95**	**2.19**	**0.6**	**2.1**
210	1276	A	31	3	2	3	1081.97				**258**	**5.44**	**3.60**	**3**	**292**	**112**	**110**	**113**	**100**	**86**	**2.34**	**0.7**	
210	1276	A	31	3	10	11	1082.05	2.84	**-24.05**	**301**	**244**	**5.20**	**2.60**	**3**	**321**	**120**	**208**	**105**	**195**	**111**	**1.25**	**0.5**	**1.1**
210	1276	A	31	3	15	16	1082.1	1.97	**-23.78**	**233**	**218**	**5.24**	**5.12**	**4**	**225**	**168**	**83**	**95**	**116**	**94**	**3.74**	**1.0**	**1.8**
210	1276	A	31	3	22	23	1082.17	2.43	**-23.72**	**98**	**643**	**5.03**	**2.84**	**1**	**119**	**1235**	**44**	**34**	**70**	**71**	**1.30**	**0.6**	**0.5**
210	1276	A	31	3	27	28	1082.22	2.13	**-23.89**	**79**	**694**	**4.19**	**4.09**	**5**	**88**	**1731**	**50**	**51**	**50**	**61**	**2.94**	**1.0**	**2.5**
210	1276	A	31	3	32	33	1082.27	4.17	**-23.96**	**224**	**480**	**5.56**	**4.12**	**3**	**101**	**367**	**52**	**34**	**82**	**77**	**2.74**	**0.7**	**0.6**
210	1276	A	31	3	37	38	1082.32	4.01	**-23.83**	**274**	**377**	**5.15**	**3.76**	**2**	**102**	**469**	**93**	**37**	**80**	**75**	**2.57**	**0.7**	**0.5**
210	1276	A	31	3	44	45	1082.39	3.23	**-23.84**	**126**	**661**	**5.63**	**4.62**	**2**	**129**	**433**	**40**	**42**	**82**	**84**	**3.36**	**0.8**	**0.7**
210	1276	A	31	3	66	67	1082.61	0.54	**-22.75**	**37**	**381**	**6.43**	**4.12**	**1**	**217**	**716**	**91**	**40**	**82**	**128**	**1.85**	**0.6**	**2.1**
210	1276	A	31	3	80	81	1082.75	0.83	**-23.23**	**65**	**327**	**6.24**	**3.28**	**1**	**132**	**207**	**66**	**35**	**81**	**111**	**0.88**	**0.5**	**1.0**
210	1276	A	31	3	85	86	1082.8	0.97	**-23.58**	**76**	**331**	**6.51**	**4.01**	**1**	**129**	**376**	**86**	**45**	**66**	**105**	**2.06**	**0.6**	**1.2**
210	1276	A	31	3	91	92	1082.86	1.96	**-23.69**	**144**	**352**	**6.99**	**6.26**	**3**	**254**	**498**	**401**	**136**	**152**	**205**	**4.59**	**0.9**	**1.6**
210	1276	A	31	3	98	99	1082.93	1.19	**-23.87**	**102**	**300**	**6.96**	**6.13**	**2**	**242**	**408**	**612**	**111**	**127**	**148**	**4.39**	**0.9**	**1.7**

Leg	Site	Hole	Core	Section	Top depth (cm)	Base depth (cm)	Sample depth (mbsf)	TOC (%)	$\delta^{13}C_{org/TOC}$ (‰ VPDB)	C_{org}/P_{tot} (mol/mol)	P (ppm)	Al (%)	Fe (%)	Mo (ppm)	V (ppm)	Mn (ppm)	Zn (ppm)	Ni (ppm)	Cu (ppm)	Cr (ppm)	S (%)	Fe/Al (%/%)	Mo(s)/TOC
210	1276	A	31	3	105	106	1083	1.25	-24.11	**82**	**393**	**5.87**	**3.47**	**1**	**145**	**2161**	**110**	**47**	**112**	**97**	**1.29**	**0.6**	**0.8**
210	1276	A	31	3	110	111	1083.05	2.28	-23.58	**126**	**466**	**5.86**	**6.80**	**3**	**138**	**2047**	**144**	**93**	**107**	**91**	**5.22**	**1.2**	**1.1**
210	1276	A	31	3	118	119	1083.13	0.6	-23.67	**38**	**407**	**6.31**	**2.63**	**1**	**131**	**121**	**75**	**29**	**81**	**89**	**0.27**	**0.4**	**1.0**
210	1276	A	31	3	15	16	1083.54	13.36	-26.17	**295**	**1168**	**5.13**	**7.72**	**10**	**160**	**276**	**162**	**268**	**172**	**70**	**7.02**	**1.5**	**0.7**
210	1276	A	31	4	27	28	1083.66	4.27	-26.47	**48**	**2315**	**6.02**	**6.23**	**8**	**243**	**136**	**78**	**109**	**105**	**101**	**4.81**	**1.0**	**1.8**
210	1276	A	31	4	49	50	1083.88	6.58	-26.82	**246**	**691**	**5.83**	**5.27**	**24**	**1171**	**106**	**1171**	**312**	**269**	**144**	**3.71**	**0.9**	**3.7**
210	1276	A	31	4	64	65	1084.03	5.2	-26.8	**313**	**429**	**7.15**	**5.76**	**15**	**566**	**129**	**293**	**296**	**158**	**119**	**4.14**	**0.8**	**2.9**
210	1276	A	31	4	69	70	1084.08	7.14	-26.8	**235**	**784**	**6.04**	**4.66**	**10**	**698**	**103**	**245**	**357**	**218**	**179**	**3.08**	**0.8**	**1.4**
210	1276	A	31	4	85	86	1084.24	0.78	-26.68	**81**	**248**	**8.62**	**3.70**	**1**	**226**	**135**	**101**	**54**	**61**	**105**	**1.13**	**0.4**	**1.8**
210	1276	A	31	4	120	121	1084.59	0.16	-25.42	**16**	**265**	**5.25**	**2.33**	**1**	**88**	**774**	**56**	**101**	**34**	**57**	**0.27**	**0.4**	**4.3**
210	1276	A	31	5	5	6	1084.94	0.51	-25.8	**44**	**297**	**4.36**	**2.30**	**1**	**79**	**2776**	**92**	**28**	**35**	**53**	**0.31**	**0.5**	
210	1276	A	31	5	40	41	1085.29	0.06	-24.73	**4**	**435**	**5.89**	**2.59**	**2**	**126**	**110**	**50**	**37**	**34**	**69**	**0.08**	**0.4**	
210	1276	A	31	6	3	4	1085.96	0.54	-25.43	**44**	**319**	**5.18**	**2.25**	**1**	**91**	**1296**	**63**	**37**	**38**	**64**	**0.29**	**0.4**	

7

Reassessing the nitrogen isotope composition of sediments from the proto-North Atlantic during Oceanic Anoxic Event 2

"Wisdom is knowing when you can't be wise."

Mohammed Ali

Abstract

Sediment records of the stable isotopic composition of nitrogen ($\delta^{15}N$) show exceptionally light $\delta^{15}N$ values at several sites in the proto-North Atlantic during Oceanic Anoxic Event 2 around the Cenomanian-Turonian boundary (~94 Ma) The low $\delta^{15}N$ during the event is generally attributed to an increase in N_2-fixation. Surprisingly, published $\delta^{15}N$ values for OAE2 vary widely, even for similar locations. Using analyses of $\delta^{15}N$ for sediments from three open ocean and two coastal sites, we show that this reported variation is likely related to the pre-treatment of sediment samples with acid prior to the $\delta^{15}N$ analysis. A compilation of all available data for unacidified OAE2 samples for the proto North-Atlantic demonstrates that the most pronounced negative shift in $\delta^{15}N$ from pre-OAE2 to OAE2 occurs in the open ocean, with $\delta^{15}N$ never lower than -3‰. Using a box model of N cycling for the proto-North Atlantic during OAE2, we show that N_2-fixation is a major contributor to the $\delta^{15}N$ signal, especially in the open ocean. Incomplete uptake of NH_4^+ for phytoplankton growth is important in regions dominated by downwelling, with lateral transport of NH_4^+ acting as a major source. In the southern proto-North Atlantic, where bottom waters were euxinic, the light $\delta^{15}N$ signature is largely explained by upwelling of NH_4^+. Our study provides an overview of regional differences in $\delta^{15}N$ in the proto-North Atlantic and highlights the role of lateral exchange of water and nutrients, in addition to local biogeochemical processes, in determining $\delta^{15}N$ values of OAE2 sediments.

1. Introduction

Nitrogen (N) is an essential and often limiting nutrient for primary production in the ocean. Nitrogen fixation, a process in which certain members of the plankton community reduce atmospheric N_2 to ammonium (NH_4^+; Paerl, 1992), is the major source of new N in the ocean (Gruber, 2004). Although many factors may limit N_2-fixation, it is commonly favoured in environments where there is a deficit of N relative to phosphorus (P; Tyrrell, 1999). Denitrification (here used to refer to all biological processes that remove inorganic N) is the major sink of fixed N in the ocean. It is largely restricted to low-oxygen zones in the water column (Codispoti et al., 2001) and continental shelf and slope sediments (Middelburg et al., 1996).

Global rates of denitrification and N_2-fixation can vary in time due to changes in climate and ocean oxygenation (e.g., Codispoti et al., 2001; Algeo et al., 2014). Consequently, the N inventory in the global ocean may also change with time. Because of preferential biological uptake of the lighter N isotope (^{14}N) over the heavier one (^{15}N) (DeNiro and Epstein, 1981; Minagawa and Wada, 1984), the N-isotope composition ($\delta^{15}N$) of bulk sediments and buried organic matter can be used to identify such perturbations of the N cycle (e.g., Bauersachs et al., 2009; Deutsch et al., 2004). Based on $\delta^{15}N$ records, it has been suggested, for example, that water-column denitrification was significantly reduced during glacial periods (Ganeshram et al., 1995). This would have increased the oceanic N inventory relative to P, possibly suppressing N_2-fixation (Ganeshram et al., 2002).

All biological N reactions lead to N isotope fractionation, though the impact may vary for each process. While denitrification reduces the size of the nitrite and nitrate (NO_x^-) reservoir and increases the $\delta^{15}N$ of the remaining NO_x^- pool, N_2-fixation adds N with low (slightly negative to zero) $\delta^{15}N$ to the ocean. This may counteract both the mass and isotopic effects of denitrification (Ryabenko, 2013). In a system with both NH_4^+ and NO_x^- present, NH_4^+ will be preferentially assimilated by phytoplankton. In anoxic environments, NH_4^+ is the dominant form of N. If low-oxygen, ammonium-rich waters are upwelled, the isotopic fractionation of NH_4^+ during primary production may significantly decrease $\delta^{15}N$ values of particulate organic nitrogen (PON) (Waser et al., 1998; Higgins et al., 2012).

Records of $\delta^{15}N$ for sediments from the proto-North Atlantic suggest a particularly strong perturbation of the N cycle during Oceanic Anoxic Event (OAE2) around the Cenomanian-Turonian boundary (93.9 Ma; Meyers et al., 2012a). The exceptionally light $\delta^{15}N$ values during the event have been interpreted as indicators of high rates of N_2-fixation (Table 1; Kuypers et al., 2004b; Junium and Arthur, 2007) and NH_4^+ upwelling (Higgins et al., 2012). A dominant role for long-term diagenesis is generally discounted because of similar trends in compound-specific and bulk $\delta^{15}N$ records (Higgins et al., 2012; Robinson et al., 2012). At many sites, such as at Demerara Rise, in the southern part of the basin, the decline in $\delta^{15}N$ coincides with the rise in the stable carbon isotopic composition ($\delta^{13}C$) of sedimentary carbonate ($\delta^{13}C_{carb}$) and organic matter ($\delta^{13}C_{org}$) which is characteristic for OAE2 (e.g., Kuypers et al., 2002; Tsikos et al., 2004). The increase in

N_2-fixation is assumed to be due to enhanced denitrification and an increase in P recycling linked to the expansion of low-oxygen conditions during the event (Kuypers et al., 2002). The widespread N_2-fixation during OAE2 is supported by recent model studies of the biogeochemistry in the proto-North Atlantic (Monteiro et al., 2012; Ruvalcaba Baroni et al., 2014b).

Surprisingly, however, several studies of OAE2 sediments report a parallel rise in $\delta^{15}N$ and $\delta^{13}C$ during the event (Jenkyns et al., 2007) or the lack of a clear trend, whereas others have shown that such a trend exists (e.g., Deep Sea Drilling Project [DSDP] Site 367; Rau et al., 1987 versus Kuypers et al., 2004b). Comparison of the methods used to analyse sediment $\delta^{15}N$ in the above examples suggests that such deviations from the expected trend are only observed for sediments that have first been subjected to acid treatment to remove carbonates prior to the $\delta^{15}N$ measurement. Acid treatment (Lohse et al., 2000; Brodie et al., 2011), in particular when followed by removal of the supernatant, is known to lead to removal of N compounds (Nieuwenhuize et al., 1994). As a consequence, changes in the $\delta^{15}N$ of sediments may no longer reflect changes in N dynamics in the proto-North Atlantic.

In this study, we compiled all the available $\delta^{15}N$ data in the proto-North Atlantic for coastal and deep-sea sediments from OAE2 that have not been pre-treated with acid. Since little is known about the N dynamics in the open ocean and along the northern coast of the proto-North Atlantic, we expand the existing data set with new data for three open ocean sites and two coastal sites. We also demonstrate how acid-pre-treatment of the samples would have affected our results. Finally, we use a box model for the proto-North Atlantic to assess whether the observed $\delta^{15}N$ values in the various coastal and open ocean settings can be explained by enhanced N_2-fixation and/or incomplete use of NH_4^+. While the overall proto-North Atlantic was low in dissolved oxygen, clear regional trends in its distribution can be distinguished, based on geological records (e.g., Owens et al., 2012; Ruvalcaba Baroni et al., 2014a). As the N cycle is strongly affected by changes in dissolved oxygen, regional differences in sediment N isotope values in the proto-North Atlantic are expected.

2. Material and Methods

2.1. Study sites

All published isotope ratios of total sediment N ($\delta^{15}N_{TN}$) for non-acidified samples from the proto-North Atlantic were compiled (Fig. 1; Table 1). This data compilation comprises four sites in the south (DSDP Site 367 and Ocean Drilling Program [ODP] Sites 1258, 1260 and 1261 at Demerara Rise; Kuypers et al., 2004b; Junium and Arthur, 2007; Higgins et al., 2012) and one site in the north (Wunstorf; Blumenberg and Wiese, 2012). Sediments from five additional sites were selected for analysis in areas in the proto North-Atlantic for which there is either limited data or where previous records have a low depth resolution. These sites are located in the northern coast (Wunstorf and Bass River) and distributed over the central open ocean (DSDP Site 386, ODP Sites 641 and 1276).

Site	Estimated Water depth (m)	$\delta^{15}N_{TN}$(min,max) pre-OAE2	OAE2	Shift	Reference
Central Open Ocean					
DSDP 386 (new)	2000-3800	1.3(-2.5,2.6)	-2 (-2.8,1.1)		This study
ODP 641 (new)	3500	2.2(1.8,2.7)	-0.2 (-2.7,3)		This study
ODP 1276 (new)	>2000	1.9(1.1,2.8)	-1,1 (-2.7,1.9)		This study
Mean		*1.8*	*-1.1*	*-3*	
Southern Open Ocean					
DSDP 367	3700	-1.3 (-2,-0.8)*	-1.4(-2.3,0.1)*	-0.1	Kuypers et al. (2004b)
Southern Coast					
ODP 1258		-0.8 (-1.9,-0.2	-1.8 (-2.2,-0.3)		Higgins et al. (2012)
ODP 1260	1000	-1 (-1.6,-0.5)	-2 (-3,-0.3)		Junium and Arthur(2007)
ODP 1261	1000	n.a.	-2 (-3,-0.3)		Junium and Arthur(2007)
Mean		*-0.9*	*-1,9*	*-1*	
Northern Coast					
Bass River (new)	<30	1.4(1.2,1.7)	1.3(-0.2,2)	-0.1	This study
East.-North. Coast					
Wunstorf	100-150	n.a.	1 (-0.9,1)*		Blumenberg and Wiese (2012)
Wunstorf (new)		1,4(0.6,2.6)	0.8(-1.5,3.3)		This study
Mean		*1.4*	*0.9*	*-0.5*	

Table 1. *Compilation of sites where published and new data of $\delta^{15}N_{TN}$ (‰) in sediments not treated with acid are available for the proto-North Atlantic. The mean $\delta^{15}N_{TN}$ before and during OAE2 is presented, as well as the maximum and minimum values for each time interval. Evidence from biomarkers indicating a relatively high abundance of N_2-fixing cyanobacteria are indicated where available/present (*), n.a. is not available. Standard deviations are shown as error bars in Fig. 7.*

2.1.1. Wunstorf: Northwest Germany

The Wunstorf core was drilled ~25 km west of Hannover, Germany (TK 25 Wunstorf, no. 3522, 52°23.942'N, 9°28.824'E). During the Late Cretaceous the Hannover region was part of the epicontinental shelf sea that formed when large parts of Eurasia were flooded during the global Cenomanian transgression. The Upper Cenomanian sediments, belonging to the Brochterbeck Formation (71.5-49.6 meters below surface – mbs), generally consist of white limestones and light-gray marly limestones. The Brochterbeck Formation is overlain by the Hesseltal Formation (49.6-23.1 mbs), which comprises the ~13.5 m-thick OAE2-interval. The Hesseltal Formation consists of rhythmically alternating multicolored marls, light gray (marly) limestones and black shales, with a maximum TOC content of ~3% (Hetzel et al., 2011). The retrieved sediments are estimated to have been deposited in water depths of 100 to 150 m (Wilmsen, 2003). The OAE2-interval was previously identified based on detailed biostratigraphy (Voigt et al., 2008, and references therein). The exact placement of the OAE2-interval was based on a ~2‰ positive shift in the $\delta^{13}C_{carb}$ (Voigt et al., 2008), which was recently also observed in the $\delta^{13}C_{org}$ (Du Vivier et al., 2014).

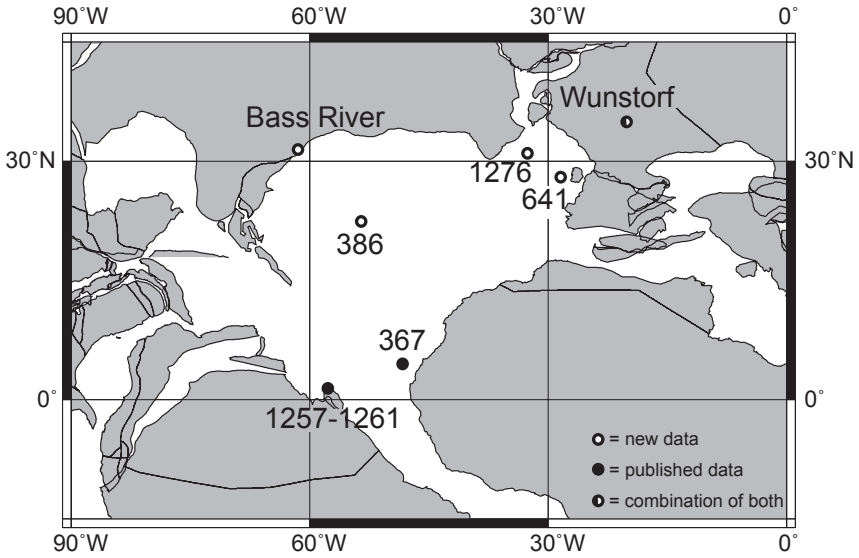

Figure 1. *Paleogeographic map of the proto-North Atlantic during OAE2, indicating the location of the sites where $\delta^{15}N$ data for samples that where not pre-treated with acid are available for the Cenomanian-Turonian transition. Open circles indicate the sites for which new $\delta^{15}N$ data are presented in this study: Bass River, 386, 641 and 1276. Black circles are sites for which data of $\delta^{15}N$ were published previously: DSDP 367 (Kuypers et al., 2004b) and ODP 1258, 1260 and 1261 (Higgins et al., 2012; Junium and Arthur, 2007). Black- and white circles indicate the sites where both $\delta^{15}N$ data were previously published (Wunstorf; Blumenberg and Wiese, 2012) and where new $\delta^{15}N$ data with a higher resolution are presented. The map was generated at http://www.odsn.de/odsn/services/paleomap/paleomap.html.*

2.1.2. Bass River: New Jersey Shelf

The Bass River borehole was drilled as part of the New Jersey Coastal Plain, ODP Leg 174AX, New Jersey, USA (39°36'42"N, 74°26'12"W, Miller et al., 1998). The retrieved Upper Cenomanian to Lower Turonian sediments consist of homogenous dark gray, (micro)fossil rich, micaceous silty clays to clayey silts, with a relatively low average total organic carbon content (TOC) of ~1% and a maximum of ~2.5% (Bowman and Bralower, 2005). The persistent presence of benthic foraminifera and relatively modest TOC to total P ratios (C_{org}/P_{tot}), indicate that the bottom waters were never completely depleted in oxygen (Chapter 3). Assemblages of benthic foraminifera indicate that the entire sequence was deposited on a shallow shelf, predominantly in an inner neritic setting (water depth <30 m; Sugarman et al. 1999). The approximately 13 m long OAE2-interval was identified based on nannofossil biostratigraphy and ~2.5‰ positive shifts in $\delta^{13}C_{carb}$ and $\delta^{13}C_{org}$ (Sugarman et al., 1999; Bowman and Bralower, 2005; Chapter 3).

2.1.3. *Site 386: Central Bermuda Rise*

Site 386 was drilled on the Central Bermuda Rise by DSDP Leg 43, some km south-southeast of Bermuda (31°11.21'N, 64°14.94'W, 4793 m water depth). Site 386 is the most centrally located proto-North Atlantic site yielding upper Cenomanian to lower Turonian sediments. The Late Cretaceous sediments predominantly consist of green, gray and black clay,- and mudstones, with a maximum TOC content up to 13%

(Chapter 6), that were deposited at a water depth >2000 m (Chenet and Francheteau, 1980). The OAE2-interval was clearly identified by a ~2.5‰ positive shift in $\delta^{13}C_{org}$ (Chapter 6).

2.1.4. *Site 641: Galicia Bank*

Site 641 was drilled during ODP Leg 103, and is located on the western margin of the Galicia Bank, offshore northwestern Spain (42°09.3'N, 12°10.9'W, 4646 m water depth). The Upper Cenomanian to Lower Turonian sediments generally consist of green and gray claystones, deposited at an estimated water depth of 3500 m. The sequence may contain significant hiatuses. The OAE2-interval itself is represented by a ~0.3 m of dark green and black shales (Shipboard Scientific Party, 1987b), which is marked by a ~2.5‰ positive shift in $\delta^{13}C_{org}$ and an average TOC content of ~9%. The organic carbon background values are typically <0.1% (Thurow et al., 1988; Chapter 6).

2.1.5. *Site 1276: Newfoundland Basin*

Site 1276 was drilled during ODP Leg 210, in the Newfoundland Basin, offshore the eastern Canadian continental margin (45°24.3198'N, 44°47.1496'W, 4565 m water depth). The mid-Cretaceous sequence consists of mud-dominated gravity flow deposits (Shipboard Scientific Party, 2004). The OAE2-interval itself, however, consists of a 3.5 m thick stack of mainly pelagic sediments (Urquhart et al., 2007), supported by a drastic drop of terrestrial palynomorphs, with an average TOC content of 4% and maximum values up to 13% (Sinninghe Damsté et al., 2010). Large positive shifts of ~4.5‰ in $\delta^{13}C_{org}$ and >5‰ in the stable carbon isotopes of the bacterial biomarker, $C_{31}17\beta,21\beta(H)$-hopane, define the OAE2-interval (Sinninghe Damsté et al., 2010).

2.2. *Sediment geochemistry*

The Bass River core was sampled at and by the Rutgers Core Repository (Rutgers University, New Jersey, USA). The Wunstorf core, Site 386, Site 641 and Site 1276 were sampled at the IODP core repository in Bremen (Marum, Bremen University, Germany). After shipment to Utrecht aliquots of the samples were cleaned, ground, freeze dried and subsequently stored cool and dry until analysis. All five cores contain sediments of the Cenomanian-Turonian transition.

Total sediment N (wt. %) and $\delta^{15}N_{TN}$ were measured using a Fisons Instruments CNS NA 1500 analyzer coupled to a Thermo Delta Plus isotope ratio spectrometer. The average

analytical uncertainty based on analyses of duplicate sediment samples was 0.0041 wt. % (1σ = 0.0043) for N and 0.173 (1σ = 0.177) for $\delta^{15}N_{TN}$.

Samples were still available for a few intervals of Site 386, Site 641, Bass River and Wunstorf. Aliquots of 0.5 g dried sediment from each of these intervals were decalcified by shaking in excess 1M HCl, initially for 4 h and for a further 12 h after addition of new acid. The supernatant was discarded after centrifugation and the residue was rinsed with demineralized water in two consecutive steps. The sediment that was pre-treated with acid was dried, ground in an agate mortar and analyzed for isotope ratios of sediment N ($\delta^{15}N_{TNacid}$). Decalcified samples were also available for an additional site (DSDP Site 367), for which we measured $\delta^{15}N_{TNacid}$ as well. Supporting geochemical data, which here includes total organic carbon (TOC wt. %), total phosphorous (P_{tot} wt. %), $\delta^{13}C_{carb}$ and $\delta^{13}C_{org}$, for all cores were obtained from the literature (Bowman and Bralower, 2005; Voigt et al., 2008; Sinninghe Damsté et al., 2010; Hetzel et al., 2011; Du Vivier et al., 2014; Chapters 3 and 6). The profile of $\delta^{15}N_{TN}$ for Site 367 was previously measured by Kuypers et al. (2004b).

					Coast					
	Open Ocean		**Northern**		**North.-east**		**Southern**		**Tethys Gate.**	
	pre-OAE2	OAE2	pre-OAE2	OAE2	pre-OAE2	OAE2	pre-OAE2	OAE2	pre-OAE2	OAE2
NH_4^+UP	0	0.02	0	1.1	0	0	0	3.9	0	0.5
NO_3^-UP	2	2.4	6.8	1.3	0.2	0.4	4.8	1.2	1.1	0.7
NH_4^+LT	0	2.8	0	0.7	0	0.1	0	0.3	-	-
NO_3^-LT	5.1	2.1	2	1.5	0.2	0.9	0.2	0.4	-	-
TOTNin	7.1	7.32	8.8	4.6	0.4	1.4	5	5.8	1.1	1.2
N2FIX	0.25	5.2	0.3	1.5	0.1	0.3	3	1.5	0.04	1.2
DENW	1.2	9.7	0	0.3	0	0.04	0.1	0.1	0	0.03
DENS	0.84	1.5	0.2	1.1	0	0.06	2	0	0.02	0.1
DENtot	2.04	11.5	0.2	1.4	0	0.1	2.1	0.1	0.02	0.14
NIT	3.18	0	2	0	0.5	0	3.2	0	0.5	0
$[NH_4^+]_{sub}$	0	29	0	11	0	0	0	31	0	9
$[NO_x^-]_{sub}$	44	0	26	12	16	14	35	10	16	7
$[O_2]_{sub}$	144	11	116	11	157	94	30	0	140	27

Table 2. *Relevant rates and components affecting the $\delta^{15}N$ in the MB2 model for pre-OAE2 and OAE2 conditions. Major processes in the N cycle (Tmol N y^{-1}) and concentrations (μM) of subsurface ammonium ($[NH_4^+]_{sub}$), nitrate ($[NO_x^-]_{sub}$) and oxygen ($[O_2]_{sub}$) in the central open ocean and in coastal regions are listed. The abbreviations NH_4^+LT, NH_4^+UP and DEN_{TOT} refer to the upwelling flux of recycled NH_4^+, lateral transport of NH_4^+ and the sum of water column (DENW) and sedimentary denitrification (DENS) for each region. NO_3^-LT, NO_3^-UP and TOTNin refer to the upwelling flux of NO_3^-, lateral transport of NO_3^- and total input of N to surface waters. N_2-fixation and nitrification are referred to as N2FIX and NIT.*

2.3. *Model*

The model used in this study is a simplified version of the multi-box model of Ruvalcaba Baroni et al. (2014b), that describes the coupled dynamics of particulate organic carbon, particulate organic and dissolved N and P and dissolved oxygen in the proto North-Atlantic during OAE2. Here, we use the same settings for all cycles as those in their multi-box model (MB1), but we exclude regions for which data of $\delta^{15}N_{TN}$ are not available (e.g., Western Interior Seaway). Based on results of MB1, Ruvalcaba Baroni et al. (2014b), suggest that N_2-fixation was widespread during OAE2. Uptake of NH_4^+ by primary producers is suggested to be important in all upwelling areas. Denitrification is significant in the central open ocean and along the northern coast. All rates of N processes in our simplified model (MB2) are summarized in Table 2.

2.3.1. *Model structure*

We use the MB2 model to assess whether we can explain the $\delta^{15}N$ values for sediments in the central open ocean and 4 coastal regions during OAE2. The central open-ocean box includes Sites 386, 603 and 1276. The coastal boxes are: the Southern Coast (upwelling region where Demerara Rise is located), the Northern Coast (upwelling region where Bass River is located) and the Northeastern Coast (downwelling region where Wunstorf is located). The Tethys Gateway is also included in the MB2 model because lateral exchange from the gateway into the central open ocean is important in the multi-box model. Further details on the segmentation and water fluxes of the model are presented in Supplements S1.

The N pools included in the model are NO_x^-, NH_4^+ and PON. In surface waters, only one combined inorganic nitrogen reservoir is considered which is also referred to as NO_x^- because NH_4^+ is initially close to zero. A full description of the model can be found in Ruvalcaba Baroni et al. (2014a) and in Ruvalcaba Baroni et al. (2014b). Rate laws for N processes are summarized in Table 3. Perturbations in the MB2 model to simulate OAE2 conditions are taken from the baseline OAE2 scenario in Ruvalcaba Baroni et al. (2014b) their (BsLi-N).

2.3.2. *Nitrogen isotope dynamics*

The MB2 model resolves the dynamics of the two stable N isotopes, ^{15}N and ^{14}N. The conventional δ-notation (‰) for N isotope ratios with respect to atmospheric N (R_{atm}) is:

$$\delta^{15}N_{res} = \left(\frac{R_{Nres}}{R_{atm}} - 1 \right) \cdot 1000 , \quad (1)$$

where R_{Nres} is the ratio between $^{15}N_{res}$ and $^{14}N_{res}$ of the corresponding N reservoir (N_{res}) in the ocean. We explicitly model the reservoir for $^{15}N_{res}$ and we calculate $^{14}N_{res}$ from the total N pool ($^{14}N_{res} = TOTN_{res} - {}^{15}N_{res}$) to detect changes in $\delta^{15}N_{res}$ with time. The ^{15}N pools included in the model are for NO_x^-, NH_4^+ and PON.

In our initial conditions, $^{15}N_{res}$ in the ocean accounts for the same percentage as in the atmosphere (0.366 % of the total atmospheric N):

N process	^{15}N equation	ε range	ε in model
NO_x^- uptake	$NUPTAKE15 = \alpha_{PP} \cdot R_{NOx} \cdot NUPTAKE$	-5 to 0 [b]	0**
NH_4^+ uptake	$NUPTAKE15 = \alpha_{PP} \cdot R_{NH4} \cdot NUPTAKE$	-15 to -4 [a,c,f]	-4**
N_2-fixation	$N2FIX15 = \alpha N2FIX \cdot R_{atm} \cdot N2FIX$	-3 to 0 [d,k,l]	-3
N release	$NREM15 = \alpha NREM \cdot R_{PON} \cdot NREM$	0	0
PON export	$NEXP15 = \alpha_{EX} \cdot R_{PON} \cdot NEXP$	-1 to 0 [f]	-1
Ammonification	$AMMONI15 = \alpha_{AMMONI} \cdot R_{PON} \cdot AMMONI$	0	0
Nitrification	$NIT15 = \alpha_{NIT} \cdot R_{NH4} \cdot NIT$	-25 to -7 [g,h]	-20
Water column Denitrification	$DENW15 = \alpha_{DENW} \cdot R_{NOx} \cdot DENW$	-23 to -5 [d,e,i,j]	-10
Sediment Denitrification	$DENS15 = \alpha_{DENS} \cdot R_{NOx} \cdot DENS$	-6 to -1 [d,j,k]	-4
PON burial	$NBUR15 = \alpha_{BURN} \cdot R_{PON} \cdot NBUR$	-6 to 0 [d]	0
Transport of inorganic N	$N15T = R_{source} \cdot NT$	none	none

Table 3. *Rate equations for the ^{15}N processes, the corresponding range of enrichment factors (ε in ‰) found in the literature and the values used in the model. The fractionation factor is calculated as* $\alpha = \frac{\varepsilon}{1000} + 1$ *for each corresponding process (in subscripts). R is the* $\frac{^{15}N}{^{14}N}$ *ratio of the corresponding source pool indicated with subscripts. For a full description of ε values of* NO_x^- *uptake and* NH_4^+ *uptake (**) see section 2.3.3 and S3. [a] Altabet and Francois (1994), [b] Waser et al. (1998), [c] Hoch et al. (1994), [d] Brandes and Devol (2002), [e] Gruber (2004), [f] Higgins et al. (2011), [g] Brandes and Devol (1997), [h] Mariotti et al. (1981), [i] Sigman et al. (2000), [j] Kritee et al. (2012), [k] Carpenter et al. (1997), [l] Capone et al. (1997).*

$$^{15}N_{res} = TOTN_{res} \cdot 0.00366, \quad (2)$$

hence $\delta^{15}N_{res}^{initial} = 0$. After reaching a geochemical steady state for N pools during pre-OAE2, fractionation factors for all N processes are included, with the exception of N uptake (initially zero). The model is then run until a new isotopic equilibrium state is reached before implementing OAE2 perturbations.

The distribution of components with time are calculated using the set of differential equations shown in Supplements S2 and Table S1. The equations for individual ^{15}N processes are summarized in Table 3.

Reported values of enrichment factors (ϵ) for key N processes differ widely, especially regarding denitrification in sediments and the water column, uptake of NH_4^+ and nitrification. N_2-fixation has a small fractionation effect, producing cells with a $\delta^{15}N$ that is relatively close or slightly depleted (-3‰) to atmospheric values (Hoering and Ford, 1960; Minagawa and Wada, 1986; Carpenter et al., 1997; Capone et al., 1997; Brandes and Devol, 2002). In general, we chose the most commonly used and/or most recently suggested for each process. For denitrification and nitrification, we chose mid-range values for in our simulations. In order to assess whether the isotopic signal of N could be explained by N_2-fixation alone, we chose the most negative reported in literature. The compilation of the reported as well as the chosen values for this study are listed in Table 3.

As records of $\delta^{15}N_{TN}$ mainly represent the isotopic composition of organic matter, comparison between model results and data are only possible for the $\delta^{15}N$ of PON. Because we aim to capture the major shift in $\delta^{15}N_{TN}$ for each region during the Cenomanian-Turonian transition, we average the $\delta^{15}N_{TN}$ values measured for pre-OAE2 and OAE2-intervals, respectively. Additionally, we calculate the standard deviation of each averaged $\delta^{15}N_{TN}$ and identify the full range for both time intervals. In the case where several $\delta^{15}N_{TN}$ records are available for one single region and data matched our stringent quality criteria (i.e., no acidification; Table 1), all $\delta^{15}N_{TN}$ values for that region are included in the average. In order to differentiate the $\delta^{15}N$ from records and from the model, we refer to the modeled isotopic composition of the organic N as $\delta^{15}N_{model}$.

2.3.3. Numerical Experiments

We perform three main numerical experiments (E1, E2 and E3) with the MB2 model in order to identify which processes in the N cycle could potentially contribute to the $\delta^{15}N_{TN}$ observed in OAE2 sediments. Denitrification and nitrification, when unbalanced, may influence the $\delta^{15}N$ of the water column (Ryabenko, 2013) and, thus, the signal of the buried organic N. We build an additional model (MB3) with all the same characteristics as the MB2 model, but with new parameterizations of nitrification and water-column denitrification (Supplements S3). The new parameterization in MB3 reduces water-column denitrification and increases nitrification without the need to alter the initial conditions. We then repeat the three experiments with the MB3 model in order to assess the effect of reduced denitrification on $\delta^{15}N_{TN}$. The experiments performed with the MB2 model are denoted with subscript MB2 and those carried out with the MB3 model with subscript $_{MB3}$.

We start with a simple experiment (E1) assuming complete N assimilation by phytoplankton. Therefore, primary production has no fractionation ($\alpha_{PP} = 1$). For experiment two (E2), we assess the fractionation effect of primary productivity due to incomplete uptake of N in surface waters. We assume that the upwelled NH_4^+ is neither fully consumed nor fully oxidized in surface waters due to excess NH_4^+. Because N uptake in the surface layer is modelled as one single pool, α_{PP} accounts for the contribution of all inorganic N, including NH_4^+, and their isotope effect. Moreover, α_{PP} is adjusted for each region according to the amount of upwelled NH_4^+ relative to the total upwelled N. The fractionation factor is then calculated as:

$$\alpha_{PP} = (P_{NH_4^+} \cdot \epsilon_{PP_{NH}} + P_{NO_x^-} \cdot \epsilon_{PP_{NO}}) / 1000 + 1, \quad (3)$$

where P_{NH4+} and P_{NOx-} are the portion of upwelled NH_4^+ and NO_x^- relative to total upwelled N, respectively (e.g., $P_{NH_4^+} = \frac{NH_4^+ UP}{TOTNUP}$, where NH_4^+ and TOTNUP represent upwelling of NH_4^+ and total dissolved N, respectively). We consider an enrichment factor of $\epsilon_{PP_{NO}} = 0\%$ when NO_x^- is the only N nutrient for primary production and of $\epsilon_{PP_{NH}} = 4‰$ (Higgins et al., 2011; Algeo et al., 2014) when NH_4^+ replaces NO_x^-. In Table 2, we show the upwelling fluxes for NH_4^+ and NO_x^- given by the model in each region. In E2, α_{PP}

values in the central open ocean and the Northeastern Coast are assumed to be 1, because the upwelled NH_4^+ is very small.

Lateral transport in the multi-box model is important even in surface waters. All regions are influenced by the incoming waters of one or more neighboring areas. As a third experiment (E3), we consider the additional effect that lateral transport of NH_4^+ to surface waters can have on fractionation during primary production. We estimate the lateral transport of NH_4^+ and NO_x^- for each region and calculate α_{PP} following equation 3, but including both upward and lateral transport of N (full description in Supplements S4). A summary of calculated α_{PP} values for each experiment is given in Table S3.

3. Results

3.1. Relationship between TOC, C_{org}/N and $\delta^{15}N_{TN}$

A scatter plot of $\delta^{15}N_{TN}$ versus TOC for all 5 locations reveals a clear, non-linear, negative relation between TOC and $\delta^{15}N_{TN}$ at both coastal and open ocean sites (Fig. 2a). When the TOC content is low (<2%), $\delta^{15}N_{TN}$ decreases sharply with increasing TOC, with most $\delta^{15}N_{TN}$ being positive. With further increasing TOC, all $\delta^{15}N_{TN}$ values are negative until they become nearly constant with a distinct minimum of ca. -3‰ (when TOC>4%). A

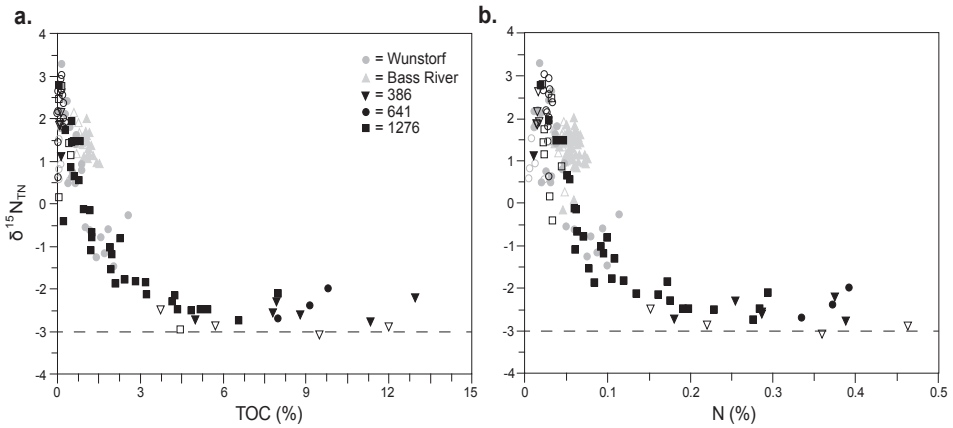

Figure 2. *Total organic carbon (TOC) (a) and total nitrogen (N) (b) versus $\delta^{15}N_{TN}$. Coastal sites are indicated in light gray. Open and closed symbols indicate pre-OAE2 and OAE2 sediments, respectively. The lower limit of $\delta^{15}N_{TN}$ is indicated with the dashed horizontal line.*

similar relation is observed between $\delta^{15}N_{TN}$ versus total N (Fig. 2b). A Keeling plot of OAE2 $\delta^{15}N_{TN}$ revealed an "end-member" value for N_2-fixation of -3. Note that most $\delta^{15}N_{TN}$ at both coastal sites (Wunstorf and Bass River), together with most values for pre-OAE2 conditions at the other sites, are positive.

3.2. *Effect of acidification on $\delta^{15}N_{TN}$*

The $\delta^{15}N_{TN}$ measured in untreated and acid-treated samples from Sites 367 and 386 differs (Fig. 3). At both sites, $\delta^{15}N_{TNacid}$ is more negative than $\delta^{15}N_{TN}$ and shows an opposite trend, especially at Site 386.

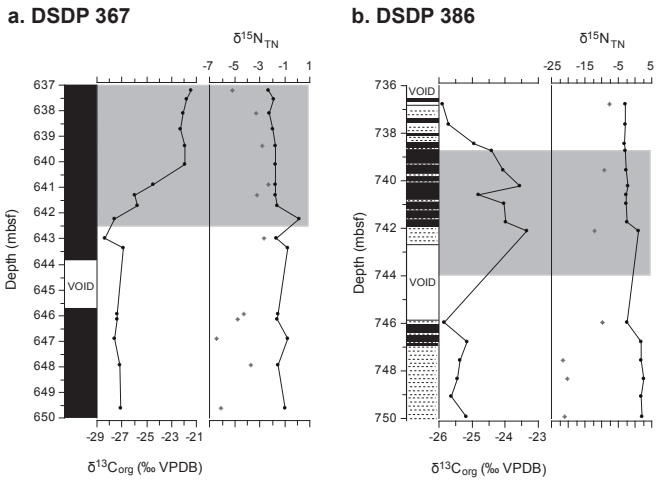

Figure 3. *$\delta^{15}N_{TN}$ measured in the original, untreated samples (black) and in samples pre-treated with acid (grey dots) for (a) DSDP 367 and (b) DSDP 386. The stratigraphy and isotope composition of organic carbon are used as a reference for the OAE2-interval (shaded). In (a) the N-isotope record in non-acidified samples is from Kuypers et al. (2004b).*

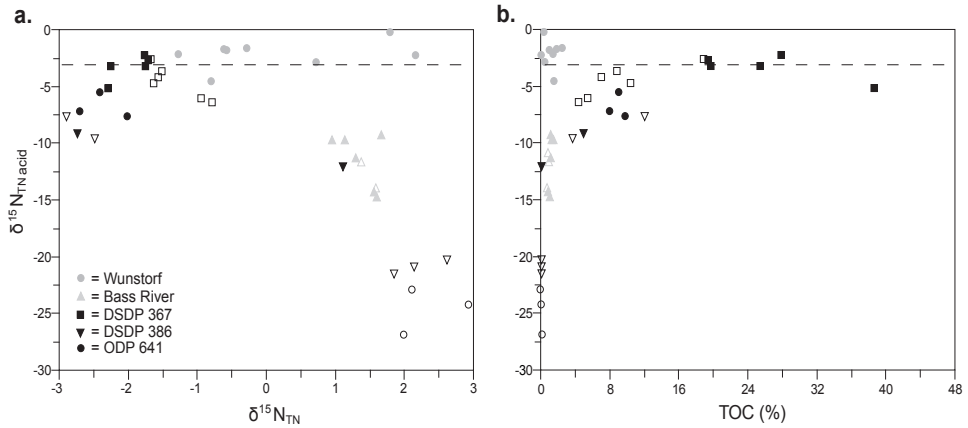

Figure 4. *(a) N-isotope signal measured in samples that where not pre-treated with acid ($\delta^{15}N_{TN}$) versus the signal measured in samples pre-treated with acid ($\delta^{15}N_{TNacid}$) at all measured sites. (b) Relation between TOC content and $\delta^{15}N_{TNacid}$. The minimum $\delta^{15}N_{TN}$ of -3‰ observed in our records is plotted as a reference (dashed horizontal line). Open and closed symbols are as indicated in Fig. 2.*

A scatter plot of $\delta^{15}N_{TN}$ versus $\delta^{15}N_{TNacid}$ for all sites (Fig. 4a) reveals three distinct groups of samples, with all $\delta^{15}N_{TNacid}$ being more negative than $\delta^{15}N_{TN}$: one with $\delta^{15}N_{TNacid}$ between -10 and -1‰, a second with $\delta^{15}N_{TNacid}$ smaller than -10‰ and a third (containing only Wunstorf samples) with $\delta^{15}N_{TNacid}$ close to -1‰. The $\delta^{15}N_{TNacid}$ at all sites shows a positive, but non-linear relationship with TOC content (Fig. 4b), except at Wunstorf where no trend is observed.

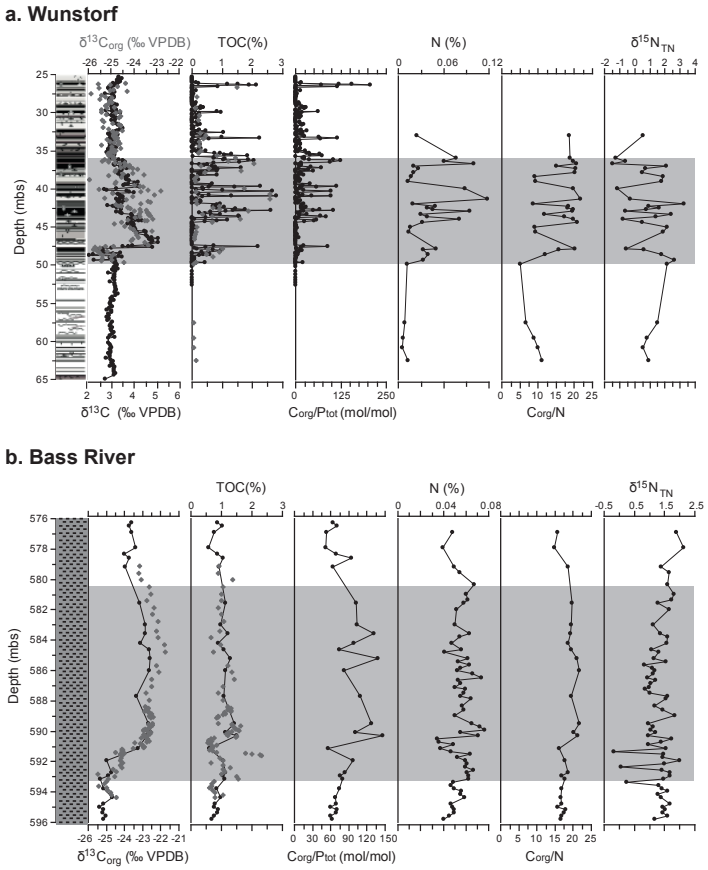

Figure 5. *Geochemical results across Oceanic Anoxic Event 2 (OAE2) at two coastal sites: (a) Wunstorf and (b) Bass River, where mbs is meters below surface. From left to right, $\delta^{13}C$, TOC content, total organic carbon to total phosphorus ratio (C_{org}/P_{tot}), total nitrogen content (N), C_{org}/N ratios and isotopic signal of total nitrogen ($\delta^{15}N_{TN}$) in bulk sediments, VPDB – Vienna Peedee Belemnite. $\delta^{13}C_{org}$ values in (a) are from Voigt et al. (2008; black) and Du Vivier et al. (2014) (grey). Measurements of TOC and C_{org}/P_{tot} are from Hetzel et al. (2011; black). TOC measurements (grey) are from Chapter 4. Stratigraphy is from Voigt et al. (2008). In (b) $\delta^{13}C_{org}$ and TOC values are from Chapter 3 (black) and Bowman and Bralower (2005; grey). C_{org}/P_{tot} are from Chapter 3. New measurements for both sites are for N and $\delta^{15}N_{TN}$*

3.3. *Coastal sites: Wunstorf and Bass River*

The OAE2-interval at Wunstorf and Bass River (Fig. 5) is well demarcated by the positive excursion of $\delta^{13}C_{org}$ that includes the onset and the final recovery phase at both coastal sites (e.g., Voigt et al., 2008; Chapter 3). Although more extreme at Wunstorf than at Bass River, all chemical profiles show large changes during OAE2 relative to pre-excursion values, with TOC, C_{org}/P_{tot} and N increasing and $\delta^{15}N_{TN}$ decreasing. In general, the Wunstorf site is characterized by higher TOC (~3%), C_{org}/P_{tot} (~125) and N (~0.1%), as well as lower $\delta^{15}N_{TN}$ (-1‰) when compared to Bass River.

All chemical profiles for the two coastal sites show a higher variability during OAE2 compared to pre-OAE2 conditions. This is most pronounced at Wunstorf. While at Bass River, a negative $\delta^{15}N_{TN}$ (<0‰) occurs near the onset of OAE2, at Wunstorf, large negative shifts in $\delta^{15}N_{TN}$ are observed throughout the entire OAE2-interval. During OAE2, $\delta^{15}N_{TN}$ ranges from -1.5 to 3 and from -0.5 to 1.5‰, at Wunstorf and Bass River, respectively. In both $\delta^{15}N_{TN}$ profiles, all major negative shifts are related to maxima in $\delta^{13}C_{org}$, TOC, C_{org}/P_{tot} and N. While C_{org}/N ratios mirror the $\delta^{15}N_{TN}$ signal at Wunstorf, at Bass river they are fairly constant throughout the OAE2-interval (~20).

3.4. *Central open ocean: Sites 386, 641 and 1276*

During the OAE2-interval, identified by the positive excursion of $\delta^{13}C_{org}$, a large increase in TOC, C_{org}/P_{tot}, C_{org}/N and N content occurs at all three open ocean sites (Fig. 6). Contents of TOC are highest at Sites 386 and 1276 (~13%).

At Site 386 (Fig. 6a), the actual initiation of OAE2 was not recorded. At the first point within OAE2, TOC, C_{org}/P_{tot} and N are near background values. From then onward, $\delta^{15}N_{TN}$ mirrors the TOC and N data until the termination where there is a decoupling between TOC, C_{org}/P_{tot}, N and $\delta^{15}N_{TN}$. Nonetheless, TOC, C_{org}/P_{tot} and N remain high and $\delta^{15}N_{TN}$ is fairly constant around -3‰. The $\delta^{15}N_{TN}$ during OAE2 at this location ranges from -3 to 2‰, while the absolute shift from pre-OAE2 to OAE2 conditions is -5.5‰.

At Site 641 (Fig. 6b), the $\delta^{15}N_{TN}$ profile presents a sharp decrease at the onset and a relatively fast recovery towards the termination of OAE2. In this case, the most negative value $\delta^{15}N_{TN}$ (-3‰) coincides with the highest C_{org}/P_{tot} (~240). The largest absolute $\delta^{15}N_{TN}$ shift from pre-OAE2 to OAE2 of all three sites, is observed at this site (-6).

At Site 1276 (Fig. 6c), all profiles show a high variability with several maxima and minima throughout the OAE2-interval. Most peaks in $\delta^{15}N_{TN}$ coincide with lows in TOC, C_{org}/P_{tot} and N. While C_{org}/P_{tot} increases significantly at the onset of OAE2, the highest value (457) occurs towards the termination of OAE2. The lower $\delta^{15}N_{TN}$ values are close to -3, as observed at Sites 386 and 641. The absolute shift from pre-OAE2 to OAE2 in $\delta^{15}N_{TN}$ is similar to that at Site 386 (-5.5‰).

3.5. *Model Results*

In the MB2 model, rates of N_2-fixation are higher than rates of upwelled NH_4^+ in all regions, except in the Southern coast (Table 2). With the new set of equations described in section S2, NH_4^+ concentrations increase significantly and, therefore, rates of

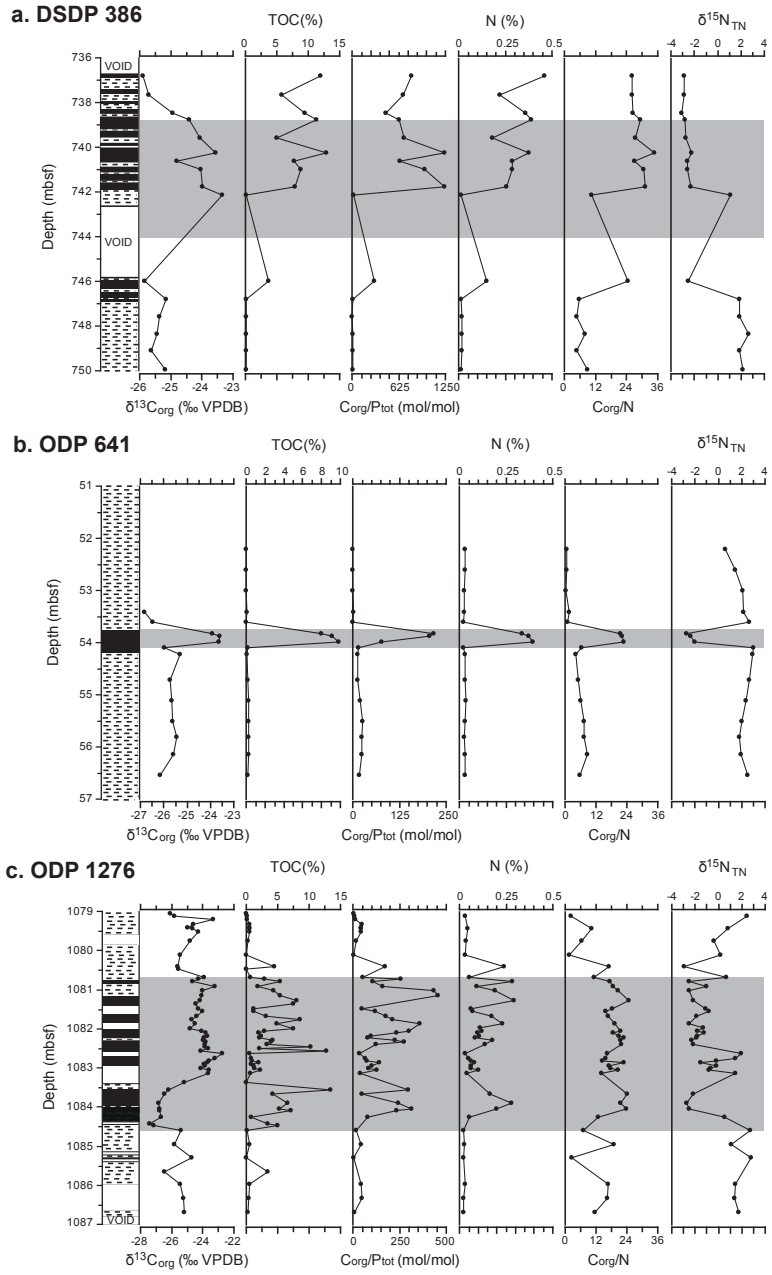

Figure 6. *Geochemical results across Oceanic Anoxic Event 2 (OAE2) at (a) DSDP 386, (b) ODP 641 and (c) ODP 1276 plotted against depth (mbsf). From left to right, $\delta^{13}C_{org}$ and TOC content, C_{org}/P_{tot}, N, C_{org}/N ratios and $\delta^{15}N_{TN}$. Abbreviations as in Fig. 5. Supporting data are from Chapter 6 and Sinninghe Damsté et al. (2010).*

transported NH_4^+ in the MB3 model are higher than rates of N_2-fixation (Table S1). While denitrification is lower in the MB3 than in the MB2 model, total nitrification, oxygen and NO_x^- concentrations are higher. This is reflected in the generally more depleted $\delta^{15}N_{model}$.

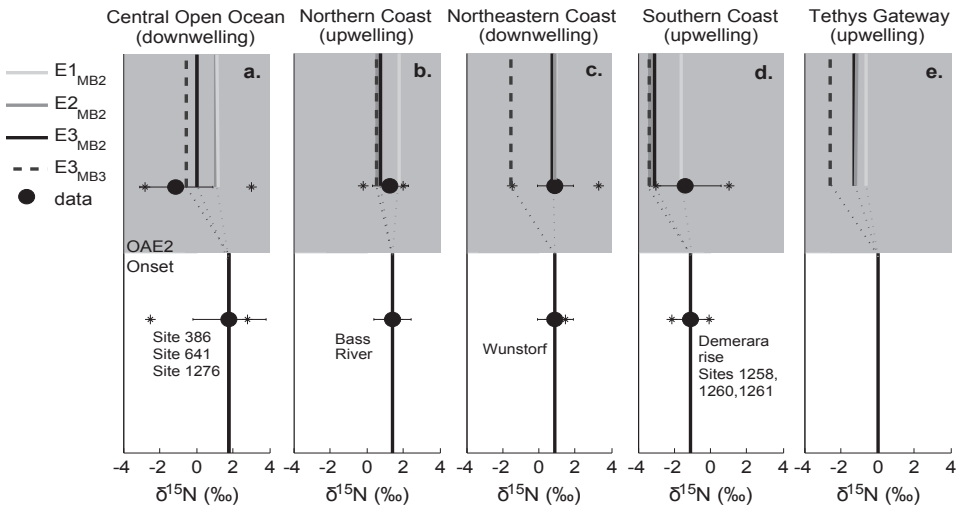

Figure 7. *Model results (bold lines) for experiments 1 to 3, simulating the mean shift in $\delta^{15}N$ from pre-OAE2 to OAE2 (gray shade) in (a) the central open ocean, (b) Northern Coast, (c) Northeastern Coast, (d) Southern Coast and (e) Tethys Gateway. Experiments are: no fractionation due to primary productivity (E1), fractionation effect by primary productivity due to NH_4^+ input to surface waters from upwelling (E2), fractionation effect by primary productivity due to NH_4^+ input to surface waters from upwelling and lateral transport (E3). E2 and E3 assume incomplete uptake of NH_4^+ by phytoplankton growth. Results performed with the MB2 and MB3 model are indicated with subscripts MB2 and MB3, respectively. Observations of the mean $\delta^{15}N_{TN}$ shift from pre-OAE to OAE2 (black plain circles), together with the ± standard deviation (horizontal black lines) and the lowest and highest value during OAE2 (stars) are plotted in each corresponding region for comparison. The $\delta^{15}N_{TN}$ of Sites 386, 641 and 1276 are averaged in a). $\delta^{15}N_{TN}$ values at Demerara Rise are taken from bulk sediment data of Higgins et al. (2012).*

In Fig. 7, we show the results of $\delta^{15}N_{model}$ for all numerical experiments and compare them to the average $\delta^{15}N_{TN}$, as well as its standard deviation and the most extreme values for the pre-OAE2 and OAE2-intervals. With the exception of $E3_{MB3}$, results of the MB2 and MB3 model are very similar, therefore $E1_{MB3}$ and $E2_{MB3}$ results are not shown. The $\delta^{15}N_{model}$ in all experiments besides $E3_{MB3}$ during OAE2 are close to the mean $\delta^{15}N_{TN}$ or within the ± standard deviation in most regions. The experiment that shows most negative values is experiment $E3_{MB3}$, notably Northeastern Coast. In the central open ocean the full range in $\delta^{15}N_{model}$ is not captured (Fig. 7a).

4. Discussion

4.1. $\delta^{15}N_{TN}$ artifact due to sample treatment

Measurements of $\delta^{15}N_{TN}$ in OAE2 sediments are not systematically determined with a standard method. While some researchers use untreated samples, others decalcify with acid and discard the supernatant after centrifugation. Concentrations of acid and exposure times may also vary between studies (e.g., Jenkyns et al., 2007; Meyers et al., 2009). We demonstrate that the isotope composition of organic N measured in samples treated with acid is consistently more negative than that of untreated samples. Trends of $\delta^{15}N_{TN}$ and $\delta^{15}N_{TNacid}$ with depth may be opposite depending on sample pre-treatment (Figs. 3 and 2a versus 4b). Addition of acid to samples leads to hydrolysis of proteins and other N-bearing compounds and thus potentially to selective removal of N compounds (Lohse et al., 2000; Brodie et al., 2011), which significantly alters the isotopic composition of the remaining organic N, resulting in negative values that can be as low as -30‰ (Fig. 4). The effect may depend on the nature and strength of the acid, the duration of exposure and the acid addition procedure (in-situ or with discarded acid; Nieuwenhuize et al. 1994; Kennedy et al., 2005). Samples with low TOC, total N and high carbonate should be treated with additional care (Bahlmann et al., 2010). Our results demonstrate that the N-isotope composition measured in samples treated with acid and subsequent removal of supernatant cannot be used as an indicator of N dynamics in past environments.

4.2. Trends in $\delta^{15}N_{TN}$ during OAE2: N_2-fixation and NH_4^+ uptake

Reliable $\delta^{15}N_{TN}$ data for OAE2 are only available for a few sites (Table 1). At all these sites, similar trends are observed, with the perturbation due to OAE2 being most pronounced in the central open ocean (Figs. 6 and 7). The magnitude of the absolute shift in $\delta^{15}N_{TN}$ per region is tightly linked to the redox conditions in the proto-North Atlantic. When considering mean values, the smallest absolute $\delta^{15}N_{TN}$ shift from pre-OAE2 to OAE2 occurred at Bass River and Wunstorf (-0.1 and -0.5‰, respectively). As indicated by the C_{org}/P_{tot} ratios, conditions along the north coast, in particular at Bass River (Chapter 3), were not as reducing as in the open ocean (van Bentum et al., 2012; Chapter 6) and Southern Coast (e.g., Sinninghe Damsté and Köster, 1998; Kuypers et al., 2002). In the euxinic southern proto-North Atlantic (at Demerara Rise and at Site 367), the absolute shift in $\delta^{15}N_{TN}$ is, however, smaller than in the central open ocean. The small $\delta^{15}N_{TN}$ shift during the Cenomanian-Turonian transition can be explained by sporadic anoxia prior to OAE2 in the south (e.g., Sinninghe Damsté and Köster, 1998; Kuypers et al., 2004a).

Our models (MB2 and MB3) aim to explain the mean absolute shifts in $\delta^{15}N_{TN}$ from pre-OAE2 to OAE2 conditions. In general, the MB2 model captures the mean $\delta^{15}N_{TN}$ values in all regions (Fig. 7). In experiments $E1_{MB2}$ to $E3_{MB2}$, the largest shift occurs in the open ocean (Fig. 7a) in agreement with observations of Table 1. In the MB2 model, N_2-fixation rates are high everywhere, being highest in the central open ocean during OAE2 (Table 2). This suggests that N_2-fixation was a major process controlling the $\delta^{15}N_{TN}$ signal throughout the entire OAE2. This is in agreement with what was previously

suggested (e.g., Junium and Arthur, 2007; Kuypers et al., 2004b; Blumenberg and Wiese, 2012), although each of these studies was based on sites from a single region. Our model results and data show that N_2-fixation was also significant in the central open ocean.

The effect of early diagenesis on $\delta^{15}N_{TN}$ is expected to increase with water depth due to prolonged oxygen exposure of sediments in low sedimentation rate environments (e.g., Moodley et al., 2005; Möbius et al., 2010; Robinson et al., 2012). In the central open ocean, the pristine $\delta^{15}N_{TN}$ signal in pre-OAE2 conditions may have been lower than the one measured in our samples, leading to a smaller shift in $\delta^{15}N_{TN}$ from pre-OAE2 to OAE2 conditions.

Because our model does not include diagenesis, the $\delta^{15}N_{model}$ in the central open ocean only captures the N-isotope signal of the intact deposited organic matter (Fig. 7a).

Extreme values recorded in the $\delta^{15}N_{TN}$ profiles (Fig. 6) are best captured by experiment $E3_{MB3}$ (performed with the MB3 model) in both the central open ocean and coastal areas. In the MB3 model, accumulation of NH_4^+ in bottom waters is higher than in the MB2 model (Table S2), leading to a higher fractionation effect of primary production due to incomplete uptake of NH_4^+ in $E3_{MB3}$ when compared to $E3_{MB2}$. The more pronounced $\delta^{15}N_{TN}$ shifts in $E3_{MB3}$, which best matches the data, suggests that lateral transport of NH_4^+, in addition to upwelling (E2), was important during OAE2. Thus, high lateral regional exchange may have contributed to a further decrease in $\delta^{15}N_{TN}$, especially in areas dominated by downwelling, such as the Northeastern coast and central open ocean. The presence of N_2 fixers using an alternative nitrogenase enzyme in the water column and with significantly larger fractionations (-6 to -7) may have also contributed to the negative $\delta^{15}N_{TN}$ signal (Zhang et al., 2014).

In the Southern Coast, all numerical experiments that consider a fractionation effect by primary production due to incomplete uptake of NH_4 (E2 and E3 performed with both models) capture the $\delta^{15}N_{TN}$ signal of the most negative values recorded during OAE2 (Fig. 7d). This suggests that upwelling rather than lateral input of NH_4^+ or N_2-fixation likely dominated the $\delta^{15}N_{TN}$ because inputs of NH_4^+ due to lateral fluxes and N_2-fixation do not significantly affect the $\delta^{15}N_{TN}$. This is best explained by the highly reducing conditions and is consistent with model results of Higgins et al. (2012), based on records of $\delta^{15}N_{TN}$ at Demerara Rise.

Temporal variations in oxygen conditions may have occurred within the OAE2-interval (e.g., Hetzel et al., 2011). Periods of strong oxygen depletion may have first led to an increase in denitrification and N_2-fixation and thus primary production. As a consequence, oxygen further decreased in bottom waters (due to enhanced respiration), while NH_4^+ may have increased, as well as its vertical and lateral transport. This would have affected not only the area where NH_4^+ was being produced (such as the Southern Coast), but also areas where conditions were less reducing, such as the Northern Coast. This may explain the high variability observed in most $\delta^{15}N_{TN}$ records, especially at Bass River, Wunstorf and Site 1276 (Figs. 5 and 6). At Bass River, which is a shallow coastal site, the largest variability may also be linked to high riverine influence (Chapter 3), while

at Wunstorf this may be associated to the large changes in lithology observed at this site (Voigt et al., 2008).

5. Conclusions

Our results indicate that measurements of $\delta^{15}N_{TN}$ in sediments that have been treated with acid followed by removal of supernatant cannot be used to draw conclusions about N dynamics in past environments. We recommend to not acidify samples for $\delta^{15}N_{TN}$ analysis. Our compilation of $\delta^{15}N_{TN}$ values for untreated sediment samples from the literature and from five new sites presented in this study highlight a consistent shift of $\delta^{15}N_{TN}$ to lighter values during OAE2 with a distinct lower limit of -3‰. We find large regional differences in the magnitude of this shift with the largest shift being observed in the central open ocean and a relatively minor one at more oxygenated coastal sites. Box model results for N dynamics indicate that enhanced N_2-fixation likely explains most of the shift in $\delta^{15}N_{TN}$. Upwelling NH_4^+ was likely of additional importance along the Southern Coast of the proto-North Atlantic, linked to the presence of highly reducing bottom waters. Lateral transport of NH_4^+ may also have contributed to the $\delta^{15}N_{TN}$ at many locations. The high temporal variability in $\delta^{15}N_{TN}$ may be the result of waxing and waning of the low oxygen conditions, leading to temporal variations in N_2-fixation and NH_4^+ supply.

Supplements to Chapter 7

S1 Geographical segmentation and water cycle

A simplified version of the multi-box model described in Ruvalcaba Baroni et al. (2014b) has been expanded with ^{15}N dynamics. The ordinary differential equations describing mass conservation are solved using R, a free software package (R Development Core team, 2006; Soetaert et al., 2010). The code of the model can be requested by sending an email to the first author of this paper.

In the original multi-box model (MB1), the proto-North Atlantic is divided into seven boxes based on the location of upwelling and downwelling areas and the bathymetry during OAE2. The water cycle of the multi-box model is based on the proto-North Atlantic circulation as derived by Topper et al. (2011). Here, we select four of these regions that include sites where $\delta^{15}N_{TN}$ was measured in samples untreated with acid: the central open ocean, the Southern Coast, the Northern Coast and the Northeastern Coast. One additional region, the Tethys Gateway, is also considered in the new version of the model (MB2) because it plays a major role in exchanging solutes with the central open ocean. The central open ocean is defined as the area above ~15°N with a water depth greater than 700 m (about 61% of the total area of the proto-North Atlantic). The central open ocean is divided into three boxes: the surface (0 to 100 m), intermediate (100 to 700 m) and bottom waters (700 to 5000 m). The coastal regions are divided into two boxes: the surface (0 to 100 m) and bottom waters (100 to 700 m).

S2 Mass balance equations for ^{15}N

In this section, we describe the mass balance equations as implemented in the MB2 model for the dissolved inorganic ($^{15}NO_x^-$ and $^{15}NH_4^+$) and particulate organic ($PO^{15}N$) pools of the heavy N-isotope (^{15}N). Equations are described for each box of the model. Boxes are surface (0 to 100 m), intermediate (100 to 700 m) and bottom waters (700 to 5000 m) for the central open ocean and surface (0 to 100 m) and bottom water (100 to 700 m) for the coastal areas (Southern Coast, Tethys Gateway, Northern Coast and Northeastern Coast). Processes relevant to the N cycle in surface waters that are included: N uptake by phytoplankton (*NUPTAKE*), N_2-fixation (*N2FIX*), remineralization of organic N (*REM*) and input and output of inorganic N (*NTin* and *NTout*) through vertical and lateral transport. Input of N also includes riverine supply from continents to coastal waters. In subsurface waters (intermediate and bottom waters), other relevant processes are nitrification (*NIT*), ammonification (*AMMONI*), denitrification in water column (*DENW*) and sediments (*DENS*), export production of organic N (*EXP*) and burial of organic N (*NBUR*). Note that N_2-fixation in bottom waters is only included in coastal areas. In the MB2 model, all these processes are considered for the mass balance of the included ^{15}N pools. The mass balance equations for each ^{15}N pool are summarized in Table S1 and the individual equations of the ^{15}N processes (indicated with a "15") are given in Table 3 (main text).

Reservoir	box	Equation
$^{15}NO_x^-$	surface	$\frac{\partial^{15}NO_x^-}{\partial t}_s = N15Tin - N15Tout + REM15 + N2FIX15_s - NUPTAKE15$
$PO^{15}N$	surface	$\frac{\partial PO^{15}N}{\partial t}_s = NUPTAKE15 - REM15 - NEXP15$
$^{15}NO_x^-$	intermediate	$\frac{\partial^{15}NO_x^-}{\partial t}_i = N15Tin - N15Tout - NIT15_i - DENW15_i$
$^{15}NH_4^+$	intermediate	$\frac{\partial^{15}NH_4^+}{\partial t}_i = N15Tin - N15Tout + AMMONI15_i - NIT15_i$
$PO^{15}N$	intermediate	$\frac{\partial PO^{15}N}{\partial t}_i = NEXP15_s - AMMONI15_i - NEXP15_i$
$^{15}NO_x^-$	bottom	$\frac{\partial^{15}NO_x^-}{\partial t}_b = N15Tin + N2FIX15_b - N15Tout - NIT15_b - DENW15_b - DEN15S$
$^{15}NH_4^+$	bottom	$\frac{\partial^{15}NH_4^+}{\partial t}_b = N15Tin - N15Tout + AMMONI15_b - NIT15_b$
$PO^{15}N$	bottom	$\frac{\partial PO^{15}N}{\partial t}_b = NEXP15_i - AMMONI15_b - NBUR15$

Table S1. *Mass balance equation for all ^{15}N reservoirs in the water column. The indexes $_s$, $_i$ and $_b$ correspond to surface, intermediate and bottom waters, respectively and in and out indicate input and output fluxes. To simplify the notation, the lateral and vertical transport, which are different for each N pool, are summarized as N15Tin and N15Tout depending on their direction relative to the source pool.*

S3 New parametrization for denitrification and nitrification

Nitrification, the biological conversion of NH_4^+ to nitrate and nitrite (NO_x^-) in the presence of oxygen, is a key process controlling the amount of $NO_x^-$and NH_4^+ in the water column. Since denitrification depends on the availability of NO_x^- it is linked to nitrification. While denitrification enriches the NO_x^- reservoir in ^{15}N, nitrification adds ^{14}N to this reservoir by taking it from the NH_4^+ reservoir. When unbalanced, these processes may influence $\delta^{15}N$ (Ryabenko, 2013) ratios of the water column and, thus, the signal of the buried organic N. Because both processes are poorly constrained for the proto-North Atlantic and to further assess their influence on $\delta^{15}N_{TN}$, we built an additional model (MB3) with the same characteristics as the MB2 model in order to assess the effect of changes in watercolumn denitrification and nitrification on ^{15}N dynamics under similar conditions as those of the base line scenario (BsLi-N) in Ruvalcaba Baroni et al. (2014b). A detailed description of the new parametrizations is given in this section.

Denitrification in the water column is assumed to be low and constant above an oxygen concentration of 30 μM. Below this oxygen concentration, water-column denitrification is then defined as:

$$DENW = \sqrt{kden^{water} \cdot [NO_x^-] \cdot W} \cdot \frac{[NO_x^-]}{[NO_x^-] + K_{NO}} \cdot \left(\frac{K_{O2}}{[O_2] + K_{O2}}\right)^{dnfO}, \quad (1)$$

where $kden^{water}$ is the rate constant for denitrification in the water column, W is the water reservoir where the process is occurring and K_{NO} is the Monod constant for NO_x^- involved in denitrification. The exponential factor to the Monod kinetics (*dnfO*) in the MB3 model (*dnfO*=1 in all boxes) differs from the original ones used in Ruvalcaba Baroni et al. (2014b) (*dnfO*=1.8 and 1.5). This reduces the sensitivity of denitrification to low-oxygen (Fig. S1). The Monod constant for denitrification for oxygen (K_{O2}) differ with respect to the original (K_{O2} = 10 μM and K_{NO} = 0.1 μM), so that denitrification becomes more sensitive to oxygen than to NO_x^- concentrations ($[O_2]$ and $[NO_x^-]$, respectively).

Unlike the original parametrization, which considered a linear relationship between NH_4^+ and nitrification, in the MB3 model we assume a non-linear dependency on NH_4^+. In this case, the non-linear dependency on NH_4^+ is represented by the power 0.7, which was chosen from a sensitivity analysis (not shown). Here, nitrification when oxygen is above 30 µmol (NIT_{ho}) is defined as:

$$NIT_{ho} = kox \cdot [NH_4]^{0.7} \cdot W \cdot \frac{[O_2]}{[O_2] + K_{O2}}, \quad (2)$$

where *kox* is the rate constant for nitrification in oxic waters. When oxygen is below 30 µmol, nitrification (NIT_{lo}) is calculated as:

$$NIT_{lo} = klox \cdot [NH_4]^{0.7} \cdot W \cdot \frac{[O_2]}{[O_2] + K_{O2}} \cdot \frac{K_{NH4}}{[NH_4] + K_{NH4}}, \quad (3)$$

where *klox* is the rate constant for nitrification in low-oxygen conditions and K_{NH4} (=1 µM) is the Monod constants for NH_4^+. The Monod constant for oxygen involved in nitrification was chosen from a sensitivity analysis and leads to a more gradual response to decreasing oxygen concentrations (Fig. S2). The resulting new rates for all relevant N processes given by the MB3 model are presented in Table S2.

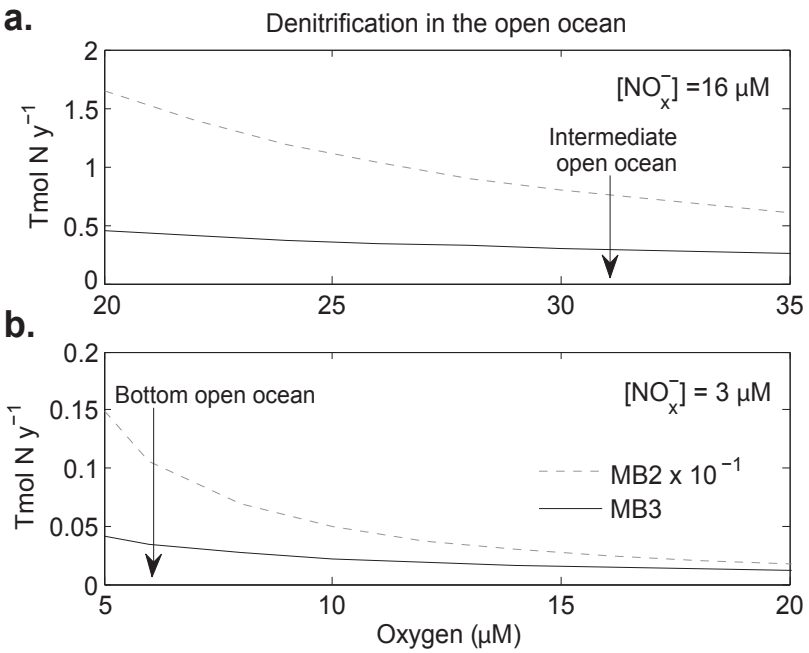

Figure S1. *Response of denitrification to oxygen with constant NO_x^- concentrations in the original (MB1 and MB2; dashed line) and in the MB3 model (black line). Nitrate concentrations are the ones given by the original model for (a) the intermediate and (b) bottom waters of the central open ocean. Oxygen concentrations given by the original model in the central open ocean are indicated with arrows.*

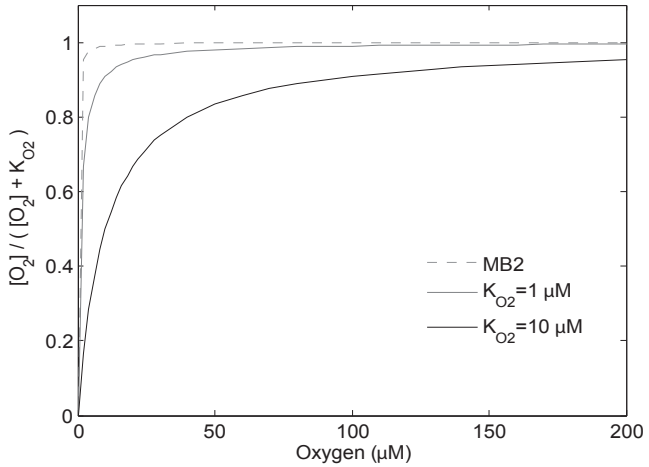

Figure S2. *Sensitivity to oxygen of the Monod term in the parametrisation of nitrification with a Monod constant for denitrification (K_{O2}) of 0.1 (original value in model), 1 and 10 µM (chosen one for new parametrisation).*

		Coast			
	Open Ocean	**Northern**	**Northeast.**	**Southern**	**Tethys Gate.**
NH_4^+UP	1.2	2.177	0.01	5.724	1.69
NO_3^-UP	0.4	1.978	0.589	0.289	0.41
NH_4^+LT	4.87	1.347	0.37	0.3	-
NO_3^-LT	1.67	1.288	0.1	0.399	-
TOTNin	8.14	6.789	1.072	6.713	2.1
N2FIX	4	1	0.2	3.2	1
DENW	2.1	0.1	0	3	0.01
DENS	0	1.2	0.01	0	0.1
DEN_{TOT}	2.1	1.3	0.01	3	0.11
NIT	2.1	2.3	2.7	0	1.1
$[NH_4^+]_{sub}$	23	21	0	45	22
$[NO_x^-]_{sub}$	3	19	23	2	5.5
$[O_2]_{sub}$	6.5	8	87	0	18

Table S2. *Relevant rates and components affecting the $\delta^{15}N$ in the MB3 model for for OAE2 conditions (pre-OAE2 values are the same as in Table 2, main text). Abbreviations are the same as in Table 2 (main text). Rates are in Tmol N y^{-1} and concentrations in µM.*

S4 Estimates of lateral NH_x^- and NH_4^+ transport into surface waters

In this section, we describe all calculations performed to obtain the α_{PP} for each region in Experiment E3 (main text). Because in our model NH_4^+ and NO_x^- are modeled as one single reservoir in surface waters, we first estimate all individual incoming lateral

transport of NH_4^+ and NO_x^-. The individual (j) incoming lateral transport of NH_4^+ and NO_x^- ($NH_4^+LT_j$ and $NO_x^-LT_j$) in each region are based on the P_{NH4+} and P_{NOx}- of the source region and are approximated as follows:

$$NH_4^+LTj = P_{NH4+} \cdot TNLTj \quad (4)$$

$$NO_3^- LTj = P_{NO3-} \cdot TNLTj, \quad (5)$$

where $TNLT_j$ is the individual lateral transport of total N into surface waters for each region in both the MB2 and MB3 model. With this we calculate the total lateral transport of NH_4^+ and NO_x^- entering each surface region (the sum of all individual fluxes; NH_4^+LT and NO_x^-LT). We then adjust the α_{PP} values following equation 3 (main text). In this case P_{NH4+} and P_{NOx-} take into account both the vertical and total lateral portion of NH_4^+ and NO_x^- relative to the total N input ($TOTNin$) in surface waters, (e.g., $P_{NH4+} = \frac{TOTNH_4^+in}{TOTNin}$, where $TOTNH_4^+in = NH_4^+LT + NH_4^+UP$). Relevant values for experiment E3 performed with the MB3 model are listed in Table S2. A summary of all calculated α_{PP} for each experiment performed with both the MB2 and MB3 models is given in Table S3.

			Coast		
Experiments	**Open Ocean**	**Northern**	**NorthEast.**	**Southern**	**Tethys Gate.**
$E1_o$	1	1	1	1	1
$E2_o$	1	0.998	1	0.9969	0.998
$E3_o$	0.998	0.998	0.999	0.9971	0.998
$E3_{new}$	0.997	0.998	0.9985	0.9964	0.99698

Table S3. *Calculated values of α_{PP} in each box for the relevant numerical experiment. Experiments are: No fractionation due to primary productivity (E1), fractionation effect by primary productivity due to NH_4^+ input to surface waters from upwelling (E2), fractionation effect by primary productivity due to NH_4^+ input to surface waters from upwelling and lateral transport (E3). E2 and E3 assume a fractionation effect due to incomplete uptake of NH_4^+ by phytoplankton growth.*

References

Adams, D.D., Hurtgen, M.T., and Sageman, B.B. (2010). Volcanic triggering of a biogeochemical cascade during Oceanic Anoxic Event 2. *Nature Geoscience* 3, 201-204.

Aksu, A.E., Abrajano, J., Mudie, P.J., and Yaşar, D. (1999). Organic geochemical and palynological evidence for terrigeneous origin of the organic matter in Aegean Sea sapropel S1. *Marine Geology* 153, 303-318.

Algeo, T.J., and Maynard J.B. (2004). Trace-element behavior and redox facies in core shales of Upper Pennsylvanian Kansas-type cyclothems. *Chemical Geology* 206, 289-318.

Algeo, T.J., and Lyons, T.W. (2006). Mo-total organic carbon covariation in modern anoxic marine environments: implications for analysis of paleoredox and paleohydrographic conditions. *Paleoceanography* 21, PA1016.

Algeo, T.J., and Ingall, E. (2007). Sedimentary Corg:P ratios, paleocean ventilation, and Phanerozoic atmospheric pO_2. *Palaeogeography, Palaeoclimatology, Palaeoecology* 256, 130–155.

Algeo, T.J., and Heckel, P.H. (2008). The Late Pennsylvanian midcontinent sea of North America: a review. *Palaeogeography, Palaeoclimatology, Palaeoecology* 268, 205-221.

Algeo, T.J., and Rowe, H., (2012). Paleoceanographic applications of trace-metal concentration data. *Chemical Geology* 324 – 325, 6-18.

Algeo, T.J., Meyers, P.A., Robinson, R.S., Rowe, H., and Jiang, G. (2014). Icehouse-greenhouse variations in marine denitrification. *Biogeosciences* 11, 1273-1295.

Alley, R.B., Mayewski, P.A., Sowers, T., Stuiver, M., Taylor, K.C., and Clark, P.U. (1997). Holocene climatic instability: A prominent, widespread event 8200 yr ago. *Geology* 25, 483-486.

Altabet, M.A., and Francois, R., (1994). Sedimentary nitrogen isotopic ratio as a recorder for surface ocean nitrate utilization. *Global Biogeochemical Cycles* 8, 103-116.

Anderson, J.J., and Devol, A.H. (1973). Deep water renewal in Saanich Inlet, an intermittently anoxic basin. *Estuarine and Coastal Marine Science* 1, 1-10.

Arthur, M.A. (1979). North Atlantic Cretaceous black shales: the record at Site 398 and a brief comparison with other occurrences. *In: Ryan, W.B.F., Sibuet, J. C. et al., Initial Reports of the Deep Sea Drilling Project* 47/2. Washington, U.S., Government Printing Office, 719-738.

Arthur, M.A., and Sageman, B.B. (1994). Marine black shales: Depositional mechanisms and environments of ancient deposits. *Annual Review of Earth and Planetary Sciences* 22, 499-551.

Arthur, M.A., and Sageman, B.B. (2005). Sea-level control on source-rock development: perspectives from the Holocene Black Sea, the mid-Cretaceous Western Interior Basin of North America, and the Late Devonian Appalachian Basin. *In: Harris, N.B. (Ed.), The deposition of organic-carbon-rich sediments: models, mechanisms, and consequences. SEPM Special Publication* 82, 35-59.

Arthur, M.A., Dean, W.E., and Pratt, L.M. (1988). Geochemical and climatic effects of increased marine organic-carbon burial at the Cenomanian-Turonian boundary. *Nature* 335, 714-717.

Bahlmann, E., Bernasconi, S. M., Bouillon, S., Houtekamer, M., Korntheuer, M., Langenberg, F., Mayr, C., Metzke, M., Middelburg, J. J., Nagel, B., Struck, U., Voß, M., and Emeis, K.-C. (2010). Performance evaluation of nitrogen isotope ratio determination in marine and lacustrine sediments: An inter-laboratory comparison. *Organic Geochemistry* 41, 3-12.

Barclay, R.S., McElwain, J.C., and Sageman, B.B. (2010). Carbon sequestration activated by a volcanic CO_2 pulse during Ocean Anoxic Event 2. *Nature Geoscience* 3, 205-208,

Bar-Matthews M., Ayalon A., Kaufman A., and Wasserburg, G.J. (1999). The Eastern Mediterranean paleoclimate as a reflection of regional events: Soreq Cave, Israel. *Earth and Planetary Science Letters* 166, 85-95.

Barron, E.J. (1983). A warm, equable Cretaceous: the nature of the problem. *Earth-Science Reviews* 19, 305-338.

Bauersachs, T., Schouten, S., Compaoré, J., Wollenzien, U., Stal, L.J., and Sinninghe Damsté, J.S. (2009). Nitrogen isotopic fractionation associated with growth on dinitrogen gas and nitrate by cyanobacteria. *Limnology and Oceanography* 54, 1403-1411.

Bayon, G., Dupré, S., Ponzevera, E., Etoubleau, J., Chéron, S., Pierre, C., Mascle, J., Boetius, A., and De Lange, G.J. (2013). Formation of carbonate chimneys in the Mediterranean Sea linked to deep-water oxygen depletion. *Nature Geoscience* 6, 755-760.

Beckmann, B., Flögel, S., Hofmann, P., Schulz, M., and Wagner, T. (2005). Orbital forcing of Cretaceous river discharge in tropical Africa and ocean response. *Nature* 437, 241-244.

Beerling, D.J., Lomas, M.R., and Gröcke, D.R. (2002). On the nature of methane gas-hydrate dissociation during the Toarcian and Aptian oceanic anoxic events. *American Journal of Science* 302, 28-49.

Berner, R.A., and Canfield, D.E. (1989). A new model for atmospheric oxygen over Phanerozoic time. *American Journal of Science* 289, 333-361.

Berry, W.B.N., and Wilde, P. (1978). Progressive ventilation of the oceans-an explanation of the distribution of the lower Paleozoic black shales. *American Journal of Science* 278, 257-275.

Bethoux, J.P. (1989). Oxygen consumption, new production, vertical advection and environmental evolution of the Mediterranean Sea. *Deep-Sea Research* 36, 769-781.

Betts, R.A., Boucher, O., Collins, M., Cox, P.M., Falloon, P.D., Gedney, N., Hemming, D.L., Huntingford, C., Jones, C.D., Sexton, D.M.H., and Webb, M.J. (2007). Projected increase in continental runoff due to plant responses to increasing carbon dioxide. *Nature* 448, 1037-1041.

Bice, K.L., Birgel, D., Meyers, P.A., Dahl, K.A., Hinrichs, K.-U., and Norris, R.D. (2006). A multiple proxy and model study of the Cretaceous upper ocean temperatures and atmospheric CO_2 concentrations. *Paleoceanography* 21, PA2002.

Birks H.J.B., and Line, J.M. (1992). The use of rarefaction analysis for estimating palynological richness from Quaternary pollen-analytical data. *Holocene* 2, 1-10.

Blättler, C.L., Jenkyns, H.C., Reynard, L.M., and Henderson, G.M. (2011). Significant increases in global weathering during Oceanic Anoxic Events 1a and 2 indicated by calcium isotopes. *Earth and Planetary Science Letters* 309, 77-88.

Blumenberg, M., and Wiese, F. (2012). Imbalanced nutrients as triggers for black shale formation in a shallow shelf setting during the OAE2 (Wunstorf, Germany). *Biogeosciences* 9, 4139-4153.

Boessenkool, K.P., Brinkhuis, H., Schönfeld, J., and Targarona, J. (2001). North Atlantic sea-surface temperature changes and the climate of western Iberia during the last deglaciation; a marine palynological approach. *Global and Planetary Change* 30, 33-39.

Bopp, L., Le Queré, C., Heimann, M., Manning, A.C., and Monfray, P. (2002). Climate-induced oxygen fluxes: implications for the contemporary carbon budget. *Global Biogeochemical Cycles* 16, GB1022.

Bowman, A.R., and Bralower, T.J. (2005). Paleoceanographic significance of high-resolution carbon isotope records across the Cenomanian-Turonian boundary in the western interior and New Jersey coastal plain, USA. *Marine Geology* 217, 305-321.

Bradford, M.R., and Wall, D.A. (1984). The distribution of Recent organic-walled dinoflagellate cysts in the Persian Gulf, Gulf of Oman, and northwestern Arabian Sea. *Palaeontographica B* 192, 16-84.

Bralower, T.J., Fullagar, P.D., Paull, C.K., Dwyer, G.S., and Leckie, R.M. (1997). Mid-Cretaceous strontium-isotope stratigraphy of deep-sea sections. *Geological Society of America Bulletin* 109, 1421-1442.

Brandes, J.A., and Devol, A.H. (1997). Isotopic fractionation of oxygen and nitrogen in coastal marine sediments. *Geochimica et Cosmochimica Acta* 61, 1793-1801.

Brandes, J.A., and Devol, A.H. (2002). A global marine-fixed nitrogen isotopic budget: Implications for Holocene nitrogen cycling. *Global Biogeochemical Cycles* 16, 1120.

Brasier, M.D. (1985), Fossil indicators of nutrient levels. 1. Eutrophication and climate change. *In: Bosence, D.W.J. & Allison, P.A. (Eds.), Marine Palaeoenvironmental analysis from Fossils. Geological Society of London, Special Publication* 83, 113-132.

Brinkhuis, H. (1994). Late Eocene to Early Oligocene dinoflagellate cysts from the Priabonian type-area (northeast Italy): biostratigraphy and palaeoenvironmental interpretation. *Palaeogeography, Palaeoclimatology, Palaeoecology* 107, 121-163.

Brinkhuis, H., Bujak, J.P., Smit, J., Versteegh, G.J.M., and Visscher, H. (1998). Dinoflagellate-based sea surface temperature reconstructions across the Cretaceous – Tertiary boundary. *Palaeogeography, Palaeoclimatology, Palaeoecology* 141, 67-83.

Brinkhuis, H., Schouten, S., Collinson, M.E., Sluijs, A., Sinninghe Damsté, J.S., Dickens, G.R., Huber, M., Cronin, T.M., Onodera, J., Takahashi, K., Bujak, J.P., Stein, R., van der Burgh, J., Eldrett, J.S., Harding, I.C., Lotter, A.F., Sangiorgi, F., van Konijnenburg-f Cittert, H., de Leeuw, J.W., Matthiessen, J., Backman, J., Moran, K., and the Expedition 302 Scientists (2006). Episodic fresh surface waters in the Eocene Arctic Ocean. *Nature* 441, 606-609.

Brodie, C.R., Leng, M.J., Casford, J.S., Kendrick, C.P., Lloyd, J.M., Yongqiang, Z., and Bird, M.I. (2011). Evidence for bias in C and N concentrations and ^{13}C composition of terrestrial and aquatic organic materials due to pre-analysis acid preparation methods. *Chemical Geology* 282, 67-83.

Broecker, W.S. (1991). The great ocean conveyor. *Oceanography* 4, 79-89.

Brumsack, H.J. (1980). Geochemistry of Cretaceous black shales from the Atlantic Ocean (DSDP Legs 11, 14, 36 and 41). *Chemical Geology* 31, 1-25.

Butzer, K. (2002). Geoarchaeological implications of recent research in the Nile Delta. *In: van den Brink, E.C.M., Levy, T.E. (Eds.), Egypt and the Levant*. Leicester University Press, London, 83-97.

Calvert, S.E. (1983). Geochemistry of Pleistocene sapropels and associated sediments from the Eastern Mediterranean. *Oceanologica Acta* 6, 255-267.

Calvert, S.E. (1990). Geochemistry and origin of the Holocene sapropel in the Black Sea. *In: Ittekkot, V., Kempe, S., Michealis, W., Spitzy, A. (Eds.), Facets of Modern Biogeochemistry*. Springer-Verlag, Berlin, 328-353.

Calvert, S.E., and Pedersen, T.F. (1992). Organic carbon accumulation and preservation in marine sediments: how important is anoxia? *In: Whelan, J.K., Farrington, J.W. (Eds.), Productivity,*

Accumulation and Preservation of Organic Matter in Recent and Ancient Sediments. Columbia University Press, 231-263.

Canfield, D.E., Lyons, T.W., and Raiswell, R. (1996). A model for iron deposition to euxinic Black Sea sediments. *American Journal of Science* 296, 818–834.

Capone, D.G., Zehr, J.P., Paerl, H.W., Bergman, B., and Carpenter, E.J. (1997). *Trichodesmium*, a globally significant marine cyanobacterium. *Science* 276, 1221-1229.

Carpenter, E.J., Harvey, H.R., Fry, B., and Capone, D.G. (1997). Biogeochemical tracers of the marine cyanobacterium *Trichodesmium*. *Deep Sea Research Part I: Oceanographic Research Papers* 44, 27-38.

Casford, J.S.L., Rohling, E.J., Abu-Zied, R., Cooke, S., Fontanier, C., Leng, M., and Lykousis, V. (2002). Circulation changes and nutrient concentrations in the late Quaternary Aegean Sea: A nonsteady state concept for sapropel formation. *Paleoceanography* 17.

Castañeda, I.S., Schefuß, E., Patzold, J., Sinninghe Damsté, J.S., Weldeab, S. and Schouten, S. (2010). Millennial-scale sea surface temperature changes in the eastern Mediterranean (Nile River Delta region) over the last 27,000 years. *Paleoceanography* 25, PA1208.

Castradori, D. (1993). Calcareous nannofossils and the origin of eastern Mediterranean sapropels. *Paleoceanography* 8, 459-471.

Čech, S., Hradecká, L., Svobodová, M., and Švábenická, L. (2005). Cenomanian and Cenomanian-Turonian boundary in the southern part of the Bohemian Cretaceous Basin, Czech Republic. *Bulletin of Geosciences* 80, 321-354.

Cheddadi, R., and Rossignol-Strick, M. (1995). Improved preservation of organic matter and pollen in eastern Mediterranean sapropels. *Paleoceanography* 10, 301-309.

Chénet, P.Y., and Francheteau, J. (1979). Bathymetric reconstruction method: application to the Central Atlantic Basin between 10°N and 40°N. *In: Donnelly, T., Francheteau, J., Bryan, W., Robinson, P., Flower, M., Salisbury, M., et al. (Eds.), Initial Reports of the Deep Sea Drilling Project DSDP*, 51, 52, 53, Pt. 2, 1501-1514.

Childress, J.J., and Seibel, B.A. (1998). Life at stable low oxygen levels: adaptations of animals to oceanic oxygen minimum layers. *The Journal of Experimental Biology* 201, 1223 – 1232.

Claussen, V., and Gayler, V. (1997). The greening of the Sahara during the mid-Holocene: Results of an interactive atmosphere-biome model. *Global Ecology and Biogeography Letters* 6, 369-377.

Codispoti, L.A., Brandes, J.A., Christensen, J.P., Devol, A.H., Naqvi, S.W.A., Paerl, H.W., and Yoshinari, T. (2001). The oceanic fixed nitrogen and nitrous oxide budgets: Moving targets as we enter the anthropocene? *Scientia Marina* 65, 85-105.

Cogné, J.P., and Humler, E. (2004). Temporal variation of oceanic spreading and crustal production rates during the last 180 My. *Earth and Planetary Science Letters* 227, 427-439.

Condie, K.C., Des Marais, D.J., and Abbot, D. (2001). Precambrian superplumes and supercontinents: a record in black shales, carbon isotopes, and paleoclimates? *Precambrian Research* 106, 239-260.

Conley, D.J., Humborg, C., Rahm, L., Savchuk, O.P., and Wulff, F. (2002). Hypoxia in the Baltic Sea and basin-scale changes in phosphorus biogeochemistry. *Environmental Science and Technology* 3, 5315 – 5320.

Cookson, I.C., and Eisenack, A. (1962). Additional microplankton from Australian Cretaceous sediments. *Micropaleontology* 8, 485-507.

Courtinat, B., Crumière, J.P., Méon, H., and Schaaf, A. (1991). Les associations de kystes de dinoflagellés du Cénomanien-Turonien de Vergons (Bassin Vocontien France). *Geobios* 24, 649-666.

Crampton, J.S., Raine, I., Strong, C.P., and Wilson, G.J. (2001). Integrated biostratigraphy of the Raukumara Series stratotype (Cenomanian to Coniacian) at Mangaotane Stream, Raukumara Peninsula, New Zealand. *New Zealand Journal of Geology and Geophysics* 44, 365-389.

Creaney, S., and Passey, Q.R. (1993). Recurring Patterns of Total Organic Carbon and Source Rock Quality within a Sequence Stratigraphic Framework. *AAPG Bulletin* 77, 386-401.

Crudeli, D., Young, J.R., Erba, E., De Lange, G.J., Henriksen, K., Kinkel, H., Slomp, C.P., and Ziveri, P. (2004). Abnormal carbonate diagenesis in Holocene – Late Pleistocene sapropel-associated sediments from Eastern Mediterranean; evidence from *Emiliania huxleyi* coccolith morphology. *In: Villa, G., Lees, J.A., Bown, P.R. (Eds.), Calcareous Nannofossil Palaeoecology and Palaeocenographic Reconstructions. Marine Micropaleontology* 52, 217-240.

Crudeli, D., Young, J.R., Erba, E., Geisen, M., Ziveri, P., De Lange, G.J., and Slomp, C.P. (2006). Fossil record of holococcoliths and selected hetero-holococcolith associations from the Mediterranean (Holocene-late Pleistocene): evaluation of carbonate diagenesis and paleoecological – paleogeographic implications. *Palaeogeography, Palaeoclimatology, Palaeoecology* 237, 191-212.

Dale, B. (1996). Dinoflagellate cyst ecology: Modeling and geological applications. *In: Jansonius, J. and McGregor, D.C., (Eds.), Palynology: Principles and Applications.* American Association of Stratigraphic Palynologists Foundation, Dallas, USA, 1249-1276.

Dalsgaard, T., Thamdrup, B., and Canfield, D.E. (2005). Anaerobic ammonium oxidation (anammox) in the marine environment. *Research in Microbiology* 156, 457-464.

De Lange, G.J., and Ten Haven, H.L. (1983). Recent sapropel formation in the Eastern Mediterranean. *Nature* 305, 797-798.

Deflandre, G., and Cookson, I.C. (1955). Fossil microplankton from Australian late Mesozoic and Tertiary sediments. *Marine and Freshwater Research* 6, 242-314.

DeNiro, M.J., and Epstein, S. (1981). Influence of diet on the distribution of nitrogen isotopes in animals. *Geochimica et Cosmochimica Acta* 45, 341-351.

Deutsch, C., Sigman, D.M., Thunell, R.C., Meckler, A.N., and Haug, G.H. (2004). Isotopic constraints on glacial/interglacial changes in the oceanic nitrogen budget. *Global Biogeochemical Cycles* 18, GB4012.

Devol, A.H., and Hartnett, H.E. (2001). Role of the oxygen-deficient zone in transfer of organic carbon to the deep ocean. *Limnology and Oceanography* 46, 1684-1690.

Diaz, R.J., and Rosenberg, R. (2008). Spreading dead zones and consequences for marine ecosystems. *Science* 321, 926-929.

Dodsworth, P. (1996). Stratigraphy, microfossils and depositional environments of the lowermost part of the Welton Chalk Formation, late Cenomanian to early Turonian (Cretaceous) in eastern England. *Proceedings of the Yorkshire Geological Society* 51, 45-64.

Dodsworth, P. (2000). Trans-Atlantic dinoflagellate cyst stratigraphy across the Cenomanian – Turonian (Cretaceous) Stage boundary. *Journal of Micropalaeontology* 19, 69-84.

Dodsworth, P. (2004a). The distribution of dinoflagellate cysts across a Late Cenomanian carbon isotope ($\delta^{13}C$) anomaly in the Pulawy borehole, central Poland. *Journal of Micropalaeontology* 23, 77-80.

Dodsworth, P. (2004b). The palynology of the Cenomanian-Turonian (Cretaceous) boundary succession at Aksudere in Crimea, Ukraine. *Palynology* 28, 129-141.

Donders, T.H., Weijers, J.W.H., Munsterman, D.K., Kloosterboer-van Hoeve, M.L., Buckles, L.K., Pancost, R.D., Schouten, S., Sinninghe Damsté, J.S., and Brinkhuis, H. (2009). Strong climate coupling of terrestrial and marine environments in the Miocene of northwest Europe. *Earth and Planetary Science Letters* 281, 215-225.

Doney, S.C. (2010). The growing human footprint on coastal and open-ocean biogeochemistry. *Science* 328, 1512-1516.

Douville E., Charlou, J.L., Oelkers, E.H., Bienvenu, P., Jove Colon, C.F., Donval, J.P., Fouquet, Y., Prieur, D., and Appriou, P. (2002). The rainbow vent fluids (36°14'N, MAR): the influence of ultramafic rocks and phase separation on trace metal content in Mid-Atlantic Ridge hydrothermal fluids. *Chemical Geology* 184, 37-48.

D'Ortenzio, F., and Ribera d'Alcala, M. (2009). On the trophic regimes of the Mediterranean Sea: a satellite analysis. *Biogeosciences* 6, 139-148.

Du Vivier, A.D.C., Selby, D., Sageman, B.B., Jarvis, I., Gröcke, D.R., and Voigt, S. (2014). Marine $^{187}Os/^{188}Os$ isotope stratigraphy reveals the interaction of volcanism and ocean circulation during Oceanic Anoxic Event 2. *Earth and Planetary Science Letters* 389, 23-33.

Dugdale, R.C., and Wilkerson, F.P. (1988). Nutrient sources and primary production in the Eastern Mediterranean. *Oceanologica Acta* 9, 179-184.

Eckert, S., Brümsack, H.-J., Severmann, S., Schnetger, B., März, C., and Fröllje, H., (2013). Establishment of euxinic conditions in the Holocene Black Sea. *Geology* 41, 431–434.

Elder, W.P. (1989). Molluscan extinction patterns across the Cenomanian-Turonian Stage boundary in the western interior of the United States. *Paleobiology* 15, 299-320.

Eldrett, J.S., Minisini, D., and Bergman, S.C. (2014). Decoupling of the carbon cycle during Ocean Anoxic Event 2. *Geology* 42, 567-570.

Elshanawany, R., Zonneveld, K.A.F., Ibrahim, M.I., and Kholeif, S.E.A. (2010). Distribution patterns of recent organic-walled dinoflagellate cysts in relation to environmental parameters in the Mediterranean Sea. *Palynology* 34, 233-260.

Emerson, S.R., and Huested, S.S. (1991). Ocean anoxia and the concentrations of molybdenum and vanadium in seawater. *Marine Chemistry* 34, 177-196.

Erba, E. (2004). Calcareous nannofossils and Mesozoic oceanic anoxic events. *Marine Micropaleontology* 52, 85-106.

Erbacher, J., Thurow, J., and Littke, R. (1996). Evolution patterns of radiolariaand organic matter variations: A new approach to identify sea-level changes in mid-Cretaceous pelagic environments. *Geology* 6, 499-502.

Erbacher, J., Mutterlose, J., Wilmsen, M., Wonik, T., and the Wunstorf Drilling Scientific Party (2007). The Wunstorf Drilling Project: Coring a global stratigraphic reference section of the Oceanic Anoxic Event 2. *Scientific Drilling* 4, 19-21.

Erdtman, G. (1943). An Introduction to Pollen Analysis. *Chronica Botanica*, Waltham, Massachusetts, USA.

Erdtman, G. (1960). The Acetolysis Method. *Svensk Botanisk Tidskrift* 54, 561-564.

Ernst, G., Wood, C.J., and Hilbrecht, H. (1984). The Cenomanian-Turonian boundary problem in NW-Germany with comments on the north-south correlation to the Regensburg area. *Bulletin of the Geological Society of Denmark* 33, 103-113.

Farley, M.B. (1987). Palynomorphs from surface water of the eastern and central Caribbean Sea. *Micropaleontology* 33, 270-279.

Fauconnier, D. and Masure, E. (2004). Les dinoflagellés fossiles: guide pratique de détermination: les genres à processus et à archéopyle apical. *Editions BRGM*, Collection Scientifique, Orléans, 600 pp.

Feinsinger, P., and Busby, W.H. (1987). Pollen carryover: experimental comparisons between morphs of Palicourea lasiorrachis (Rubiaceae), a distylous, bird-pollinated, tropical treelet. *Oecologia* 73, 231-235.

Fensome, R.A., and Williams, G.L. (2004). The Lentin and Williams Index of Fossil Dinoflagellates – 2004 Edition. *American Association of Stratigraphic Palynologists Contribution Series* 42, 909 pp.

Fensome, R.A., Gocht, H., and Williams, G.L. (1996). The Eisenack Catalog of Fossil Dinoflagellates. *New Series*, 4. E. Schweizerbart'sche Verlagsbuchhandlung, Stuttgart, Germany, 2009–2548.

Forster, A., Schouten, S., Baas, M., and Sinninghe Damsté, J.S. (2007a). Mid-Cretaceous (Albian – Santonian) sea-surface temperature record of the tropical Atlantic Ocean. *Geology* 35, 919-922.

Forster, A., Schouten, S., Moriya, K., Wilson, P.A., and Sinninghe Damsté, J.S. (2007b). Tropical warming and intermittent cooling during the Cenomanian/Turonian Oceanic Anoxic Event (OAE 2): Sea surface temperature records from the equatorial Atlantic. *Paleoceanography* 22, PA1219.

Forster, A., Kuypers, M.M.M., Turgeon, S.C., Brumsack, H.-J., Petrizzo, M.R., and Sinninghe Damsté, J.S. (2008). The Cenomanian/Turonian oceanic anoxic event in the South Atlantic: new insights from a geochemical study of DSDP Site 530A. *Palaeogeography, Palaeoclimatology, Palaeoecology* 267, 256-283.

Freeman, K.H., and Hayes, J.M. (1992). Fractionation of carbon isotopes by phytoplankton and estimates of ancient CO_2 levels. *Global Biogeochemical Cycles* 6, 185-198.

Frölicher, T.L., Joos, F., Plattner, G.K., Steinacher, M., and Doney, S.C. (2009). Natural variability and anthropogenic trends in oceanic oxygen in a coupled carbon-climate model ensemble, *Global Biogeochemical Cycles* 23, GB1003.

Gächter, R., Meyer, J.S., and Mares, A. (1988). Contribution of bacteria to release and fixation of phosphorus in lake-sediments. *Limnology and Oceanography* 33, 1542-1558.

Gale, A.S., and Christensen, W.K. (1996). Occurrence of the belemnite Actinocamax plenus in the Cenomanian of SE France and its significance. *Bulletin of the Geological Society of Denmark* 43, 68-77.

Gale, A.S., Jenkyns, H.C., Kennedy, W.J., and Corfield, R.M. (1993). Chemostratigraphy versus biostratigraphy: DATA from around the Cenomanian – Turonian boundary. *Journal of the Geological Society of London* 150, 29-32.

Gale, A.S., Kennedy, W.J., Voigt, S., and Walaszczyk, I. (2005). Stratigraphy of the Upper Cenomanian – Lower Turonian Chalk succession at Eastbourne, Sussex, UK: ammonites, inoceramid bivalves and stable carbon isotopes. *Cretaceous Research* 26, 460-487.

Galeotti, S., Brinkhuis, H., and Huber, M. (2004). Records of post – Cretaceous-Tertiary boundary millennial-scale cooling from the western Tethys: A smoking gun for the impact-winter hypothesis? *Geology* 32, 529-532.

Gallego-Torres, D., Martinez-Ruiz, F., Meyers, P.A., Paytan, A., Jimenez-Espejo, F.J., and Ortega-

Huertas, M. (2011). Productivity patterns and N-fixation associated with Pliocene – Holocene sapropel: paleoceanographic and paleoecological significance. *Biogeosciences* 8, 415-431.

Ganeshram, R.S., Pedersen, T.F., Calvert, S.E., and Murray, J.W. (1995). Large changes in oceanic nutrient inventories from glacial to interglacial periods. *Nature* 376, 755-758.

Ganeshram, R.S., Pedersen, T.F., Calvert, S.E., and François, R. (2002). Reduced nitrogen fixation in the glacial ocean inferred from changes in marine nitrogen and phosphorus inventories. *Nature* 415, 156-159.

Gasse, F. (2000). Hydrological changes in the African tropics since the Last Glacial Maximum. *Quaternary Science Reviews* 19, 189-211.

Gill, B.C., Lyons, T.W., and Jenkyns, H.C. (2011). A global perturbation to the sulfur cycle during the Toarcian Oceanic Anoxic Event. *Earth and Planetary Science Letters* 312, 484-496.

Giunta, S., Negri, A., Maffioli, P., Sangiorgi, F., Capotondi, L., Morigi, C., Principato, M.S., and Corselli, C. (2006). Phytoplankton dynamics in the eastern Mediterranean Sea during marine isotopic stage 5e. *Palaeogeography, Palaeoclimatology, Palaeoecology* 235, 28-47.

Goodman, D.K. (1987). Dinoflagellate cysts in ancient and modern sediments. *In: Taylor, F.J.R. (Ed.), The Biology of the Dinoflagellates. Botanical Monographs*. Blackwell Scientific, Oxford, 649-722.

Gradstein, F.M., Ogg, J.G., Schmitz, M.D., and Ogg, G.M. (2012). *The Geologic Time Scale 2012, 1st ed*., Oxford, UK, Elsevier, 1176 pp.

Grant, K.M., Rohling, E.J., Bar-Matthews, M., Ayalon, A., Medina-Elizalde, M., Bronk, Ramsey, C., Satow, C., and Roberts, A.P. (2012). Rapid coupling between ice volume and polar temperature over the past 150,000 years. *Nature* 491, 744-747.

Gray, J.S., and Ying, Y.O. (2002). Effects of hypoxia and organic enrichment on the coastal marine environment. *Marine Ecology Progress Series* 238, 249-279.

Grelaud, M., Marino, G., Ziveri, P., and Rohling, E.J. (2012). Abrupt shoaling of the nutricline in response to massive freshwater flooding at the onset of the last interglacial sapropel event. *Paleoceanography* 27, PA3208.

Gruber, N. (2004). The dynamics of the marine nitrogen cycle and its influence on atmospheric CO_2 variations. *In: The ocean carbon cycle and climate*. Springer, Netherlands, 97-148.

Habib, D., and Drugg, W.S. (1987). Palynology of Sites 603 and 605, Leg 93, Deep Sea Drilling Project. *Initial Reports of the Deep Sea Drilling Project* 93. Washington, U.S., Government Printing Office 751-775.

Hamann, Y., Ehrmann, W., Schmiedl, G., Krüger, S., Stuut, J.B., and Kuhnt, T. (2008). Sedimentation processes in the Eastern Mediterranean Sea during the Late Glacial and Holocene revealed by end-member modelling of the terrigenous fraction in marine sediments. *Marine Geology* 248, 97-114.

Hancock, J.M., and Kauffman, E.G. (1979). The great transgressions of the Late Cretaceous. *Journal of the Geological Society of London* 136, 175-186.

Haq, B.U., Hardenbol, J., and Vail, P.R. (1987). Chronology of fluctuating sea levels since the Triassic. *Science* 235, 1156-1167.

Hardas, P. and Mutterlose, J. (2007). Calcareous nannofossil assemblages of Oceanic Anoxic Event 2 in the equatorial Atlantic: Evidence of an eutrophication event. *Marine Micropaleontology* 66, 52-69.

Harland, R. (1973). Dinoflagellate cysts and acritarchs from the Bear-paw Formation (Upper Campanian) of southern Alberta, Canada. *Palaeontology* 16, 665-703.

Harland, R. (1983). Distribution maps of recent dinoflagellate cysts in bottom sediments from the North Atlantic Ocean and adjacent seas. *Palaeontology* 26, 321-387.

Harris, A.J., and Tocher, B.A. (2003). Palaeoenvironmental analysis of Late Cretaceous dinoflagellate cyst assemblages using high-resolution sample correlation from the Western Interior Basin, USA. *Marine Micropaleontology* 48, 127-148.

Hasegawa, T., Crampton, J.S., Schiøler, P., Field, B., Fukushi, K., and Kakizaki, Y. (2013). Carbon isotope stratigraphy and depositional oxia through Cenomanian/Turonian boundary sequences (Upper Cretaceous) in New Zealand. *Cretaceous Research* 40, 61-80.

Hay, W.W., and Flögel, S. (2012). New thoughts about the Cretaceous climate and oceans. *Earth-Science Reviews* 115, 262-272.

Hays, J.D., and Pitman III, W.C. (1973). Lithospheric plate motion, sea level changes and climatic and ecological consequences. *Nature* 246, 18-22.

Head, M.J. (1996). Modern dinoflagellate cysts and their biological affinities. *Palynology: principles and applications* 3, 1197-1248.

Hedberg, H.D. (1936). Gravitational compaction of clays and shales. *American Journal of Science* 184, 241-287.

Helz, G.R., Miller, C.V., Charnock, J.M., Mosselmans, J.F.W., Pattrick, R.A.D., Garner, C.D., and Vaughan, D.J. (1996). Mechanism of molybdenum removal from the sea and its concentration in black shales: EXAFS evidence. *Geochimica et Cosmochimica Acta* 60, 3631-3642.

Hennekam, R., and De Lange, G.J. (2012). X-ray fluorescence core scanning of wet marine sediments: methods to improve quality and reproducibility of high-resolution paleoenvironmental records. *Limnology and Oceanography: Methods* 10, 991-1003.

Hennekam, R., Jilbert, T., Schnetger, B., and De Lange, G.J. (2014). Solar forcing of Nile discharge and sapropel S1 formation in the early- to mid-Holocene eastern Mediterranean. *Paleoceanography* 29, 343-356.

Herbin, J.P., Masure, E., and Roucaché, J. (1987). Cretaceous formations from the lower continental rise off Cape Hatteras: organic geochemistry, dinoflagellate cysts, and the Cenomanian/Turonian boundary event at Sites 603 (Leg 93) and 105 (Leg 11). *Initial Reports of the Deep Sea Drilling Project* 93. Washington, U.S., Government Printing Office, 1139-1160.

Hesselbo, S.P., Gröcke, D.R., Jenkyns, H.C., Bjerrum, C.J., Farrimond, P., Morgans Bell, H.S., and Green, O.R. (2000). Massive dissociation of gas hydrate during a Jurassic oceanic event. *Nature* 406, 392-395.

Hetzel, A., Böttcher, M.E., Wortmann, U.G., and Brumsack, H.-J. (2009). Paleo-redox conditions during OAE 2 reflected in Demerara Rise sediment geochemistry (ODP Leg 207). *Palaeogeography, Palaeoclimatology, Palaeoecology* 273, 302-328.

Hetzel, A., März, C., Vogt, C., and Brumsack, H.-J. (2011). Geochemical environment of Cenomanian – Turonian black shale deposition at Wunstorf (northern Germany). *Cretaceous Research* 32, 480-494.

Heusser, L.E. (1988). Pollen distribution in marine sediments on the continental margin off northern California. *Marine Geology* 80, 131-147.

Higgins, M.B., Wolfe-Simon, F., Robinson, R.S., Qin, Y., Saito, M.A., and Pearson, A. (2011). Paleoenvironmental implications of taxonomic variation among $\delta^{15}N$ values of chloropigments. *Geochimica et Cosmochimica Acta* 75, 7351-7363.

Higgins, M.B., Robinson, R.S., Husson, J.M., Carter, S.J., and Pearson, A. (2012). Dominant eukaryotic export production during ocean anoxic events reflects the importance of recycled NH_4^+. *Proceedings of the National Academy of Sciences of the U.S.A*. 109, 2269-2274.

Hilgen, F.J. (1991). Astronomical calibration of Gauss to Matuyama sapropels in the Mediterranean and implication for the geomagnetic Polarity Time Scale. *Earth and Planetary Science Letters* 104, 226-244.

Hoch, M.P., Fogel, M.L., and Kirchman, D.L. (1994). Isotope fractionation during ammonium uptake by marine microbial assemblages. *Geomicrobiology Journal* 12, 113-127.

Hoering, T.C., and Ford, H.T. (1960). The isotope effect in the fixation of nitrogen by *Azotobacter*. *Journal of the American Chemical Society* 82, 376-378.

Holmes, P.L. (1990). Differential transport of pollen and spores: a laboratory study. *Review of Palaeobotany and Palynology* 64, 289-296.

Hooghiemstra, H. (1988). Palynological records from northwest African marine sediments: a general outline of the interpretation of the pollen signal. *Philosophical Transactions of the Royal Society of London* 318, 431-449.

Hopmans, E.C., Weijers, J.W.H., Schefuß, E., Herfort, L., Sinninghe Damsté, J.S., and Schouten, S. (2004). A novel proxy for terrestrial organic matter in sediments based on branched and isoprenoid tetraether lipids. *Earth and Planetary Science Letters* 224, 107-116.

Huber, B.T., Hodell, D.A., and Hamilton, C.P. (1995). Middle – Late Cretaceous climate of the southern high latitudes: stable isotopic evidence for minimal equator-to-pole thermal gradients. *Geological Society of America Bulletin* 107, 1164-1191.

Huguet, C., Hopmans, E.C., Febo-Ayala, W., Thompson, D.H., Sinninghe Damsté, J.S., and Schouten, S. (2006). An improved method to determine the absolute abundance of glycerol dibiphytanyl glycerol tetraether lipids. *Organic Geochemistry* 37, 1036-1041.

Huguet, C., de Lange, G.J., Middelburg, J.J., Sinninghe Damsté, J.S., and Schouten, S. (2008). Selective preservation of soil organic matter in oxidized marine sediments (Madeira Abyssal Plain). *Geochimica et Cosmochimica Acta* 72, 6061-6068.

Huguet, C., Kim, J.-H., de Lange, G.J., Sinninghe Damsté, J.S., and Schouten, S. (2009). Effects of long-term oxic degradation on the $U^{K'}_{37}$, TEX_{86} and BIT organic proxies. *Organic Geochemistry* 40, 1188-1194.

Ingall, E., and Jahnke, R. (1994). Evidence for enhanced phosphorus regeneration from marine sediments overlain by oxygen depleted waters. *Geochimica et Cosmochimica Acta* 58, 2571-2575.

Ingall, E.D., Bustin, R.M., and van Cappellen, P. (1993). Influence of water column anoxia on the burial and preservation of carbon and phosphorus in marine shales. *Geochimica et Cosmochimica Acta* 57, 303-316.

IPCC, (2013). Climate Change 2013: The Physical Science Basis. *In: Stocker, T.F., D. Qin, G.-K. Plattner, M. Tignor, S.K. Allen, J. Boschung, A. Nauels, Y. Xia, V. Bex and P.M. Midgley (Eds.): Contribution of Working Group I to the Fifth Assessment Report of the Intergovernmental Panel on Climate Change*. Cambridge University Press, Cambridge, United Kingdom and New York, New York, USA, 1535 pp.

IPCC, (2014). Climate Change 2014: Impacts, Adaptation, and Vulnerability. *In: Barros, V.R., Field, C.B., et al. (Eds.), Part B: Regional Aspects. Contribution of Working Group II to the Fifth Assessment Report*

of the Intergovernmental Panel on Climate Change. Cambridge University Press, Cambridge, United Kingdom and New York, New York, USA, in progress.

Jaccard, S.L., and Galbraith, E.D. (2012). Large climate-driven changes of oceanic oxygen concentrations during the last deglaciation. *Nature Geoscience* 5, 151-156.

Jacobs, L., Emerson, S., and Skei, J. (1985). Partitioning and transport of metals across the O_2/H_2S interface in a permanently anoxic basin: Framvaren Fjord, Norway. *Geochimica, et Cosmochimica Acta* 49, 1433-1444.

Jacobsen, D.M., and Anderson, D.M. (1986). Thecate heterotrophic dinoflagellates: feeding behaviour and mechanisms. *Journal of Phycology* 22, 249-258.

Jarvis, I., Carson, G.A., Cooper, M.K.E., Hart, M.B., Leary, P.N., Tocher, B.A., Horne, D., and Rosenfeld, A. (1988). Microfossils and the Cenomanian – Turonian (Late Cretaceous) oceanic anoxic event. *Cretaceous Research* 9, 3-103.

Jarvis, I., Lignum, J.S., Gröcke, D.R., Jenkyns, H.C., and Pearce, M.A. (2011). Black shale deposition, atmospheric CO_2 drawdown, and cooling during the Cenomanian-Turonian Oceanic Anoxic Event. *Paleoceanography* 26, PA3201.

Jefferies, R.P.S. (1962). The palaeoecology of the Actinocamax plenus subzone (lowest Turonian) in the Anglo-Paris Basin. *Palaeontology* 4, 609-647.

Jenkyns, H.C. (1988). The Early Toarcian (Jurassic) anoxic event: stratigraphic, sedimentary, and geochemical evidence. *American Journal of Science* 288, 101-151.

Jenkyns, H.C. (2010). Geochemistry of oceanic anoxic events. *Geochemistry, Geophysics, Geosystems* 11, Q03004.

Jenkyns, H.C., Matthews, A., Tsikos, H., and Erel, Y. (2007). Nitrate reduction, sulfate reduction, and sedimentary iron isotope evolution during the Cenomanian-Turonian oceanic anoxic event. *Paleoceanography* 22, PA3208.

Jilbert, T., and Slomp, C.P. (2013). Rapid high amplitude variability in Baltic Sea hypoxia during the Holocene. *Geology* 41, 1183-1186.

Jørgensen, B.B. (1982). Mineralization of organic matter in the sea bed: the role of sulfate reduction. *Nature* 296, 643-645.

Junium, C.K., and Arthur, M.A. (2007). Nitrogen cycling during the Cretaceous, Cenomanian-Turonian Oceanic Anoxic Event II. *Geochemistry, Geophysics, Geosystems* 8, Q03002.

Kaiho, K. (1994). Planktonic and benthic foraminiferal extinction events during the last 100 my. *Palaeogeography, Palaeoclimatology, Palaeoecology* 111, 45-71.

Keeling, R.F., and Garcia, H. (2002). The change in oceanic O_2 inventory associated with recent global warming. *Proceedings of the National Academy of Sciences of the U.S.A.* 99, 7848-7853.

Keil, R.G., Hu, E.S., Tsamakis, E.C., and Hedges, J.I. (1994). Pollen in marine sediments as an indicator of oxidation of organic matter. *Nature* 369, 639-641.

Kemp, A.E.S., Pearce, R.B., Koizumi, I., Pike, J., and Rance, S.J. (1999). The role of mat-forming diatoms in the formation of Mediterranean sapropels. *Nature* 398, 57-61.

Kennedy, P., Kennedy, H., and Papadimitriou, S. (2005). The effect of acidification on the determination of organic carbon, total nitrogen and their stable isotopic composition in algae and marine sediment. *Rapid Communications in Mass Spectrometry* 19, 1063-1068.

Kerr, A.C. (1998). Oceanic plateau formation: a cause of mass extinction and black shale deposition around the Cenomanian – Turonian boundary? *Journal of the Geological Society of London* 155, 619-626.

Kholeif, S.E.A., and Mudie, P.J. (2009). Palynological records of climate and oceanic conditions in the late Pleistocene and Holocene of the Nile Cone, southeastern Mediterranean, Egypt. *Palynology* 33, 1-24.

Kim, J.-H., van der Meer, J., Schouten, S., Helmke, P., Willmott, V., Sangiorgi, F., Koç, N., Hopmans, E.C., and Sinninghe Damsté, J.S. (2010). New indices and calibrations derived from the distribution of crenarchaeal isoprenoid tetraether lipids: Implications for past sea surface temperature reconstructions. *Geochimica et Cosmochimica Acta* 74, 4639-4654.

Kraal, P., Slomp, C.P., Forster, A., and Kuypers M.M.M. (2010). Phosphorus cycling from the margin to abyssal depths in the proto-Atlantic during oceanic anoxic event 2. *Palaeogeography, Palaeoclimatology, Palaeoecology* 295, 42-54.

Kritee, K., Sigman, D.M., Granger, J., Ward, B.B., Jayakumar, A., and Deutsch, C. (2012). Reduced isotope fractionation by denitrification under conditions relevant to the ocean. *Geochimica et Cosmochimica Acta* 92, 243-259.

Krom, M.D., Kress, N., Brenner, S., and Gordon, L.I. (1991). Phosphorus limitation of primary productivity in the Eastern Mediterranean-Sea. *Limnology and Oceanography* 36, 424-432.

Krom, M.D., Stanley, J.D., Cliff, R.A., and Woodward, J.C. (2002). Nile River sediment fluctuations over the past 7000 yr and their key role in sapropel development. *Geology* 30, 71-74.

Kukal, Z. (1990). The rate of geological processes. *Earth-Science Reviews* 28, 7-258.

Kullenberg, B. (1952). On the salinity of water contained in marine sediments. *Göteborgs Kungliga Vetenskaps- och Vitterhetssamhället Handling, Series B* 6, 3-37.

Kuroda, J., Ogawa, N.O., Tanimizu, M., Coffin, M.F., Tokuyama, H., Kitazato, H., and Ohkouchi, N. (2007). Contemporaneous massive subaerial volcanism and Late Cretaceous oceanic anoxic event 2. *Earth and Planetary Science Letters* 256, 211-223.

Kuypers, M.M.M., Pancost, R.D., and Sinninghe Damsté, J.S. (1999). A large and abrupt fall in atmospheric CO_2 concentration during Cretaceous times. *Nature* 399, 342-345.

Kuypers, M.M.M., Pancost, R.D., Nijenhuis, I.A., and Sinninghe Damsté, J.S. (2002). Enhanced productivity led to increased organic carbon burial in the euxinic North Atlantic basin during the late Cenomanian oceanic anoxic event. *Paleoceanography* 17, PA1052.

Kuypers, M.M.M., Lourens, L.J., Rijpstra, W.R.C., Pancost, R.D., Nijenhuis, I.A., and Sinninghe Damsté, J.S. (2004a). Orbital forcing of organic carbon burial in the proto-North Atlantic during oceanic anoxic event 2. *Earth and Planetary Science Letters* 228, 465-482.

Kuypers, M.M.M., van Breugel, Y., Schouten, S., Erba, E., and Sinninghe Damsté, J.S. (2004b). N_2-fixing cyanobacteria supplied nutrient N for Cretaceous oceanic anoxic events. *Geology* 32, 853-856.

Lamolda, M.A., and Mao, S. (1999). The Cenomanian – Turonian boundary event and dinocyst record at Ganuza (northern Spain). *Palaeogeography, Palaeoclimatology, Palaeoecology* 150, 65-82.

Larson, R.L. (1991). Latest pulse of Earth: Evidence for a mid-Cretaceous superplume. *Geology* 19, 547-550.

Laskar, J., Robutel, P., Joutel, F., Gastineau, M., Correia, A.C.M., and Levrard, B. (2004). A long-term numerical solution for the insolation quantities of the Earth. *Astronomy and Astrophysics* 428, 261-285.

Leckie, R.M., Bralower, T.J., and Cashman, R. (2002). Oceanic anoxic events and plankton evolution: biotic response to tectonic forcing during the Mid-Cretaceous. *Paleoceanography* 17, PA1041.

Leggett, J.K., McKerrow, W.S., Cocks, L.R.M., and Rickards, R.B. (1981). Periodicity in the Palaeozoic marine realm. *Journal of the Geological Society of London* 138, 167-176.

Lengger, S.K., Kraaij, M., Tjallingii, R., Baas, M., Stuut, J.B., Hopmans, E.C., Sinninghe Damsté, J.S., and Schouten, S. (2013). Differential degradation of intact polar and core glycerol dialkyl glycerol tetraether lipids upon post-depositional oxidation. *Organic Geochemistry* 65, 83-93.

Lenz, C., Behrends, T., Jilbert, T., Silveira, M., and Slomp, C.P. (2014). Redox-dependent changes in manganese speciation in Baltic Sea sediments from the Holocene Thermal Maximum: an EXAFS, XANES and LA-ICP-MS study. *Chemical Geology* 370, 49-57.

Lewis, J., Dodge J.D., and Powell, J. (1990). Quaternary dinoflagllate cysts from the upwelling system offshore Peru, Hole 686B, ODP Leg 112. *In: Suess, E., Von Huene, R., et al. (Eds.), Proceedings of the Ocean Drilling Program, Scientific Results* 112. Washington, U.S., Government Printing Office, 323-328.

Li, H., and Habib, D. (1996). Dinoflagellate stratigraphy and its response to sea level change in Cenomanian-Turonian sections of the Western Interior of the United States. *Palaios*, 15-30.

Lignum, J.S. (2009). Cenomanian (upper Cretaceous) palynology and chemostratigraphy: Dinoflagellate cysts as indicators of palaeoenvironmental and sea-level change. *PhD thesis, Kingston University London*, Kingston upon Thames, UK, 582 pp.

Linnert, C., Mutterlose, J., and Erbacher, J. (2010). Calcareous nannofossils of the Cenomanian/Turonian boundary interval from the Boreal Realm (Wunstorf, northwest Germany). *Marine Micropaleontology* 74, 38-58.

Lohse, L., Kloosterhuis, R.T., de Stigter, H.C., Helder, W., van Raaphorst, W., and Van Weering, T.C. (2000). Carbonate removal by acidification causes loss of nitrogenous compounds in continental margin sediments. *Marine Chemistry* 69, 193-201.

Lovley, D.R., and Phillips, E.J. (1988). Novel mode of microbial energy metabolism: organic carbon oxidation coupled to dissimilatory reduction of iron or manganese. *Applied Environmental Microbiology* 54, 1472-1480.

Luciani, V., and Cobianchi, M. (1999). The Bonarelli Level and other black shales in the Cenomanian-Turonian of the northeastern Dolomites (Italy): calcareous nannofossil and foraminiferal data. *Cretaceous Research* 20, 135-167

Lyons, T.W. and Severmann, S. (2006). A critical look at iron paleoredox proxies: New insights from modern euxinic marine basins. *Geochimica et Cosmochimica Acta* 70, 5698-5722.

Lyons, T.W., Werne, J.P., Hollander, D.J., and Murray, R.W. (2003). Contrasting sulfur geochemistry and Fe/Al and Mo/Al ratios across the last oxic-to-anoxic transition in the Cariaco Basin, Venezuela. *Chemical Geology* 195, 131-157.

Malinverno, A., Erba, E., and Herbert, T.D. (2010). Orbital tuning as an inverse problem: chronology of the early Aptian oceanic anoxic event 1a (Selli Level) in the Cismon APTICORE. *Paleoceanography* 25, PA2203.

Marino, G., Rohling, E.J., Sangiorgi, F., Hayes, A., Casford, J.L., Lotter, A.F., Kucera, M., and Brinkhuis, H. (2009). Early and middle Holocene in the Aegean Sea: Interplay between high and low latitude climate variability. *Quaternary Science Reviews* 28, 3246-3262.

Mariotti, A., Germon, J.C., Hubert, P., Kaiser, P., Letolle, R., Tardieux, A., and Tardieux, P. (1981). Experimental determination of nitrogen kinetic isotope fractionation: some principles; illustration for the denitrification and nitrification processes. *Plant and Soil* 62, 413-430.

Marshall, K.L., and Batten, D.J. (1988). Dinoflagellate cyst associations in Cenomanian – Turonian "black shale" sequences of northern Europe. *Review of Palaeobotany and Palynology* 54, 85-103.

Matear, R.J., and Hirst, A.C. (2003). Long-term changes in dissolved oxygen concentrations in the ocean caused by protracted global warming. *Global Biogeochemical Cycles* 17, GB1125.

Matear, R.J., Hirst, A.C., and McNeil, B.J. (2000). Changes in dissolved oxygen in the Southern Ocean with climate change. *Geochemistry, Geophysics, Geosystems* 1.

Mazzini, A., Svensen, H., Leanza, H.A., Corfu, F., and Planke, S. (2010). Early Jurassic shale chemostratigraphy and U – Pb ages from the Neuquén Basin (Argentina): implications for the Toarcian Oceanic Anoxic Event. *Earth and Planetary Science Letters* 297, 633-645.

McArthur, J.M., Algeo, T.J., van de Schootbrugge, B., Li, Q., and Howarth, R.J. (2008). Basinal restriction, black shales, Re – Os dating, and the early Toarcian (Jurassic) oceanic anoxic event. *Paleoceanography* 23, PA4217.

McMinn, A. (1988). Outline of a Late Cretaceous dinoflagellate zonation of northern Australia. *Alcheringa* 12, 137-156.

Meyer, K.M., and Kump, L.R. (2008). Oceanic euxinia in Earth history: Causes and consequences. *Annual Review of Earth and Planetary Sciences* 36, 251-288.

Meyers, P.A., Bernasconi, S.M., and Yum, J.-G. (2009). 20 My of nitrogen fixation during deposition of mid-Cretaceous black shales on the Demerara Rise, equatorial Atlantic Ocean. *Organic Geochemistry* 40, 158-166.

Meyers, S.R., Siewert, S.E., Singer, B.S., Sageman, B.B., Condon, D.J., Obradovich, J.D., Jicha, B.R., and Sawyer, D.A. (2012a). Intercalibration of radio isotopic and astrochronologic time scales for the Cenomanian-Turonian boundary interval, Western Interior Basin, USA. *Geology* 40, 7-10.

Meyers, S.R., Sageman, B.B., and Arthur, M.A. (2012b). Obliquity forcing and the amplification of high-latitude climate processes during Oceanic Anoxic Event 2. *Paleoceanography* 27, PA3212.

Middelburg, J.J., and Levin, L.A. (2009). Coastal hypoxia and sediment biogeochemistry. *Biogeosciences* 6, 1273-1293.

Middelburg, J.J., Soetaert, K., Herman, P.M., and Heip, C.H. (1996). Denitrification in marine sediments: A model study. *Global Biogeochemical Cycles* 10, 661-673.

Miller, K.G., Sugarman, P.J., Browning, J.V., Olsson, R.K., Pekar, S.F., Reilly, T.J., Cramer, B.S., Aubry, M.-P., Lawrence, R.P., Curran, J., Stewart, M., Metzger, J.M., Uptegrove, J., Bukry, D., Burckle, L.H., Wright, J.D., Feigenson, M.D., Brenner, G.J., and Dalton, R.F. (1998). Bass River site report. *Proceedings of the Ocean Drilling Program, Initial Reports* 174AX. Washington, U.S., Government Printing Office, 5-43.

Miller, K.G., Kominz, M.A., Browning, J.V., Wright, J.D., Mountain, G.S., Katz, M.E., Sugarman, P.J., Cramer, B.S., Christie-Blick, N., and Pekar, S.F. (2005). The Phanerozoic record of global sea-level change. *Science* 310, 1293-1298.

Minagawa, M., and Wada, E. (1984). Stepwise enrichment of ^{15}N along food chains: Further evidence and the relation between $\delta^{15}N$ and animal age. *Geochimica et Cosmochimica Acta* 48, 1135-1140.

Minagawa, M., and Wada, E. (1986). Nitrogen isotope ratios of red tide organisms in the East China Sea: A characterization of biological nitrogen fixation. *Marine Chemistry* 19, 245-259.

Möbius, J., Lahajnar, N., and Emeis, K.-C. (2010). Diagenetic control of nitrogen isotope ratios in Holocene sapropels and recent sediments from the Eastern Mediterranean Sea. *Biogeosciences* 7, 3901-3914.

Monteiro, F.M., Pancost, R.D., Ridgwell, A. and Donnadieu, Y. (2012). Nutrients as the dominant control on the spread of anoxia and euxinia across the Cenomanian – Turonian oceanic anoxic event (OAE2): model – data comparison. *Paleoceanography* 27, PA4209.

Montresor, M., Zingone, A., and Sarno, D. (1998). Dinoflagellate cyst production at a coastal Mediterranean site. *Journal of Plankton Research* 20, 2291-2312.

Moodley, L., Middelburg, J.J., Herman, P.M.J., Soetaert, K., and De Lange, G.J. (2005). Oxygenation and organic-matter preservation in marine sediments: Direct experimental evidence from ancient organic carbon-rich deposits. *Geology* 33, 889-892.

Morel, F.M.M., and Price, N.M. (2003). The biogeochemical cycles of trace metals in the oceans. *Science* 300, 944-947.

Mort, M., Adatte, T., Föllmi, K.B., Keller, G., Steinmann, P., Matera, V., Berner, Z., and Stüben, D. (2007). Phosphorus and the roles of productivity and nutrient recycling during oceanic anoxic event 2. *Geology* 35, 483-486.

Mudie, P.J., (1982). Pollen distribution in recent marine sediments, eastern Canada. *Canadian Journal of Earth Sciences* 19, 729-747.

Mudie, P.J., and McCarthy, F.M.G. (1994). Late Quaternary pollen transport processes, western north Atlantic: Data from box models, cross-margin and N – S transects. *Marine Geology* 118, 79-105.

Mudie, P.J., and McCarthy, F.M. (2006). Marine palynology: potentials for onshore-offshore correlation of Pleistocene-Holocene records. *Transactions of the Royal Society of South Africa* 61, 139-157.

Müller, R.D., Sdrolias, M., Gaina, C., Steinberge, R.B., and Heine, C. (2008). Long-term sea-level fluctuations driven by ocean basin dynamics. *Science* 319, 1357-1362.

Naqvi, S.W.A., Naik, H., Pratihary, A., D'Souza, W., Narvekar, P.V., Jayakumar, D.A., Devol, A.H., Yoshinari, T., and Saino, T. (2006). Coastal versus open-ocean denitrification in the Arabian Sea. *Biogeosciences* 3, 621-633.

Negri, A., and Giunta, S. (2001). Calcareous nannofossil paleoecology in the sapropel S1 of the eastern Ionian Sea: paleoceanographic implications. *Palaeogeography, Palaeoclimatology, Palaeoecology* 169, 101-112.

Negri, A., Capotondi, L., and Keller, J. (1999). Calcareous nannofossils, planktic foraminifers and oxygen isotope in the late Quaternary sapropels of the Ionian Sea. *Marine Geology* 157, 84-99.

Nieuwenhuize, J., Maas, Y.E.M., and Middelburg, J.J. (1994). Rapid analysis of organic carbon and nitrogen in particulate materials. *Marine Chemistry* 45, 217-224.

Oschliess A., Schulz K.G., Riebesell U., and Schmittner, A. (2008). Simulated 21st century's increase in oceanic suboxia by CO_2-enhanced biotic carbon export. *Global Biogeochemical Cycles* 22, GB4008.

Owens, J.D., Lyons, T.W., Li, X., Macleod, K.G., Gordon, G., Kuypers, M.M.M., Anbar, A., Kuhnt, W., and Severmann, S. (2012). Iron isotope and trace metal records of iron cycling in the proto-North Atlantic during the Cenomanian – Turonian oceanic anoxic event (OAE-2). *Paleoceanography* 27, PA3223.

Paerl, H.W. (1992). Marine pelagic cyanobacteria: *Trichodesmium* and other diazotrophs. Springer, Netherlands, 287-307.

Pálfy, J., and Smith, P.L. (2000). Synchrony between Early Jurassic extinction, oceanic anoxic event, and the Karoo – Ferrar flood basalt volcanism. *Geology* 28, 747-750.

Pancost, R.D., Crawford, N., Magness, S., Turner, A., Jenkyns, H.C., and Maxwell, J.R. (2004). Further evidence for the development of photic zone euxinic conditions during Mesozoic oceanic anoxic events. *Journal of the Geological Society of London* 161, 353-364.

Parente, M., Frijia, G., Di Lucia, M., Jenkyns, H.C., Woodfine, R.G., and Baroncini F. (2008). Stepwise extinction of larger foraminifers at the Cenomanian-Turonian boundary: A shallow-water perspective on nutrient fluctuations during Oceanic Anoxic Event 2 (Bonarelli Event). *Geology* 36, 715-718.

Paul, C.R.C., Lamolda, M.A., Mitchell, S.F., Vaziri, M.R., Gorostidi, A., and Marshall, J.D. (1999). The Cenomanian/Turonian boundary at Eastbourne (Sussex, UK): A proposed European reference section. *Palaeogeography, Palaeoclimatology, Palaeoecology* 150, 83-121.

Paulmier, A., Ruiz- Pino, D., Garçon, V., and Farias, L. (2006). Maintaining of the eastern south Pacific oxygen minimum zone (OMZ) off Chile. *Geophysical Research Letters* 33, L20601.

Pavlishina, P., and Wagreich, M. (2012). Biostratigraphy and paleoenvironments in a northwestern Tethyan Cenomanian-Turonian boundary section (Austria) based on palynology and calcareous nannofossils. *Cretaceous Research* 38, 103-112.

Pearce, M.A., Jarvis, I., and Tocher, B.A. (2009). The Cenomanian-Turonian boundary event, OAE 2 and palaeoenvironmental change in epicontinental seas: new insights from the dinocyst and geochemical records. *Palaeogeography, Palaeoclimatology, Palaeoecology* 280, 207-234.

Peterse, F., van der Meer, J., Schouten, S., Weijers, J.W.H., Fierer, N., Jackson, R.B., Kim, J.-H., and Sinninghe Damsté, J.S. (2012). Revised calibration of the MBT – CBT paleotemperature proxy based on branched tetraether membrane lipids in surface soils. *Geochimica et Cosmochimica Acta* 96, 215-229.

Peyrot, D., Barroso-Barcenilla, F., Barrón, E., and Comas-Rengifo, M.J. (2011). Palaeoenvironmental analysis of Cenomanian – Turonian dinocyst assemblages from the Castilian Platform (northern-Central Spain). *Cretaceous Research* 32, 504-526.

Peyrot, D., Barroso-Barcenilla, F., and Feist-Burkhardt, S. (2012). Palaeoenvironmental controls on late Cenomanian – early Turonian dinoflagellate cyst assemblages from Condemios (Central Spain). *Review of Palaeobotany and Palynology* 180, 25-40.

Pierrehumbert, R.T. (2002). The hydrologic cycle in deep-time climate problems. *Nature* 419, 191-198.

Pinardi, N., and Masetti, E. (2000). Variability of the large scale general circulation of the Mediterranean Sea from observations and modelling: a review. *Palaeogeography, Palaeoclimatology, Palaeoecology* 158, 153-174.

Plattner, G.K., Joos, F., Stocker, T.F., and Marchal, O. (2001). Feedback mechanisms and sensitivities of ocean carbon uptake under global warming. *Tellus B: Chemical and Physical Meteorology* 53, 564-592.

Pogge von Strandmann, P.A.E., Jenkyns, H.C., and Woodfine, R.G. (2013). Lithium isotope evidence for enhanced weathering during Oceanic Anoxic Event 2. *Nature Geoscience* 6, 668-672.

Poulsen, J. C., Barron, E.J., Arthur, A., and Peterson, H. (2001). Response of the mid-Cretaceous global oceanic circulation to tectonic and CO_2 forcings. *Paleoceanography* 16, 576-592.

Powell, A.J., Dodge, J.D., and Lewis, J. (1990). Late Neogene to Pleistocene palynological facies of the Peruvian continental margin upwelling, Leg 112. *In: Suess, E., Von Huene, R., et al. (Eds.), Proceedings of the Ocean Drilling Program, Scientific Results* 112. Washington, U.S., Government Printing Office, 297-321.

Prauss, M.L. (2006). The Cenomanian – Turonian Boundary Event (CTBE) at Wunstorf, north-west Germany, as reflected by marine palynology. *Cretaceous Research* 27, 872-886.

Prauss, M.L. (2012). The Cenomanian/Turonian Boundary event (CTBE) at Tarfaya, Morocco: Palaeoecological aspects as reflected by marine palynology. *Cretaceous Research* 34, 233-256.

Presley B.J., Kolodny, Y., Nissenbaum, A., and Kaplan, I.R. (1972). Early diagenesis in a reducing fiord, Saanich Inlet, British Columbia II. Trace elements distribution in interstitial water and sediment. *Geochimica et Cosmochimica Acta* 36, 1073-1090.

Prince, I.M., Jarvis, I., Pearce, M.A., and Tocher, B.A. (2008). Dinoflagellate cyst biostratigraphy of the Coniacian – Santonian (Upper Cretaceous): new data from the English Chalk. *Review of Paleobotany and Palynology* 150, 59-96.

Pross, J., and Brinkhuis, H. (2005). Organic-walled dinoflagellate cysts as paleoenvironmental indicators in the Paleogene; a synopsis of concepts. *Paläontologische Zeitschrift* 79, 53-59.

Pross, J., Kotthoff, U., Müller, U.C., Peyron, O., Dormoy, I., Schmiedl, G., Kalaitzidis, S., and Smith, A.M. (2009). Massive perturbation in terrestrial ecosystems of the Eastern Mediterranean region associated with the 8.2 kyr B.P. climatic event. *Geology* 37, 887-890.

R Development Core team (2006). R: A Language and Environment for Statistical Computing. *R Foundation for Statistical Computing*.

Rabalais, N.N., Turner, R.E., and Wiseman, W.J. (2002). Gulf of Mexico hypoxia, aka "The dead zone". *Annual Review of Ecology and Systematics* 33, 235 – 263.

Rau, G.H., Arthur, M.A., and Dean, W.E. (1987). $^{15}N/^{14}N$ variations in Cretaceous Atlantic sedimentary sequences: implication for past changes in marine nitrogen biogeochemistry. *Earth and Planetary Science Letters* 82, 269-279.

Raup, D.M., and Sepkoski, J.J. (1982). Mass extinctions in the marine fossil record. *Science* 215, 1501-1503.

Raup, D.M., and Sepkoski, J.J. (1986). Periodic extinctions of families and genera. *Science* 231, 833-836.

Reed, D.C., Slomp, C.P. and De Lange, G.J. (2011). A quantitative reconstruction of organic matter and nutrient diagenesis in Mediterranean Sea sediments over the Holocene. *Geochimica et Cosmochimica Acta* 75, 5540-5558.

Renssen, H., Brovkin, V., Fichefet, T., and Goosse, H. (2003). Holocene climatic instability during the termination of the African Humid Period. *Geophysical Research Letters* 30, 1184.

Robertson, A.H.F., Emeis, K.-C., Richter, C., and Camerlenghi, A. (1998). *Proceedings of the Ocean Drilling Program, Scientific Results* 160. Washington, U.S., Government Printing Office, 817 pp.

Robinson, R.S., Kienast, M., Luiza Albuquerque, A., Altabet, M., Contreras, S., De Pol Holz, R., Dubois, N., Francois, R., Galbraith, E., Hsu, T.-C., Ivanochko, T., Jaccard, S., Kao, S.-J., Kiefer, T., Kienast, S., Lehmann, M.F., Martinez, P., McCarthy, M., Möbius, J., Pedersen, T., Quan, T.M., Ryabenko, E., Schmittner, A., Schneider, R., Schneider-Mor, A., Shigemitsu, M., Sinclair, D., Somes, C., Studer, A., Thunell, R., and Yang, J.-Y. (2012). A review of nitrogen isotopic alteration in marine sediments. *Paleoceanography* 27, PA4203.

Rochon, A., de Vernal, A., Turon, J.L., Mathiessen, J., and Head, M.J. (1999). Distribution of recent dinoflagellate cysts in surface sediments from the North Atlantic Ocean and adjacent seas in relation to sea-surface parameters. *AASP Contributions Series number* 35. American Association of Stratigraphic Palynologists Foundation, Dallas, Texas, 152 pp.

Rohling, E.J. (1994). Review and new aspects concerning the formation of Eastern Mediterranean sapropels. *Marine Geology* 122, 1-28.

Rohling, E.J., and Gieskes, W.W. (1989). Late Quaternary changes in Mediterranean intermediate water density and formation rate. *Paleoceanography* 4, 531-545.

Rohling, E.J., and Pälike, H. (2005). Centennial-scale climate cooling with a sudden cold event around 8,200 years ago. *Nature* 434, 975-979.

Rossignol-Strick, M. (1985). Mediterranean Quaternary sapropels, an immediate response of the African monsoon to variation of insolation. *Palaeogeography, Palaeoclimatology, Palaeoecology* 49, 237-263.

Rossignol-Strick, M. (1999). The Holocene climatic optimum and pollen records of sapropel 1 in the eastern Mediterranean, 9000 – 6000 BP. *Quaternary Science Reviews* 18, 515-530.

Ruddiman, W.F. (2000). Earth's Climate: past and future. W.H. Freeman, New York.

Ruvalcaba Baroni, I., Biogeochemical response to widespread anoxia in the past ocean *PhD-thesis, Utrecht University*, in press.

Ruvalcaba Baroni, I., Topper, R.P.M., van Helmond, N.A.G.M., Brinkhuis, H., and Slomp, C.P. (2014). Biogeochemistry of the North Atlantic during oceanic anoxic event 2: role of changes in ocean circulation and phosphorus input. *Biogeosciences* 11, 977-993.

Ruvalcaba Baroni, I., Tsandev, I., and Slomp, C.P. (2014). Enhanced N_2-fixation and NH_4^+ recycling during oceanic anoxic event 2 in the proto-North Atlantic. *Geochemistry, Geophysics, Geosystems* 15.

Ryabenko, E. (2013). Stable Isotope Methods for the Study of the Nitrogen Cycle. *In: Zambianchi, E., (Ed.): Topics in Oceanography 49*.

Sageman, B.B., Meyers, S.R., and Arthur, M.A. (2006). Orbital time scale and new C-isotope record for Cenomanian-Turonian stratotype. *Geology* 34, 125-128.

Sangiorgi, F., Donders, T.H. (2004). Reconstructing 150 years of eutrophication in the north western Adriatic Sea (Italy) using dinoflagellate cysts, pollen and spores. *Estuarine, Coastal and Shelf Science* 60, 69-79.

Sangiorgi, F., Capotondi, L., Combourieu Nebout, N., Vigliotti, L., Brinkhuis, H., Giunta, S., Lotter, A.F., Morigi, C., Negri, A., and Reichart, G.-J. (2003). Holocene seasonal sea-surface temperature variations in the southern Adriatic Sea inferred from a multiproxy approach. *Journal of Quaternary Science* 18, 723-732.

Sangiorgi, F., Fabbri, D., Comandini, M., Gabbianelli, G., and Tagliavini, E. (2005). The distribution of sterols and organic-walled dinoflagellate cysts in surface sedimentsof the North-western Adriatic Sea (Italy). *Estuarine, Coastal and Shelf Sciences* 64, 395-406.

Sarmiento J.L., Hughes T.M.C., Stouffer R.J., and Manabe, S. (1998). Simulated response of the ocean carbon cycle to anthropogenic climate warming. *Nature* 393, 245-249. .

Schiøler, P., and Crampton, J.S. (2014). Dinoflagellate biostratigraphy of the Arowhanan Stage (upper Cenomanian – lower Turonian) in the East Coast Basin, New Zealand. *Cretaceous Research* 48, 205-224.

Schlanger, S.O., and Jenkyns, H.C. (1976). Cretaceous Oceanic Anoxic Events: causes and consequences. *Geologie en Mijnbouw* 55, 179-184.

Scholz, F., McManus, J., Mix, A.C., Hensen, C., and Schneider, R.R. (2014). The impact of ocean deoxygenation on iron release from continental margin sediments. *Nature Geoscience* 7, 433-437.

Schouten, S., Hopmans, E.C., Schefuß, E., and Sinninghe Damsté, J.S. (2002). Distributional variations in marine crenarchaeotal membrane lipids: a new tool for reconstructing ancient sea water temperatures? *Earth and Planetary Science Letters* 204, 265-274.

Schouten, S., Hopmans, E.C., Forster, A., van Breugel, Y., Kuypers, M.M.M., and Sinninghe Damsté, J.S. (2003). Extremely high sea-surface temperatures at low latitudes during the middle Cretaceous as revealed by archaeal membrane lipids. *Geology* 31, 1069-1072.

Schouten, S., Hopmans, E.C., and Sinninghe Damsté, J.S. (2004). The effect of maturity and depositional redox conditions on archaeal tetraether lipid palaeothermometry. *Organic Geochemistry* 35, 567-571.

Schouten, S., Huguet, C., Hopmans, E.C., Kienhuis, M.V.M., and Sinninghe Damsté, J.S. (2007). Improved analytical methodology for TEX_{86} paleothermometry by high performance liquid chromatography/atmospheric pressure chemical ionization-mass spectrometry. *Analytical Chemistry* 79, 2940-2944.

Scotese, C.R., (2001). Atlas of Earth History 1, *PALEOMAP Project*, Arlington, Texas, USA.

Scott, C., and Lyons, T.W. (2012). Contrasting molybdenum cycling and isotopic properties in euxinic versus non-euxinic sediments and sedimentary rocks: Refining the paleoproxies. *Chemical Geology* 324-325, 19-27.

Scranton, M.I., Astor, Y., Bohrer, R., Ho, T.-Y., and Muller-Karger, F. (2001). Controls on temporal variability of the geochemistry of the deep Cariaco Basin. *Deep-Sea Research Part I* 48, 1605-1625.

Sewall, J.O., van de Wal, R.S.W., van der Zwan, K., van Oosterhout, C., Dijkstra, H.A., and Scotese, C.R. (2007). Climate model boundary conditions for four Cretaceous time slices. *Climate of the Past* 3, 647-657.

Shaffer G., Olsen, S.M., and Pedersen, J.O.P. (2009). Long-term ocean oxygen depletion in response to carbon dioxide emissions from fossil fuels. *Nature Geoscience* 2, 105-109.

Shimmield, G.B., and Mowbray, S.R. (1991). The inorganic geochemical record of the northwest arabian sea: a history of productivity variations over the last 400 k.y. from sites 722 and 724. *Proceedings of the Ocean Drilling Program, Scientific Results* 117. Washington, U.S., Government Printing Office, 409-443.

Shipboard Scientific Party (1977). Site 367. *In: Lancelot, Y., E. Seibold, et al., (Eds.)*, *Initial Reports of the Deep Sea Drilling Project* 41. Washington, U.S., Government Printing Office, 163-232.

Shipboard Scientific Party (1987a). Site 603. *In: van Hinte, J.E., S.W. Wise Jr., et al., (Eds.), Initial Reports of the Deep Sea Drilling Project* 93. Washington, U.S., Government Printing Office, 25-276.

Shipboard Scientific Party (1987b). Site 641. *In: Boillot, G., E.L. Winterer, et al., (Eds.), Initial Reports of the Ocean Drilling Program* 103. Washington, U.S., Government Printing Office, 571-649.

Shipboard Scientific Party (2004). Site 1276. *In: Tucholke, B.E., J.-C. Sibuet, A. Klaus, et al. (Eds.), Initial Reports of the Ocean Drilling Program* 210. Washington, U.S., Government Printing Office, 1-358.

Sigman, D.M., Altabet, M.A., McCorkle, D.C., Francois, R., and Fischer, G. (2000). The $\delta^{15}N$ of nitrate in the southern ocean: nitrogen cycling and circulation in the ocean interior. *Journal of Geophysical Research: Oceans (1978-2012)* 105, 19599-19614.

Sinninghe Damsté, J.S. and Köster, J. (1998). A euxinic southern North Atlantic Ocean during the Cenomanian/Turonian oceanic anoxic event. *Earth and Planetary Science Letters* 158, 165-173.

Sinninghe Damsté, J.S., Kenig, F., Koopmans, M.P., Köster, J., Schouten, S., Hayes, J.M., and De Leeuw, J. (1995). Evidence for gammacerane as an indicator of water column stratification. *Geochimica et Cosmochimica Acta* 59, 1895-1900.

Sinninghe Damsté, J.S., Kuypers, M.M.M., Pancost, R.D., and Schouten, S. (2008). The carbon isotopic response of algae, (cyano)bacteria, archaea and higher plants to the late Cenomanian perturbation of the global carbon cycle: insights from biomarkers in black shales from the Cape Verde Basin (DSDP Site 367). *Organic Geochemistry* 39, 1703-1718.

Sinninghe Damsté, J.S., van Bentum, E.C., Reichart, G.-J., Pross, J., and Schouten, S. (2010). A CO_2 decrease-driven cooling and increased latitudinal temperature gradient during the mid-Cretaceous Oceanic Anoxic Event 2. *Earth and Planetary Science Letters* 293, 97-103.

Sinninghe Damsté, J.S., Schouten, S., and Volkman, J.K. (2014), C_{27} – C_{30} neohop-13(18)-enes and their saturated and aromatic derivatives in sediments: Indicators for diagenesis and water column stratification. *Geochimica et Cosmochimica Acta*, 133, 402-421.

Sinton, C.W., and Duncan, R.A. (1997). Potential links between ocean plateau volcanism and global ocean anoxia at the Cenomanian – Turonian boundary. *Economic Geology* 92, 836-842.

Slomp, C.P., Thomson, J., and De Lange, G.J. (2002). Enhanced regeneration of phosphorus during formation of the most recent eastern Mediterranean sapropel (S1). *Geochimica et Cosmochimica Acta* 66, 1171-1184.

Sluijs, A., and Brinkhuis, H. (2009). A dynamic climate and ecosystem state during the Paleocene – Eocene Thermal Maximum: Inferences from dinoflagellate cyst assemblages on the New Jersey Shelf. *Biogeosciences* 6, 1755-1781.

Sluijs, A., and Dickens, G.R. (2012). Assessing offsets between the $\delta^{13}C$ of sedimentary components and the global exogenic carbon pool across early Paleogene carbon cycle perturbations. *Global Biogeochemical Cycles* 26, GB4005.

Sluijs, A., Pross, J., and Brinkhuis, H. (2005). From greenhouse to icehouse; organic-walled dinoflagellate cysts as paleoenvironmental indicators in the Paleogene. *Earth-Science Reviews* 68, 281-315.

Sluijs, A., Schouten, S., Pagani, M., Woltering, M., Brinkhuis, H., Sinninghe Damsté, J.S., Dickens, G.R., Huber, M., Reichart, G.-J., Stein, R., Matthiessen, J., Lourens, L.J., Pedentchouk, N., Backman, J., Moran, K., and the Expedition 302 Scientists (2006). Subtropical Arctic Ocean temperatures during the Palaeocene/Eocene thermal maximum. *Nature* 441, 610-613.

Sluijs, A., Bowen, G.J., Brinkhuis, H., Lourens, L.J., and Thomas, E. (2007a). The Palaeocene-Eocene Thermal Maximum super greenhouse: biotic and geochemical signatures, age models and mechanisms of global change. *Deep Time Perspectives on Climate Change: Marrying the Signal From Computer Models and Biological Proxies*, 323-347.

Sluijs, A., Brinkhuis, H., Schouten, S., Zachos, J.C., Bohaty, S., John, C., Deltrap, R., Reichart, G.-J., Sinninghe Damsté, J.S., Crouch, E., and Dickens, G.R. (2007b). Environmental precursors to rapid light carbon injection at the Palaeocene/Eocene boundary. *Nature* 450, 1218-1221.

Sluijs, A., Schouten, S., Donders, T.H., Schoon, P.L., Röhl, U., Reichart, G.-J., Sangiorgi, F., Kim, J.-H., Sinninghe Damsté, J.S., and Brinkhuis, H. (2009). Warm and wet conditions in the Arctic region during Eocene Thermal Maximum 2. *Nature Geoscience* 2, 777–780.

Snow, L.J., Duncan, R.A., and Bralower, T.J. (2005). Trace element abundances in the Rock Canyon Anticline, Pueblo, Colorado, marine sedimentary section and their relationship to Caribbean plateau construction and ocean anoxic event 2. *Paleoceanography* 20, PA4099.

Soetaert, K., Petzoldt, T., and Woodrow Setzer, R. (2010). Solving Differential Equations in R: Package deSolve. *Journal of Statistical Software* 33, 1-25.

Stanley, D.J., and Maldonado, A. (1977). Nile Cone: Late Quaternary stratigraphy and sediment dispersal. *Nature* 266, 129-135.

Stanley, J.-D., and Warne, A.G. (1993). Nile delta: recent geological evolution and human impact. *Science* 260, 628-634.

Stockmarr, J. (1971). Tablets with spores used in absolute pollen analysis. *Pollen et Spores* 13, 615-621.

Stover, L.E., Brinkhuis, H., Damassa, S.P., de Verteil, L., Helby, R.J., Moteil, E., Partridge, A.D., Powell, A.J., Riding, J.B.; Smelror, M., and Williams, G.L. (1996). Mesozoic-Tertiary dinoflagellates, acritarchs and prasinophytes. *In: Jansonius, J. and McGregor, D.C., (Eds.), Palynology: Principles and Applications.* Dallas (American Association of Stratigraphic Palynologists Foundation), 1249-1276.

Stramma, L., Johnson, G.C., Sprintall, J., and Mohrholz, V. (2008). Expanding oxygen-minimum zones in the tropical oceans. *Science* 320, 655-658.

Stramma, L., Schmidtko, S., Levin, L.A., and Johnson, G.C. (2010). Ocean oxygen minima expansions and their biological impacts. *Deep-Sea Research Part* I 57, 587-595.

Stramma, L., Oschlies, A., and Schmidtko, S. (2012). Mismatch between observed and modeled trends in dissolved upper-ocean oxygen over the last 50 yr. *Biogeosciences* 9-10, 4045-4057.

Strauss, H. (2006). Anoxia through time. *In: Neretin, L.N. (Ed.), Past and Present Water Column Anoxia. NATO Science Series. IV. Earth and Environmental Sciences*. Springer, Netherlands, 3-19.

Sugarman, P.J., Miller, K.G., Olsson, R.K., Browning, J.V., Wright, J.D., De Romero, L.M., White, T.S., Muller, F.L., and Uptegrove, J. (1999). The Cenomanian/Turonian carbon burial event, Bass River, NJ, USA: Geochemical, paleoecological, and sea-level changes. *Journal of Foraminiferal Research* 29, 438-452.

Summerhayes, C.P. (1987). Organic-rich Cretaceous sediments from the North Atlantic. *Geological Society of London Special Publication* 26, 301-316.

Takashima, R., Nishi, H., Yamanaka, T., Tomosugi, T., Fernando, A.G., Tanabe, K., Moriya, K., Kawabe, F., and Hayashi, K. (2011). Prevailing oxic environments in the Pacific Ocean during the mid-Cretaceous Oceanic Anoxic Event 2. *Nature Communications* 2, 234.

Taylor, S.R., and McLennan, S.M. (1995). The Geochemical Evolution of the Continental Crust. *Review of Geophysics* 33, 241-265.

Thomson, J.D. (1986). Pollen transport and deposition by bumble bees in Erythronium: influences of floral nectar and bee grooming. *The Journal of Ecology* 74, 329-341.

Thomson, J., Higgs, N.C., Wilson, T.R.S., Croudace, I.W., De Lange, G.J., and van Santvoort, P.J.M. (1995). Redistribution and geochemical behaviour of redox-sensitive elements around S1, the most recent eastern Mediterranean sapropel. *Geochimica et Cosmochimica Acta* 59, 3487-3501.

Thomson, J., Crudeli, D., De Lange, G.J., Slomp, C.P., Erba, E., Corselli, C., and Calvert, S.E. (2004). Florisphaera profunda and the origin and diagenesis of carbonate phases in eastern Mediterranean sapropel units. *Paleoceanography* 19, PA3003.

Thurow, J.W., Moullade, M., Brumsack, H.-J., Masure, E., Taugourdou, J., and Dunham, K. (1988). The

Cenomanian-Turonian Boundary Event (CTBE) at Leg 103/Hole 641. *Proceedings of the Ocean Drilling Program, Scientific Results* 103. Washington, U.S., Government Printing Office, 587-634.

Tinner, W., van Leeuwen, J.F.N., Colombaroli, D., Vescovi, E., Van der Knaap, W.O., Henne, P.D., Pasta, S., D'Angelo, S., and La Mantia, T. (2009). Holocene environmental and climatic changes at Gorgo Basso, a coastal lake in southern Sicily, Italy. *Quaternary Science Reviews* 28, 1498-1510.

Tocher, B.A., and Jarvis, I. (1995). Dinocyst distributions and stratigraphy of two Cenomanian-Turonian boundary (Upper Cretaceous) sections from the western Anglo-Paris Basin. *Journal of Micropalaeontology* 14, 97-105.

Topper, R.P.M., Trabucho Alexandre, J., Tuenter, E., and Meijer, P.T. (2011). A regional ocean circulation model for the mid-Cretaceous North Atlantic Basin: implications for black shale formation. *Climate of the Past* 7, 277-297.

Trabucho-Alexandre, J., Tuenter, E., Henstra, G.A., van der Zwan, K.J., van de Wal, R.S.W., Dijkstra, H.A., and De Boer, P.A. (2010). The mid-Cretaceous North Atlantic nutrient trap: Black shales and OAEs. *Paleoceanography* 25, PA4201.

Traverse, A., and Ginsburg, R.N. (1966). Palynology of the surface sediments of Great Bahama Bank, as related to water movement and sedimentation. *Marine Geology* 4, 417-459.

Traverse, A. (1990). Studies of pollen and spores in rivers and other bodies of water, in terms of source vegetation and sedimentation, with special reference to Trinity River and Bay, Texas. *Review of Palaeobotany and Palynology* 64, 297-303.

Traverse, A. (1994). Sedimentation of Organic Particles. Cambridge University Press, New York, 544 pp.

Tsandev, I., and Slomp, C.P. (2009). Modeling phosphorus cycling and carbon burial during Cretaceous Oceanic Anoxic Events. *Earth and Planetary Science Letters* 286, 71-79.

Tsikos, H., Jenkyns, H.C., Walsworth-Bell, B., Petrizzo, M.R., Forster, A., Kolonic, S., Erba, E., Premoli Silva, I., Baas, M., Wagner, T. and Sinninghe Damsté, J.S. (2004). Carbon-isotope stratigraphy recorded by the Cenomanian – Turonian Oceanic Anoxic Event: correlation and implications based on three key localities. *Journal of the Geological Society of London* 161, 711-719.

Tucholke, B.E., and Vogt, P.R. (1979). Western North Atlantic: Sedimentary evolution and aspects of tectonic history. *Initial Reports of the Deep Sea Drilling Project* 43. Washington, U.S., Government Printing Office, 791-825.

Turgeon, S.C., and Creaser, R.A. (2008). Cretaceous oceanic anoxic event 2 triggered by a massive magmatic episode. *Nature* 454, 323 – 326.

Turon, J.L., Lézine, A.M., and Denèfle, M. (2003). Land–sea correlations for the last glaciation inferred from a pollen and dinocyst record from the Portuguese margin. *Quaternary Research* 59, 88-96.

Tyrrell, T. (1999). The relative influences of nitrogen and phosphorus on oceanic primary production. *Nature* 400, 525-531.

Tyson, R.V., and Pearson, T.H. (1991). Modern and ancient continental shelf anoxia: an overview. *Geological Society of London Special Publication* 58, 1-24.

Tzortzaki, E., Karakitsios, V., and Tsikos, H. (2013). Biomarker evidence for intermittent photic zone euxinia in the Aptian–Albian organic sedimentary record from the Ionian Zone (Epirus, Greece). *Organic Geochemistry* 64, 84-93.

Uitz, J., Claustre, H., Gentili, B., and Stramski, D. (2010). Phytoplankton class-specific primary production in the world's oceans: Seasonal and inter-annual variability from satellite observations. *Global Biogeochemical Cycles* 24, 3016-3035.

Urquhart, E., Gardin, S., Leckie, R.M., Wood, S.A., Pross, J., Georgescu, M.D., Ladner, B., and Takata, H. (2007). A paleontological synthesis of ODP Leg 210, Newfoundland Basin. *In: Tucholke, B.E., Sibuet, J.-C., Klaus, A., (Eds.), Proceedings of the Ocean Drilling Program, Scientific. Results* 210. Washington, U.S., Government Printing Office, 1-53.

Van Bentum, E.C., Hetzel, A., Brumsack, H.J., Forster, A., Reichart, G.-J., and Sinninghe Damsté, J.S. (2009). Reconstruction of water column anoxia in the equatorial Atlantic during the Cenomanian–Turonian oceanic anoxic event using biomarker and trace metal proxies. *Palaeogeography, Palaeoclimatology, Palaeoecology* 280, 489-498.

Van Bentum, E.C., Reichart, G.-J., and Sinninghe Damsté, J.S. (2012). Organic matter provenance, palaeoproductivity and bottom water anoxia during the Cenomanian/Turonian oceanic anoxic event in the Newfoundland Basin (northern proto North Atlantic Ocean). *Organic Geochemistry* 50, 11-18.

Van Campo, M.M. (1984). Relations entre la végétation de l'Europe et les températures de surface océaniques après le dernier maximum glaciair. *Pollen Spores* 26, 497 – 518.

Van Cappellen, P., and Ingall, E.D. (1994). Benthic phosphorus regeneration, net primary production, and ocean anoxia: a model of the coupled marine biogeochemical cycles of carbon and phosphorus. *Paleoceanography* 9, 677-692.

Van Simaeys, S., Brinkhuis, H., Pross, J., Williams, G.L., and Zachos, J.C. (2005). Arctic dinoflagellate migrations mark the strongest Oligocene glaciations. *Geology* 33, 709-712.

Varban, B.L., and Plint, A.G. (2008). Palaeoenvironments, palaeogeography, and physiography of a large, shallow, muddy ramp: Late Cenomanian- Turonian Kaskapau Formation, Western Canada foreland basin. *Sedimentology* 55, 201-233.

Vellekoop, J., Sluijs, A., Smit, J., Schouten, S., Weijers, J.W.H., Sinninghe Damsté, J.S., and Brinkhuis, H. (2014). Rapid short-term cooling following the Chicxulub impact at the Cretaceous – Paleogene boundary. *Proceedings of the National Academy of Sciences of the U.S.A.* 111, 7537-7541.

Versteegh, G.J.M., Zonneveld, K.A.F. (2002). Use of selective degradation to separate preservation from productivity. *Geology* 30, 615-618.

Voigt, S., Gale, A.S., and Flögel, S. (2004). Midlatitude shelf seas in the Cenomanian-Turonian greenhouse world: Temperature evolution and North Atlantic circulation. *Paleoceanography* 19, PA4020.

Voigt, S., Gale, A.S., and Voigt, T. (2006). Sea-level change, carbon cycling and palaeoclimate during the Late Cenomanian of northwest Europe; An integrated palaeoenvironmental analysis. *Cretaceous Research* 27, 836-858.

Voigt, S., Erbacher, J., Mutterlose, J., Weiss, W., Westerhold, T., Wiese, F., Wilmsen, M., and Wonik, T. (2008). The Cenomanian – Turonian of the Wunstorf section (north Germany): Global stratigraphic reference section and new orbital time scale for oceanic anoxic event 2. *Newsletters on Stratigraphy* 43, 65-89.

Wall, D., and Dale, B. (1966). "Living fossils" in Western Atlantic plankton. *Nature* 211, 1025-1026.

Wall, D., Dale, B., Lohmann, G.P., and Smith, W.K. (1977). The environment and climatic distribution of dinoflagellate cysts in modern marine sediments from regions in the North and South Atlantic Oceans and adjacent seas. *Marine Micropaleontology* 2, 121-200.

Waser, N.A.D., Harrison, P.J., Nielsen, B., Calvert, S.E., and Turpin, D.H., (1998). Nitrogen isotope fractionation during the uptake and assimilation of nitrate, nitrite, ammonium, and urea by a marine diatom. *Limnology and Oceanography* 43, 215-224.

Weijers, J.W.H., Schouten, S., Spaargaren, O.C., and Sinninghe Damsté, J.S., (2006). Occurrence and distribution of tetraether membrane lipids in soils: Implications for the use of the TEX_{86} proxy and the BIT index. *Organic Geochemistry* 37, 1680-1693.

Weijers, J.W.H., Schouten, S., van den Donker, J.C., Hopmans, E.C., and Sinninghe Damsté, J.S. (2007). Environmental controls on bacterial tetraether membrane lipid distribution in soils. *Geochimica et Cosmochimica Acta* 71, 703-713.

Weldeab, S., Emeis, K.-C., Hemleben, C., and Siebel, W. (2002). Provenance lithogenic surface sediments and path ways of riverine suspended matters in the eastern Mediterranean Sea: Evidence from $^{143}Nd/^{144}Nd$ and $^{87}Sr/^{86}Sr$ ratios. *Chemical Geology* 186, 139-149.

Weldeab, S., Emeis, K.-C., Hemleben, C., Schmiedl, G., and Schulz, H. (2003). Spatial productivity during formation of Sapropels S5 and S6 in the Mediterranean Sea: evidence from Ba contents. *Palaeogeography, Palaeoclimatology, Palaeoecology* 191, 169-190.

Weldeab, S., Menke, V., and Schmiedl, G. (2014). The Pace of East African Monsoon Evolution during the Holocene. *Geophysical Research Letters* 41, 1724-1732.

Wendler, I. (2013). A critical evaluation of carbon isotope stratigraphy and biostratigraphic implications for Late Cretaceous global correlation. *Earth-Science Reviews* 126, 116-146.

Westermann, S., Stein, M., Matera, V., Fiet, N., Fleitmann, D., Adatte, T., and Föllmi, K.B. (2013). Rapid changes in the redox conditions of the western Tethys Ocean during the early Aptian oceanic anoxic event. *Geochimica et Cosmochimica Acta* 121, 467-486.

Whitney F.A., Freeland H.J., and Robert, M. (2007). Persistently declining oxygen levels in the interior waters of the eastern subarctic Pacific. *Progress in Oceanography* 75, 179-199.

Wilkin R.T., Arthur, M.A., and Dean, W.E. (1997). History of water-column anoxia in the Black Sea indicated by pyrite framboid size distributions. *Earth and Planetary Science Letters* 148, 517-525.

Willard, D.A., Weimer, L.M., and Riegel, W.L. (2001). Pollen assemblages as paleoenvironmental proxies in the Florida Everglades. *Review of Palaeobotany and Palynology* 113, 213-235.

Williams, D.F., Thunell, R.C., and Kennett, J.P. (1978). Periodic freshwater flooding and stagnation of the eastern Mediterranean Sea during the late Quaternary. *Science* 201, 252-254.

Willis, K.J., Bennett, K.D. and Birks, H.J.B. (1998). The late Quaternary dynamics of pines in Europe. *In: Richardson, D.M. (Ed.), Ecology and Biogeography of Pinus*. Cambridge University Press, Cambridge, 107-121.

Wilmsen, M. (2003). Sequence stratigraphy and palaeoceanography of the Cenomanian stage in northern Germany. *Cretaceous Research* 24, 525-568.

Zhang, X., Sigman, D.M., Morel, F.M.M., and Kraepiel, A.M.L. (2014). Nitrogen isotope fractionation by alternative nitrogenases and past ocean anoxia. *Proceedings of the National Academy of Sciences of the U.S.A.* 111, 4782-4787.

Zonneveld, K.A.F., Versteegh, G.J.M., and De Lange, G.J. (1997). Preservation of organic walled dinoflagellate cysts in different oxygen regimes: a 10,000 yr natural experiment. *Marine Micropaleontology* 29, 393-405.

Zonneveld, K.A.F., Versteegh, G.J.M., and De Lange, G.J. (2001). Palaeoproductivity and postdepositional

aerobic organic matter decay reflected by dinoflagellate cyst assemblages of the Eastern Mediterranean S1 sapropel. *Marine Geology* 172, 181-195.

Zonneveld, K.A.F., Versteegh, G., and Kodrans-Nsiah, M. (2008). Preservation and organic chemistry of Late Cenozoic organic-walled dinoflagellate cysts: A review. *Marine Micropaleontology* 68, 179-197.

Zonneveld, K.A.F., Chen, L., Möbius, J., and Mahmoud, M.S. (2009). Environmental significance of dinoflagellate cysts from the proximal part of the Po-river discharge plume (off southern Italy, Eastern Mediterranean). *Journal of Sea Research* 62, 189-213.

Zonneveld, K.A., Chen, L., Elshanawany, R., Fischer, H.W., Hoins, M., Ibrahim, M.I., Pittauerova, D., and Versteegh, G.J. (2012). The use of dinoflagellate cysts to separate human-induced from natural variability in the trophic state of the Po-River discharge plume over the last two centuries. *Marine Pollution Bulletin* 64, 114-132.

Zonneveld, K.A.F., Marret, F., Versteegh, G.J.M., Bogus, K., Bonnet, S., Bouimetarhan, I., Crouch, E., de Vernal, A., Elshanawany, R., Edwards, L., Esper, O., Forke, S., Grøsfjeld, K., Henry, M., Holzwarth, U., Kielt, J.F., Kim, S.Y., Ladouceur, S., Ledu, D., Chen, L., Limoges, A., Londeix, L., Lu, S.H., Mahmoud, M.S., Marino, G., Matsouka, K., Matthiessen, J., Mildenhal, D.C., Mudie, P., Neil, H.L., Pospelova, V., Qi, Y., Radi, T., Richerol, T., Rochon, A., Sangiorgi, F., Solignac, S., Turon, J.L., Verleye, T., Wang, Y., Wang, Z., and Young, M. (2013). Atlas of modern dinoflagellate cyst distribution based on 2405 data points. *Review of Palaeobotany and Palynology* 191, 1-197.

"Most of the fundamental ideas of science are essentially simple, and may, as a rule, be expressed in a language comprehensible to everyone."

Albert Einstein

Summary in dutch (Samenvatting in het Nederlands)

1. Oceanische zuurstofconcentraties

Zuurstof is essentieel voor veel leven op Aarde. Zowel op het land als in de oceanen. De concentratie van zuurstof in de atmosfeer is gelijkmatig verdeeld over de Aarde, en door de tijd heen relatief constant. Grote variaties in de atmosferische zuurstofconcentratie vinden we alleen als we kijken naar tijdschalen van miljoenen jaren. De zuurstofconcentratie in de oceanen verschilt per locatie en kan zelfs variëren per seizoen. Zuurstofconcentraties in de oceanen zijn van invloed op de groei en de stofwisseling van alle macro-organismen, zoals vissen, krabben, kreeften en weekdieren, en een (te) lage zuurstofconcentratie kan uiteindelijk zelfs fataal zijn. Oceanische zuurstofconcentraties bepalen dus voor een belangrijk deel de distributie en diversiteit van het leven in de oceanen. Verder is de zuurstofconcentratie van invloed op veel biogeochemische kringlopen, omdat de zuurstofconcentratie bepaalt welke microbiële processen zich af kunnen spelen in de waterkolom en in de oppervlaktesedimenten. Veranderingen in oceanische zuurstofconcentraties kunnen daarom ook worden gerelateerd aan grote verstoringen van de koolstofkringloop, de kringloop van voedingsstoffen als fosfor en stikstof en mondiaal klimaat.

Een breed scala aan fysische en biogeochemische processen bepaalt de zuurstofconcentraties in de oceanen. Een groot deel van het huidige oceaanoppervlak is voorzien van voldoende zuurstof door gasuitwisseling met de atmosfeer en door zuurstofproductie van fytoplankton (primaire productie door fotosynthese). De oplosbaarheid van zuurstof in de oceanen wordt echter bepaald door de temperatuur en het zoutgehalte van het zeewater, welke variëren door tijd en ruimte. In het diepere deel van de oceanen (dieper dan ~100m) wordt zuurstof verbruikt bij de afbraak van organisch materiaal (respiratie). In dieper water kan zuurstof alleen worden aangevuld door menging met zuurstofrijk water. De interactie tussen oceaancirculatie en biogeochemische processen leidt daarom tot een complexe verdeling van opgelost zuurstof in de oceanen.

In sommige regio's wordt het opgeloste zuurstof sneller opgebruikt dan dat het aangevuld kan worden, dit leidt tot het ontstaan van zuurstofloze zones. In de huidige oceanen vinden we deze zuurstofloze zones vaak langs de westkust van de continenten. Daar zorgen door wind gedreven stromingen voor opstuwing van water dat rijk is aan voedingsstoffen, dit stimuleert vervolgens planktongroei (primaire productiviteit), oftewel de productie van organisch materiaal. Nadat het plankton sterft zakt het naar dieper water, waar het wordt afgebroken, hierbij wordt zuurstof verbruikt. In dit soort gebieden zorgt hoge primaire productiviteit dus voor dalende zuurstofconcentraties. Een fractie van het geproduceerde organisch materiaal wordt geëxporteerd naar de zeebodem, waar het kan worden begraven voor een langere periode (miljoenen jaren). Op plekken waar zuurstofloze zones zijn wordt echter relatief veel organisch materiaal in het sediment begraven, omdat afbraak van organisch materiaal veel efficiënter is onder zuurstofrijke omstandigheden.

In de huidige oceanen vinden we zuurstofloze zones in het oostelijk deel van de Pacifische Oceaan, in de Atlantische Oceaan, in de Golf van Mexico en in de Arabische Zee. Verder komt zuurstofloosheid voor in (nagenoeg) afgesloten bekkens als de Oostzee, de Zwarte Zee, het Cariaco bekken (voor de kust van Venezuela) en in fjorden.

Toch is de hedendaagse oceaan over het algemeen voorzien van voldoende zuurstof door een stroming, de "Ocean Conveyor Belt", die koud en zuurstofrijk water van de polen naar de diepte van de oceanen transporteert. Echter, door menselijke activiteit verandert de dynamiek en biogeochemie van de oceanen. Metingen en modelresultaten laten zien dat de zeewatertemperatuur sterk is gestegen en dat oceanische zuurstofconcentraties in grote delen van de oceaan gedaald zijn in de laatste decennia. Het uitbreiden van zuurstofloze zones in de hedendaagse oceaan kan direct gekoppeld worden aan de menselijke uitstoot van koolstofdioxide (CO_2), een sterk broeikasgas dat zorgt voor opwarming van de Aarde. Zowel het vermogen van zuurstof om op te lossen in zeewater, als de ventilatie van de oceaan neemt hierdoor af. Verder is er in kustgebieden meer primaire productiviteit door toenemende toevoer van voedingsstoffen door menselijke activiteit. Menselijke activiteit en de opwarming van de Aarde zullen dus leiden tot een verdere uitbreiding van zuurstofloze zones en langdurige zuurstofloosheid in steeds grotere delen van de oceaan.

Een toenemend aantal onderzoeken naar zuurstof in de oceanen zorgt voor een steeds beter inzicht in de oorzaken en gevolgen van zuurstofloosheid in de huidige oceanen en de gevoeligheid van bepaalde gebieden om zuurstofloos te worden. Toch is onze kennis over de reacties van veel biogeochemische processen op veranderende oceanische zuurstofconcentraties en de koppelingen tussen biologie en klimaat nog altijd beperkt. We weten echter dat oceanische zuurstofconcentraties flink varieerden in het geologisch verleden. Deze variaties gingen samen met grote verstoringen in de kringlopen van koolstof, stikstof, fosfor en andere elementen, welke hun sporen hebben achtergelaten in de sedimenten die toentertijd zijn afgezet. Deze sedimenten kunnen we nu gebruiken om de oorzaken en gevolgen van zuurstofloosheid in het verleden te onderzoeken. De resultaten van dit soort onderzoek helpen ons vervolgens om de ontwikkeling van zuurstofloosheid in de oceanen, en de gevolgen daarvan, in het heden en de toekomst beter te begrijpen.

2. Zuurstofloosheid in het geologisch verleden

Tijdens bepaalde perioden in het (geologisch) verleden van de Aarde zijn er donkere, fijnkorrelige, vaak gelaagde mariene sedimenten afgezet. Deze afzettingen zijn over het algemeen rijk aan organisch materiaal en sulfiden, terwijl er geen graafgangen, gemaakt door bodemleven, te vinden zijn. Deze sedimenten worden "zwarte schalies" genoemd, en zijn gevormd onder zuurstofloze omstandigheden. De specifieke oorzaken en gevolgen van de verschillende zuurstofloze perioden verschillen in tijd en ruimte, hoewel ze meestal lijken voor te komen tijdens perioden met een broeikasklimaat. De duur van de verschillende zuurstofloze perioden in het geologisch verleden varieert van enkele

tientallen jaren tot wel een miljoen jaar, van een enkel geïsoleerd bekken tot de mondiale oceaan en van kustgebieden tot de diepste delen van de open oceaan.

Een goed voorbeeld van zuurstoffloosheid in een bekken uit het recente verleden is de herhaaldelijke afzetting van organisch rijke sedimenten, "sapropelen", in het oostelijk deel van de Middellandse Zee. Maxima in zonne-instraling op het noordelijk halfrond, zorgen voor perioden met een versterkte moesson boven Noord-Afrika. Vervolgens zorgt de toegenomen zoetwaterafvoer voor verstoring van de stroming in de Middellandse Zee, omdat er gelaagdheid in de zee ontstaat doordat (licht) zoetwater op (zwaarder) zout zeewater blijft drijven. Hierdoor kan zuurstofrijk oppervlaktewater niet meer met het diepere water mengen, waardoor het organisch materiaal, dat in de oppervlaktewateren geproduceerd wordt, tijdens zijn afbraak al het zuurstof verbruikt in het dieper water. Als alle zuurstof opgebruikt is blijft een groot deel van het organisch materiaal bewaard op de zeebodem, die lagen van organisch materiaal zijn de sapropelen.

In een dieper verleden, met name tijdens het Mesozoïcum (252 tot 66 miljoen jaar geleden) zijn er verschillende perioden waarin zwarte schalies zijn afgezet. Deze perioden duurden typische een paar honderdduizend tot een miljoen jaar, en worden "Oceanic Anoxic Events" (OAEs) genoemd. De meeste OAEs kunnen worden gekoppeld aan grootschalig vulkanisme en het oplossen van methaanhydraten in de oceanen. In een dergelijk scenario vond een snelle stijging van atmosferische CO_2 concentraties plaats, waardoor een vaak al warm klimaat nog warmer werd. Vervolgens leidde dit tot een toename in de chemische verwering van gesteenten op het land, waardoor er meer voedingsstoffen terecht kwamen in de oceanen. Dit leidde dan weer tot verhoogde primaire productiviteit en uiteindelijk tot grootschalige zuurstoffloosheid. Daarnaast zijn er ook aanwijzingen dat bepaalde spoorelementen (bijv. ijzer en koper) die vrijkomen bij vulkanisme hebben bijgedragen aan verhoogde primaire productiviteit. Tijdens de meeste OAEs was de waterkolom zelfs (deels) "euxinisch", oftewel zuurstofloos en sulfidisch. Vrije waterstofsulfide in de waterkolom is giftig, zelfs in lage concentraties. Zowel zuurstoffloosheid als euxinia worden daarom vaak gekoppeld aan massa-extincties.

3. Oceanic Anoxic Event 2

Eén van de best gedocumenteerde en onderzochte OAEs is OAE2. OAE2 vond plaats rond de Cenomaan-Turoon grens (ongeveer 94 miljoen jaar geleden), midden in de geologisch tijdsperiode het Krijt. Het noorden van de 'Atlantische Oceaan' was toen nog relatief afgesloten, omdat de continenten nog veel dichter bij elkaar lagen in vergelijking met de huidige situatie. Daarnaast was het klimaat veel warmer en kwamen er geen grote ijskappen voor, dat zorgde, samen met verhoogde tektonische activiteit voor een veel hogere zeespiegel in vergelijking met tegenwoordig (~150 meter hoger). Hierdoor werden grote delen van de continenten door ondiepe zeeën bedekt. Zo was Europa toentertijd een eilandengroep, vergelijkbaar met het hedendaagse Indonesië. Het afgesloten karakter van de Noord-Atlantische Oceaan was waarschijnlijk een belangrijke factor in de formatie van zuurstoffloosheid en de daaropvolgende afzetting van organisch rijke sedimenten. Met

name het zuidelijk deel van de Noord-Atlantische Oceaan, voor de kust van het huidige Marokko, Kaapverdië, Senegal en Suriname, was al voor aanvang van OAE2 grotendeels zuurstofloos. Tijdens OAE2 kreeg de zuurstoffloosheid een meer globaal karakter.

De toegenomen begraving van organisch materiaal tijdens OAE2 leidde tot verhoogde begraving van organisch materiaal dat relatief veel "lichte koolstof atomen", koolstof-12, bevat. Dit resulteerde in een exogene koolstofbron die verrijkt was in koolstof-13, oftewel "zware koolstof atomen". Deze "verzwaring van de exogene koolstofbron" is vastgelegd als een positieve afwijking in de stabiele koolstof isotopensamenstelling van sedimentaire componenten, inclusief organisch materiaal en carbonaten. Deze positieve afwijking is karakteristiek voor OAE2 en kan over de hele wereld getraceerd worden. Daarom kan deze niet alleen gebruikt worden om sedimenten, afgezet tijdens OAE2, te identificeren, maar ook om verschillende OAE2-secties aan elkaar te koppelen. Recent onderzoek heeft laten zien dat de positieve afwijking in de stabiele koolstof isotopensamenstelling een tijdsduur had van tussen de vierhonderdvijfendertigduizend en zeshonderdduizend jaar.

Terwijl wijdverbreid vulkanisme, hoofdzakelijk toegeschreven aan activiteit van het Caribische Plateau, een voor de hand liggende tektonische aanstichter was van OAE2, worden de daaropvolgende processen en terugkoppelingen nog steeds niet volledig begrepen.

Hoewel OAE2 niet tot de grote vijf massa-extincties gerekend wordt, behoord het wel tot de acht grootste oceanische extincties sinds de start van het Mesozoïcum. OAE2 wordt geassocieerd met, in het algemeen stapsgewijze, grote veranderingen in veel groepen, bijvoorbeeld nanoplankton, stralendiertjes, weekdieren en bodem en planktonische foraminiferen. Deze veranderingen worden toegeschreven aan onderzees vulkanisme, vergrootte zuurstofloze zones en veranderende concentraties van voedingsstoffen.

4. Scope van het proefschrift

Het doel van dit proefschrift is om de oorzaken van grootschalige zuurstoffloosheid en de gevolgen daarvan op biogeochemische kringlopen, de diversiteit en distributie van biota en globaal klimaat te onderzoeken. Om dit doel te bereiken zijn bestaande paleobiologische en geochemische datasets verzameld en aangevuld met nieuwe data, met name voor OAE2. Om een vergelijking te kunnen maken met meer recente perioden van zuurstoffloosheid en de huidige ontwikkelingen hebben we ook de meest recente sapropel geanalyseerd. De combinatie van mariene (voornamelijk capsules van dinoflagellaten) en terrestrische (pollen en sporen) palynologie, verschaft een goede mogelijkheid om belangrijke informatie te verkrijgen over bijvoorbeeld de temperatuur en het zoutgehalte van het zeewater en vegetatieveranderingen op het land. Verder zijn er verschillende geochemische indicatoren die gebruikt kunnen worden om de temperatuur van het zeewater en de oceanische concentraties van zuurstof en voedingsstoffen in het verleden te herleiden.

Dinoflagellaten zijn samen met kiezelwieren en haptophyte algen de belangrijkste eukaryotische primaire producenten van organisch materiaal in de huidige oceaan en

spelen daarom een belangrijke rol in de mondiale koolstofkringloop. Iets minder dan 20% van de huidige dinoflagellaten soorten produceert een resistente capsule van organisch materiaal tijdens een soort van sluimerfase in hun levenscyclus. Deze capsules blijven vaak bewaard in sedimenten die niet volledig blootgesteld zijn aan zuurstof. De diversiteit in (paleo)ecologische voorkeuren van dinoflagellaten die deze capsules maken is groot. Hierdoor kan de samenstelling van dinoflagellaten capsules in sedimenten ons informatie verschaffen over rivierwaterafvoer, stratificatie (gelaagdheid van de waterkolom) en relatieve hoogte van de zeespiegel. Als we de soortensamenstelling van dinoflagellaten capsules combineren met analyses van pollen en sporen, kunnen we zowel inzicht krijgen in veranderingen op het land als in de zee. Ondanks het grote potentieel van dit soort onderzoek is het nog nauwelijks toegepast op sedimenten die afgezet zijn tijdens OAE2.

In aanvulling op het palynologisch onderzoek kan ook geochemisch onderzoek ons helpen bij het reconstrueren van het milieu. Onderzoek naar de kringloop van fosfor heeft laten zien dat fosfor vrijkomt uit sedimenten onder lage zuurstofconcentraties. Fosfor is de limiterende voedingsstof in grote delen van de oceaan, vrijgekomen fosfor stimuleert daarom de productie van organisch materiaal. Daarom kan de ratio van koolstof en fosfor in oude sedimenten ons iets vertellen over oceanische zuurstofconcentraties en het vrijkomen van fosfor. Ook kunnen de concentraties van allerlei spoorelementen, bijvoorbeeld molybdeen en vanadium, worden gebruikt om oceanische zuurstofconcentraties van het verleden te reconstrueren, omdat deze pas worden vastgelegd in sedimenten als er geen zuurstof meer beschikbaar is in de waterkolom. Verder kan de verdeling van specifieke membraanlipiden in sedimenten, gemaakt door bepaalde groepen aquatische microben en bodembacteriën, worden gebruikt om de oppervlaktetemperatuur van (zee)water en de temperatuur op land te reconstrueren.

De implementatie van de resultaten van dit soort onderzoek in biogeochemische modellen voor de oceaan, verbetert ons begrip van hoe grootschalige zuurstoflоosheid tijdens OAE2 ontstond. Uiteindelijk is zulke geïntegreerde kennis nodig om preciezere voorspellingen te kunnen doen over het lot van onze oceanen (en het leven daarin) in de nabije toekomst.

5. Synopsis

De relatieve bijdrage van de aanvoer en productie van organisch materiaal ten opzichte van een betere bewaring van organisch materiaal onder zuurstofloze omstandigheden, blijft tot op heden onduidelijk. Zelfs voor de (relatief) recente, en zeer uitgebreid bestudeerde sapropelen, is hier nog veel discussie over. In **hoofdstuk 2** proberen we de relatieve invloed te bepalen van de productiviteit ‘en van betere preservatie van organisch materiaal op de vorming van sapropel S1 (afgezet tussen 10.000 en 6.000 jaar geleden in de Middellandse Zee). De bestudeerde sedimentkern is genomen voor de kust van Israël, waar de rivier de Nijl een dik pakket sediment heeft afgezet. Dit dikke pakket sediment geeft de mogelijkheid om de veranderingen in het verleden in hoge resolutie te bestuderen. Gebaseerd op de totale hoeveelheid dinoflagellaten capsules en biologisch geproduceerd

carbonaat zien we dat primaire productiviteit zo'n duizend jaar voor het begin van de afzetting van de sapropel al begon toe te nemen, waarschijnlijk in reactie op toegenomen voedingsstoffen afvoer door de Nijl. Een verandering in dinoflagellaten groepen tijdens het begin van de sapropel doet vermoeden dat de waterkolom relatief snel gelaagd werd (binnen honderd jaar). Naast de dinoflagellaten capsules, neemt ook het aantal pollen en sporen toe voor aanvang van de sapropel. De pollen samenstelling wijst eerst op een savannelandschap, maar verandert al snel naar een moeraskustgebied, wat een grotere invloed van de Nijl suggereert. Drie eeuwen na aanvang van de sapropel begint de totale hoeveelheid dinoflagellaten capsules en biologisch geproduceerde carbonaat af te nemen, hoewel de vorming van de sapropel gewoon doorgaat. Op basis hiervan concluderen we dat verhoogde primaire productiviteit samen met de, door gelaagdheid van de waterkolom geïnitieerde, betere bewaring van organisch materiaal leidde tot formatie van sapropel S1, en dat hoge primair productiviteit alleen belangrijk was tijdens de beginfase.

Het ontstaan van OAE2 wordt vaak gekoppeld aan een extreem warm broeikasklimaat. De gevolgen hiervan op de hydrologische kringloop (neerslag en verdamping) worden echter nog niet volledig begrepen. In **hoofdstuk 3** gebruiken we zowel palynologische als geochemische methoden om het klimaat tijdens OAE2 te reconstrueren, daarbij focussen we met name op de temperatuur van het zeewater en de hydrologische kringloop. De bestudeerde sedimenten zijn afkomstig van een sedimentkern, de Bass River kern, genomen in New Jersey (VS). Uit analyse van de kern blijkt dat vlak voor OAE2 de temperatuur van zeewater met ~2.5°C toeneemt naar 36.5°C, en de palynologie laat een toename in rivierwaterafvoer zien. Direct na het begin van OAE2 wordt het echter snel droger en ~3°C kouder, een periode die we het "Plenus Cold Event" noemen. Deze afkoeling is in eerdere studies waargenomen en wordt toegeschreven aan een daling in atmosferische CO_2 concentraties door mondiale koolstofbegraving tijdens de beginfase van OAE2. Gedurende de rest van OAE2 was de zeewatertemperatuur relatief hoog (36-37°C) en het klimaat was het ook erg vochtig. Na OAE2 daalde de zeewatertemperatuur naar het niveau van voor OAE2 en werd het klimaat ook weer droger. Op basis van deze resultaten concluderen we dat een versnelde hydrologische kringloop heeft bijgedragen aan een toevoer van voedingsstoffen naar kustwateren en een toename van gelaagdheid van de waterkolom, waardoor zuurstofloze zones ontstonden of verder uitbreidden.

Het scheiden van de effecten van (1) een warmer wordend klimaat, (2) veranderingen in de hydrologische kringloop en (3) een toename van primaire productiviteit op afnemende oceanische zuurstofconcentraties blijft een groot wetenschappelijk probleem. In **hoofdstuk 4** proberen we de effecten van deze verschillende factoren te bepalen voor het OAE2 interval in de Wunstorf kern (Noord-Duitsland). Wederom gebruiken we een combinatie van palynologische en geochemische methoden. Hoewel het afzettingsmilieu in Wunstorf erg wisselend was lijkt de ontwikkeling van de zeewatertemperatuur sterk op die we hebben gezien in de Bass River kern en andere eerder onderzochte locaties in de Noord-Atlantische Oceaan. Op een onderbreking van de zwarte schalies door afkoeling tijdens het zogenaamde Plenus Cold Event na, blijft de zeewatertemperatuur constant, terwijl er wel variatie is in het afgezette gesteente. Dit suggereert dat veranderingen in

zeewatertemperatuur geen direct effect hadden op de vorming van de zwarte schalies. Absolute en relatief hogere aantallen pollen in de zwarte schalie lagen wijzen op een toename van neerslag en rivierwaterafvoer. Laatstgenoemde bracht waarschijnlijk extra voedingsstoffen met zich mee, wat resulteerde in een toename van productiviteit, blijkens de toename in dinoflagellaten capsules. Daarom concluderen we dat toegenomen neerslag en rivierwaterafvoer, samen met een toename in primaire productiviteit zorgden voor de vorming van zwarte schalies in de Europese kustgebieden tijdens OAE2.

Vrijwel alle soorten organismen, inclusief dinoflagellaten, migreren door klimaatverandering of andere veranderingen in hun leefmilieu. De afkoeling tijdens OAE2 (Plenus Cold Event) zou een soortgelijke migratie teweeg gebracht kunnen hebben. Vooral het exclusief voorkomen van dinoflagellaten capsules behorend tot de *Cyclonephelium compactum – membraniphorum* (*Ccm*) groep in de Bass River kern ten tijde van het Plenus Cold Event, versterkt dit vermoeden. In **hoofdstuk 5** is de mondiale verspreiding van deze soort voor en tijdens OAE2 in kaart gebracht. De resultaten laten zien dat *Ccm* voor OAE2 alomtegenwoordig was in gebieden op hoge breedtegraden, maar tijdens OAE2 komt *Ccm* ook in gebieden voor op lagere breedtegraden. Dit wijst er op dat *Ccm* richting de evenaar migreerde ten gevolge van de afkoeling tijdens het Plenus Cold Event. Het voorkomen van *Ccm* in sedimenten op lagere breedtegraden kan daarom goed gebruikt worden om te bepalen wanneer de sedimenten zijn afgezet.

Het is niet duidelijk of het diepe deel van de Noord-Atlantische Oceaan geheel zuurstofloos was tijdens OAE2. Daarom hebben we in **hoofdstuk 6** bestaande geochemische data verzameld en nieuwe data gegenereerd voor vijf sedimentkernen verspreid over het diepe deel van de Noord-Atlantische oceaan. De resultaten laten zien dat het diepere water in de gehele Noord-Atlantische oceaan zuurstofloos was gedurende een groot deel van OAE2. Verder blijkt dat de circulatie in de Noord-Atlantische Oceaan ook veel minder efficiënt was dan tegenwoordig het geval is. Ten slotte hebben we aanwijzingen gevonden dat het Plenus Cold Event ook invloed heeft gehad op de zuurstofconcentraties in de diepzee.

Het ontstaan van grootschalige zuurstofloosheid tijdens OAE2 wordt vaak gekoppeld aan een toename in primaire productiviteit, deels toegeschreven aan veranderingen in de kringloop van stikstof. Sedimenten van verschillende locaties in de Noord-Atlantische oceaan worden gekenmerkt door een bijzonder "zware" stabiele isotopensamenstelling van stikstof. Dit wordt weer gekoppeld aan de vastlegging van atmosferisch stikstof door microben in oppervlaktewater. Gepubliceerde stabiele isotopensamenstellingen van stikstof voor OAE2 verschillen echter nogal per locatie. In **hoofdstuk 7** hebben we de gepubliceerde stabiele isotopensamenstellingen van stikstof verzameld en nieuwe data gegenereerd voor verschillende locaties in de Noord-Atlantische Oceaan ten tijde van OAE2. Onze data laat zien dat de variatie in de gepubliceerde stabiele isotopensamenstellingen van stikstof waarschijnlijk te wijten is aan het opwerken van sedimenten met zuur, voordat de isotopensamenstelling geanalyseerd wordt. Toch geven ook de sedimenten zonder zuurbehandeling opvallend zware waarden voor OAE2. Wanneer we deze data in een stikstofkringloopmodel voor de Noord-Atlantische Oceaan

tijdens OAE2 verwerken, blijkt dat vastfging van atmosferisch stikstof door microben in de oceaan een belangrijke bijdrage levert aan het isotopensignaal, met name voor het centrale deel van de Noord-Atlantische Oceaan. Daarnaast laten we zien dat lateraal transport en opstuwing van ammonium en onvolledige opname van ammonium tijdens de groei van fytoplankton bijdraagt aan de zwaardere stabiele isotopensamenstellingen van stikstof.

6. Conclusie

De belangrijkste resultaten en conclusies van dit proefschrift laten zien dat verstoringen van het klimaat in het verleden, inclusief het ontstaan van gelaagdheid van de waterkolom door toegenomen rivierwaterafvoer en een versterkte meststoffen kringloop, kettingreacties opleverden waardoor uiteindelijk grootschalige zuurstofloosheid ontstond. Werkgroep 1 van het "Intergovernmental Panel on Climate Change" (IPCC), voorspelt, naast opwarming, ook een toename in neerslag in veel regio's. Verder zijn er veel meer extremen in neerslag en rivierwaterafvoer waargenomen in de afgelopen jaren. In het meest recente IPCC rapport wordt al uitgebreid stil gestaan bij de afname van de oplosbaarheid van zuurstof in zeewater, dalende zuurstofconcentraties in de oceaan en uitbreidende zuurstofloze zones. Deze observaties en voorspellingen, in combinatie met de belangrijkste conclusies van dit proefschrift, suggereren dat de zuurstofloze zones zich zullen blijven uitbreiden. Regio's waar tot op heden geen zuurstoftekort is, zullen hier in de nabije toekomst mogelijk wel mee te maken krijgen, met name kustgebieden.

De resultaten in dit proefschrift vormen een belangrijke bijdrage aan een beter begrip van de vele terugkoppelingsmechanismen (positief en negatief) die samen zorgen voor een versterking of een vermindering van zuurstofloosheid in de oceaan. Deze inzichten zijn cruciaal om voorspellingen over de toekomst van de oceaan te optimaliseren en om het beleid te bepalen dat de toekomst van het leven in de oceaan waarborgt.

Acknowledgements (Dankwoord)

HET IS AF! Einde, ende, fin, fine, finish, maar toch nog niet helemaal… Dit proefschrift was namelijk nooit tot stand gekomen zonder de steun van de geweldige groep mensen om me heen, die ik bij deze nog even genoemd wil hebben.

Allereerst wil ik mijn drie mentoren bedanken: Henk Brinkhuis, Appy Sluijs en Caroline Slomp. Toen ik tegen het einde van mijn Master Biogeologie op zoek was naar een PhD-positie kwam ik wonderbaarlijk genoeg voor het eerst in contact met Henk en Appy. Vier jaar later kan ik concluderen dat ik in geen mooier team had kunnen "spelen" dan team MPP - Marine Palynologie en Paleoceanografie.

Henk, jouw ideeën, suggesties en commentaren waren altijd vlijmscherp, maar ook de vrijheid die je me hebt gegeven binnen het project heb ik zeer gewaardeerd. Het principe iedereen kent Henk en Henk kent iedereen heeft vele deuren geopend, waardoor ik een aantal mooie reizen heb kunnen maken en heel veel interessante mensen heb mogen ontmoeten, enorm bedankt!

Appy, jij bent de gedroomde dagelijkse begeleider geweest! Jouw aanhoudende enthousiasme en positivisme hebben me meermaals uit een dipje gesleurd, en ondanks je overvolle agenda stond je altijd klaar om mee naar data te kijken en jouw visie te geven. Verder was het elke keer weer super om met jouw commentaar op een manuscript aan de slag te gaan, zelden negatief, altijd constructief! De tripjes naar Liverpool, San Francisco en Sitges waren grandioos om aan jouw zijde mee te hebben mogen maken. Niet alleen stelde je me voor aan de juiste mensen, vaak wist je ook de beste kroegen en restaurants te vinden. Ik vind het een grote eer om de eerste promovendus te zijn met jou als promotor!

Caroline, vanaf het begin van het project heb ik bijzonder prettig met jou samen gewerkt. Met name door jouw goede coördinatie en communicatie is de koppeling tussen de twee componenten van het Focus & Massa OAE-project zo mooi tot stand gekomen. Ik ben dan ook erg blij dat we die goede samenwerking nu voortzetten in mijn eerste postdoc.

Then my fellow PhD colleague in the OAE-project, Itzel. Thanks for the great collaboration and your inspiring thoughts and ideas. I particularly enjoyed our joined trips to Bremen and of course (sunny) Bergen! I'm sure you have a very bright future ahead of you.

De basis van dit proefschrift ligt voor een groot deel bij de positieve (werk)sfeer binnen het Laboratorium voor Palaeobotanie en Palynologie (LPP), die voortkomt uit het dagelijkse espressootje in de koffiehoek, een potje tafelvoetbal na de lunch, de PPGU activiteiten en de spontane VrijMiBo's. Marjolein, Rieke, Bas, Linda, Chloë, Jan, Natasja, Hans, Leonard, Zwier, Gea, Han, Johan en Wim bedankt voor jullie hulp en gezelligheid. Francesca en Timme: ik vond het geweldig om met jullie aan de sapropelen te werken, en als eenzame postdoc was Peter vaak degene waarbij ik terecht kon met een vraag, bedankt! Verder heeft

de door de jaren heen variërende groep studenten een belangrijk aandeel gehad in de goede groepssfeer. Met name het begeleiden van afstudeerprojecten vond ik ontzettend leerzaam en leuk: Bastiaan, Karlijn, Daan, Gideon, Karin en Nina, bedankt voor jullie inzet en enthousiasme!

Dan mag ik natuurlijk mijn lotgenoten, collega PhD's bij LPP, niet vergeten te noemen. De eerste twee jaren waren daar nog de veteranen Peter, Emmy en Sander, die het goede voorbeeld hebben gegeven. Maar ook de huidige bezetting zorgt voor een zeer inspirerende werkomgeving. Johan, Alex, Arjen, Joost, Mariska, Mirja, Tjerk en Julian bedankt voor het aanhoren van een hele hoop gezanik tijdens de lunch, de (wetenschappelijke) discussies maar vooral ook voor de gezelligheid tijdens de koffiepauzes en borrels. Succes met de afronding van jullie projecten!

Met name het grondige commentaar en de vele suggesties van Jaap Sinninghe Damsté en Gert-Jan Reichart hebben mijn manuscripten flink verbeterd, dank daarvoor. Verder wil ik Stefan Schouten, Ellen Hopmans en Jort Ossebaar van de mariene organische biogeochemie groep van het NIOZ bedanken voor hun hulp bij de analyse en interpretaties van de GDGT-data. Discussies met Jack Middelburg, Gert de Lange, Lucas Lourens, Dirk Munsterman, Frans Bunnik, Roel Verreussel, Poppe de Boer, João Trabucho-Alexandre, Lennart de Nooijer, Klaas Nierop (ook voor de betere voetbalfeitjes), Francien Peterse, Tom Jilbert, Peter Kraal en Johan Weijers heb ik zeer gewaardeerd. Waarbij ik Johan nog speciaal wil bedanken voor zijn aanmoedigingen en enthousiasme tijdens mijn masteronderzoek, anders was ik waarschijnlijk niet eens aan een PhD begonnen. Verder wil ik de vele PhD collega's en analisten van (organische) geochemie en de mensen van Geo-Media bedanken: Rick, Marie-Louise, Matthias, Nikki, Jiawang, Mathilde, Anne, Fatimah, Alwina, Alejandra, Amalia, Moji, Jos, Els, Laura, Marieke, Loes, Mohamed, Jiefei, Dineke, Jan, Ton Zalm, Thom, Helen, Anita, Dominika, Michiel, Arnold, Ton Markus, Margot Stoete en al degenen die ik hier nog vergeet.

Of course this dissertation could never have been written without collaboration and/or discussion with a large group of internationally-based co-workers: Simone Galeotti, Elisabetta Erba, Robert Speijer, James Eldrett, Martin Pearce, Darren Gröcke, Guy Plint, Jörg Pross, Jochen Erbacher, Wolfram Kürschner, Dan Reed, Silke Voigt, Tim Bralower, Stephen Meyers and many others, including all the participants of the Utrecht OAE-meeting in January 2011, the lecturers and students of the 8th Urbino Summer School in Paleoclimatology (USSP) in July 2011 and the lecturers of the 2012 Utrecht Dinocourse. Furthermore the Integrated Ocean Drilling Program (IODP), Wunstorf Drilling Scientific Party and the PASSAP cruise members are acknowledged for providing the studied materials, and Statoil for additional financial support.

The USSP has been a great source for collaborations and friendships. I particularly treasure the friendship with three PhD colleagues from Utrecht, that started in Urbino. Helen, Vittoria and Rick, thanks for all the great coffee moments, dinners and nights out.

With exception of the shots of tequila, they made my PhD-time just that little bit easier. I hope we can continue to solve ALL paleoclimate-related problems on the back of beermats!

Dan mijn paranimfen: Joost en Arjen. Jullie zijn fijne collega's, maar ik beschouw jullie vooral als goede vrienden, waarmee een biertje drinken of bijv. een congres of voetbalwedstrijd bezoeken altijd een feest is.

Arjen, jij bent drie jaar lang mijn kamergenoot geweest, buiten het bespreken van data was het een prettige afleiding om met jou (soms verhit) te discussiëren over de actualiteiten, politiek en voetbal. Jouw gouden regel bij het gebruik van software "als je het kan bedenken dat een functie er is, dan is die er ook" heeft me veelvuldig geholpen.

Joost, jou ken ik al vanaf onze introductieweek bij AW, sinds die tijd hebben we bij veel cursussen samengewerkt. Ik kon altijd bij je terecht als ik iemand nodig had om even mee naar data te kijken of als ik een probleem had met software of gewoon voor een koffie. Verder was het een feest om samen de koers te volgen, waarschijnlijk kunnen we allebei de winnaars van alle wielerkoersen van de laatste vier jaar opnoemen...

Mijn dank is groot heren!

Het werk als promovendus vergt ontspanning op zijn tijd, iets wat het zaalvoetbal bij Olympos op de donderdagavonden naar hartelust biedt. Teamgenoten, supporters en natuurlijk onze sponsor en naamgever Sciencemedia.nl - Dan Brinkhuis, bedankt!

Ook was daar de "Little Deurne groep" waarmee we op maandagavonden als team "Lord of the Ruins" deelnamen aan de Mick O'Connells pubquiz, PhD-stress was dan echt even verleden tijd. Tom, Gert-Jan, Geert, Ashlee, Leon, Carla, Dianne en Job, bedankt!

Hans, Stephan en Tom, de Carnavals-tripjes naar Andalusië en de vele avondjes Deurne/Tilburg/Breda/R'dam met goede gesprekken maar vooral ook bier, whisky, sushi, toepen, casino, en wat al niet meer, hebben me fantastisch steun geboden de afgelopen vier jaar, bedankt!

Verder wil ik alle vrienden, kennissen en (schoon)familie, met Geert en Marie-José in het bijzonder, bedanken voor hun aanmoedigingen en interesse in mijn onderzoek.

Ten slotte wil ik graag mijn ouders bedanken. Zonder jullie oneindige steun en aanmoedigingen was ik nooit op het punt gekomen dat ik dit dankwoord überhaupt mocht schrijven. Jullie hebben mijn interesses voor natuur, geografie en klimaat van jongs af aan geprikkeld en me een flinke dosis doorzettingsvermogen en werklust meegegeven. De vele weekendjes Deurne vorm(d)en altijd een oase van rust, waardoor ik weer met frisse moed aan een nieuwe week kon beginnen. Pap en mam, bedankt!

Dan als allerlaatste, Sophie. Je hebt alle "highs" en "lows" van mijn PhD-traject van dichtbij meegemaakt. Ondanks dat, heb ik altijd op jouw onvoorwaardelijke steun en liefde kunnen rekenen en waren de afgelopen vier jaar vooral een hele mooie tijd. Dankjewel!

Niels, Utrecht, November 2014

"Scientia potentia est."

Francis Bacon, in: *Meditationes Sacrae (1597)*

Curriculum Vitae

Niels van Helmond was born on the 26th of August 1987 in Deurne, the Netherlands. He completed his pre-university education (gymnasium) at the Willibrord Gymnasium in Deurne in 2005. In September 2005 he started studying Earth Sciences at Utrecht University. He obtained his Bachelor's degree with the specialization Biogeology (with distinction) in July 2008, after a graduation research project with Prof. dr. Esther Jansma. In this project he performed dendrochronological analysis to study the provenance of wood used in the Roman harbour of Forum Hadriani (Voorburg, the Netherlands). Niels started with the Master Biogeology in September 2008. The second year of his master consisted of a graduation research project, under supervision of Dr. Johan Weijers, Dr. Timme Donders (TNO) and Prof. dr. Gert-Jan Reichart. In this project the climate of northwest Europe at the onset of Northern Hemisphere glaciations in the Early Pleistocene was reconstructed, applying both organic geochemical and palynological proxies. Part of that project was a three-month internship at TNO Petroleum Geosciences. In August 2010 Niels obtained his Master's degree (with distinction). From October 2010 Niels was a PhD-candidate in the Marine Palynology and Paleoceanography group at Utrecht University, under supervision of Prof. dr. Henk Brinkhuis, Prof. dr. Appy Sluijs and Prof. dr. ir. Caroline Slomp, which resulted in this dissertation. From October 2014 onwards Niels is a postdoctoral researcher in the Marine Biogeochemistry group of Prof. dr. ir. Caroline Slomp.

Peer-reviewed articles

Published

Van Helmond, N.A.G.M., Sluijs, A., Reichart, G.-J., Sinninghe Damsté, J.S., Slomp, C.P., and Brinkhuis, H. (2014). A perturbed hydrological cycle during Oceanic Anoxic Event 2. *Geology* 42, 123–126.

Ruvalcaba Baroni, I., Topper, R.P.M., van Helmond, N.A.G.M., Brinkhuis, H., and Slomp, C.P. (2014). Biogeochemistry of the North Atlantic during oceanic anoxic event 2: role of changes in ocean circulation and phosphorus input. *Biogeosciences* 11, 977-993.

Domínguez Delmás, M., Driessen, M., García González, I., van Helmond, N.A.G.M., Visser, R., and Jansma, E. (2014). Long-distance oak supply in mid-2nd century AD revealed: the case of a Roman harbour (Voorburg-Arentsburg) in the Netherlands. *Journal of Archaeological Science* 41, 642-654.

Van Helmond, N.A.G.M., Ruvalcaba Baroni, I., Sluijs, A., Sinninghe Damsté, J.S., and Slomp, C.P. (2014). Spatial extent and degree of oxygen depletion in the deep proto-North Atlantic Basin during Oceanic Anoxic Event 2. *Geochemistry, Geophysics, Geosystems* 15.

Van Helmond, N.A.G.M., Sluijs, A., Sinninghe Damsté, J.S., Reichart, G.-J., Voigt, S., Erbacher, J., Pross, J., and Brinkhuis, H. (2014). Freshwater discharge controlled deposition of Cenomanian-Turonian black shales on the NW European epicontinental shelf (Wunstorf, North Germany). *Climate of the Past Discussions* 10, 3755-3786 (*under review for Climate of the Past*).

Submitted

Van Helmond, N.A.G.M., Hennekam, F.M., Donders, T., Bunnik, F.P.M., de Lange, G.J., Brinkhuis, H., and Sangiorgi, F., Marine productivity leads organic matter preservation in sapropel S1: palynological evidence from a core along the path of the Nile River outflow. *In revision for Quaternary Science Reviews.*

Van Helmond, N.A.G.M., Sluijs, A., Papadomanolaki, N.M., Plint, A.G., Gröcke, D.R., Pearce, M.A., Eldrett, J.S., Trabucho-Alexandre, J., van de Schootbrugge, B., and Brinkhuis, H., Equatorward migration of dinoflagellates during the Plenus Cold Event, Oceanic Anoxic Event 2. *Under review for Geology*.

Ruvalcaba Baroni, I., van Helmond, N.A.G.M., Tsandev, I., Middelburg, J.J., and Slomp, C.P., Reassessing the nitrogen isotope composition of sediments from the proto-North Atlantic during Oceanic Anoxic Event 2. *Under review for Paleoceanography*.